P-T-t-d evolution paths within the Gander Zone, NE Newfoundland

Tanya R. King (1987)

P-T-t-d evolution paths within the Gander Zone, NE Newfoundland.

TANYA RACHEL KING

A thesis submitted in partial fulfilment of the requirements of Oxford Brookes University for the degree of Doctor of Philosophy

May 1997

PAGES NOT SCANNED AT THE REQUEST OF THE UNIVERSITY

SEE ORIGINAL COPY OF THE THESIS FOR THIS MATERIAL

To my family and friends for all their support

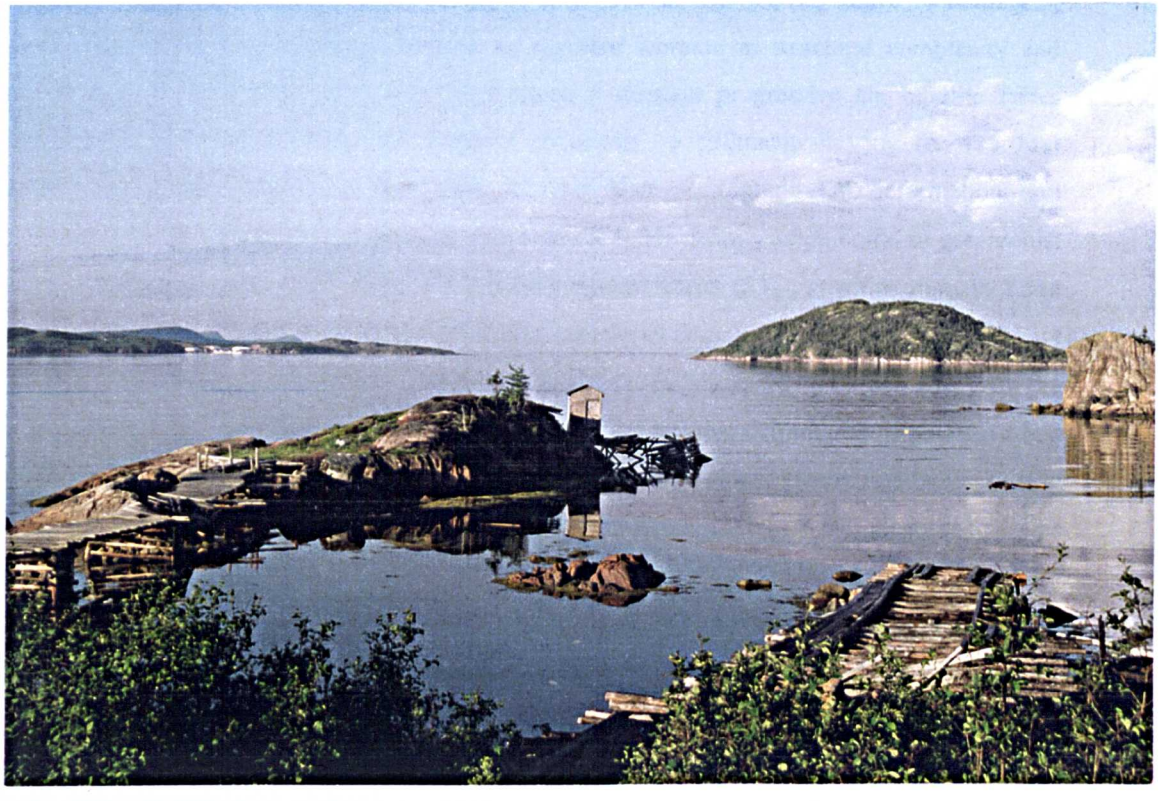

Abstract

The Gander Lake Subzone of northeast Newfoundland preserves a complex tectonothermal evolution resulting from continental collision of Gondwana and Laurentia following closure of the Iapetus ocean. Field, petrographic, geothermobarometric studies and isotopic age data define five northeast-southwest trending domains, each with a characteristic P-T-t-d evolutionary path, which reveal elements of the overall tectonothermal evolution in this sector of the Appalachians.

Domain 1 preserves deformed low grade metasediments and east vergent flat-lying D2 folds formed at *c.* 470 Ma. Domain 2 preserves focusing of later progressive deformation ($D3_{WEST}$) into a steep, predominantly sinistral high strain zone characterised by andalusite → kyanite → sillimanite indicative of a clockwise metamorphic path (peak conditions *c.* 650 °C, 5.5 kbar). In domain 3, deformed metasediments ($D2\text{-}D3_{EAST}$) display an eastward increase in structural complexity and metamorphic grade to a peak of *c.* 600 °C. Domain 4 displays progressive amphibolite facies deformation ($D3_{EAST}$) characterised by prograde andalusite → sillimanite-bearing (*c.* 425 Ma) migmatites with peak conditions of *c.* 700 °C, 4.5 kbar. Retrograde D4 deformation and metamorphism is concentrated in steep narrow high strain zones. $S4_{WEST}$ amphibolite to greenschist facies shear fabrics (predominantly dextral) overprint prograde fabrics ($S3_{WEST}$) within domain 2 and are cross-cut by the *c.* 427 Ma Middle Brook Granite. Locally in domains 3 and 4 prograde ($D3_{EAST}$) fabrics are overprinted by amphibolite to upper greenschist facies $S4_{EAST}$ fabrics which also form the dominant fabric in *c.* 417 Ma syntectonic granites. D5-D6 retrogressive deformation is pervasive in a *c.* 2 km wide mylonitic zone adjacent to the Dover Fault. D5 dextral greenschist-facies ductile structures are cut by the *c.* 385 Ma Newport Granite which in turn is cut by D6 sub-greenschist facies brittle dextral faults.

In combination, the domains preserve A) low grade deformation (Ordovician?) associated with easterly thrusting of the Dunnage Zone over the Gander Zone, B) Silurian metamorphism and deformation progressively partitioned into high strain zones and, C) Devonian retrograde ductile-brittle shearing and brittle faulting local to the Dover Fault. The spatial and temporal coincidence of transpressive deformation, moderate to high grade metamorphism and voluminous granite magmatism in the east portion of the Gander Zone is taken to relate to sinistrally oblique collision between two major crustal blocks during the Silurian. Devonian reactivation juxtaposed part of the high grade Gander Zone against the low grade Avalon block across the brittle-ductile Dover Fault.

Acknowledgements

I would like to thank my supervisors Richard, Kevin and Bob for their support and help over the last three years. I am indebted to Richard for his help in the field, providing guidance, advice, encouragement and enthusiasm (and providing a first class rock carrying service in the field!). I would like also to thank Bob for his field supervision and guidance during the project. Kev provided invaluable help back in Oxford and introduced me to the pleasures of metamorphism (and sarcasm)!

Essential technical support was provided by the staff at Oxford Brookes University, I would like to thank Jon Wells for the numerous thin sections and probe slides, Gordon Watt and Anton Kearsley for help with the S.E.M., Kelly Davis and Ian Pope for solving my computer problems and Simon Deadman for his photography. In addition thanks to Martyn, Dave and Rob for valuable discussion and to the rest of the staff for discussion of a non-geological nature. Thanks also to Bob and Michelle, the postgrads and Donny and Lucy for their hospitality in Durham.

Thanks to the Newfoundland Department of Mines and Energy for providing logistical help in the field, without the help of Sean O'Brien field work would have been difficult and far less enjoyable, thanks also to his family and Pablo for their hospitality. Ian, Torre, Dave and Jamie were excellent field companions who provided never ending humour and great dancing partners at local Newfy dances. Safe boatmanship was given by Ed Saunders and great hospitality and food both by Ed and Ester, the mayor of Hare Bay and his wife ensured we received letters and ate well!

There are many people who have made my time at Oxford Brookes enjoyable including my long suffering office partners Martyn and Dave (sorry about the sports kit!), the 'Hard Rock Think Tank', the secretaries, and numerous other drinking partners including Ran, Jon, Gordon and Jo. Without my faithful squash partner Mike goodness knows what (or whom) I would have taken my aggression out on! Thanks to my friends in Oxford, especially Karen and housemates in 'Bully' Road for a great three years, to Suzi and Abi for girlie hols and to Katie, Rachel and Brad for putting up with me last term!

A special thankyou to James for providing me with moral support and keeping me sane through my write up. Finally I would like to thank my family Mum, Dad, Alice and Barney for their continual encouragement and backing over the last three years and especially Dad for his interest, helpful discussion and reference checking!

P-T-t-d evolutionary paths within the Gander Zone, NE Newfoundland.

Chapter 3. Domain 2: The Wing Pond Shear Zone

Chapter 4: Domain 3: The Central Gander Metasedimentary Belt

Chapter 5. Domain 4: The Eastern Gander Migmatite Belt

Chapter 6. Domain 5: The Dover Fault Shear Zone

Chapter 7. Conclusions

Appendices

List of figures

CHAPTER 1

CHAPTER 2

CHAPTER 3

CHAPTER 4

CHAPTER 5

CHAPTER 6

CHAPTER 7

Chapter 1

Introduction

Chapter 1. Introduction

1.1 Aims and scope of study

1.1.1 Use of P-T-t-d evolutionary paths

An understanding of phase equilibria and the stability of mineral assemblages, backed up by experimental work and the study of natural rocks allows pressure (P) and temperature (T) estimates to be made of a variety of rock types. Whereas in some rocks mineral assemblages simply record peak metamorphic conditions, detailed textural analysis of individual rocks or suites of rocks may reveal remnants of pre-peak prograde and post-peak retrograde metamorphic conditions each of which preserves a snap-shot of the evolving orogenic conditions recording a P-T path. Where such snap-shots can be linked in time, either relative to a specific deformational event or absolutely by isotopic dating, detailed P (pressure)-T (temperature)-t (time)-deformation (d) evolutionary paths can be constructed which enable evaluation of the progressive evolution of the orogenic belt (e.g. Ernst, 1977; Oxburgh & England, 1980; Crawford & Hollister, 1984; Thompson & England, 1984; Brown, 1993).

Orogenic metamorphism occurs in actively deforming regions of the crust leading to perturbations of the pre-orogenic thermal structure of the crust followed by post-orogenic decay back to steady-state values. The time-dependant interplay of tectonism and subsequent thermal relaxation hence control the P-T-t-d evolution of the crust. If the relationship between metamorphism and structure is well understood, P-T-t-d paths can be developed which yield significant information on the tectonothermal evolution of metamorphic terranes (e.g. Selverstone, 1985; Spear, 1990). The form of paths can provide information on tectonic processes which occurred during development of the orogenic belt (e.g. Oxburgh & Turcotte, 1974; England & Thompson, 1984) and the type of belt distinguished by the relative timing of maximum-T and maximum-P (e.g. Thompson & England, 1984; Brown, 1993).

1.1.2 Application of techniques to the Gander Lake Subzone

The Gander Lake Subzone provides an ideal region which to apply the P-T-t-d approach in order to solve the tectonothermal evolution of an ancient orogen. The region forms part of the Northern Appalachians (e.g. Williams, 1979) which has undergone protracted deformation and metamorphism (Hanmer, 1981; Holdsworth, 1994a) closely linked to magmatism following Iapetus closure (e.g. Williams & Stevens, 1974). The main deformation and metamorphism is attributed to the Silurian sinistral-oblique collision of Western Avalonia to the Gander Zone along a major terrane boundary (the Dover Fault) which allowed lateral decoupling of crustal blocks during collision (Holdsworth, as distinct from the Siluro-Devonian 'Acadian' orogeny seen elsewhere in the Appalachians (e.g. Blenkinsop *et al.* 1976).

The relative timing of deformational events within the Gander Lake Subzone can be bracketed by field relationships and linked to an absolute geochronologic framework provided by radiometric age dates from migmatites and foliated and non-foliated granites (e.g. Colman-Sadd *et al.* 1990; Dallmeyer *et al.* 1983; Dunning *et al. in prep.*). Metasedimentary, migmatitic and metabasic assemblages record the prograde and peak metamorphism conditions which can be investigated by study of petrographic and microstructure-porphyroblast relationships and the application of geothermobarometry. Post-peak, high-grade conditions are recorded by fabrics within syn-tectonic granites which can be assessed by microstructural fabric analysis. The conditions during exhumation of the region are recorded by a range of retrogressive shear-fabrics in the vicinity of the present day Dover Fault.

1.1.3 Aims of study

The Appalachians in North America have been the subject of numerous previous studies which have led to an understanding of the Palaeozoic evolution of the mountain chain. Although some parts of the chain have been the subject of numerous metamorphic and structural studies (e.g. van Staal & Fyffe, 1991; Neuman & Max, 1989; Hepburn *et al.* 1995), detailed understanding of the evolution of other parts of the belt is poor. One such region is Newfoundland situated at the north end of the belt, and in particular the Gander Zone which lies between remnants of Iapetus and Gondwanan/Avalonian crustal blocks. This study aims to better define the P-T-t-d evolution for this important part of the Appalachian chain and consider it within a regional tectonic framework.

The Gander Lake Subzone represents a key region in which to investigate the ancient initial interaction of Gondwana with Avalon. It is thought to comprise part of the Gondwanan continental margin and represents a portion of the Central Mobile Belt; remnants of the Iapetus Ocean destroyed during the Appalachian Orogeny. The region underwent deformation and magmatism (following initial Ordovician closure of the Iapetus) as a result of Silurian sinistral-oblique collision along the crustal boundary between the Central Mobile Belt and Avalon. In common with the rest of the Central Mobile Belt in Newfoundland, the Gander Lake Subzone displays variations in structural complexity, metamorphic grade and intensity of igneous intrusion. The understanding of the interplay between deformation, metamorphism and magmatism in the region requires detailed structural and geothermetric study across the region. Results and observations allow the following conclusions to be made;

1) the region can be subdivided into 5 domains each of which preserves specific structural and metamorphic conditions,

2) structures can be variably correlated across the region between individual domains,

3) assemblages record clockwise metamorphic paths,

4) peak conditions are preserved by low-pressure, high-temperature migmatites,

5) both prograde and retrograde deformation is progressive in style,

6) localised strain partitioning has occurred.

1.2 Outline of study area

1.2.1 Geographical setting

The area of study; the Gander Lake Subzone is located in north-eastern Newfoundland. Newfoundland is an island measuring *c.* 500km × 500km situated at the northern end of the Appalachian orogen in the Atlantic Ocean forming part of maritime Canada (fig. 1.1). The Gander Lake Subzone is characterised by an undulating low topography and rocky coastline. Inland exposure is generally poor, or poorly accessible due to peat bogs and dense vegetation which comprise pine forests and scrub. Good inland exposure is provided along the Trans Canada Highway (TCH) and Trans Canada Railway (TCR) sections which transect the study region, and locally on the shores of lakes and in quarries and road cuts. Coastal exposure is excellent comprising clean wave washed outcrops.

1.2.2 Regional geological setting & tectonic evolution

The Appalachian orogen preserves a record of Neoproterozoic to middle Palaeozoic ocean opening and closure and continental collision (e.g. Williams, 1984), Newfoundland provides a cross-section across the northern part of the orogen. The timing and kinematics of tectonic accretion within Newfoundland is complex and most likely involved several independent collisions (e.g. Williams & Hatcher, 1982; Colman-Sadd *et al.* 1992a; van Staal, 1994; van Staal & de Roo, 1995). Original relationships between accreted terranes, and the timing of their accretion are however commonly enigmatic due to post-accretionary transpressive and transtensional adjustments (e.g. Barr *et al.* 1995).

Newfoundland, in common with other parts of the Northern Appalachian Orogen has traditionally been subdivided into four tectonostratigraphic zones (fig. 1.1; Williams, 1979) termed the Humber, Dunnage, Gander and Avalon Zones. These are thought to represent (fig. 1.3) various lithotectonic terranes (Williams & Hatcher, 1983) formed during development and destruction of the Iapetus Ocean between Laurentia and Western Avalonia (representing a fragment of Gondwana) with Laurentia represented by the Humber Zone in the west and Avalonia by the Gander and Avalon Zones in the east (e.g. Dewey and Bird, 1970; Williams, 1979). In between these continental vestiges, the Dunnage Zone preserves the remnants of the early Palaeozoic Iapetus Ocean and associated arcs (e.g. Williams *et al.* 1988), which interacted both with the Humber and Gander Zones during the Ordovician (Arenig) with the emplacement of ophiolites onto the opposing margins of the Iapetus (e.g. Colman-Sadd *et al.* 1992a). The Humber Zone comprises crystalline basement overlain by a cover sequence of Neoproterozoic to Middle Ordovician limestones and siliciclastic sediments, structurally overlain by Taconian allochthons comprising sedimentary and igneous thrust sheets. The Dunnage Zone is characterised by Cambrian to Middle Ordovician submarine volcanics and Early Ordovician ophiolitic suites. The Dunnage Zone is subdivided into the Notre Dame and Exploits Subzones, separated by the

Fig. 1.1 Tectonostratigraphic map of Newfoundland (modified after Williams *et al.* 1988).

Red Indian Line (interpreted as an Ordovician suture closed by the early Llandovery; Williams *et al.* 1993) and with contrasting crustal affinity. The Notre Dame Subzone comprises Grenvillian basement unconformably overlain by non-marine Silurian sequences. The Exploits Subzone comprises Neoproterozoic volcanics overlain by Middle Ordovician to Early Silurian shales and turbidites conformably overlain by Silurian strata. The Gander Zone is characterised by siliciclastic Cambro-Ordovician sediments and is subdivided into the geographically distinct Gander Lake, Meelpaeg and Mount Cormack Subzones. The Avalon Zone comprises Neoproterozoic volcanic and sedimentary rocks unconformably overlain by Neoproterozoic and early Palaeozoic marine sediments with a Acado-Baltic trilobite fauna (Hutchinson, 1962; O'Brien *et al.* 1983). The majority of the Precambrian rocks record a complex history of bimodal volcanism, plutonism and sedimentation within fault-bounded basins associated with a long lived arc (O'Brien *et al.* 1983) followed by deformation and low-grade metamorphism accompanying the Precambrian Avalonian Orogeny (prior to deposition of Cambrian sediments; Hughes, 1970).

Fig. 1.2 a) Tectonostratigraphic map of Newfoundland showing crustal blocks; b) seismic cross-section across Newfoundland showing relationship between tectonostratigraphic terranes and the underlying crustal blocks (after Keen *et al.* 1986).

a)

Fig.1.3 Summary of the units within the Newfoundland Appalachians showing their probable affinities in relation to the Iapetus Ocean (modified after Holdsworth, 1994a).

Tectonostratigraphic unit		Affinities
HUMBER ZONE		Continental, Laurentian
DUNNAGE ZONE	Notre Dame Subzone Undifferentiated ophiolite Exploits Subzone	Fragmented arcs; Laurentian/Gondwanan?
GANDER ZONE		Continental, uncertain origin?
AVALON ZONE		Continental, Avalonian (Gondwanan)

The deep structure of the Appalachian Orogen in Newfoundland has been investigated by interpretation of seismic reflection studies (e.g. Keen *et al.* 1986; Marillier *et al.* 1989; Stockmal *et al.* 1990) combined with results of isotopic studies of basement rocks (e.g. Fryer *et al.* 1992; D'Lemos & Holdsworth, 1995). Results (fig. 1.2) suggest that the region is underlain by three crustal blocks, 1) the Grenvillian basement Block (corresponding to the partially overridden Laurentian margin) which at the surface is characterised by the Humber Zone; 2) the Central Block which underlies the Gander Zone and part of the Dunnage Zone and 3) the Avalonian Crustal Block, directly coinciding with the Avalon Zone. It is unclear whether the Central Block is continuous with the surface rocks of the Dunnage and Gander Zones. It appears that the Dunnage Zone forms a thin allochthonous sheet detached from the lower crust (fig. 1.2b) bounded against the Gander Zone which is itself bounded to the southeast by the steeply dipping Dover Fault (e.g. Williams & Stevens, 1974).

Recent models suggest that the main juxtaposition of the Dunnage components (Notre Dame and Exploits) occurred prior to the closure of the Ordovician Iapetus Ocean ('Iapetus 1' of van der Pluijm & van Staal, 1988). Closure of the Iapetus is thought to have been initiated in the mid-Ordovician and is attributed to Taconic subduction-related thrusting of oceanic thrust sheets (of Dunnage Notre-Dame Subzone affinity) over the Humber continental margin (*c.* 470 Ma; Williams & Stevens, 1974; Williams, 1984; Colman-Sadd, 1980, 1982; Colman-Sadd *et al.* 1992a & b). In western Newfoundland, the mid-Ordovician Taconic Orogeny was marked by the emplacement of two major allochthons consisting of slices of ophiolitic, volcanic and sedimentary rocks which are variably interpreted as pre-assembled slices (Waldron & Stockmal, 1991), and late-stage emplaced ophiolitic components (Cawood, 1995). At about the same time as the interaction of the Dunnage and Humber Zones, ophiolitic assemblages of the Exploits Subzone (of the Dunnage Zone) were juxtaposed over rocks of the underlying Gander Zone (correlated with the Penobscottian event in Maine, e.g. Colman-Sadd *et al.* 1992a). The timing of this deformation in Newfoundland is constrained by a U-Pb zircon age of *c.* 474 Ma of the Partridge Berry Hill Granite which intrudes the ophiolites and the Gander Zone, and by Arenig-Llanvirn fauna which oversteps the zonal boundary (e.g. Piasecki *et al.* 1990, Colman-Sadd *et al.* 1992a). Evidence for the continued generation and consumption of ocean crust in the late Ordovician is seen in the Miramichi region of New Brunswick (van Staal & Fyffe, 1991) aswell as locally in the

Buchans Roberts Arm Belt of Newfoundland (O'Brien & Szybinski, 1989). Subsequent reactivation of pre-existing tectonic boundaries and widespread deformation occurred during closure of a back arc basin ('Iapetus 2' of van der Pluijm & van Staal, 1988) which resulted in mid-Silurian Acadian (termed 'Salinic' Orogeny in the Gander Zone; Dunning *et al.* 1990) metamorphism and plutonism (Colman-Sadd, 1982; van der Pluijm & van Staal, 1988; Stockmal *et al.* 1990). This event is thought to be a progressive deformational event involving Laurentian/Gondwanan interactions (e.g. van Staal *et al.* 1990; Williams, 1993; Hibbard, 1994), the precise timing and kinematics of which are unclear. It has been proposed in New Brunswick that late-Silurian sinistral transpression changed through extensional collapse into dextral transpression in the early to mid Devonian, and is attributed to a continual modification of stresses due to rearrangement of crustal units (van Staal & De Roo, 1995).

The western margin of the Gander Lake Subzone against the Dunnage Zone is generally interpreted as tectonic (e.g. Currie, *et al.* 1979; Pajari *et al.* 1979; Blackwood, 1982, O' Neill, 1991), marked along much of its length by ophiolitic assemblages of the Gander River Complex (formerly GRUB; Jenness, 1958; Blackwood, 1978, 1982; O' Neill, 1991). The various detailed field observations and interpretations of the relationships formed during the juxtaposition of the Dunnage and Gander lake Subzones are summarised in fig. 1.4. The eastern margin of the Gander Lake Subzone with Avalon (marked by the Dover Fault; Yonce, 1970) separates upper amphibolite-facies Gander Zone rocks (Hare Bay Gneiss and foliated granite) from greenschist-facies Avalon zone volcanic rocks. Rocks across the Dover Fault preserve totally different geological histories (Blackwood & Kennedy, 1975) and are interpreted to be unrelated prior to juxtaposition.

Fig. 1.4 Summary of previous interpretations of the nature of the Dunnage/Gander boundary.

Author	Contribution
Kennedy & McGonigal (1972)	Noted detrital mineral and rock fragments in basal conglomerate of the Davidsville group in the Dunnage Zone hence inferred major angular unconformity between Davidsville and Gander groups.
Uzuakpunwa (1973)	Noted that Gander Group had acquired a deformation fabric prior to emplacement of the Davidsville Group also that metamorphic fragments in the Davidsville melange preserve earlier deformation.
Currie & Pajari (1977)	Proposed conformable relationship between Davidsville and Gander groups in Carmanville area where Gander River Complex is absent however provides contradicting evidence for a structural discontinuity between the sequences.
Blackwood (1978, 1982)	Suggested nature of the Davidsville Group/Gander Group contact is enigmatic where the Gander River Complex is present. Interpreted contact south of Gander Lake as conformable however elsewhere suggested a non-conformably overlain faulted contact
Piasecki (1988)	Proposed tectonic contact between Davidsville and Gander Groups shown around Weirs Pond by a km-wide mylonitic zone.
O'Neill (1991)	Suggested juxtaposition of the Gander Group with Dunnage occurred by transcurrent movement along the Gander River Complex.

Fig. 1.5 Simplified geology map of the Gander Lake Subzone, NE Newfoundland.

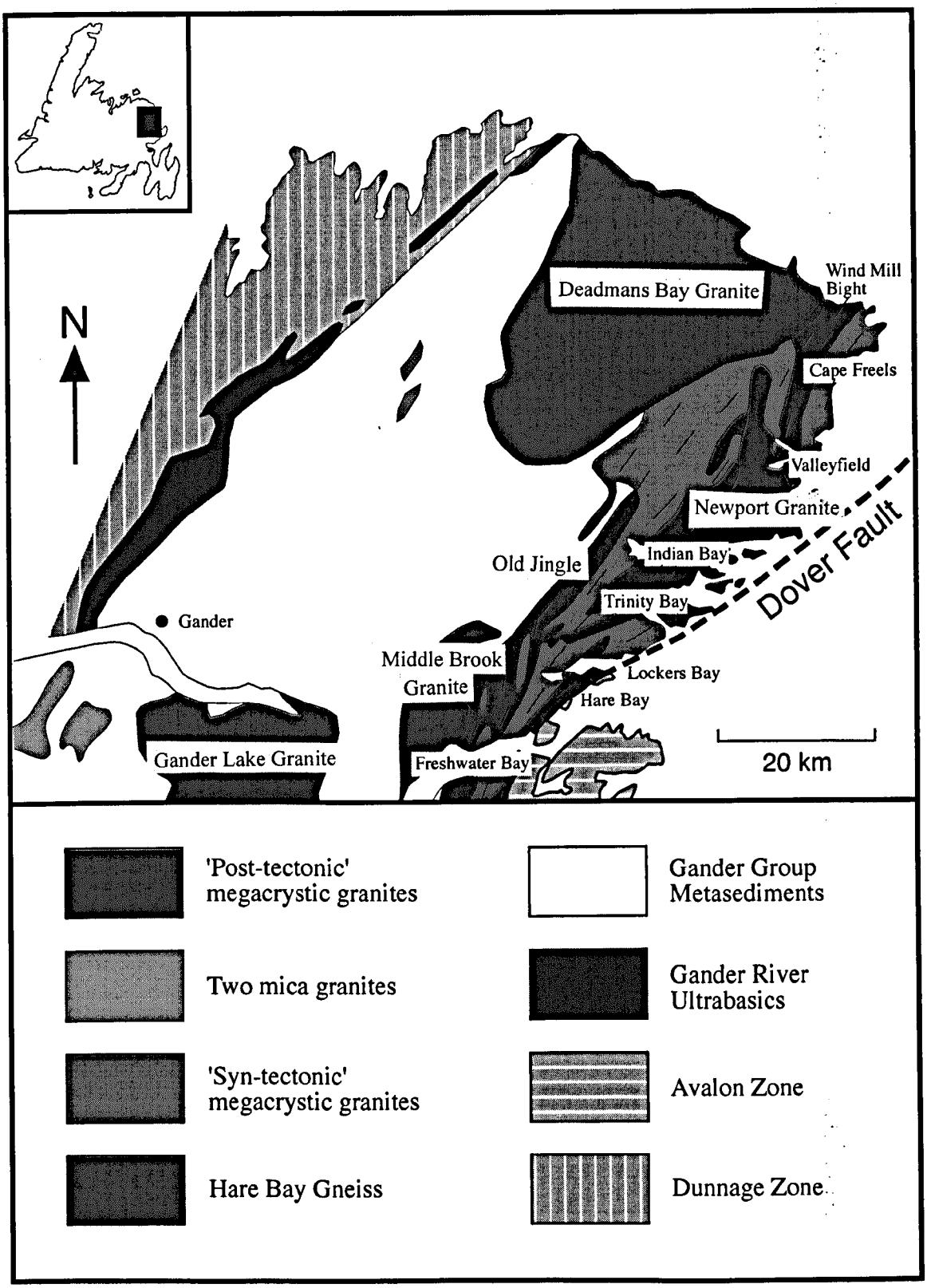

1.3 Geology of the Gander Lake Subzone

1.3.1 Introduction

The Gander Lake Subzone forms the northern part of the Gander Zone in Newfoundland and comprises (fig. 1.5) a thick variably deformed and metamorphosed sequence of siliciclastic Gander Group metasediments which are intruded by numerous foliated and unfoliated granites (Jenness, 1963; McGonigal, 1973, Blackwood & Kennedy, 1975; Blackwood, 1977; Williams *et al*, 1988). The west of the region comprises low grade metasediments whereas the east records sillimanite-grade regional metamorphism and migmatisation within a belt of migmatites, orthogneiss and metabasite (termed the Hare Bay Gneiss; Blackwood & Kennedy, 1975; Blackwood, 1977) associated with foliated granites (Jayasinghe & Berger, 1976; Blackwood, 1976, 1978; Jayasinghe, 1978).

1.3.2 Structure and metamorphism

Fig. 1.6 Summary of previous structural observations and classifications within the Gander Lake Subzone.

Author	Contribution
Kennedy & McGonigal (1972)	Defined 3 phases of deformation in Gander Group: D1-local weak & deformation, D2-SE facing isoclinal folds & axial planar fabric, D3-tight SE facing folds. Recognised NE-SW trending sub-horizontal mineral lineation.
Uzuakpunwa (1973)	Described 4 main phases of deformation in the Gander Group and recognised that it had acquired a composite fabric before emplacement of Davidsville Group (i.e. Dunnage obduction).
Blackwood (1977)	Recognised early S1 schistosity, main S2 fabric in Gander Group (flat in the west and steepens eastwards) and upright F3 folds. Recognised complex metamorphic and deformational history in the gneisses.
Jayasinghe (1978)	Recognised refolding in gneisses and effect of strain variation on style of deformation in migmatites, described 'cataclastic' fabrics in migmatites adjacent to Cape Freels Granite.
Hanmer (1981)	Defined 'flat belt' of low grade metasediments and 'steep belt' of metasediments, gneisses and migmatites. Proposed region as a sinistral Acadian shear zone with increase of deformation eastwards and ductile deformation synchronous with granite intrusion.
O'Neill & Knight (1988)	Described early S1, defined principal foliation S2 axial planar to isoclinal F2 folds which steepen into anomalous metamorphic zone around Wing Pond.
Holdsworth (1991)	Recognised sinistral 'early ductile' fabrics in migmatites and foliated granites, variably overprinted by sinistral-dextral 'late ductile' and dextral 'late-brittle' fabrics.
Holdsworth (1994a)	Described flat-lying F2 folds in Gander Group which are progressively deformed eastwards into migmatites by upright F3 and F4 folds (also present in foliated granitoids). Correlated F4 folds with 'early ductile' fabrics in migmatites and granites.

The Gander Lake Subzone displays evidence for protracted prograde heterogeneous deformation (e.g. Kennedy & McGonigal, 1972; Hanmer, 1981; O'Neill, 1991; Holdsworth, 1994a) shown by coincident regions of increased structural complexity and higher metamorphic grade (Kennedy & McGonigal, 1972; Hanmer, 1981; O'Neill, 1991; Holdsworth, 1994a, b). Low-grade flat-lying deformed assemblages (the 'flat-belt' of Hanmer, 1981) in the west are overprinted by the effects of sinistral transpression which were focused into a steep sinistral shear zone (e.g. Hanmer, 1981; Caron & Williams, 1988a, b). Rocks in the 'steep-belt' (Hanmer, 1981) are characterised by syn-tectonic sillimanite-grade regional metamorphism, migmatisation and granite plutonism (Holdsworth, 1994a). Effects of protracted retrogressive deformation are preserved within the Dover Fault Shear Zone (e.g. Holdsworth, 1991; Holdsworth & O'Brien, 1993; Holdsworth *et al.* 1993) where sinistral transpressive deformation is overprinted by dextral ductile shear-fabrics. Cross-cutting dextral brittle deformation is localised along the Gander-Avalon boundary marked by the present day Dover Fault (Holdsworth, 1991). The onset of down-temperature deformation is interpreted to record exhumation and possible onset of orogenic collapse (Holdsworth, 1994a).

The flat-lying structures preserved in the west are regionally interpreted as D2 (attributed to the eastwards obduction of Dunnage over the Gander Zone; Williams & Stevens, 1974; Williams, 1984; Colman-Sadd, 1980, 1982; Colman-Sadd *et al.* 1992a) associated with development of a northeast-southwest trending sub-horizontal stretching lineation (e.g. Kennedy & McGonigal, 1972; Blackwood, 1977; O'Neill, 1991). The D2 structures are in several regions overprinted by upright folds (termed F3; e.g. Blackwood, 1977) and later structures with the intensity of later deformations accompanied by an increase in metamorphic grade. The upright deformation is progressive in style (Holdsworth, 1994a), deforming high-grade metasediments which pass laterally into deformed sillimanite-grade migmatites. Steep amphibolite facies fabrics form the dominant fabric in the majority of the syn-tectonic granitoids (Hanmer, 1981; Holdsworth, 1991, 1994a). High grade (early ductile, Holdsworth, 1991) deformed migmatitic and granitic assemblages are overprinted by lower-grade shear fabrics and brittle faults (termed late ductile & late brittle respectively; Holdsworth, 1991). A summary of previous structural interpretations and classifications is shown in fig. 1.6.

1.4 Lithological classifications

1.4.1 Gander Group Metasediments

The previous classifications and stratigraphic interpretations of metasediments of the Gander Lake Subzone are summarised in fig. 1.7. Metasediments comprise a thick sequence of interbanded pelitic, semi-pelitic and psammitic lithologies with subordinate bands and pods of calc-silicate (Blackwood, 1977, O'Neill, 1991) which is termed the Gander Group (thought to

Fig. 1.7 Summary of contributions in the recognition, description and division of Gander Zone rocks.

Author	Contribution
Murray & Howley (1881)	Reconnaissance work, proposed Silurian age for metasediments and described NE-trending mafic and ultramafic rocks.
Twenhofel (1947)	Phyllite, slate and quartzite along Gander Lake assigned to Silurian 'Gander Lake Series'.
Baird *et al.* (1951)	Earliest regional mapping proposed Ordovician age for Gander Lake rocks.
Jenness (1954, 1958, 1963)	Redefined 'Gander Lake Series' to Ordovician group based on graptolite and brachiopod fauna. Subdivided Gander Lake Group into 3 conformable units. Detailed description of ultramafics.
Williams (1964)	Extended 3 fold division of Jenness' northwards.
Kennedy & McGonigal (1972)	Redefined Gander Lake Group to consist of only lower arenaceous unit of Jenness. Davidsville Group proposed for middle and upper fossiliferous units. Interpreted rocks as part of a continental prism which thinned east onto Avalon platform. Interpreted Gander Group metasediments as cover sequence to eastern gneissic basement.
McGonigal (1973)	Recognised two contrasting terranes; 1) metasedimentary 2) sedimentary and volcanic which he defined as the Gander Group and Davidsville Groups respectively.
Blackwood & Kennedy (1975)	Termed eastern gneissic rocks the Bonavista Bay Gneissic Complex and interpreted it as representing basement.
Blackwood (1976, 1977)	Subdivided gneissic complex into 1) paragneiss 2) Square Pond Gneiss 3) Hare Bay Gneiss (migmatite) with 'migmatite front' between gneissic units.
Blackwood (1978)	Reinterpreted gneissic units as single conformable sequence with eastward increase in metamorphic grade and interpreted it as basement.
Strong *et al.* (1974)	Sampled granite intrusions in the Gander Zone for geochemical study.
Jayasinghe (1976, 1978)	Undertook regional mapping in the Gander Lake Subzone; described various foliated megacrystic granites (e.g. Wareham, Cape Freels & North Pond) and unfoliated granites (e.g. Deadmans Bay & Newport).
Wonderley & Neuman (1984)	Defined the Indian Bay Formation, interpreted fossils from boulders as 'in situ' assigned to late Arenig age-early Llandeilian age.
O'Neill & Blackwood (1989)	Subdivided Gander Group into the Jonathans Pond and Indian Bay formations, defined Gander River Complex.
O'Neill (1991), O'Neill & Colman-Sadd, (1993)	Recognised and described Wing Pond Shear Zone and contact metamorphic aureoles around Deadmans Bay and Ocean Pond Granites.
Hanmer (1981)	Described low-strain and mylonitic types of migmatite; recognised syn-tectonic foliated granites
Holdsworth (1991)	Subdivided Hare Bay Gneiss Migmatites into coherent, mobilised and schlieric types; suggested a syn-tectonic in origin for the majority of the foliated megacrystic granites.
D'Lemos & Holdsworth (1995)	Described the range of stromatic, schlieric, inhomogeneous diatexitic and anatectic granitic types of migmatite.
Schofield, D'Lemos & King (1996)	Described the structural relationship between the syn-tectonic Cape Freels Granite and its country rocks.

include the lower Jonathans Pond Formation and the overlying Indian Bay Big Pond Formation; O'Neill, 1991). Early work (e.g. Kennedy & McGonigal, 1972; Blackwood & Kennedy, 1975; Blackwood, 1976, 1977), interpreted Gander Group metasediments as a cover sequence to basement schists and gneisses in the east (the Bonavista Bay Gneiss Complex;

Blackwood & Kennedy, 1975). Subsequent field and isotopic work has shown the metasediments to be part of a continuous sequence of increasing chlorite to sillimanite grade which passes into migmatites (Blackwood, 1978; O'Neill, 1991; D'Lemos & Holdsworth, 1995).

Metasedimentary assemblages in the west of the Gander Lake Subzone are typically low grade and chlorite-muscovite-bearing. Regions of increased grade in the metasediments include assemblages within the Wing Pond Shear Zone (O'Neill, 1991) typified by development of andalusite, kyanite, sillimanite and staurolite and assemblages in the east (termed the Square Pond Gneiss, Blackwood, 1977) adjacent to the migmatites (e.g. at Old-Jingle; fig. 1.5) which show local development of garnet and sillimanite. Metasedimentary assemblages show local development of contact metamorphic index minerals within the aureoles of undeformed granite plutons such as the Ocean Pond and Deadmans Bay Granites (O'Neill, 1991; fig. 1.5).

1.4.2 Hare Bay Gneiss Migmatite

Migmatites form part of the Hare Bay Gneiss sequence (Blackwood, 1977) which are characteristically of sillimanite-grade (Blackwood & Kennedy, 1975, Blackwood, 1977) and are interpreted to represent high grade equivalents of Gander Group metasediments (e.g. Blackwood, 1978). The migmatites form a variety of types (e.g. Holdsworth, 1991) ranging from coherent stromatic metatexites through to 'mobilised gneiss' and 'schlieren-rich xenolithic granite'. Migmatites display varying degrees of metamorphic segregation, partial melting, melt segregation as well as disruption and disaggregation of restite into melt portions (D'Lemos & Holdsworth, 1995). The stromatic migmatites are characterised by subparallel leucosome/melanosome layers which are variably deformed into folds (termed early ductile fabrics; Holdsworth, 1991) and show local evidence for melt migration. Migmatites displaying higher degrees of partial melting have been broadly classified as schlieric migmatites and inhomogeneous diatexites, products of advanced melting are described as heterogeneous xenolithic anatectic granite (D'Lemos & Holdsworth, 1995).

1.4.3 Orthogneiss

Orthogneisses comprise a series of locally homogeneous tonalitic to granitic bodies which lack numerous country rock xenoliths and schlieren leading to the interpretation that they were not derived from the migmatites (Blackwood, 1977). The majority of the orthogneisses have been previously included as part of the Hare Bay Gneiss sequence (Blackwood, 1977) although a small number of orthogneissic bodies have been classified as part of later intrusive suites (e.g. Hanmer, 1981). The 'Hare Bay Gneiss' orthogneisses locally cross-cut layering in the migmatite but are deformed by the main phase of deformation in the country rocks (Holdsworth & O'Brien, 1993), and are interpreted as early intrusions. The orthogneisses display a distinct gneissic fabric defined

by alkali feldspar augen wrapped by a plagioclase / quartz banding which show effects of high-temperature ductile recrystallisation (Holdsworth & O'Brien, 1993).

1.4.4 Metabasite

Metabasite is contained mostly within a suite of felsic / mafic complexes close to the Dover Fault (Hanmer, 1981) and is classified as part of the Hare Bay Gneiss sequence (Blackwood, 1977). The bodies comprise a diverse series of foliated sheets which carry fabrics preserved within paragneissic migmatite and are hence interpreted to represent early mafic intrusions (Holdsworth, 1991, 1994a). Lesser deformed massive metadioritic / metabasic bodies have been described from within the migmatites which are interpreted as being slightly younger (e.g. D'Lemos & Holdsworth, 1995). Rare metabasic units within the Gander Group metasediments (O'Neill, 1991) are interpreted to broadly correlate with those within the migmatites (classified as Hare Bay Gneiss) further east (Holdsworth, 1994a).

1.4.5 Intrusive bodies in the Hare Bay Gneiss

Igneous intrusions are dominantly granitic and sub-divided into applogranite veins, mixed sheet complexes, alkali feldspar megacrystic granites, two-mica garnetiferous granites and gabbros (Strong *et al.* 1974; Jayasinghe & Berger, 1976; Blackwood, 1977; Jayasinghe, 1978; Holdsworth, 1991; O'Brien & Holdsworth, 1992; D'Lemos & Holdsworth, 1995; D'Lemos *et al.* 1995; Schofield *et al.* 1996).

Silurian alkali feldspar megacrystic granites (e.g. the Wareham, Lockers Bay, Dover Fault and Cape Freels Granites) and mixed sheeted complexes form a distinct group of early foliated granites which occur as elongate bodies restricted to the Hare Bay Gneiss (Blackwood, 1977) and parallel the regional foliation. The majority of the granites form vertical sheets, although, the Wareham granite is thought to be flat-lying in attitude (D. Schofield *pers. comm.*). Structures within these granites and relationships with host rocks, have led to them being termed 'syn-tectonic' (e.g. Hanmer, 1981; Holdsworth, 1991, 1994a; Schofield *et al.* 1996). A second distinctive group of Devonian alkali feldspar megacrystic granites (e.g. the Deadmans Bay, Newport and Gander Lake plutons) form bodies which are unfoliated, discordant to structures in the country rocks (e.g. D'Lemos *et al.* 1995) and display development of contact metamorphic aureoles (e.g. O'Neill. 1991). These bodies cross-cut both the foliated megacrystic granites and the two-mica granites, and are sharply terminated by the Gander-Avalon tectonic boundary (except the Ackley Granite which reportedly cross-cuts the Dover Fault; Dallmeyer *et al.* 1983; Tuach, 1987). The unfoliated nature of these granites has led to them being termed 'post-tectonic' (Colman-Sadd *et al.* 1990; Kerr *et al.* 1993; D'Lemos *et al.* 1995). The Middle Brook Granite shows many features in common with the post-tectonic granites and has traditionally been classified as such. However, recent isotopic work (Dunning *et al. in prep.*) suggests an age

significantly older than nearby syn-tectonic granites. A spectrum of so called 'two-mica granites' range from early foliated to non-foliated bodies (e.g. Jayasinghe & Berger, 1976; Jayasinghe, 1978) which occur throughout the Gander Zone (Blackwood, 1978) and in places are closely related to migmatites, while elsewhere cross-cut foliated megacrystic granites (Blackwood, 1977).

1.5 Methodology

1.5.1 Field and sampling techniques

Fieldwork was undertaken during two field seasons of four and nine weeks respectively (1994 and 1995). Field studies of regional structural and metamorphic relationships across the region, undertaken with reference to pre-existing regional maps (Blackwood, 1977; Jayasinghe, 1978; O'Neill, 1991; O'Neill & Colman-Sadd, 1993) identified key areas of interest. Detailed mapping (and sample collection) carried out in these key regions utilised standard base maps (1: 50000) and aerial photographs and concentrated on lithological, structural and metamorphic characteristics. Approximately 270 orientated samples were collected from across the Gander Lake Subzone in order to acquire a database of the different rock types and fabric generations and to establish the metamorphic mineral assemblages and reactions within the rocks.

1.4.2 Analytical techniques

Constraining P and T

Fig. 1.8 Summary of geothermobarometers and sources of calibrations applied to assemblages in the Gander Lake Subzone.

Exchange thermometers		
Garnet-biotite	$Fe_3Al_2Si_3O_{12}$ + $KMg_3AlSi_3O_{10}(OH)_2$ = $Mg_3Al_2Si_3O_{12}$ + $KFe_3AlSi_3O_{10}(OH)_2$	Ferry & Spear (1978); Perchuk & Lavrent'eva (1983); Hodges & Spear (1982); Ganguly & Saxena (1984); Indares & Martignole (1985); Berman (1990)
Amphibole-plagioclase	NaSi = CaAl	Spear (1980); Blundy & Holland (1990); Holland & Blundy (1994)
Other geothermobarometers		
Amphibole-plagioclase geothermobarometer	Empirical model based on dependence of Al content in Ca-amphiboles and coexisting plagioclase	Plyusnina (1982)
Clinopyroxene-plagioclase geobarometer	Based on reaction $CaAl_2Si_2O_8 = CaAl_2SiO_6 + SiO_2$	Ellis (1980)
Cordierite geobarometer	Based on Xmg content of cordierite	Holdaway & Lee (1977)

Microstructural petrographic analysis of *c.* 270 thin sections from assemblages across the region enabled assessment of mineral-fabric relationships, mineral assemblages and the grade of metamorphism. The results of the thin-section analysis identified specific assemblages of metamorphic interest to which more detailed petrographic study was given, and which are geothermobarometrically sensitive. S.E.M. (using a energy dispersive JOEL instrument; see Appendix B1) probe work was undertaken on these assemblages. Several tools were applied in order to investigate the metamorphic conditions of formation of assemblages including the use of mineral reactions and equilibria from petrogenetic grids, and the application of various calibrations of published geothermobarometers. The geothermobarometers and calibrations applied to specific Gander Lake Subzone assemblages are summarised in fig. 1.8. In common with other geothermobarometric studies (e.g. Chipera & Perkins, 1988), it was neccessary that the mineral assemblages to which methods were applied record a state of local equilibrium (e.g. Essene, 1982, 1989). This was ensured by the analysis of rims (non-retrogressed) of mineral pairs and avoiding analysis of recrystallised or geochemically homogenised assemblages. When choosing the most suitable calibration of geothemobarometer, their accuracy, as well as their sensitivity over a range of specific P-T conditions (discussed by Spear, 1993) were considered.

1.5.3 Layout of thesis

The thesis is divided into seven chapters. The main body (chapters 2 to 6) describe in detail the geology and metamorphic and structural evolution of five individual domains within the Gander Lake Subzone (fig. 1.9) each of which are characterised by specific structural and metamorphic assemblages. The tectonothermal development of each domain is summarised by construction (where possible) of a P-T-t-d path. The domains (from west to east) are; 1) the Western Gander Metasedimentary Belt, 2) the Wing Pond Shear Zone, 3) the Central Gander Metasedimentary Belt, 4) the Eastern Gander Migmatite Belt and 5) the Dover Fault Shear Zone (fig. 1.9).

The precise location, lithology, structural and metamorphic characteristics of each domain are discussed in the beginning of each chapter. The flat-lying regional D2 structures are correlated across the Gander Lake Subzone both in domains 1 and 3, whereas overprinting upright prograde and retrograde fabrics are classified regionally into those occurring in the west (i.e. in domains 1 & 2) and east (i.e. in domains 3, 4 & 5) of the region. The upright prograde structures in the west of the Gander Lake Subzone are termed $D3_{WEST}$ whereas those in the east are termed $D3_{EAST}$, similarly the steep micaceous fabrics in the west and east of the Gander Lake Subzone are termed $D4_{WEST}$ and $D4_{EAST}$ respectively (fig. 1.10).

Each chapter includes field and microstructural descriptions of fabric and metamorphism and the results of petrographic and geothermobarometric analysis. Prograde, peak and retrograde metamorphic conditions are assessed and related to deformation, in addition relative timing relationships are made from field observations and absolute timing relationships inferred from radiometric age dates of specific intrusions. In the concluding chapter (7) the overall structure and

Fig. 1.9 Map showing the 5 domains of the Gander Lake Subzone.

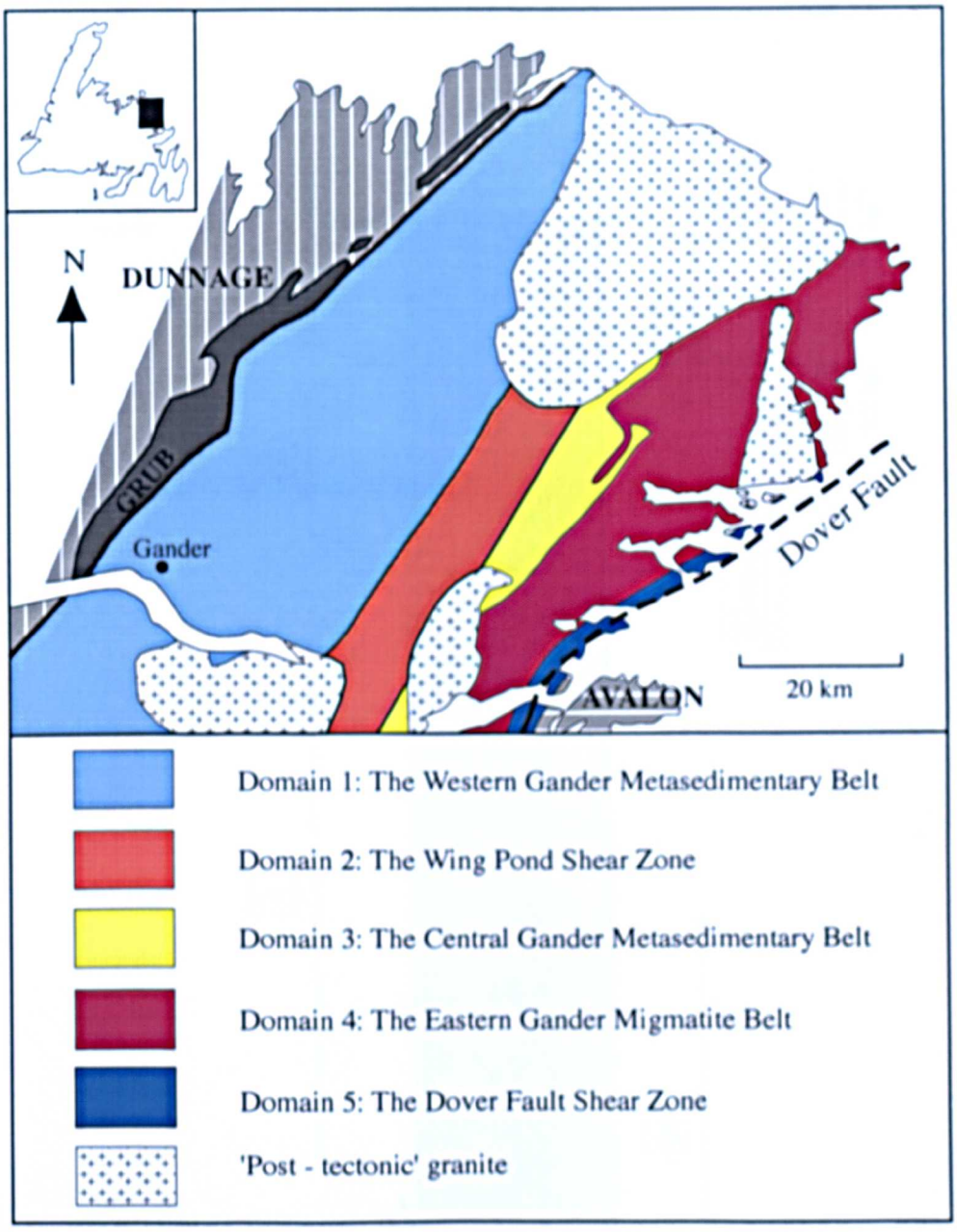

Fig.1.10 Schematic cross-section of the Gander Lake Subzone showing structural characteristics of domains 1-5.

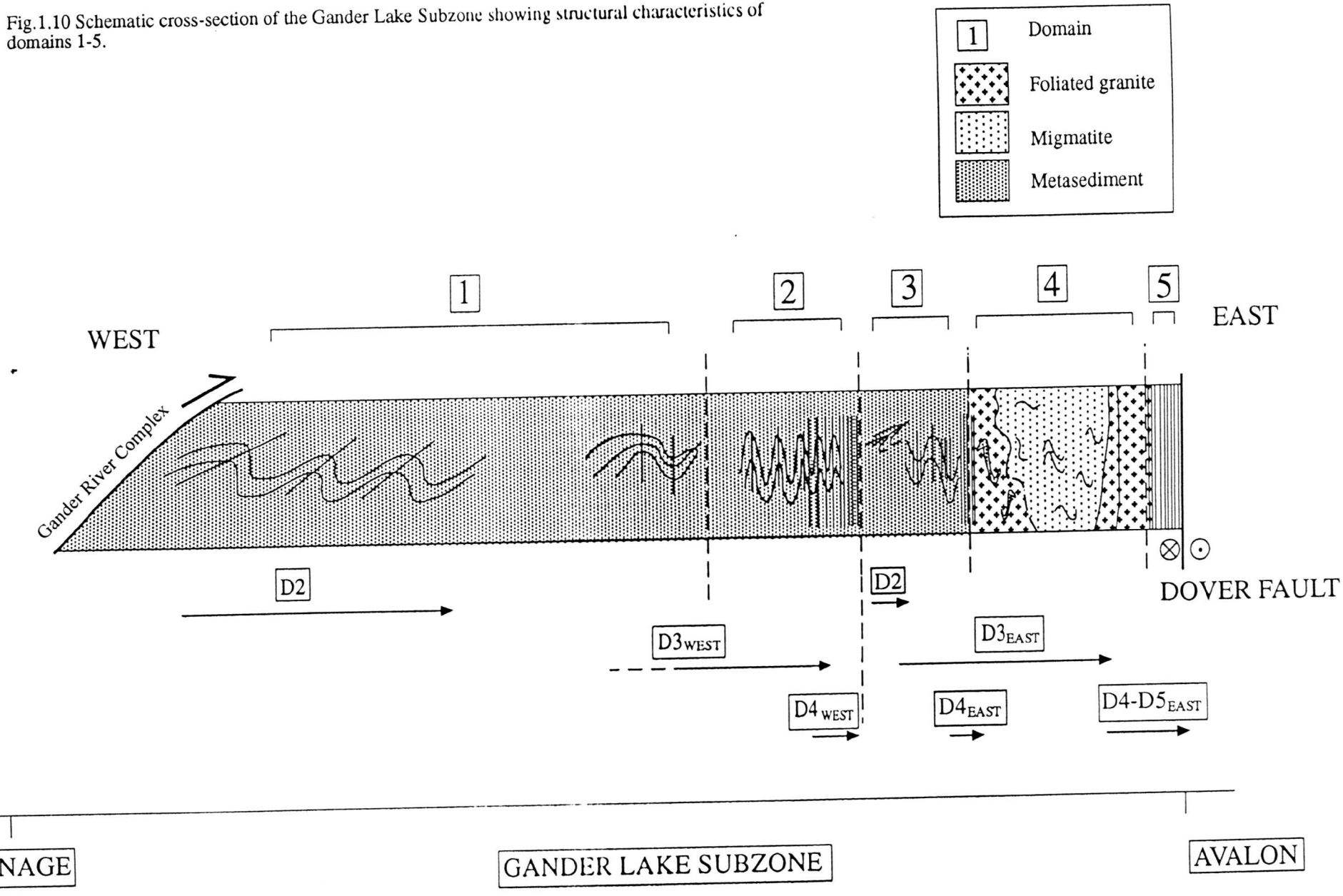

form of the individual P-T-t-d paths (characteristic of each separate domain) are compared and their implications for the overall structural and tectonic evolution of the Gander Lake Subzone are discussed.

Chapter 2.

Domain 1: The Western Gander Metasedimentary Belt

Chapter 2. Domain 1: The Western Gander Metasedimentary Belt

2.1 Introduction

The Western Gander Metasedimentary Belt (domain 1) is a northeast-southwest trending belt located to the east of the Dunnage Zone (Williams, 1979) and the west of domain 2 (the Wing Pond Shear Zone, O'Neill, 1991; fig. 2.1). The domain extends north from Gander Lake to Shoal Pond and measures 25-30 km in width. Structures in the domain are predominantly subhorizontal leading to its classification as a 'flat belt' (Hanmer, 1981). The dominant lithology in the region is Gander Group metasediment (McGonigal, 1973; Blackwood, 1982) which comprises predominantly of low-grade (Jonathan's Pond Formation; O'Neill, 1991) pelitic to semi-psammitic metasediments with minor layers of calc-silicate lithology. Other rock types within the domain include minor ultramafic bodies and large undeformed (muscovite and biotite) granites (O'Neill, 1991; O'Neill & Colman-Sadd, 1993). The western margin of the domain is an abrupt boundary marked by the Gander River Complex (O'Neill, 1991; formerly GRUB of Blackwood, 1980). The eastern boundary is gradational, and loosely marked by the transition from subhorizontal greenschist facies fabrics to steep amphibolite facies fabrics.

This chapter uses the results of field, microtextural and petrographic mineral-fabric analysis combined with the application of mineral equilibria studies to establish the conditions of metamorphism within the domain.

2.2 Structure and metamorphism

The recumbent structures which dominate the domain are easterly verging with a well developed axial planar cleavage (O'Neill, 1991; Holdsworth, 1994a), these are thought to be related to regional D2 (attributed to the mid-Ordovician accretion of the ophiolitic Dunnage Zone over the Gander Zone; Williams & Stevens, 1974; Colman-Sadd, 1980, 1982; Williams, 1984; Colman-Sadd *et al.* 1992a). Early fabrics which have been recognised at an outcrop scale include transposed bedding fabrics (S0-Sn) and a fine crenulation cleavage (S1), these are overprinted by S2 which Holdsworth (1994a) described as a pervasively developed spaced pressure solution 'pin-stripe' cleavage. A variably well developed post-D2 northeast-southwest trending subhorizontal mineral lineation has been described (e.g. Kennedy & McGonigal, 1972; Hanmer, 1981; O'Neill, 1991, Holdsworth, 1994a) which is predominantly subhorizontal, but shows complex plunge variations (fig. 2.2a). In the east of the domain D2 assemblages are locally overprinted by upright folds with associated steep fabrics which are termed $D3_{WEST}$ (previously termed D3 e.g. Blackwood, 1977) in addition local overprinting of D2 by westerly verging recumbent folds termed $D3_{LOCAL}$ is common. Cross-cutting of rocks by northeast-

Fig. 2.1 Locality/sample map for Domain 1.

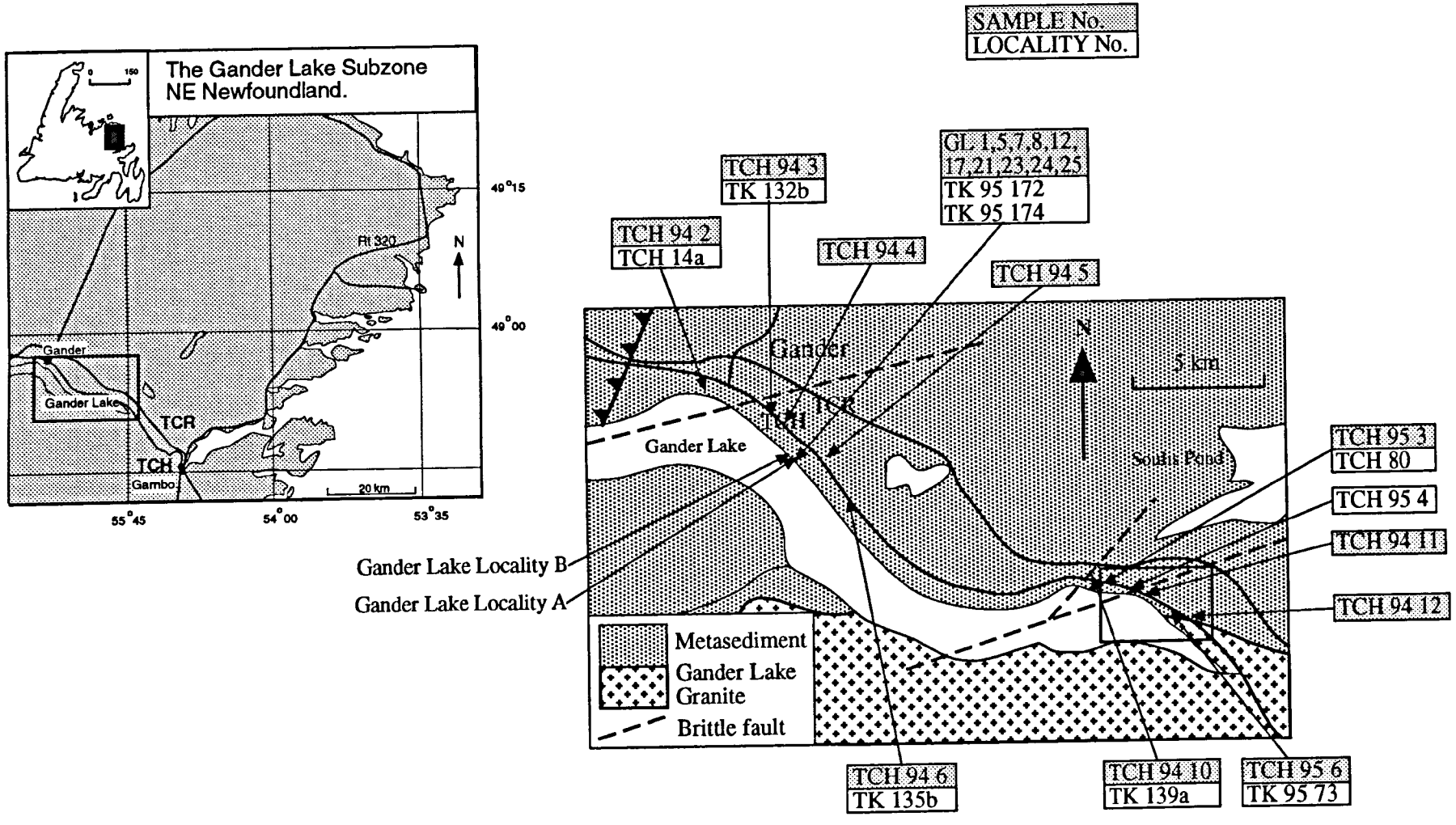

Fig. 2.2 a) & b) Structural maps for the west of the Gander Lake Subzone (from the Benton Turn to the Gander Lake Granite; for precise location see fig. 2.1) showing F2 folds and post F2 mineral lineation (after Holdsworth. *pers. comm.*).

southwest trending brittle faults occurs throughout the domain. Assessment of the relationships between D2, $D3_{WEST}$ and $D3_{LOCAL}$ deformation and metamorphism in the domain has been carried out by field, and microstructural petrographic-fabric analysis from numerous localities from across the Trans Canada Highway section, and from two key localities beside Gander Lake (fig. 2.1).

The metasedimentary assemblages within the domain are characterised by presence of chlorite and muscovite (e.g. O'Neill, 1991; Holdsworth, 1994a), however in the aureole of the Gander Lake Granite D2 and $D3_{WEST}$ assemblages are overprinted by contact heating effects (e.g. O'Neill, 1991) and show hornfelsing and variable development of contact metamorphic minerals e.g. biotite, andalusite and cordierite.

2.3 Field relationships

The dominant structures in the domain are easterly verging flat-lying folds with an associated axial planar cleavage, these deform a millimetre scale planar fabric and a lithological variation. The lithological variation is clearly defined by centimetre scale interlayered coherent pelitic, semi-pelitic and psammitic units, in places show fine laminations, graded bedding and cross-bedding and is interpreted as bedding (S0). Beds are variably transposed into S0-Sn fabrics.

Fig. 2.3 Sketch of field relationships in domain 1 (locality TCH 94 10) showing F2 folds deforming S0-Sn and relic S1 and the local development of $F3_{WEST}$ folds and associated steep axial planar $S3_{WEST}$ cleavage.

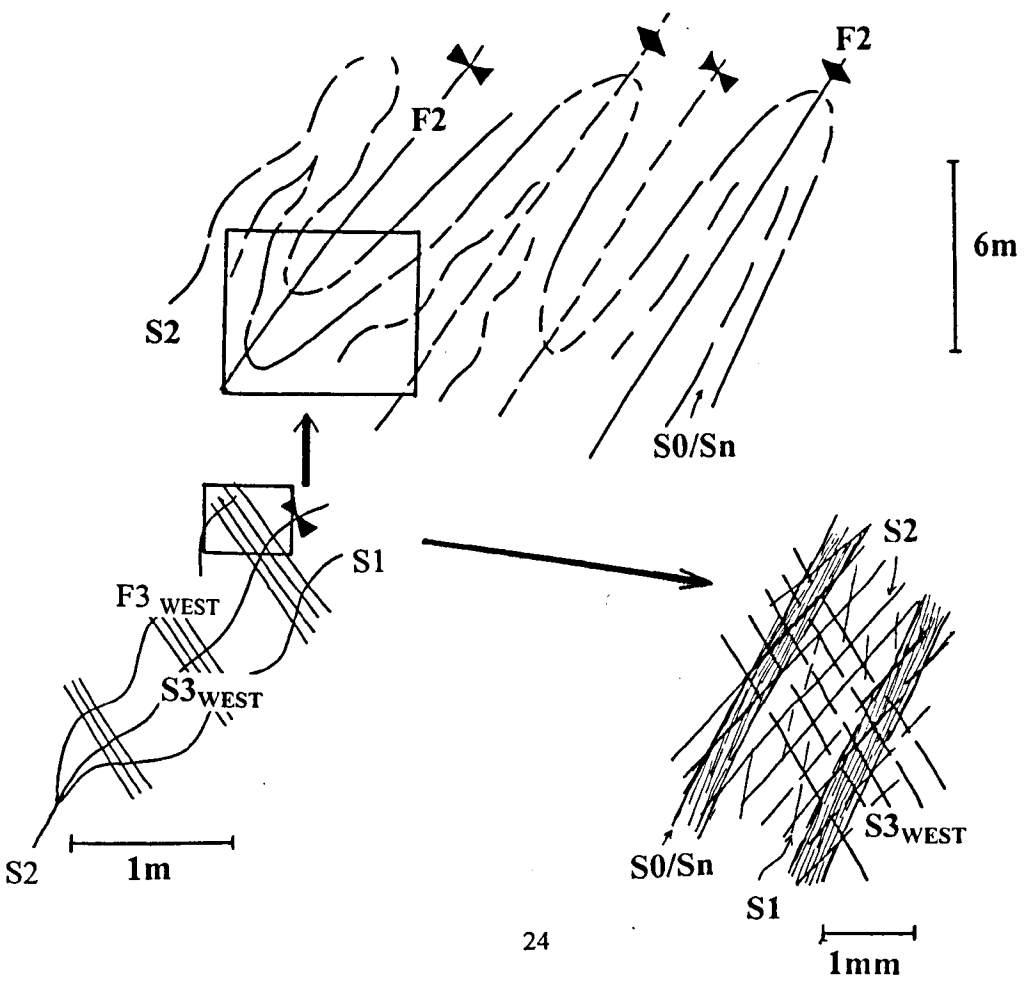

Fig. 2.4 Map of Gander Lake locality A showing deformation structures and fabrics.

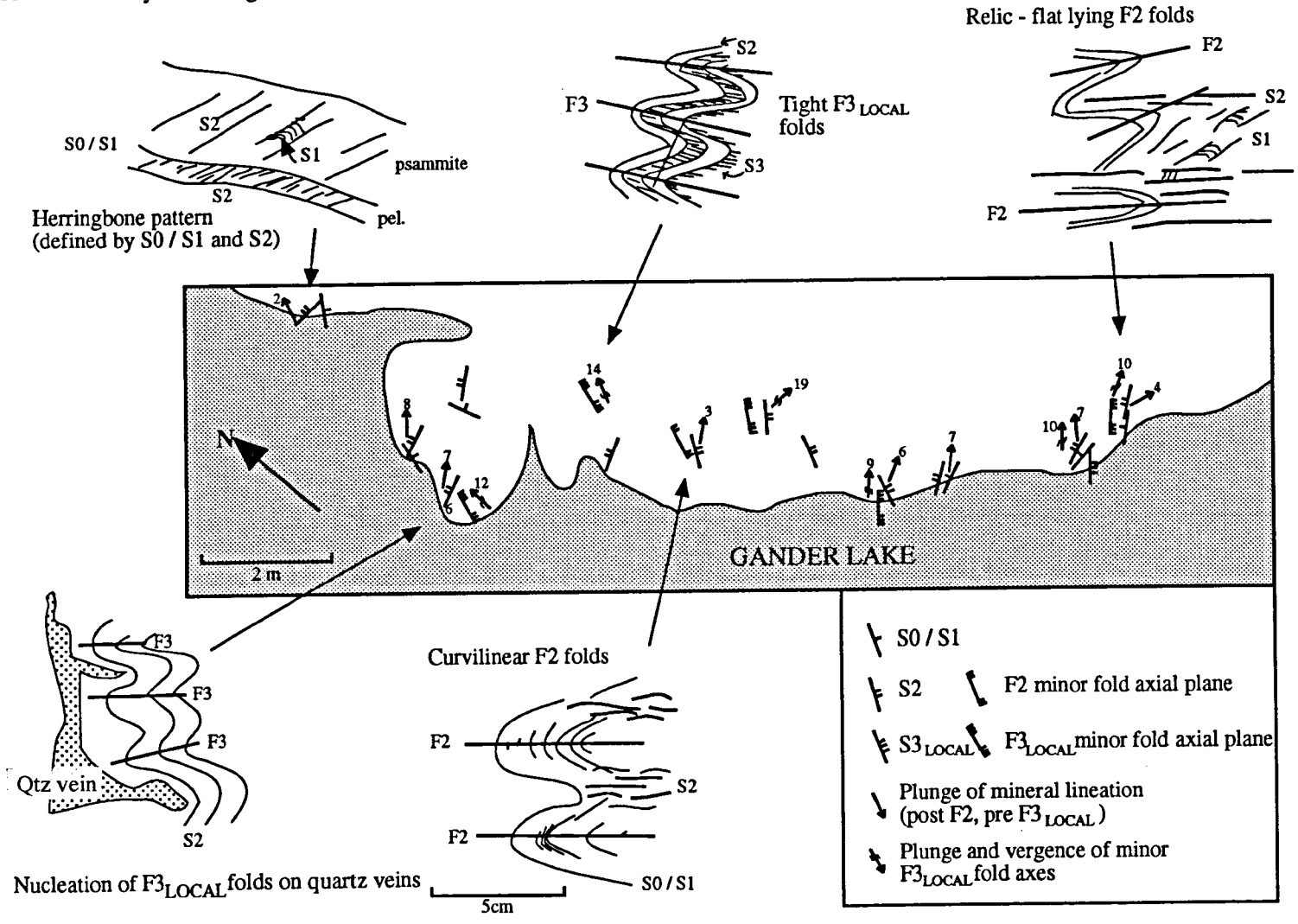

Fig.2.5 Map of Gander Lake locality B showing deformation structures & fabrics.

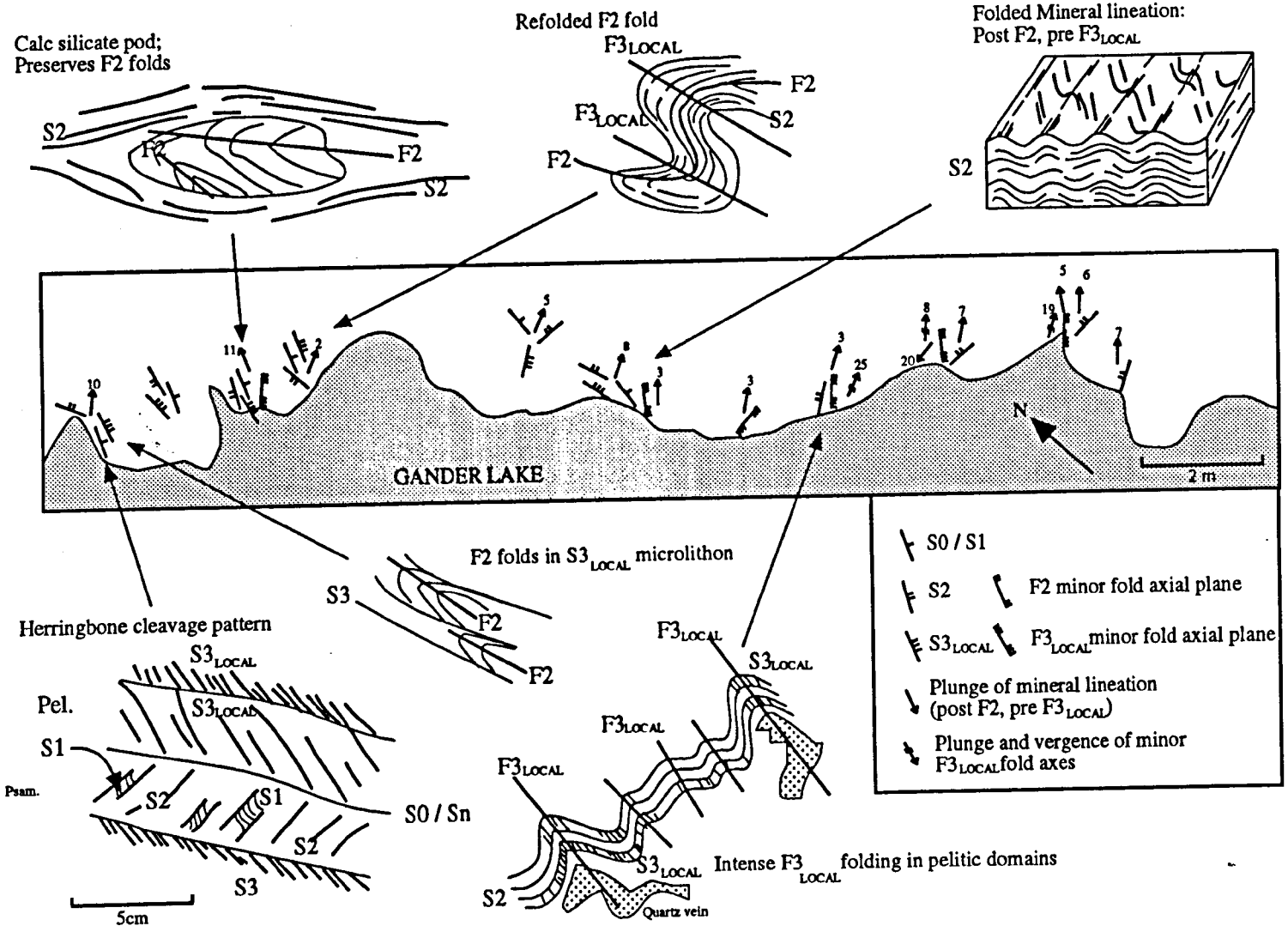

The fine layered fabric, deformed by the flat-lying folds, is orientated subparallel to S0 and is defined by aligned muscovite, chlorite , plagioclase and quartz. Quartzofeldspathic grains show an elongation parallel to the fabric and evidence for recrystallisation suggesting that it represents a low-grade S1 metamorphic as opposed to a diagenetic fabric. The flat-lying folds which deform this fabric are hence interpreted to have formed syn-D2. Detailed mapping by Holdsworth (1994a) has similarly demonstrated this D2 fold relationship by the study of local fold facing directions which suggest that the folds occur on the limbs of a larger relic D1 structure. The D2 folds and fabrics are deformed by upright folds with an associated steep axial planar fabric in the central and eastern region of the domain; however locally in the east, D2 assemblages are overprinted by westerly-verging flat-lying folds. F2 folds are overprinted by a northeast-southwest trending mineral lineation which appears to be subparallel to the upright overprinting fold axes, however is clearly deformed by the flat-lying overprinting folds (fig 2.4). The upright folds are termed $F3_{WEST}$ and the subhorizontal folds $F3_{LOCAL}$.

2.3.1 Pre-D2 structures and fabrics

The presence of transposed bedding fabric S0-Sn is widely evident across the domain however evidence for relic S1 is rare. Relic beds and bedding laminations (S0) are defined by subtle variation in quartzofeldspathic and mica content. Psammitic lithologies display 5-50 cm scale beds and semi-pelitic and pelitic units thinner 2-15 cm scale beds. Bedding laminations are commonly preserved intrafolial to S2 in pelitic lithologies and form fine (0.5-1 mm scale) dark planar fabrics which in places show cross-lamination (e.g. locality TCH 94 139). Rare local way-up criteria of beds can be recognised in psammitic assemblages (i.e.on the north shore of Gander Lake), shown by the presence of normal graded bedding and sedimentary flame structures.

S1 is in places preserved intrafolial to S2 (predominantly in the west of the domain) and forms a fine (millimetre scale) crenulation cleavage (fig. 2.6). The fabric cannot be recognised in assemblages which have undergone $D3_{WEST}$ or $D3_{LOCAL}$ overprinting. S1 (orientated parallel / sub-parallel to bedding variation, S0-Sn), is defined by fine micaceous M, and quartzofeldspathic Q domains. M domains comprise muscovite and chlorite-rich layers which appear to be locally laterally continuous. Quartzofeldspathic layers comprise fine grains of quartz and plagioclase. S1 is evident in semi-pelitic and pelitic metasediments along the west of the Trans Canada Highway (e.g. localities TCH 94 5, TCH 94 6) where it forms a faintly defined fine fabric intrafolial to S2. S1 shows a chevron pattern between S2 cleavage domains due to local refraction. At localities beside Gander Lake, evidence for relic S1 is similarly restricted to within S2 foliae within psammitic layers (e.g. localities GL 1, GL 12, GL 21, GL 24) however is notably absent from semi-pelitic and pelitic lithologies. This relationship is clearly displayed in interbedded psammitic and pelitic layers (of S0-Sn) where relic S1 is common in quartzofeldspathic layers and totally transposed in micaceous layers. At locality GL 1, psammites display < millimetre scale S1 which occurs intrafolial to S2 fabric within low-strain hinge regions of $F3_{LOCAL}$ folds (figs. 2.7, 2.8), also at this locality preservation of S1 occurs in 'strain shadows' of calc-silicate pods (8-10 cm in length) which have escaped $D3_{LOCAL}$.

Fig. 2.6 Relic S1 fabric (fine, millimetre scale) preserved intrafolial to S2 cleavage.

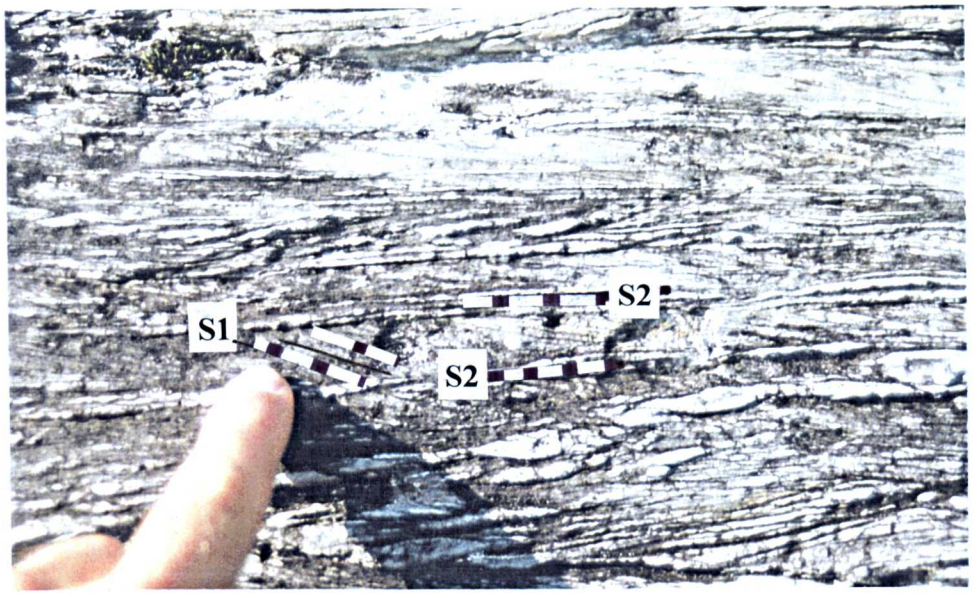

2.3.2 D2 structures and fabrics

F2 folds are best displayed in the west and central regions of the domain where transposition by axial planar S2 is non pervasive. The structures deform a S0-Sn fabric (1-15 cm scale) and show preferential development of S2 within the semi-pelitic and pelitic layers (fig. 2.8). The orientation of the F2 fold axes is northeast-southwest (fig. 2.2), folds verge eastwards and show a dominantly southeastward-directed facing (locally variable between 030 and 170 °, R.E. Holdsworth, *pers. comm.*) which is consistent across the region. Folds are recumbent and closed to tight in form (centimetre to metre scale), and are characteristically curvilinear (fig. 2.8a). Features of F2 folds are clearly displayed beside Gander Lake (localities GL 1, GL 5 GL 7) where 10 cm scale curvilinear folds occur within psammites in which S2 is absent from hinges but is pervasively developed in the limbs (figs. 2.4 & 2.5). At localities TCH 94 4, TCH 94 5, TCH 94 6, folds form similar larger scale subhorizontal structures (0.5-1m scale) within interlayered psammites and semi-pelites, in which development of S2 is restricted to pelitic lithologies. The best examples of F2 folds in the east of the region are seen within calc-silicate pods and lenses (fig. 2.7) which have internally remained largely unaffected by later deformation (e.g. $F3_{EAST}$ and $F3_{LOCAL}$). At localities GL 1 and GL 23, large elongate lenses of calc-silicate lithology, which are clearly defined by their brown weathered appearance display internal recumbent F2 folds (*c.* 10 cm scale) and show local development of spaced S2 fabric in hinge regions (fig. 2.5).

S2 forms a spaced foliation (millimetre scale) with typically anastomosing form which is defined by aligned grains of muscovite and chlorite which separate quartzofeldspathic domains. In psammitic rocks, S2 forms a spaced domainal pressure solution cleavage and in pelitic and semi-pelitic lithologies forms a well defined slatey cleavage. Where rocks have undergone later deformation (i.e. $F3_{WEST}$ or $F3_{LOCAL}$), S2 is folded and in higher strain zones is only preserved intrafolial to the later fabrics (i.e. $S3_{WEST}$ or $S3_{LOCAL}$) forming herringbone-type

cleavage patterns (millimetre to centimetre scale; figs. 2.4 & 2.5). These patterns are commonly seen at Gander Lake (e.g. GL 25) in interlayered semi-pelitic and psammitic lithologies and represent intersections of S2 with both S3 and S0-Sn.

Fig. 2.7 Calc-silicate pod within metasediment preserving recumbent F2 folds (field of view; 7cm).

2.3.3 Post-D2 structures and fabrics

The development of $F3_{WEST}$ folds is restricted to the eastern region of the domain where they are locally developed predominantly within semi-pelitic and pelitic lithologies (e.g. localities TCH 94 10, TCH 95 3, TCH 95 4). Folds form westerly-verging upright open structures and show variable development of steep axial planar fabrics. $F3_{WEST}$ folds are present at locality TCH 94 10 where they form 10-30 cm scale structures with development of $S3_{WEST}$ pressure solution fabric (millimetre scale) within the fold limbs, further east at localities TCH 95 3 and TCH 95 4 the axial planar $S3_{WEST}$ is pervasive forming a closely spaced cleavage.

$F3_{LOCAL}$ folds are similarly restricted to metasediments within the east of the domain and occur predominantly in semi-pelitic and pelitic lithologies (fig. 2.10). $F3_{LOCAL}$ folds form close to tight recumbent structures (2-20 cm scale) which display a characteristic westward-directed sense of vergence. $F3_{LOCAL}$ folds are well illustrated at Gander Lake (e.g. localities GL 8, GL 17) within pelitic lithologies (figs. 2.4 & 2.5) by symmetrical tight structures (5-10 cm scale). Folds deform a penetrative S2 foliation and show the subordinate development of an axial planar sub-horizontal to shallowly east-dipping axial planar $S3_{LOCAL}$ in the limbs. $S3_{LOCAL}$ is a closely spaced (1-2 mm scale) anastomosing crenulation cleavage which is typically chlorite and muscovite-rich. The regions affected by $F3_{LOCAL}$ folds are commonly spatially associated with abundant quartz veins, which form networks cutting through the metasediments. In places (e.g. GL 8), the $F3_{LOCAL}$ folds clearly propagate on the tips of these coarse quartz veins (fig. 2.10b), suggesting that the veining occurred syn- or prior to the associated deformation.

Fig. 2.8 D2 fold and fabric relationships; a) Recumbent curvilinear F2 fold in psammitic metasediment showing development of axial planar S2; b) Relic F2 fold deforming S1 and subordinately overprinted on limbs by axial planar S2; c) S2 pressure solution cleavage preserving intrafolial S1.

a)

b)

c)

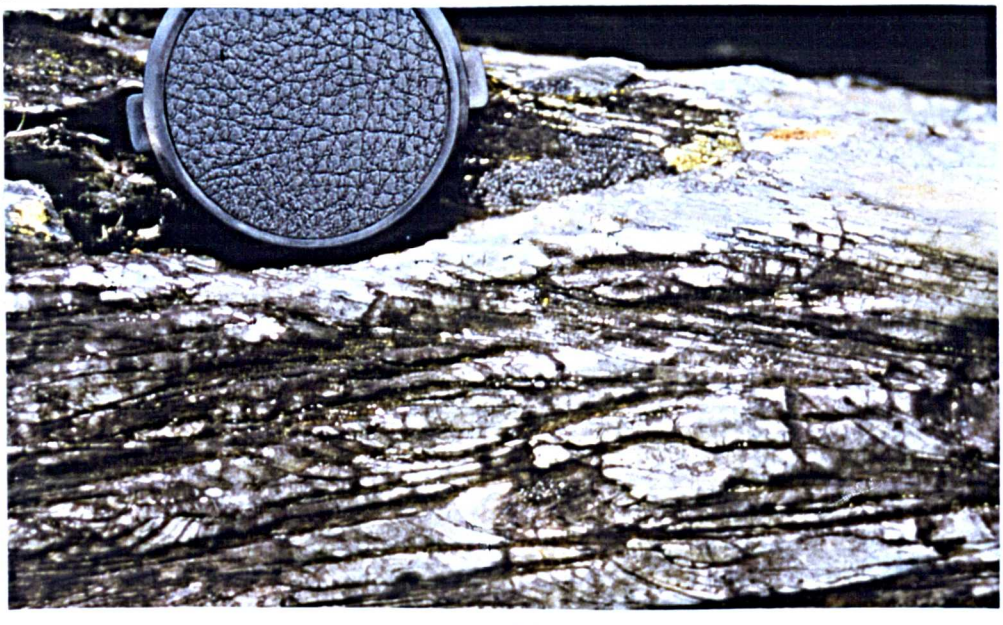

Fig. 2.9a) Upright $F3_{WEST}$ fold in pelitic metasediment deforming S2; b) Steep $S3_{WEST}$ pressure solution cleavage in psammitic metasediment overprinting S0-Sn and crenulated S2.

a) b)

Fig. 2.10 Recumbent tight $F3_{LOCAL}$ folds; a) in pelitic metasediment with deformed S2 fabric; b) in semi-pelitic metasediment showing subordinate development of axial planar $S3_{LOCAL}$ on fold limbs and quartz veining (top RHS of photograph).

a) b)

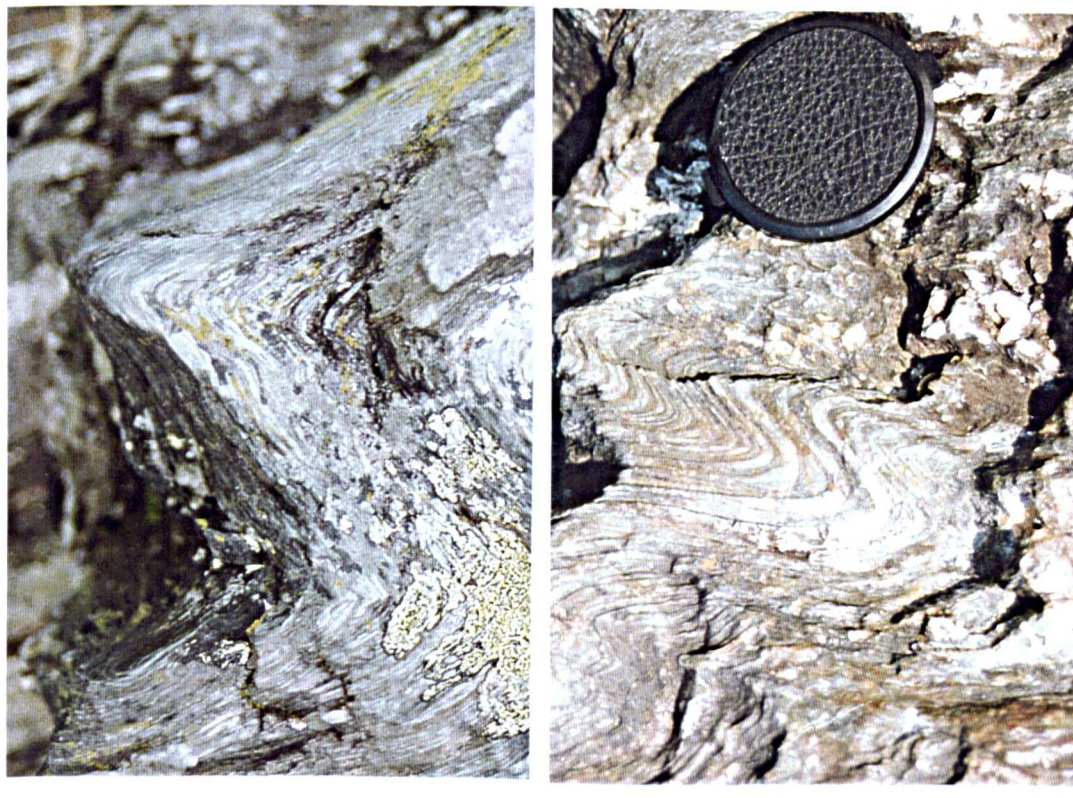

2.3.4 Contact metamorphic overprint

The metasediments in the vicinity (i.e. 2-3 km wide aureole) of the non-foliated Gander Lake Granite (e.g. localities TCH 94 10, TCH 94 12) show the effects of contact metamorphic overprinting. The boundary between the Gander Lake Granite and the metasediments is sharp, steeply dipping and clearly cross-cuts both D2 and local $F3_{WEST}$ structures, although the field relationship between the granite and $F3_{LOCAL}$ folds is unclear.

At locality TCH 94 10, rocks display a coarsely crystalline hornfelsed texture, and are characterised by the pervasive development of biotite. Further east along the Trans Canada Highway towards the granite contact (e.g. localities TCH 94 11, TCH 95 3), rocks show a similar hornfelsed texture and in addition to biotite, also show the development of coarse cordierite spots. Local development of andalusite which forms coarse (3-4 mm scale) porphyroblasts, occurs adjacent to the Gander Lake Granite (e.g. locality TCH 95 6). Detailed field observations show that these spots overprint both the subhorizontal S2, and the steep $S3_{WEST}$ fabrics.

2.4 Petrological descriptions

Fig. 2.11 Sketch of mineral-fabric relationships in domain 1 showing a) S2 pressure solution cleavage with relic S0-Sn and intrafolial S1; b) development of cordierite porphyroblasts and biotite laths overprinting steep $S3_{WEST}$ crenulation cleavage in hornfelsed metasediment.

a) b)

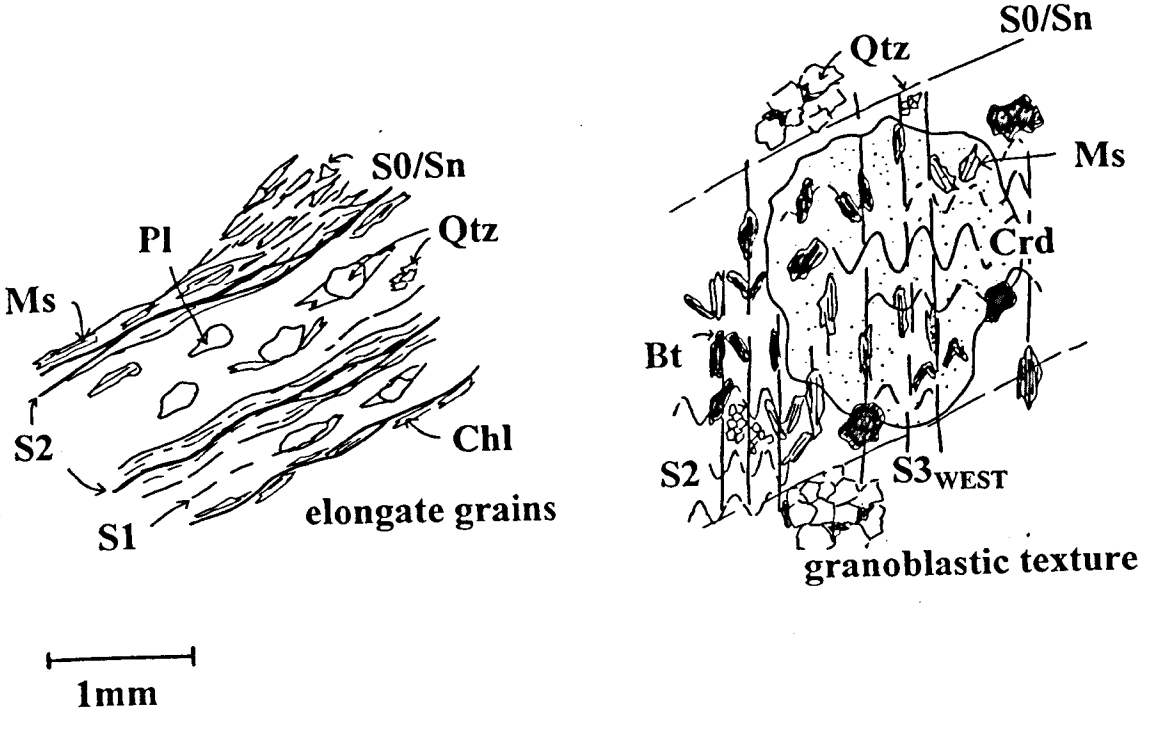

2.4.1 Pre-D2 structures and fabrics

Bedding fabrics (S0-Sn), are defined by distinct mineralogical variation in mica, and quartzofeldspathic mineral content. Psammitic beds are composed predominately of quartz with minor plagioclase, and minor muscovite and chlorite. In comparison, pelitic and semi-pelitic lithologies contain predominately muscovite and chlorite, with quartz and plagioclase forming only minor constituents. Subordinate development of ilmenite occurs in all lithologies. The muscovite and chlorites form intergrowths which are fine to medium grained, quartzofeldspathic grains are predominately medium to coarse grained.

The S1 fabric (figs. 2.11 & 2.12), is defined predominately by aligned muscovite and quartz-rich layers with minor plagioclase, chlorite and ilmenite (e.g. sample TK 95 172, locality GL 1). Muscovite in the M-domains forms fine grains which are intergrown with fine feathery chlorite. In Q-domains, quartz and plagioclase form medium / coarse grains which show deflection of muscovite around their margins. Quartz also forms fine grains which, in contrast to the coarser grains, are intergrown with the muscovite. The medium to coarse quartzofeldspathic grains display elongation and minor flattening parallel to S1. Quartz grains characteristically show undulose extinction and marginal recrystallisation, although rare annealed strain-free quartz grains are present. Plagioclase grains show no evidence for ductile recrystallisation and commonly display multiple twinning and rare sericitic alteration.

Fig. 2.12 Relic muscovite-, chlorite-rich S1 continuous cleavage; fine chlorite needles form stacks around coarse grains of quartz (field of view; 3.5mm).

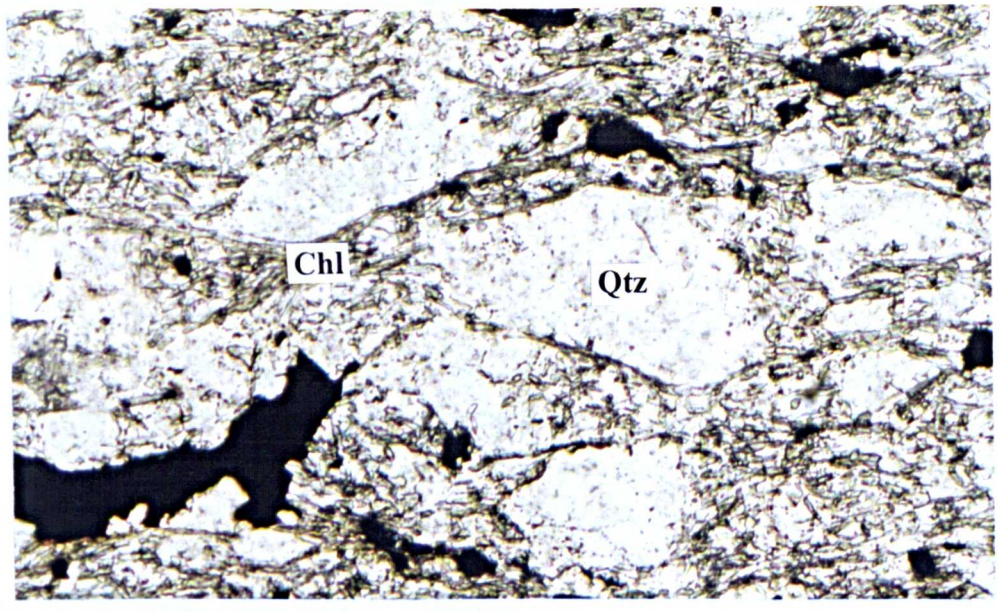

2.4.2 S2 fabric

The S2 fabric in semi-pelitic and pelitic lithologies (figs. 2.11 & 2.13) comprises M and Q domains which are defined by muscovite-rich (1-2 mm scale) and quartzofeldspathic (2-3 mm scale) layers (e.g. sample Tk132b, locality TCH 94 3). In contrast, psammitic lithologies display < millimetre scale

M domains and (2-3 mm scale) Q domains. The fabric is accentuated by the presence of dark solution seams, which contain pleochroic orange to brown coloured material, and are planar to undulating in form. The M domains comprise intergrowths of fine laths of muscovite and minor chlorite which show clear alignment, whereas Q domains comprise predominately of fine and coarse quartz and medium plagioclase grains. Coarse quartz and plagioclase grains show elongation and slight flattening parallel to S2 fabric. Quartz grains show marginal recrystallisation, development of internal subgrains and deformation lamellae; plagioclase grains display no evidence for recrystallisation. Xenomorphic ilmenite grains (medium to coarse) form a component of M domains and fine feathery chlorite, a component of both M and Q domains. Chlorite forms intergrowths which occur as stacks (fig. 2.13) around coarse quartz grains (sample TCH 14a, locality TCH 94 2).

Fig. 2.13 S2 spaced pressure solution cleavage showing quartzofeldspathic Q domains and muscovite-, chlorite-rich M domains (field of view; 3.5mm).

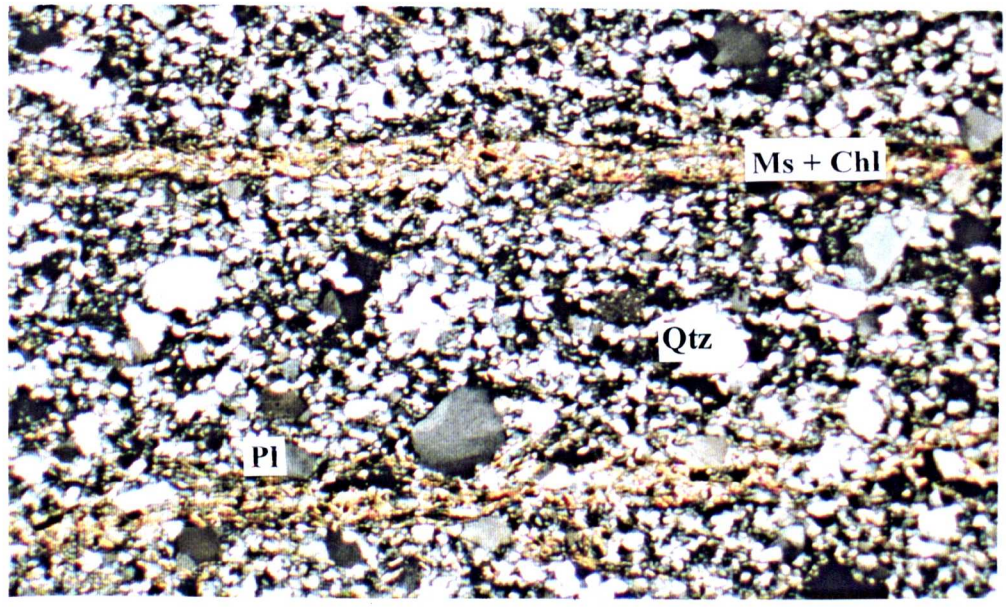

2.4.3 Post-D2 structures & fabrics

The post D2 mineral lineation is variably defined by aligned intergrowths of chlorite, muscovite and by fine rods of quartz. The $S3_{WEST}$ fabric forms a spaced domainal crenulation cleavage (1-2 mm scale) within pelitic regions of S0-Sn (e.g. sample TK 94 139, locality TCH 94 10), which corresponds to a stage 2 fabric (of Bell & Rubenach, 1983). The original mineral assemblage of steep $S3_{WEST}$ fabric which forms the axial planar fabric to upright $D3_{WEST}$ folds is obscured along both the Trans Canada Highway, and Trans Canada Railway sections by the effects of contact overprinting, and recrystallisation (see section 2.4.5) from the cross-cutting Gander Lake Granite.

The $S3_{LOCAL}$ fabric forming axial planar to the flat-lying $F3_{LOCAL}$ folds is a differentiated crenulation cleavage (fig. 2.14), which displays intrafolial symmetrical microfolds of relic S2 (e.g. samples TK 95 172, TK 95 174, locality TK GL 1). The fabric (similarly to S2), is accentuated by the subordinate development of orange to brown coloured pressure solution seams. The cleavage

domains (millimetre scale) are composed of aligned intergrowths of muscovite and chlorite with minor ilmenite, whereas the microlithons (1-3 mm scale) comprise of microfolds of muscovite-, chlorite- and quartz-rich fabric.

Fig. 2.14 $S3_{LOCAL}$ crenulation cleavage in semi-pelitic lithology with muscovite-rich symmetrical microfolds and cleavage defined by flanks of microfolds and pressure solution seams (field of view; 3.5mm).

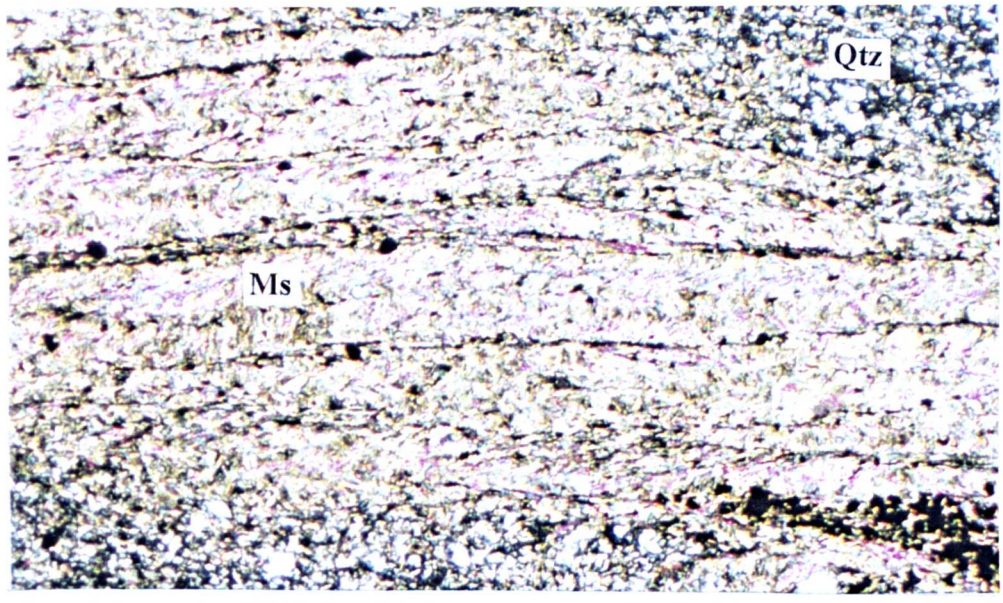

2.4.4 Contact metamorphic overprint

Pelitic regions of S0-Sn (e.g. in sample TK 94 139, locality TCH 94 10) show abundant development of medium to coarse biotite porphyroblasts (fig. 2.15), grains are commonly poikilolitic and form both subidiomorphic laths and xenoblastic grains. The biotites show a strong preferred orientation parallel to the $S3_{WEST}$ fabric, however, in places appear to be aligned along the crenulated S2 fabric. Detailed observation shows that the biotites in fact are mimetically overprinting both the S2 and $S3_{WEST}$ fabrics, this relationship is backed up by the presence of poikilolitic grains of biotite which preserve quartz inclusion trails which are continuous into the matrix fabrics (fig. 2.15b). Quartzofeldspathic regions display a coarse granoblastic texture shown by intergrowths of polygonal quartz grains. Cordierite poikiloblasts (e.g. sample TCH 80, locality TCH 95 3) are developed in addition to biotite within pelitic layers of S0-Sn (fig. 2.15a & c). The grains are subidiomorphic with numerous inclusions of quartz and aligned in trails, which correspond to stage 2 fabric development (of Bell & Rubenach, 1983). The inclusion trails, similarly to those in biotite, pass continuously into the matrix fabric which comprises crenulated S2. The relationship between andalusite porphyroblasts and the matrix fabrics is less clear due to their marginal sericitisation (e.g. sample TK 95 73, locality TCH 95 6). The porphyroblasts form subidioblastic inclusion-free laths which clearly overprint biotite-rich crenulated S2, but in places appear to show a preferential alignment parallel to $S3_{WEST}$. Detailed observations at the margins of grains (e.g. sample TCH 88, locality TCH 95 6) shows a

Fig. 2.15 Contact metamorphic overprinting relationships in Domain 1; a) cordierite spots in pelitic layers overprinting $S3_{WEST}$ crenulation cleavage, b) $S3_{WEST}$ crenulationcleavage showing development of coarse mimetic biotite; c) cordierite and biotite overprinting $S3_{WEST}$ crenulation cleavage.

a)

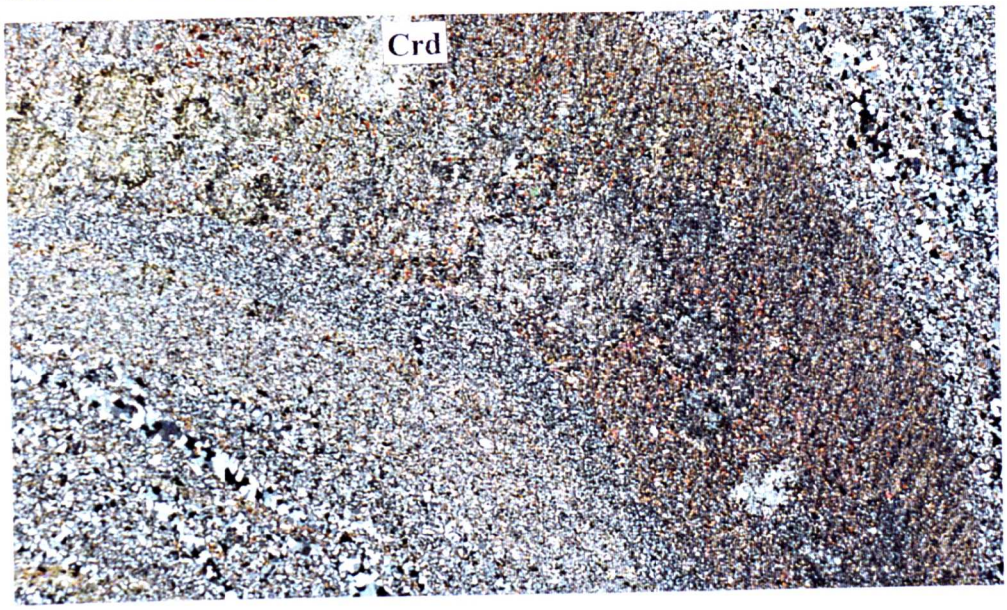

b)

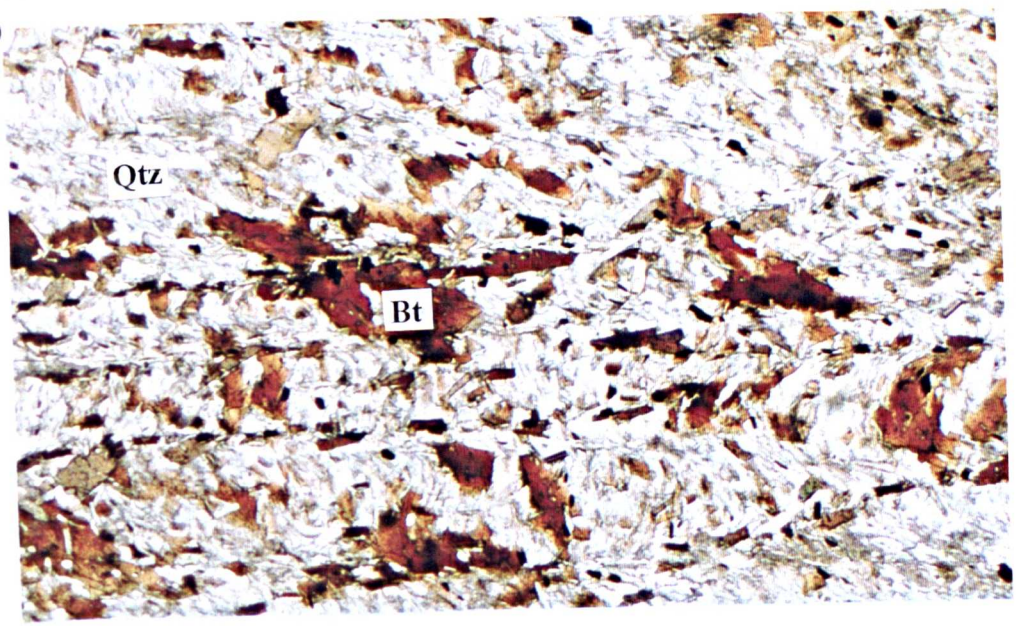

c)

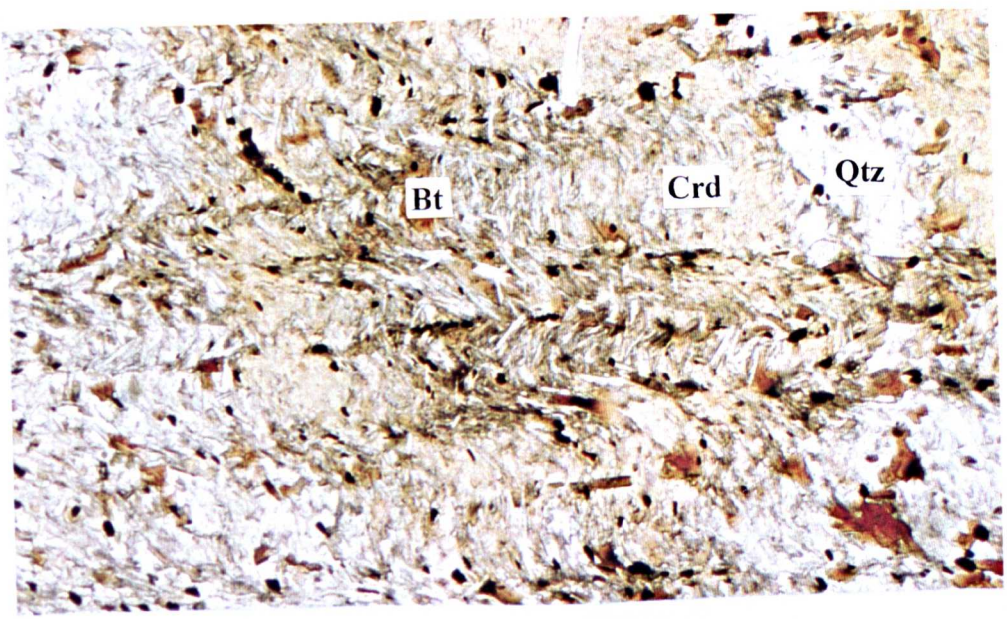

cross-cutting relationship between andalusites and the surrounding $S3_{WEST}$ crenulation cleavage implying their mimetic growth over the pre-existing $S3_{WEST}$.

2.5 Petrographic constraints on P and T

2.5.1 Methodology

The investigation of metamorphic conditions within the domain has been enabled by detailed microstructural and petrographic-fabric analysis of *c.* 35 thin sections of assemblages from across the region, and detailed petrographic analysis of key samples. The low grades of metamorphism of the metasediments however does not allow precise P-T conditions to be determined.

2.5.2 D2

The mineralogical and petrographic relationships which typify D2 assemblages are displayed within sample semi-psammitic sample TK 132b (locality TCH 94 3) and semi-pelitic sample TK 135b (locality TCH 94 6) from the west of the Trans Canada Highway section. Sample TK 132b comprises muscovite 18%, chlorite 10%, quartz 60%, plagioclase 10% and ilmenite 2%. S2 is the dominant fabric which is defined by muscovite-, chlorite-rich M domains and quartzofeldspathic Q domains and forms a characteristic spaced (1-3 mm scale) pressure solution cleavage. Sample TK 135b comprises muscovite 25%, chlorite 14%, quartz 55%, plagioclase 5% and ilmenite 1% and is characterised by a finely spaced S2 (< millimetre scale) pressure solution cleavage. In both samples, muscovite and chlorite form fine intergrowths in M domains. The Q domain contain minor amounts of chlorite which forms fine feathery intergrowths which wrap quartzofeldspathic grains. Quartz and plagioclase grains display a wide range of grain sizes from fine to coarse. The majority of grains are subidiomorphic and medium grained, however extremely coarse subidiomorphic grains which show a distinct elongation parallel to S2 are common, especially in sample TK 132b. Quartz grains do not show evidence for subgrain development although both quartz and plagioclase show marginal ductile recrystallisation.

The representative mineral compositions from within the samples TK 132b and TK 135b are presented in fig. 2.16 (full mineral analyses are displayed in Appendix A). The composition of muscovite along both the S1 and S2 fabrics plots between the muscovite and phengite end members (fig. 2.17a). Chlorites along S1 and S2 are of the same composition and classified as chamosite (with Fe 2+ dominant end-member), plots of their atomic ratios X_{Al} vs. X_{Mg} (fig. 2.17b) fall within the pelitic field (Laird, 1988). The composition of plagioclase in both samples is pure albite with X_{Ab} values between 0.99 and 1.0.

Fig. 2.16 Representative mineral analyses for S2-bearing samples TK 132b and TK 135b.

	Chl		Ms		Pl	
	Tk 132b 9	Tk 135b 13	Tk 132b 1	Tk 135b 10	Tk 132b 39	Tk 135b 22
SiO2	28.07	23.72	45.83	45.9	68.61	68.48
TiO2	0	0.23	0.71	0.56	0	0
Al2O3	21.22	21.48	31.07	32.09	20.12	20.23
FeO	26.7	29.79	4.72	4.05	0	0.17
MnO	0.4	0.19	0	0	0	0
MgO	11.61	11.91	1.31	1.64	0	0
CaO	0	0	0	0	0	0
Na2O	0	0	0.24	0	11.4	11.13
K2O	1.12	0.13	11.62	11.89	0	0.1
total	89.12	87.45	95.5	96.13	100.13	100.11
Cations per O	*28*		*22*		*32*	
Si	5.85	5.16	6.25	6.20	11.94	11.93
Al	5.21	5.51	5.00	5.11	4.13	4.15
Ti	0.00	0.04	0.07	0.06	0.00	0.00
Fe	4.65	5.42	0.54	0.46	0.00	0.02
Mn	0.07	0.04	0.00	0.00	0.00	0.00
Mg	3.61	3.86	0.27	0.33	0.00	0.00
Ca	0.00	0.00	0.00	0.00	0.00	0.00
Na	0.00	0.00	0.06	0.00	3.85	3.76
K	0.30	0.04	2.02	2.05	0.00	0.02
XAn					0	0.00
XAb					1	0.99
A	0.21	0.23				
F	0.56	0.58				
XAl	0.39	0.37				
XMg	0.44	0.42				

The abundance of chlorite and muscovite, and the presence of pure albite within the pelitic to semi-pelitic assemblages is indicative of greenschist facies conditions (in the approximate range of 350-450 °C and 2-4 kbar). The notable absence of biotite within S2 assemblages further constrains conditions to the low-T and low-P side of a biotite producing reaction i.e:

$$Cd^{1}\text{-rich Phen}^{2} + \text{Chl} \rightarrow \text{Cd-poor Phen} + \text{Chl (Al richer)} + \text{Bt} \qquad \text{(R1)}$$

(Hudson, 1980).

The elongation of the coarse quartz and albite grains is interpreted to represent flattening of detrital grains and a product of deformation at low metamorphic grade (e.g. Soper & Barber, 1982; Law, 1986).

[1] Cd = celedonite
[2] Phen = phengite

Fig. 2.17 Mineral compositions of low grade domain 1 metasedimentary samples TK 132b and TK 135b, a) Mica compositions showing the number of octahedral sites filled (di - octahedral, 4; tri - octahedral, 6) and Si, Al and M^{2+} atoms per formula unit; b) Chlorite atomic ratio Al / (Al + Fe + Mg) vs. Mg / (Mg + Fe).

a)

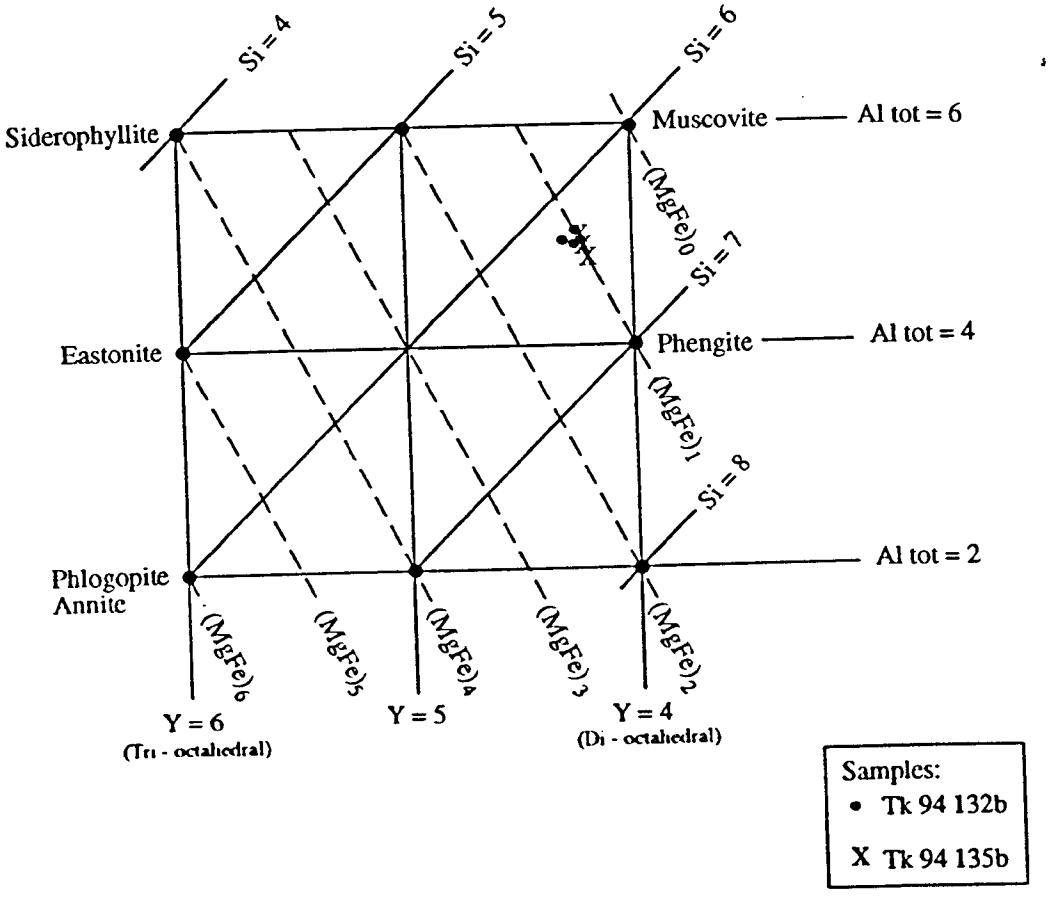

b)

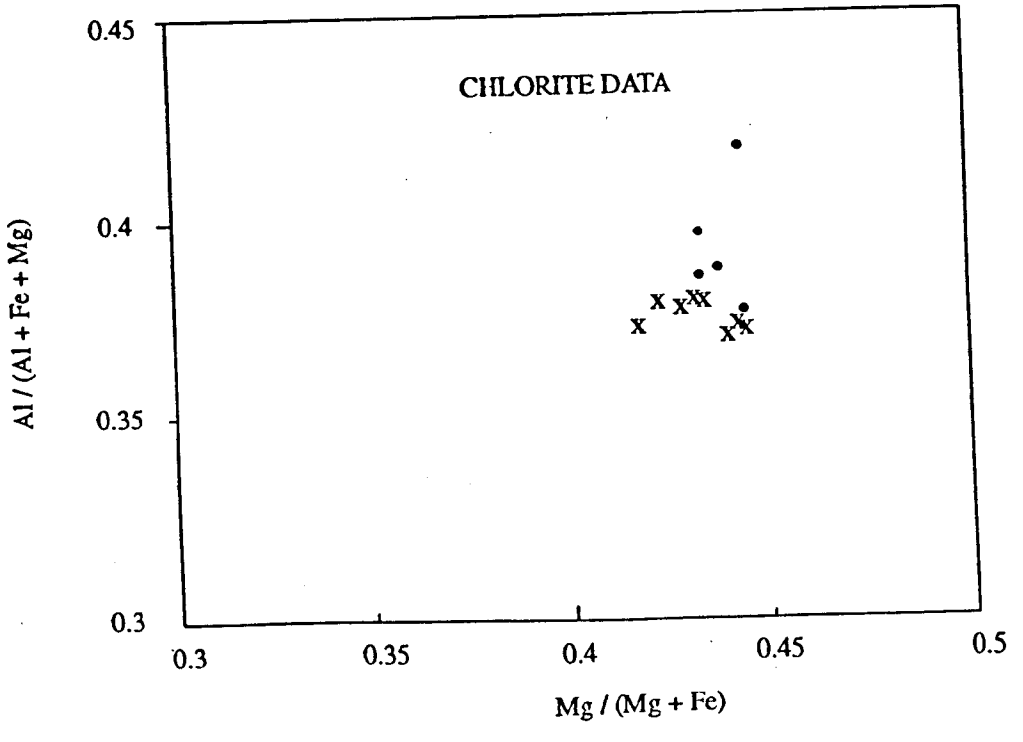

2.5.3 POST D2

The mineralogical and petrographic features of $S3_{WEST}$ are obscured by the effects of contact metamorphic overprinting by the Gander Lake Granite. However, the characteristics of $S3_{LOCAL}$ fabric are highlighted in semi-pelitic sample TK 95 172 (locality SP 1). The rock comprises the following modal proportions, muscovite 45%, chlorite 5%, plagioclase 10%, quartz 39% and ilmenite 1%. $S3_{LOCAL}$ forms a moderately well developed crenulation cleavage (corresponding to stage 3 of Bell & Rubenach, 1983) in pelitic regions of S0-Sn and a poorly developed to absent crenulation fabric in more psammitic regions. $S3_{LOCAL}$ is defined by fine to medium laths of muscovite which show a strong preferential alignment. Quartz forms fine to medium subidiomorphic grains which show evidence for undulose extinction, both quartz and plagioclase display evidence for marginal ductile recrystallisation.

The grade of the $D3_{LOCAL}$ is constrained by the presence of muscovite and chlorite and the absence of biotite to greenschist facies conditions below a biotite-in reaction (e.g. R1; Hudson, 1980) in the approximate range of 350-450 °C and 2-4 kbar.

2.5.4 Contact metamorphic overprint

Samples TK 139 (locality TCH 94 10) and TCH 80 (locality TK 95 3) illustrate the characteristic contact metamorphic features of metasediments in the aureole of the Gander Lake Granite. Sample TK 139a comprises the modal mineral proportions, biotite 35%, muscovite 3%, chlorite 10%, quartz 40%, plagioclase 11% and ilmenite 1%. The rock displays a recrystallised $S3_{WEST}$ crenulation cleavage (corresponding to stage 3 of Bell & Rubenach, 1983). Sample TCH 80 in contrast displays the addition development of cordierite and andalusite and comprises cordierite 15%, andalusite 5%, biotite 30%, muscovite 4%, chlorite 1%, quartz 35%, plagioclase 9% and ilmenite 1 %.

Both samples display extensive development of biotite, which forms both coarse idiomorphic and fine grains, the idiomorphic grains form laths and poikiloblasts which display quartz-rich inclusions trails of crenulated S2 (which passes continuously into the matrix fabric). Laths of biotite show variably alignment along both the crenulated S2 and $S3_{WEST}$ crenulation cleavage however after careful observation it is clear that the grains mimetically overprint these fabrics. The fine matrix biotites form xenomorphic grains which are intergrown with quartz. The cordierite and andalusite in sample TCH 80 form large (1-3 mm scale), xenomorphic poikiloblasts which contain inclusion trails of quartz (which pass continuously into the crenulated S2 matrix fabric). The porphyroblasts clearly overprint the crenulated S2 fabric and $S3_{WEST}$ crenulation cleavage. In both samples quartz forms granoblastic intergrowths of medium to coarse polygonal grains. The hornfelsed granoblastic texture of the quartz and the development of spots of biotite, cordierite and andalusite which overprint pre-existing fabrics and assemblages is indicative of high crustal level contact metamorphism.

2.6 Constraints on timing of deformation and metamorphism

The S1 fabric associated with the D1 event is subparallel to lithological variation S0-Sn, however is only rarely preserved, having been variably refolded and transposed by D2 throughout the domain. D2 structures are restricted to the Gander Zone metasediments and are notably absent from the adjacent Dunnage Zone (e.g. Kennedy & McGonigal, 1972). The folds are subhorizontal in attitude, and show an easterly-directed sense of vergence. The form of the structures is consistent with their development during eastward thrusting of the adjacent Gander River Ultrabasic rocks (of Dunnage) over the D1 deformed Gander Group metasediments. The thrusting of the ophiolitic Dunnage zone over the Gander Lake Subzone has been attributed to mid-Ordovician obduction and constrained using a range of data to *c.* 470 Ma (Williams & Stevens, 1974; Williams, 1984; Colman-Sadd *et al.* 1992a).

D2 assemblages are overprinted in the east of the domain by upright structures with steep axial planar fabrics ($D3_{WEST}$) which show a westward-directed sense of vergence, and are post-dated by the intrusion of the undeformed megacrystic Gander Lake Granite (interpreted as a post-tectonic Devonian pluton, e.g. Colman-Sadd *et al.* 1990). The margin of the granite clearly cross-cuts the steep $S3_{WEST}$ fabric, and the edges of the intrusion in places enclose enclaves of metasediment which show a deformed S2 fabric. Locally in the east of the domain, the S2 fabric in metasediments is folded by subhorizontal westerly-verging folds ($F3_{LOCAL}$) which show local development of an axial planar subhorizontal fabric The field relationship between the $F3_{LOCAL}$ and the upright $D3_{WEST}$ structures is unknown, also the relationship between $F3_{LOCAL}$ folds and the Gander Lake Granite is unknown.

2.7 Summary

Domain 1 (the Western Gander Metasedimentary Belt), comprises greenschist facies muscovite-, chlorite-bearing metasediments which are dominated by subhorizontal easterly verging D2 structures formed during the obduction of the ultrabasic Dunnage rocks over the Gander Group metasediments (dated as *c.* 470 Ma; Williams & Stevens, 1974; Williams, 1984; Colman-Sadd *et al.* 1992a). D2 assemblages are variably overprinted by a northeast-southwest trending mineral lineation and $F3_{WEST}$ upright folds with an associated steep axial planar fabric. $D3_{WEST}$ structures are cross-cut by the post-tectonic (e.g. Colman-Sadd *et al.* 1990) Gander Lake Granite, the margins of the granite contain rare metasedimentary rafts which preserve a deformed pin-stripe fabric. The contact metamorphic effects from the Gander Lake Granite have produced recrystallisation of the $D3_{WEST}$ fabrics therefore obsquring the original $D3_{WEST}$ mineralogy. Localised development of subhorizontal, westerly-verging folds, which deform both D2 assemblages and the mineral lineation, occurs in the east of the domain.

Chapter 3.

Domain 2: The Wing Pond Shear Zone

Chapter 3. Domain 2: The Wing Pond Shear Zone

3.1 Introduction

The Wing Pond Shear Zone is an elongate northeast-southwest trending high-strain zone in the Gander Lake Subzone (Blackwood, 1977; O'Neill & Lux, 1989; O'Neill, 1991, O'Neill & Colman-Sadd, 1993) which is bounded to the west by the Western Gander Metasedimentary Belt (domain 1), and to the east by the Central Gander Metasedimentary Belt (domain 3). It extends north from Square Pond to Indian Bay Big Pond, passing through Butts Pond, Gull Pond and Wing Pond (fig. 3.1) and measures 3 to 6 km by *c.* 40 km. The domain comprises mostly Jonathan's Pond Formation Gander Group metasediment with lesser amounts of Indian Big Pond Formation (O'Neill, 1991). The composition of the metasediments is locally variable, ranging from pelitic and semi-pelitic to semi-psammitic and psammitic. Pelitic metasediments contain variable amounts of kyanite, andalusite, sillimanite and staurolite (O'Neill, 1991). The region is intruded by minor northeast-southwest trending foliated granitic and ultrabasic bodies (O'Neill, 1991), and cross-cut by several large scale non-foliated granite intrusions (e.g. the Middle Brook, Gander Lake and Deadmans Bay granites). The western margin of domain 2 is loosely defined by the pervasive development of upright ($F3_{WEST}$) folds and associated steep fabrics. The eastern margin is defined in the south by the contact between the metasediments and the Middle Brook Granite (Blackwood, 1977), and in the north by the disappearance of steep ($S4_{WEST}$) northeast-southwest trending low-grade fabrics. Prograde and retrograde ($D3_{WEST}$ and $D4_{WEST}$) assemblages are locally masked (within the aureoles of cross-cutting, undeformed granites) by effects of contact metamorphism. In the south (e.g. around Mint Brook), field relationships are similarly obscured by effects of late-stage brittle dextral faulting (Holdsworth, 1991, 1994a; fig. 3.1).

This chapter aims through field, microtextural and metamorphic mineral-fabric analysis, to establish the conditions of prograde, peak and retrograde evolution of the domain thus enabling construction of a P-T-t-d evolutionary path.

3.2 Structure and metamorphism

The structure of the domain is dominated by upright folds and steep fabrics of variable metamorphic grade which show a wide range of mineral assemblages and structural characteristics. The deformation is progressive in style. Metasediments within the domain are characterised by a mineral-stretching lineation (e.g. O'Neill, 1991, O'Neill & Colman-Sadd, 1993; Holdsworth, 1994a & b) which displays a variable plunge (e.g. Holdsworth, 1994b). The two dominant grades of assemblages within the domain are biotite-, aluminosilicate-bearing amphibolite facies fabrics and muscovite and chlorite-bearing greenschist facies fabrics. The structural and metamorphic relationships between these assemblages are complex and have been assessed by field, petrographic and

Fig. 3.1 Locality/sample map for Domain 2.

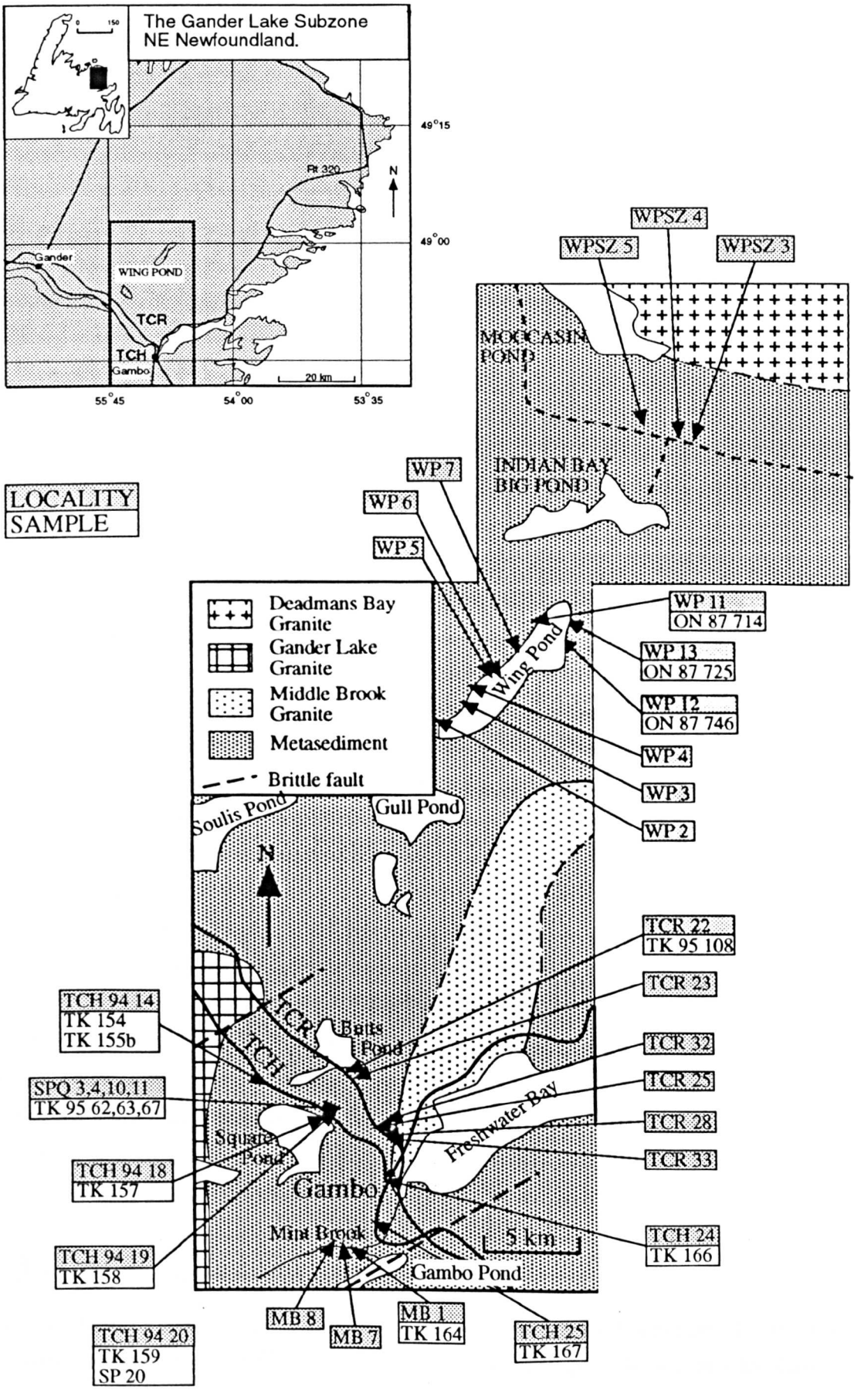

microstructural study (of *c.* 50 thin sections) of rocks from across the domain. Two key traverses, the Trans Canada Highway and Trans Canada Railway sections and key regions including Wing Pond, Gull Pond and Square Pond Quarry provide field data from across the domain, sample localities being shown on fig. 3.1.

Prograde deformation in the domain is dominated by upright folds with amphibolite facies (commonly sillimanite-bearing) axial planar fabrics which deform pre-existing easterly verging recumbent structures (regional D2) and associated spaced pressure-solution cleavage. The steep prograde fabrics preserve a predominantly sinistral sense of shear (e.g. Holdsworth, 1994b). Upright structures termed $F3_{WEST}$ become refolded and overprinted eastwards by the effects of $D3_{WEST}$ amphibolite facies deformation (e.g. Holdsworth, 1994a). The relationships between the $D3_{WEST}$ progressive deformation and metamorphism is complex with pelitic assemblages being characterised by the presence of all three aluminosilicate polymorphs (andalusite, kyanite and sillimanite) and staurolite. These have been previously interpreted as representing the mineral growth sequence kyanite → sillimanite → andalusite (O'Neill, 1991). Steep greenschist facies deformation fabrics occur locally in the centre (e.g. Square Pond), and pervasively in the east of the domain (e.g. at Mint Brook). The development of these micaceous fabrics has been previously recognised and described (e.g. O'Neill, 1991) however the relationship of the greenschist facies fabrics with the amphibolite facies fabrics has previously not been explained. Field relationships show that the greenschist facies fabrics overprint $D3_{WEST}$ folds and are hence attributed to $D4_{WEST}$ retrogression.

The assemblages both in the western and eastern regions of the domain (in the vicinity of the Gander Lake and Middle Brook Granites respectively) show effects of metamorphic contact overprinting including the development of hornfels textures and metamorphic spots. Field and petrographic analysis show that contact effects in the aureole of the Gander Lake Granite and Deadmans Bay Granites clearly overprint steep $D3_{WEST}$ fabrics, and in the aureole of the unfoliated Middle Brook Granite overprint steep $D4_{WEST}$ fabrics.

The trace of the domain broadly coincides both with the trace of a regional, positive aeromagnetic anomaly (Geological Survey of Canada, 1968a & b), and with that of a number of variably foliated minor mafic-ultramafic and granitic intrusions (O'Neill, 1993; O'Neill & Colman-Sadd, 1993) which occur around Wing Pond, Gull Pond and Square Pond. This association may be of significance in explaining the positioning of the anomalous high-strain, high-grade domain and could indicate the presence of a subcrustal mafic-ultramafic complex (suggested by O'Neill & Colman-Sadd, 1993) or a crustal heterogeneity (e.g. Miller, 1988). An alternative explanation however is that the anomalous magnetic values recorded in the vicinity of domain 2 result from the high magnetite content of the higher grade metasediments (e.g.O'Neill & Colman-Sadd, 1993).

3.3 Field relationships

The amphibolite facies $D3_{WEST}$ progressive deformation overprints pre-existing regional D2 structures (and relic S1 fabric) and is overprinted by effects of retrogressive $D4_{WEST}$. The domain is dominated

by the development of steep fabrics associated with upright fold structures. In the west these folds deform a pin-stripe fabric and are locally seen to deform axes of pre-existing recumbent folds (correlated regionally as F2). The upright folds deform a transposed bedding fabric S0-Sn (with a rarely preserved subparallel fine S1 fabric) and are hence correlated with $F3_{WEST}$. $F3_{WESTA}$ folds locally display evidence for tightening of fold axes and refolding into $F3_{WESTB}$ and locally $F3_{WESTC}$ structures (fig. 3.3) indicating the progressive nature of the deformation. Localised development of pervasive steep $S3_{WEST}$ amphibolite-grade shear fabrics occurs in discreet northeast-southwest trending (100 m scale) high-strain zones. $D3_{WEST}$ assemblages are overprinted by low-grade muscovite-rich shear fabrics which show a range of grades of amphibolite to greenschist facies, and are interpreted to have formed during retrogressive $D4_{WEST}$ deformation.

Fig. 3.2 Upright $F3_{WEST}$ fold in semi-pelitic metasediment showing development of steep axial planar $S3_{WEST}$ fabric. S0-Sn is defined by 0.5-1mm scale quartzofeldspathic and micaceous layers.

The range of $S4_{WEST}$ fabrics and their relationship with $D3_{WEST}$ are clearly displayed at Square Pond Quarry (fig. 3.6) making this a type locality for both the prograde and retrograde deformation. Field relationships in the quarry demonstrate the progressive nature of $D3_{WEST}$ shown by the presence of tight $F3_{WEST}$ folds which show evidence for local interference and refolding. The limbs of folds are variably transposed by steep micaceous retrogressive shear fabrics and locally in more pelitic regions are totally transposed by these $S4_{WEST}$ fabrics. The effects of $D4_{WEST}$ are concentrated in the southeast side of the quarry forming a large-scale (10-20m) shear zone which is

dominated by anastomosing $S4_{WEST}$ chlorite-, muscovite-rich fabrics associated with a predominately subhorizontal mineral lineation.

3.3.1 Pre-$D3_{WEST}$

The preservation of regional D2 structures and fabrics is limited to the lower strain regions of $D3_{WEST}$ which have not undergone $D4_{WEST}$ retrogression. Relic recumbent F2 folds and associated S2 fabric are seen in the west of the domain where they show evidence for refolding by $F3_{WEST}$ folds (fig. 3.6). This is illustrated along the Trans Canada Highway section (localities TCH 94 10, TCH 95 4, 5) where both centimetre, and metre scale recumbent F2 folds are deformed by open upright $F3_{WEST}$ folds. Relic F2 folds preserve a predominantly eastwards vergence direction although locally folds record a westward-directed sense of vergence (e.g. locality TCH 95 4) which is interpreted to be due to measurements taken from overturned limbs.

Relic F2 folds form close to tight structures with variably well developed axial planar fabric S2 which is characterised by a distinctive spaced (2-3 mm scale) pressure solution 'pin-stripe' cleavage. The folds deform both distinct lithological units (1-75 cm thickness) which represent transposed bedding fabric (S0-Sn) and relic S1 fabric (which forms a fine millimetre scale fabric orientated subparallel to bedding). The trace of S0-Sn fabrics are well preserved throughout of the domain and at intersections with S2, produce a herringbone-style cleavage pattern. In the central and eastern regions of the domain which are dominated by the effects of progressive $D3_{WEST}$ (e.g. around Wing Pond, Gull Pond, Square Pond and at Mint Brook), evidence for relic D2 structures and fabrics is limited, however they are locally preserved within microlithons of $S3_{WESTA}$. On the west shore of Wing Pond (locality WP 7), S2 forms a finely crenulated fabric within microlithons of $S3_{WESTA}$ in psammitic layers of metasediment. Preservation of crenulated S2 inclusion trails within large andalusite porphyroblasts are recognised by petrographic study (previously noted by O'Neill, 1991) and can be rarely observed in the field as cloudy traces within the grains (e.g. localities TCH 94 18, SPQ 11).

3.3.2 $D3_{WEST}$

The western and central portions of the domain are characterised by the development of north-northeast to south-southwest trending upright $F3_{WEST}$ structures with amphibolite facies axial planar fabrics. In the west these structures deform a spaced S2 pressure-solution cleavage and F2 flat-lying folds, and eastwards become progressively refolded and overprinted by deformation of similar style and grade (fig. 3.3). The form and grade of these structures and fabrics varies across the domain, and is characterised by open folds with a poorly developed axial planar fabrics in the west, and close to tight structures with mylonitic axial planar fabrics in narrow (10-100m) high strain zones in central and eastern regions. The shear sense on the high grade fabrics is locally variable, although is predominantly sinistral. The folds are commonly symmetrical in form although rare asymmetric,

sinistrally-verging folds are observed along the Trans Canada Railway (e.g. TCR 23) and in the vicinity of Wing Pond (e.g. WP 2, 3).

Open $F3_{WEST}$ folds which characterise $D3_{WESTA}$ are illustrated along the Trans Canada Highway (localities TCH 94 10, 14) and Trans Canada Railway (locality TCR 10) forming metre scale structures which show variable development of a closely spaced axial planar fabric (fig. 3.2). $D3_{WEST}$ mineralogical relationships in the west of the domain are obscured along the Trans Canada Highway and the Trans Canada Railway sections (fig. 3.19) by overprinting contact effects from the cross-cutting Gander Lake Granite (e.g. locality TCH 94 14).

The progressive-style of $D3_{WEST}$ is highlighted in Square Pond Quarry (localities SP 10, SP 11), and along the section at Mint Brook (locality MB 6) where a series of generations of $F3_{WEST}$ folds can be recognised (fig. 3.3 & 3.4). Locally folds can be traced from upright structures with poorly developed axial planar fabric (fig. 3.3a) into refolded structures with new axial planar fabrics which in turn, may show further refolding and development of transposing axial planar fabrics (fig. 3.3b). Specific generation of the $F3_{WEST}$ folds (i.e. $F3_{WESTA}$, $F3_{WESTB}$...) can however only be inferred if relic S2 fabric has been identified. $F3_{WEST}$ fold interference patterns observed include 'eye structures', sheath folds (10 cm scale) and other type 2 and 3 (Ramsey, 1967) interference patterns (fig. 3.3c & 3.4). This is shown at Mint Brook (localities MB 7, 8) where S2 defines refolded $F3_{WESTA}$ folds, forming type 2 interference patterns (Ramsey, 1967). Local development of $F3_{WESTC}$ structures (fig. 3.3c) occurs preferentially within pelitic lithologies and is observed along the Trans Canada Highway (e.g. locality TCH 94 3) and at Mint Brook (locality MB 6).

Fig. 3.3 Field sketch showing $D3_{WEST}$ structural overprinting relationships at Mint Brook; a) $F3_{WESTA}$ fold deforming S2 (loc. MB 7); b) $F3_{WESTA}$ fold refolded by $F3_{WESTB}$ fold with development of axial planar $S3_{WESTB}$ (loc. MB 8); c) $F3_{WESTC}$ fold of $S3_{WESTB}$ fabric preserving $F3_{WESTB}$ fold hinge (loc. MB 6).

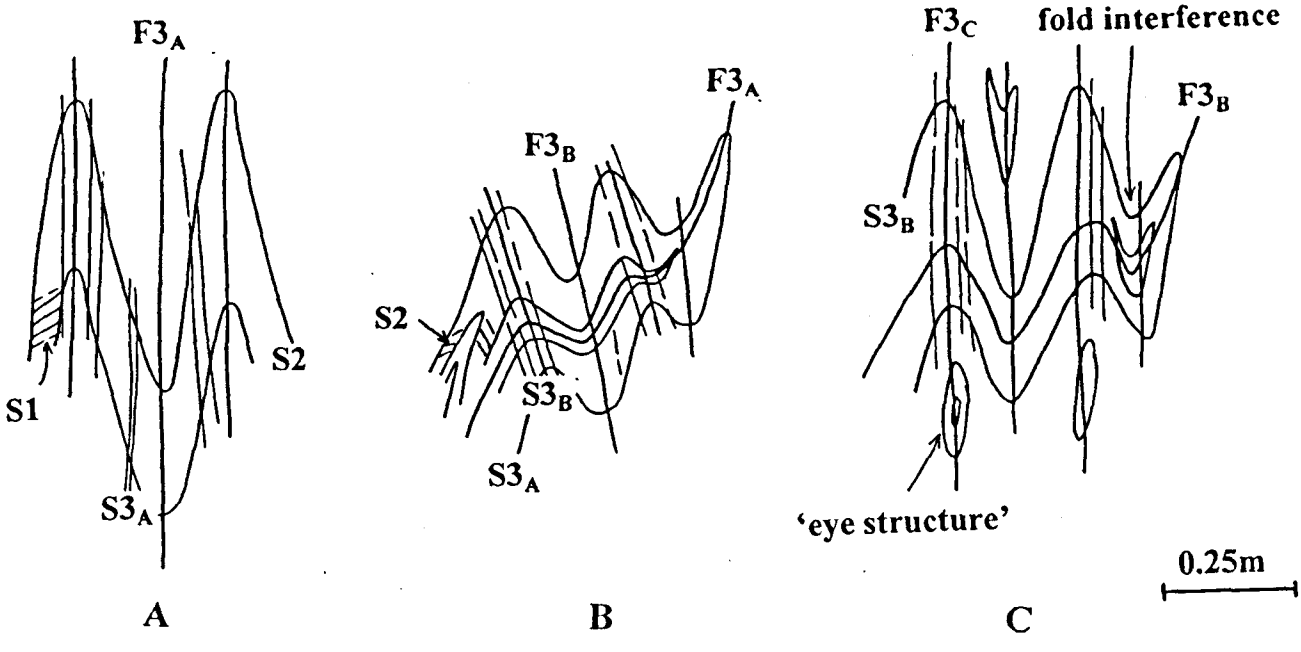

Fig. 3.4 Map of Square Pond Quarry showing the field relationships between progressive $D3_{WEST}$ and retrogressive $D4_{WEST}$ deformation.

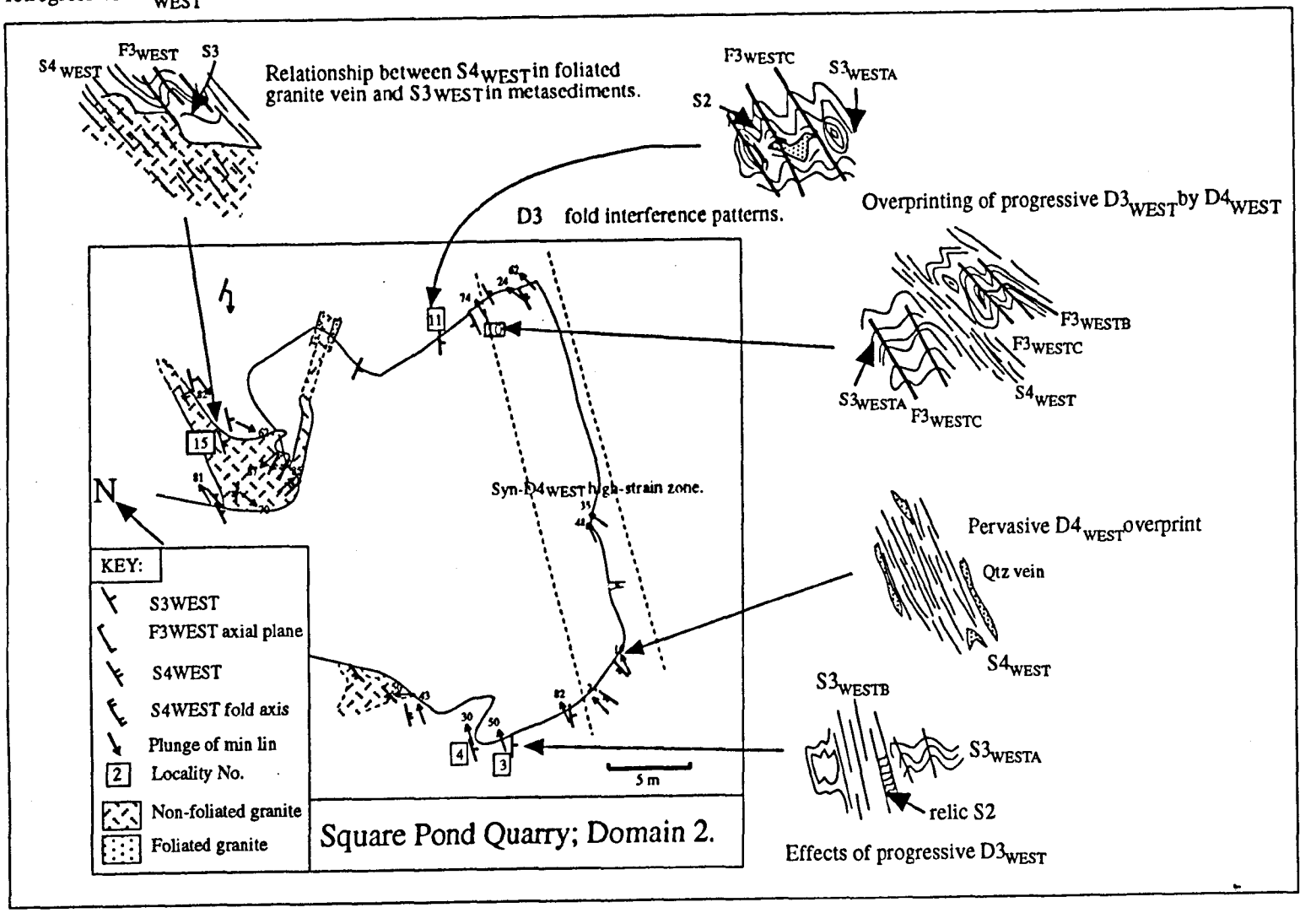

Fig. 3.5 $F3_{WEST}$ folds; a) tight folds in psammitic metasediment deforming S2 pin-stripe cleavage and showing subordinate development of steep axial planar $S3_{WEST}$; b) Folds in pelitic metasediment deforming andalusite porphyroblasts; c) Pervasive axial planar sillimanite-rich $S3_{WEST}$ wrapping andalusites, photo turned on side (in both a & b andalusites are variably pseudomorphed by kyanite).

a)

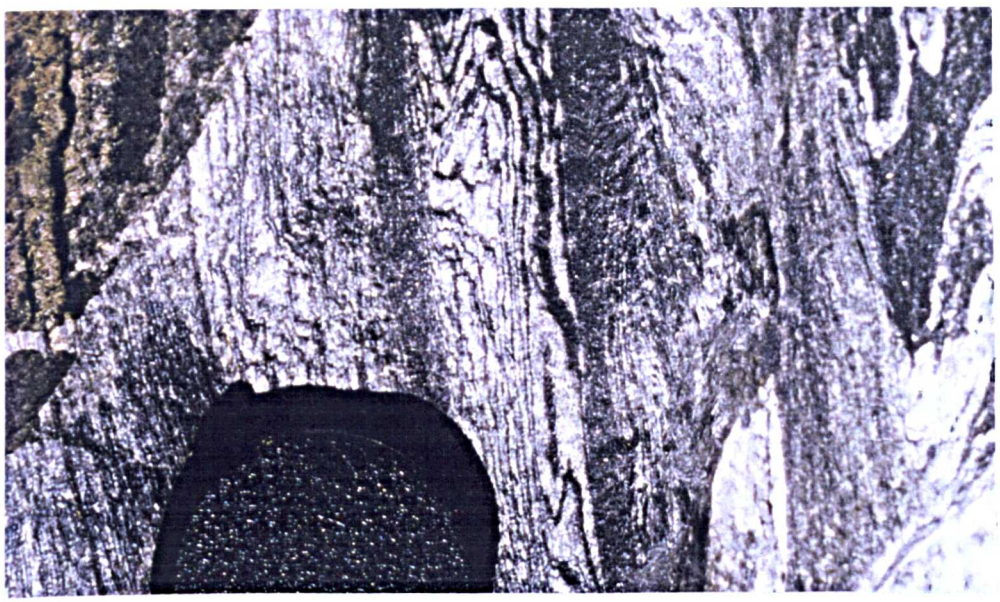

b)

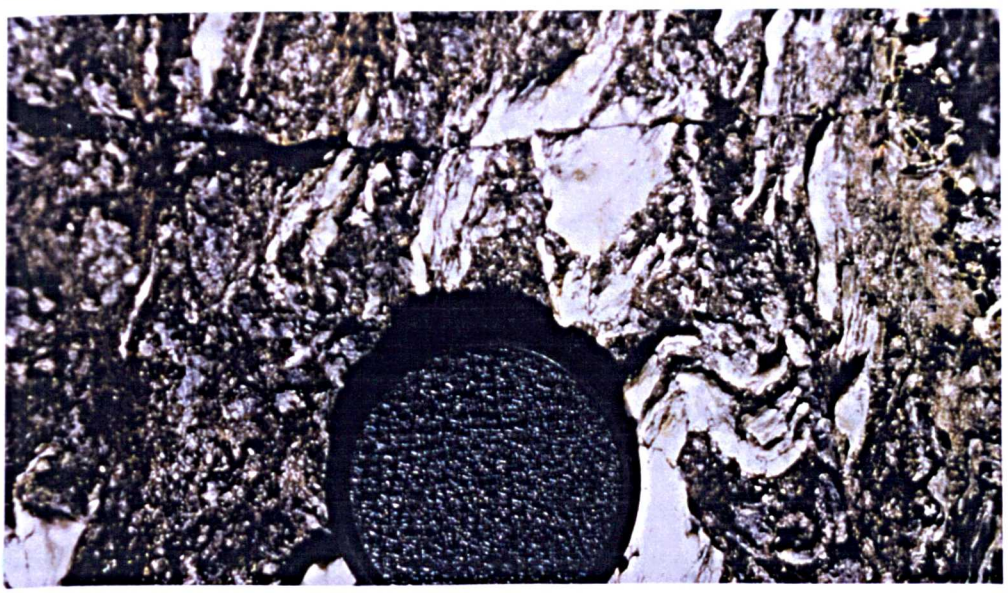

c)

The focusing of progressive $D3_{WEST}$ occurs preferentially within more pelitic lithologies of metasediments. The effects of $D3_{WEST}$ are illustrated in the central region of the domain where upright symmetrical tight $F3_{WEST}$ folds form the dominant structure (fig. 3.2) associated with well developed steep composite $S3_{WEST}$ fabrics (2-4 mm scale). The $S3_{WEST}$ mineral assemblages are locally variable, and are characterised in pelitic lithologies by the development of aluminosilicate polymorphs (andalusite, kyanite, sillimanite & fibrolite) and staurolite. Steep $S3_{WEST}$ fabrics are sillimanite and staurolite-rich and wrap tabular porphyroblasts (0.5-1 cm scale) of andalusite (fig. 3.5 b & c). Semi-pelitic and psammitic lithologies in the region display $S3_{WEST}$ fabrics which are similarly defined by quartzofeldspathic-, biotite- and muscovite-rich domains, however they do not show the development of aluminosilicates or staurolite. Around the north shore of Square Pond (localities TCH 94 18, 20) and at Square Pond Quarry (localities SP 10, 11) pelitic rocks display close upright folds with steep axial planar fabrics on limbs (fig. 3.5c) which in places refold tight $F3_{WESTA}$ assemblages (fig. 3.5b) and are termed $F3_{WESTB}$. At these localities, both $S3_{WESTA}$ and $S3_{WESTB}$ fabrics are biotite-rich and of similar appearance and grade, $S3_{WESTA}$ is characterised by the presence of aligned large tabular andalusite porphyroblasts (0.5-2 cm in length) which are variably boudinaged by $F3_{WESTB}$ folds and wrapped by a sillimanite- / fibrolite-rich $S3_{WESTB}$ fabric. The quartzofeldspathic portions of $S3_{WEST}$ are defined by discontinuous lenses and layers of quartz and a well developed pressure solution cleavage. The quartz lens commonly form asymmetric pods which show a sinistral sense of shear. Around Wing Pond and Gull Pond (WP 4, 5, 6), semi-pelitic and pelitic lithologies are characterised by relic hinges of tight to isoclinal folds (locally termed $F3_{WESTB}$), and are variably transposed by steep axial planar staurolite and sillimanite / fibrolite-rich mylonitic fabrics.

The north of the domain (e.g. WP 12, 23) comprises predominantly of semi-psammitic and psammitic metasediments, and is dominated by north-northeast to south-southwest trending $S3_{WEST}$ fabrics (fig. 3.5a). These fabrics form a distinctive pressure solution cleavage (1-2 mm scale) which is pervasively developed, and composed of aligned biotite and muscovite with anastomosing boundaries between the cleavage domains. Relic $F3_{WEST}$ folds are rarely preserved in the assemblages (WP 25). Rocks show pervasive development of a predominately steep north-northwest plunging mineral stretching lineation along $S3_{WEST}$ which is defined by aligned micas and quartz. Similar mineral stretching lineations which show a steep north-easterly directed plunge are developed within semi-pelitic and pelitic lithologies further south in the domain (e.g. SPQ 3, 4) although local variation in the attitude of the lineations is evident.

3.3.3 $D4_{WEST}$

The development of steep low-grade $S4_{WEST}$ mylonitic fabrics occurs locally throughout the domain and they form the dominant fabrics in a km-scale north-northeast to south-southwest trending tract in the east and in narrow (2-15m wide) high-strain zones internally within the domain (fig. 3.6). The assemblages at first sight show no signs of preserving relic higher grade, but through extensive field study and examination of numerous key localities along the Trans Canada Highway,

Trans Canada Railway and in Square Pond Quarry, it is clear that the fabrics have a similar orientation to, and retrogressively overprint earlier $D3_{WEST}$ assemblages (fig. 3.4). The fabrics are characterised by a range of upper to lower greenschist-facies assemblages (e.g. in Square Pond Quarry) and are locally refolded at Mint Brook (localities MB 1, 6) and Gambo Provincial Park (locality TCR 32) demonstrating the progressive style of the $D4_{WEST}$ retrogressive deformation.

Fig. 3.6 Pervasive development of steep retrogressive $S4_{WEST}$ fabrics in Square Pond Quarry (looking northeast; field of view = 6m).

Throughout the domain, $S4_{WEST}$ fabrics are mylonitic and are characteristically chlorite-, mica-rich showing presence of extensively recrystallised, and annealed quartz, biotite is notably absent from the assemblages. The fabric forms a fine (millimetre scale) penetrative slatey cleavage in semi-pelitic and pelitic lithologies and anastomosing quartz-rich mylonitic fabrics in psammitic lithologies. Associated with $D4_{WEST}$ is a well developed dominantly north-northeast to south-southwest trending mineral stretching lineation which is defined by aligned grains of chlorite, muscovite and quartz in pelites and semi-pelites (e.g. TCR 28, SP 2), and by quartz lineations in quartz veins in psammitic lithologies (e.g. MB 1). The plunge of the lineation is variable, however is predominantly subhorizontal to moderately inclined, which is clearly illustrated in the $D4_{WEST}$ retrogressive shear zone in Square Pond Quarry (fig. 3.4). The sense of shear of $D4_{WEST}$ is also variable, although appears to be predominately dextral. Dextral shear sense indicators are displayed at a key locality in Gambo Provincial Park (TCR 32) by coarse asymmetric quartz pods within pelites, and rare (centimetre scale) dextrally verging folds. Other evidence for dextral $D4_{WEST}$ deformation is given by centimetre scale shear bands in pelitic metasediments at the east of the Trans Canada Railway, and Trans Canada Highway sections (e.g. TCR 25).

3.3.4 Contact metamorphic overprint

The effects of contact metamorphism are displayed locally within the aureoles of the Gander Lake and the Middle Brook granites in the south, and the Deadmans Bay Granite in the north of the domain. After careful assessment of relationships between the contact effects and the structure and fabrics of the surrounding metasedimentary country rocks, it is clear that the contact metamorphism post-dates $D3_{WEST}$ and $D4_{WEST}$ fabric development.

The Gander Lake Granite cross-cuts $D3_{WEST}$ assemblages in the southwest of the domain producing a *c.* 2 km wide contact metamorphic aureole. The margin between the granite and metasediments is a sharp steeply-dipping contact, commonly preserved in the margins of the granite are stoped blocks of metasediment which contain a deformed pin-stripe fabric. The aureole rocks show widespread development of the metamorphic index minerals cordierite and biotite (previously described by O' Neill, 1993) and extensive hornfelsing and recrystallisation (localities TCH 94 14 and TCR 18). The cordierite porphyroblasts clearly overprint steep $S3_{WEST}$ fabrics, quartzofeldspathic portions of the metasediments display a coarse saccharoidal, granoblastic texture. In places (i.e. pelitic metasediments) fibrolite is developed in the aureole (TCH 94 14), forming as coarse knots intergrown with biotite. Away from the granite, the contact effects become less intense and are characterised by quartz recrystallisation and the subordinate development of biotite.

In the east of the domain, around the western margin of the Middle Brook Granite, low-grade $S4_{WEST}$ bearing metasediments which are characterised by steep mylonitic fabrics show variably intense effects of contact metamorphic recrystallisation (these relationships are previously undocumented). Immediately adjacent to the granite margin (TCR 33), semi-psammitic rocks are highly annealed and display a fine hornfels texture. Pelitic rocks both along the TCH and TCR sections (*c.* 1-2 km west of the contact), show intense hornfelsing and spotting which is characterised by the development of fine biotite and fine to coarse anhedral (highly sericitised) cordierite (e.g. TCH 94 23) and less commonly by the development of andalusite (e.g. MB 5).

In the north of the domain in the vicinity of Moccasin Pond and Big Bear Cove Pond (e.g. localities WPSZ 3, WPSZ 4) adjacent to the Deadmans Bay Granite (in a contact aureole *c.* 3 km wide previously described by O' Neill, 1991), assemblages display evidence for hornfelsing, and semi-pelitic to semi-psammitic metasediments show development of medium to coarse porphyroblasts of index metamorphic minerals (i.e. biotite, cordierite and andalusite). The porphyroblasts clearly overprint steep northeast-southwest orientated pressure-solution fabrics which show similar form and are correlated with retrogressive $S4_{WEST}$ fabrics seen further south (e.g. at Mint Brook). Relationships between the porphyroblasts and fabrics are tenuous in places due to the cross-cutting of the region by late-stage northeast-southwest trending brittle faults (similar to those recognised in the south of the region by Holdsworth, 1991), which appear to have locally re-oriented rocks.

3.4 Petrological descriptions

3.4.1 Pre-$D3_{WEST}$ fabrics

Relic bedding variations are defined by 1-10 cm scale layers of quartzofeldspathic and mica-rich lithology. Evidence for relic S1 subparallel to S0-Sn is rarely preserved, and is defined by aligned intergrowths of fine muscovite and quartz. The S2 foliation is characterised by millimetre scale M and Q domains which are of muscovite-, chlorite-rich, and quartzofeldspathic composition respectively (e.g. samples ON 87 714, Tk 95 62, TK 95 63). Muscovite forms fine to medium grains which are variably intergrown with fine chlorite, muscovite shows marginal recrystallisation and development of internal kink bands. Quartz grains are medium to coarse and subidiomorphic in form, grains are commonly elongate with undulating grain boundaries and show limited evidence for recovery and recrystallisation. Plagioclase grains are subidioblastic in form and show evidence for marginal ductile recrystallisation.

3.4.2 $D3_{WEST}$ progressive deformation

Inclusion geometries

Andalusite porphyroblasts contain both simple and complex inclusion trails which are consistent with the overgrowing of variably well developed $D3_{WEST}$ crenulation cleavage patterns. Within a single sample, a range of intensities of crenulation fabrics may be preserved within the andalusites (e.g. fig. 3.10) suggesting that the development of the fabric was locally inhomogeneous. The model of Bell and Rubenach (1983) describes 'stages' of crenulation cleavage development which are related to time therefore in order to classify $D3_{WEST}$ assemblages in this study a modified model is needed which refers to types of crenulation patterns and is unrelated to time (fig. 3.7).

Fig. 3.7 Types 1-6 of crenulation cleavage (corresponding to stages 1-6 of Bell & Rubenach, 1983) describing development of new foliation by crenulation and transposition of an existing foliation.

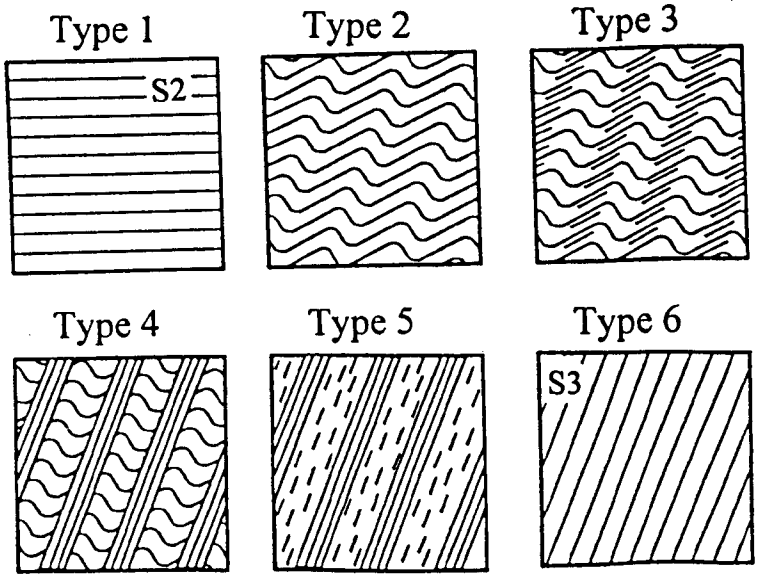

Fig. 3.8 Inclusion trail geometries in andalusites corresponding to; a) type 3-4 crenulated fabric; b) type 4-5 crenulated fabric with relic fold hooks (in a & b inclusions comprise quartz and ilmenite); c) evolved type 6 fabric with inclusions of plagioclase (modified after Bell & Rubenach, 1983; field of view; 4.5mm).

a)

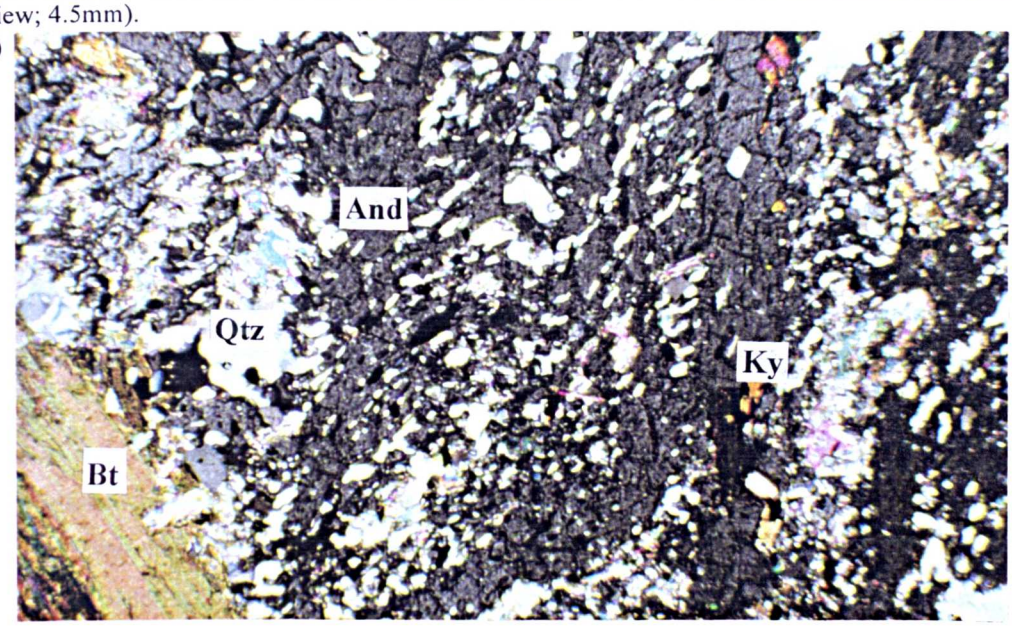

b)

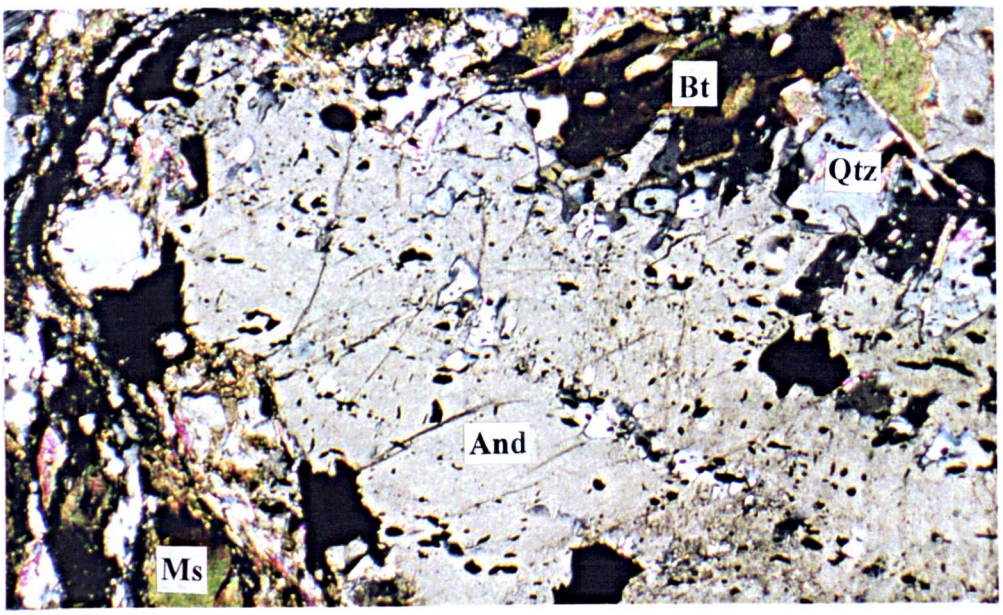

c)

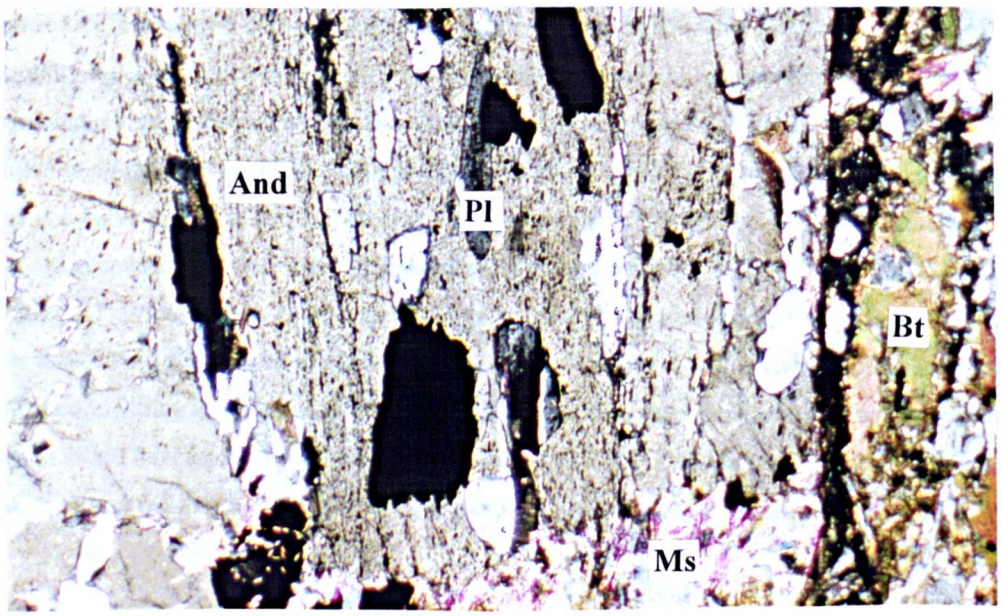

The range of types of crenulations preserved in the andalusites of domain 2 (figs. 3.8 & 3.9) appear to correspond to types 2 to 4 of crenulation cleavage (fig. 3.7). Planar trails in places preserve relic intrafolial 'fold hooks' (previously described in andalusites by Jones, 1994) which suggests that these trails represent a well developed transposition fabric corresponding to type 5 to 6 fabric development.

The mineral inclusions within the andalusites are abundant and locally comprise 30-40 % of the grain. Quartz and ilmenite are the most common inclusion phases, although biotite, muscovite, plagioclase and rutile are also present. It is apparent that in pelitic lithologies the mineralogy of inclusions is predominately ilmenite with minor quartz (fig. 3.8), whereas in semi-pelitic lithologies, and locally in more psammitic lithologies, they are predominately quartz with lesser amounts of ilmenite. The majority of quartz inclusions are medium to coarse with a lensoid to elongate form, ilmenite inclusions are fine to medium grained and subrounded. Medium to coarse grained plagioclase inclusions whose rims display concentric zoning against the andalusite are locally abundant, and show subidiomorphic form (fig. 3.8c).

In samples ON 87 746b, ON 87 714 and SP 20, open widely spaced crenulated inclusion trails (corresponding to types 2 to 3) are defined predominately by quartz inclusions, and form a close to tight pattern with a characteristic step-like form (similar to the form of trails described in andalusite by Vernon, 1986; Williams, 1994). Inclusion trail patterns show bands of fine (*c.* 0.5 mm) inclusion-poor domains which are separated by wider bands (1-1.5 mm) of inclusion-rich domains (fig. 3.9b). Within the inclusion-rich bands, inclusions are elongate and form distinct sigmoidal trails developed at a high angle to the orientation of the straight inclusion-poor fabric. However, at the margins with inclusion-poor domains, the sigmoidal trails curve into parallelism with inclusion poor domains. The crenulated inclusion trails are interpreted to represent relic S2 fabric, and the developing crenulation cleavage is interpreted as $S3_{WEST}$ (fig. 3.9). The inclusion-poor and inclusion-rich domains are thought to be related to a relic lithological variation (i.e. S0-Sn; similarly to interpretations by Bell *et al.* 1986; Vernon, 1986; Williams, 1994).

In contrast to those described above, sample TK 157b contains andalusites with inclusions which define a tightly crenulated type 4 fabric (fig. 3.8b). The inclusions are predominately composed of fine to medium opaque minerals forming linear trails which in places appear to truncate each other. Rare inclusions of quartz show relic fold hooks confirming that the porphyroblasts overprinted a highly evolved fabric (as opposed to the section being orientated parallel to the crenulation domains of the fabric). Sample ON 746a shows preservation of both similar and later stages (i.e. types 4 to 5) of fabric, however fold hooks are rare (fig. 3.9d). A fine linear fabric defined by elongate opaques is preserved within andalusites in samples TK 1591, TK 1594, TK 1571 and ON 87 746a, and corresponds to overprinting of a thoroughly transposed fabric. Sample ON 87 746a shows a spectrum of stages of fabric development preserved by inclusion trails in andalusites which are located in various regions of an $F3_{WEST}$ fold. In the core of the fold, porphyroblasts preserve type 2 to 3 of fabric development whereas on fold limbs types 4 and 5 are preserved (fig. 3.12). The above microstructural relationships suggest that the pattern of deformation partitioning changed

Fig. 3.9 Relationships between inclusion trails in andalusites and the stage of fabric development (modified after Bell & Rubenach, 1983), A) open 'type 2' crenulations (ON 87 746b); B) weakly developed 'type 3' crenulation cleavage (SP 20); C) well developed 'type 4' crenulation cleavage (ON 87 714); D) penetrative 'type 5-6' foliation (ON 87 746a).

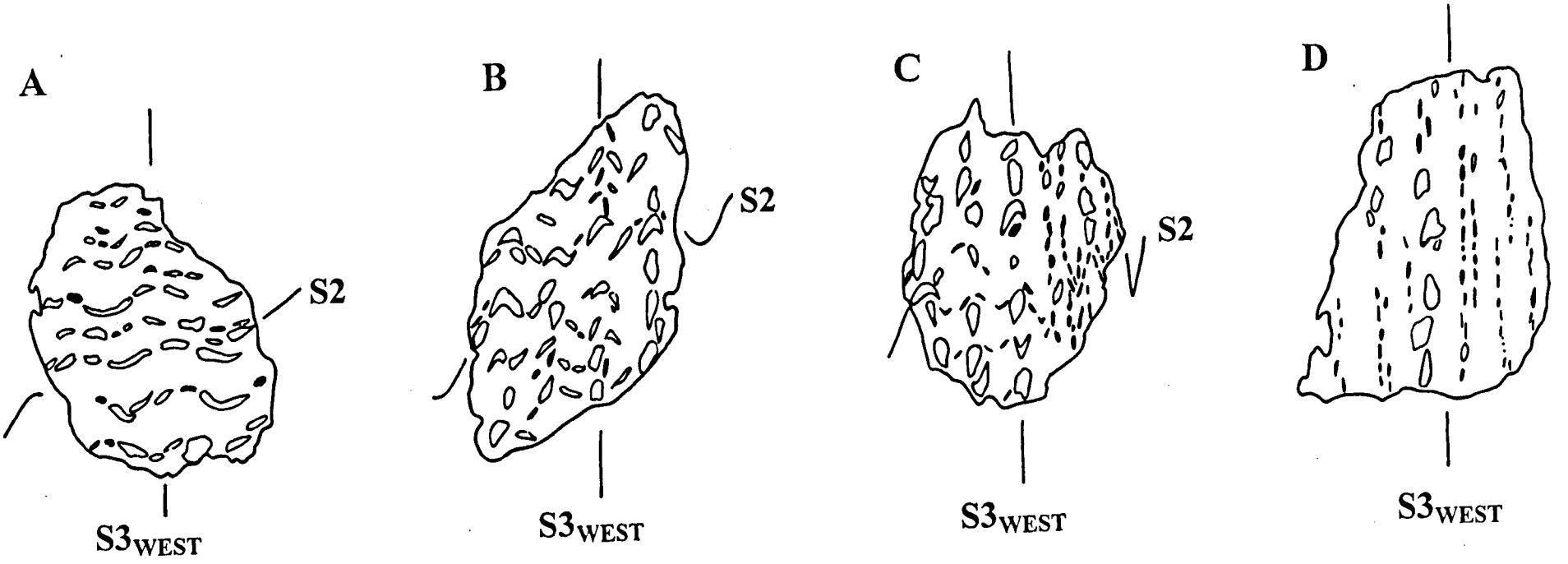

during progressive $D3_{WEST}$ which enabled the overgrowth of 'inactive' crenulations by andalusite porphyroblasts (also recognised by Vernon, 1986, Vernon *et al.* 1993). Thus, the growth of andalusite appears to have occurred at various stages during the local development of the $F3_{WEST}$ crenulations (fig. 3.10).

Fig. 3.10 Relationship between inclusion trails in andalusite porphyroblasts and the type of fabric development during $D3_{WEST}$ (modified after Bell & Rubenach, 1983 & K.A. Jones *pers. comm.*). A) type 2; B) type 3; C) type 4; D) type 5-6.

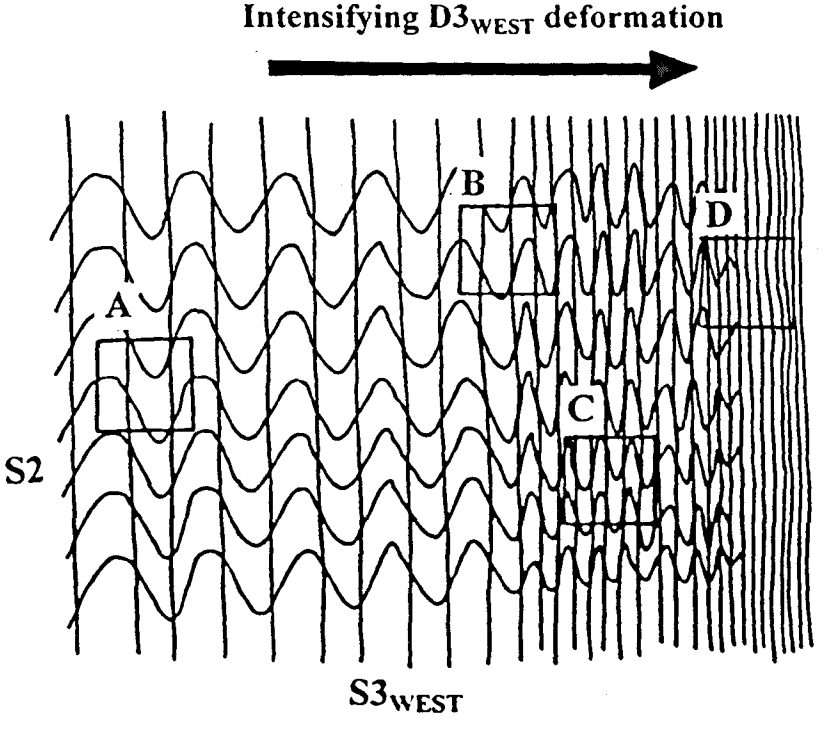

Relationships between inclusion trails and $D3_{WEST}$ matrix fabrics

The relationship between the orientation of inclusion trails within, and the wrapping prograde $S3_{WEST}$ fabrics around andalusite porphyroblasts is complex. Both the crenulated and straight fabrics defined by the inclusion trails appear to be orientated at various angles to the matrix fabric (figs. 3.11 & 3.12). Results of careful examination demonstrate that in individual specimens, the majority of the andalusite porphyroblasts show a consistent orientation which is parallel / subparallel to the wrapping $S3_{WEST}$. In samples where andalusites are preserved in low strain zones of $D3_{WEST}$ (e.g. ON 87 746b, ON 87 714), the grains consistently show a weak to moderately well developed type 2 to 3 crenulation cleavage. However where andalusites are preserved in high strain zones of $D3_{WEST}$ (e.g. SP 20, TK 157), inclusion trails display a range of type 2 to 5 fabric development. An example (fig. 3.12a) showing the development of andalusite in a $D3_{WEST}$ low-strain zone is seen in samples ON 87 714 and ON 746b, porphyroblasts overgrow early stages of $S3_{WEST}$ fabric development within pelitic regions of open to tight $F3_{WESTA}$ fold hinges. Porphyroblasts are wrapped by a poorly developed $S3_{WEST}$ fabric developed axial planar to folds. Relic crenulated S2 fabric (corresponding to

crenulated fabric in andalusites) is also preserved in the matrix intrafolial to the axial planar fabric and in strain shadows protected by the porphyroblasts. Such relationships have been described by Vernon (1986) and Bell *et al.* (1986), and have been similarly interpreted to suggest that the andalusites grew during the early stages of the progressive fabric development.

Fig. 3.11 The effects of progressive $D3_{WEST}$ deformation partitioning showing a) preservation of open crenulations in porphyroblasts and tighter crenulated fabric in strain shadows; b) partitioning of strain around porphyroblast margins; c) angular relationship between tightly crenulated inclusion trails in porphyroblasts and the wrapping high-strain fabric; d) intense strain partitioning around porphyroblast margins producing reorientation and angular relationship between inclusion trails and wrapping fabric.

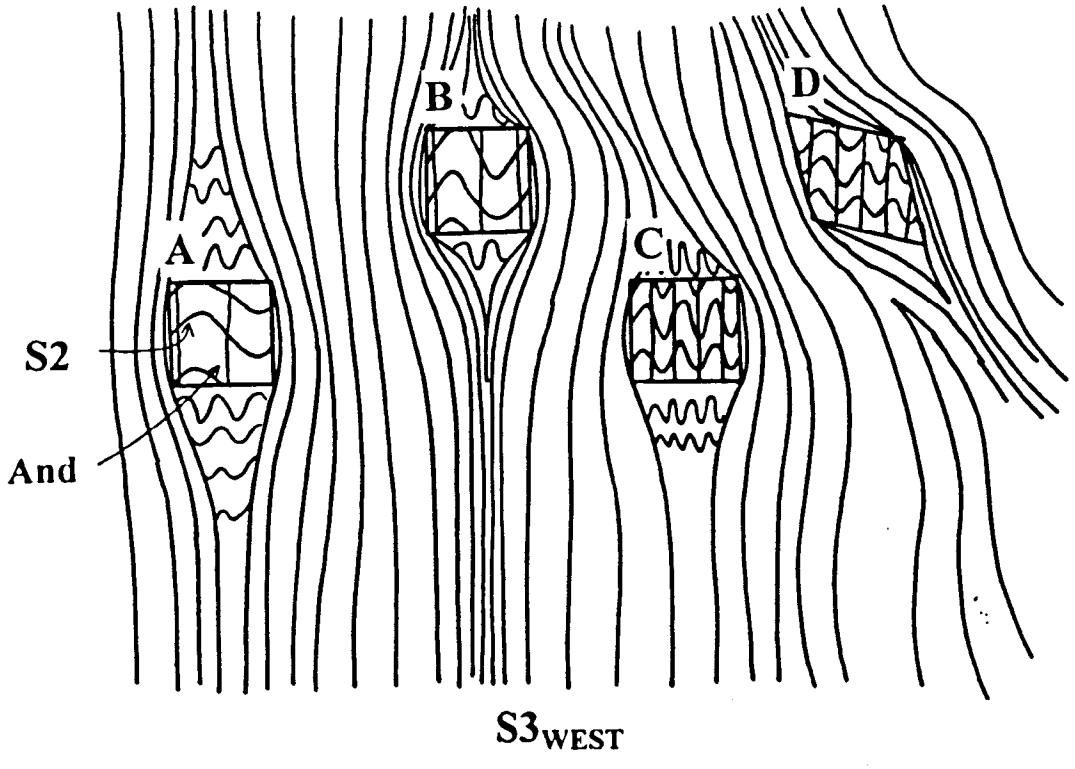

Sample SP 20 shows andalusites which are preserved in a $D3_{WEST}$ high-strain zone and similarly preserve an early stage of fabric development. In contrast to those previously described, andalusites are wrapped by an intense mylonitic $S3_{WEST}$ fabric (fig. 3.12b). In places this intense fabric slightly reorientates the andalusite porphyroblasts (i.e. sample SP 20) resulting in the development of an angular relationship with the matrix fabrics (fig. 3.11c & d). The sharp boundary between the inclusion trails at the edge of the andalusites and the wrapping matrix fabric (fig. 3.12b) indicates that these margins were sites of dissolution (similar to those described by Bell *et al.* 1986). The relationships described above between the inclusion trail geometries and the wrapping $S3_{WEST}$ fabrics suggest that porphyroblasts which developed during various stages of fabric development during $D3_{WEST}$ have been subsequently wrapped during later stages of fabric development during progressive deformation.

Fig. 3.12 Relationships between $S3_{WEST}$ inclusion trails in andalusites and the wrapping $S3_{WEST}$ fabrics; a) preservation of poorly developed 'type 2' crenulation in andalusite wrapped by well developed $S3_{WEST}$ fabric; b) angular relationship between straight inclusion trail and wrapping fabric with dissolution on porphyroblast margins.

a) b)

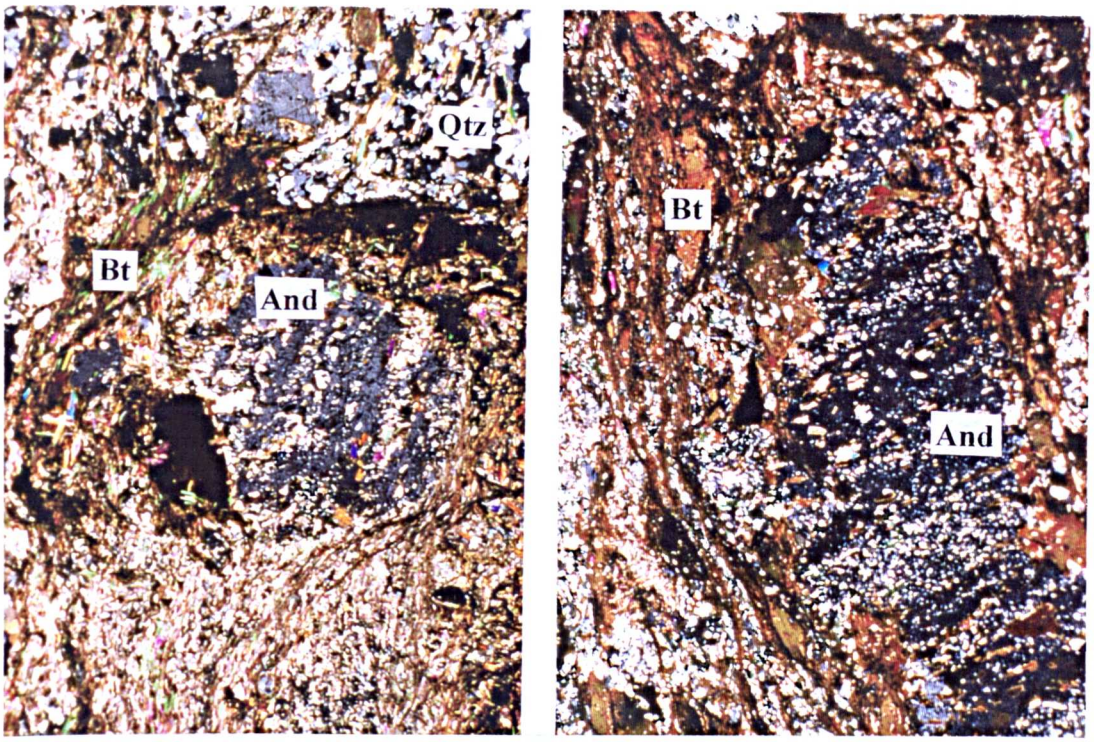

Development of kyanite

The presence of kyanite within $D3_{WEST}$ assemblages is restricted to the development of laths which are located internally within andalusite porphyroblasts, which are themselves wrapped by the $S3_{WEST}$ matrix fabrics. The andalusite grains display varying degrees of replacement by kyanite which, however, is notably absent from the $D3_{WEST}$ matrix fabrics. Kyanite forms medium to coarse grain clusters which display various growth patterns including radiating (fig. 3.13a &c) and preferentially orientated laths (fig. 3.13b). Randomly orientated kyanite laths most commonly form in a radiating growth pattern which occurs both within core and rim regions of the andalusites. In the rim regions, kyanite grains commonly radiate in from the edge towards the core of porphyroblasts whereas in the cores of andalusites, the kyanite laths radiate out uniformly (i.e. sample ON 87 725). Aggregates of kyanite laths within andalusites are preferentially orientated (fig. 3.13c), and form both a close to tight crenulated (i.e. sample TK 95 108) and straight pattern (e.g. sample TK 1591, TK 1594). The form of these kyanite growth patterns is similar to that of quartz and ilmenite inclusion trails (which preserve various types of $S3_{WEST}$ development). It can be demonstrated by microstructural relationships (fig. 3.14) that the kyanite laths cross-cut the curved crenulations (as opposed to curving around them) which suggests that they mimetically overgrew pre-existing inclusion trails.

Fig. 3.13 Growth of kyanite variably pseudomorphing andalusite; a) laths of kyanite radiating in towards core of andalusite; b) kyanite laths within andalusite showing strong preferred orientation parallel to pre-existing straight inclusion trails; c) complete pseudomorphing of andalusite by aggregates of kyanite laths (all kyanite is accompanied by fine grains of staurolite, field of view; 4.5mm).

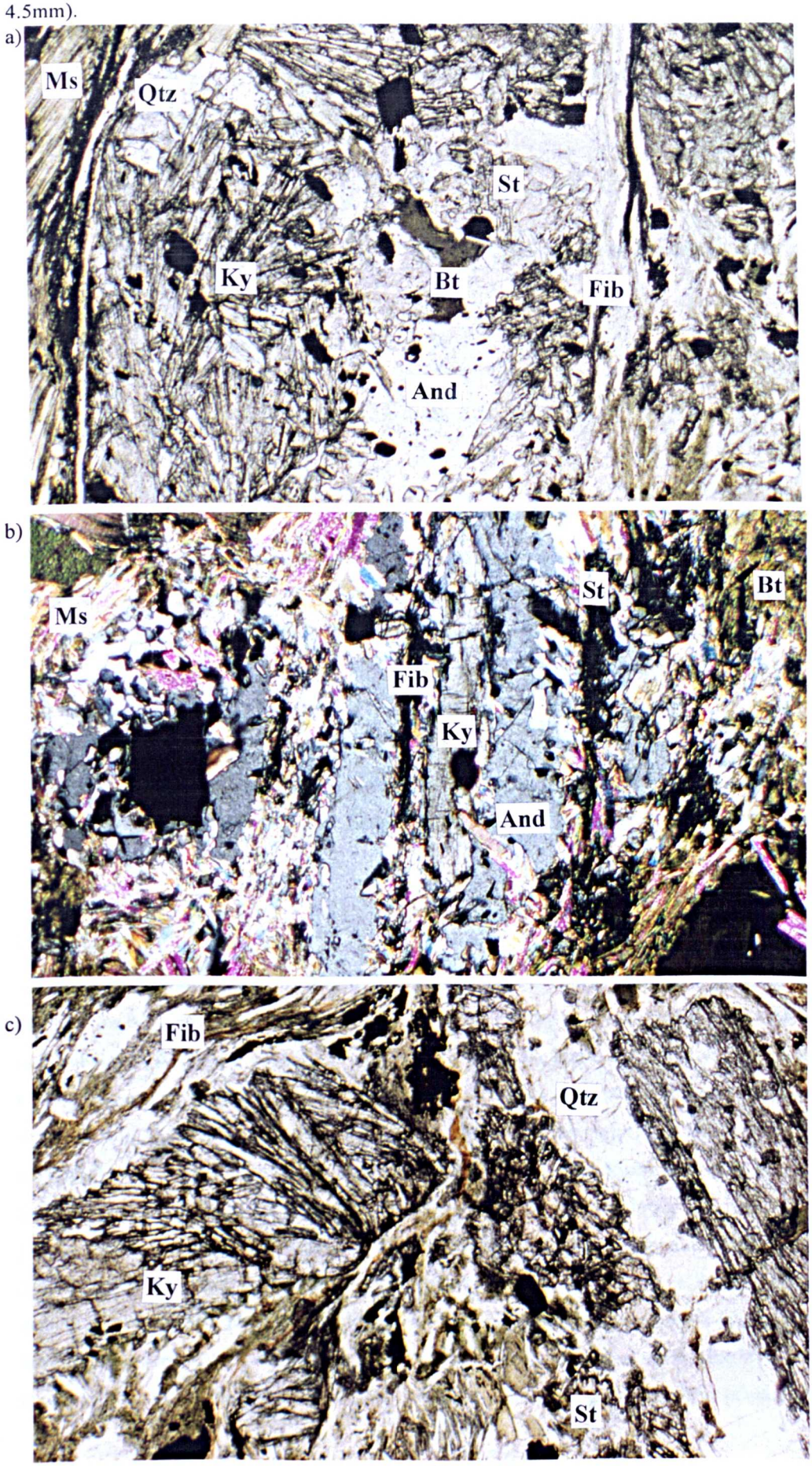

Fig. 3.14 Sketch showing the mimetic overprinting of crenulated inclusion trails in the andalusite porphyroblasts by laths of kyanite.

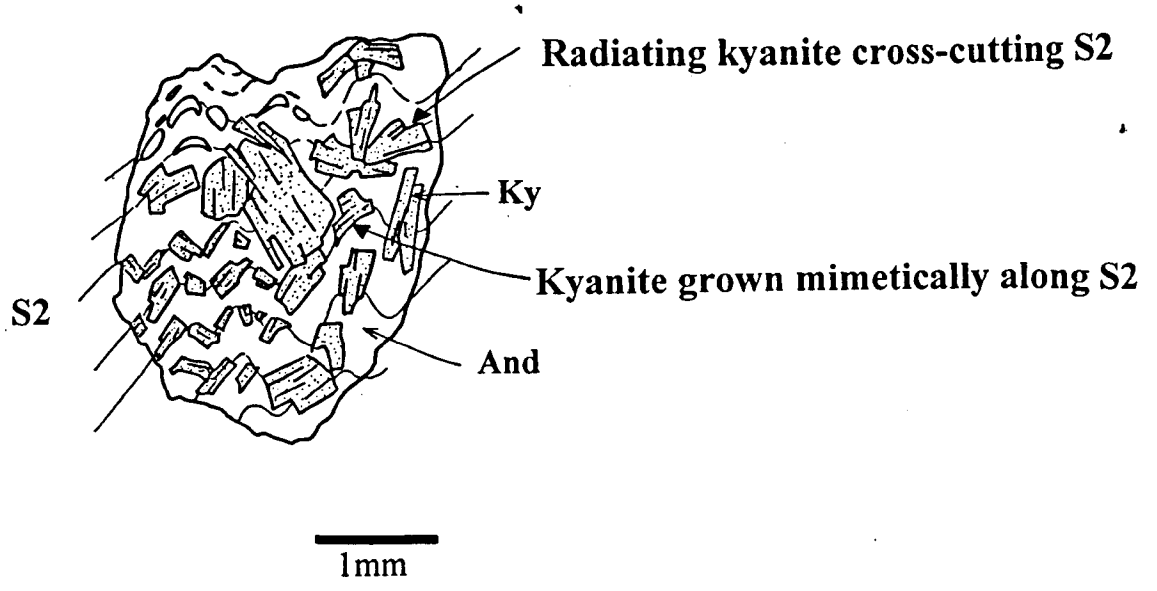

The fact that the kyanite laths in places, 1) cross-cut inclusion trails in the andalusites, 2) are orientated in optical discontinuity in contrast to the andalusite which is in optical continuity and 3) show common orientation which coincides with pre-existing fabric (i.e. inclusion trails) in andalusite, is interpreted as evidence for the direct polymorphic transition of andalusite to kyanite. In contradiction to this conclusion O' Neill (1991) interpreted the microtextures in these aluminosilicate-bearing rocks to indicate the opposite reaction, i.e. kyanite → andalusite. Microtextural relationships in rocks of comparable assemblage have been (similar to results of this study) interpreted by numerous authors (e.g. Hollister, 1969; Crawford & Mark, 1982) as representing the transition of andalusite to kyanite.

Development of staurolite

Staurolite forms in fine grain clusters (fig. 3.15a) and as fine to coarse idioblasts (fig. 3.15b & c) Grains show both 'stubby' and prismatic acicular habit, and display characteristic yellow pleochroism (α = colourless, β = pale yellow, γ = golden yellow). Staurolite grains are extensively developed within $D3_{WEST}$ assemblages where they are located both within andalusite grains and along the wrapping $S3_{WEST}$ fabrics. The development of staurolite within the majority of andalusite porphyroblasts is restricted to the regions of the grains which contain kyanite, whereas staurolite grains located along the $S3_{WEST}$ wrapping fabrics (which in places slice through variably pseudomorphed andalusites), are developed in association with either sillimanite or fibrolite (fig. 3.16a). As well as kyanite, staurolite also appears to be spatially associated (i.e. ON 87 714) with muscovite grains which form fine aggregates (within andalusites), and coarse fish (along $S3_{WEST}$ fabrics) suggesting that the development of staurolite occurred in mutual association with either kyanite, sillimanite, fibrolite and muscovite. Similarly, a link between the position of staurolite within

the assemblage and its grain size is apparent as shown by the presence of predominantly fine grains along $S3_{WEST}$ (3.16b), and coarse grains both within and in strain shadows of andalusites (fig. 3.15c).

Development of sillimanite / fibrolite

Sillimanite and fibrolite are extensively developed along the $S3_{WEST}$ matrix fabrics (fig. 3.15). $S3_{WEST}$ commonly forms a coarse anastomosing fabric which wraps variable pseudomorphed andalusites (fig. 3.15b). In high-strain domains, $S3_{WEST}$ forms an intense fabric which produces boudinage of the porphyroblasts (fig. 3.15a & c), forming microfractures and shears (i.e. sample TK 157b). These display a common orientation within the porphyroblasts with respect to the wrapping fabric (fig. 3.16), which is consistent with a Riedel shear pattern.

The $S3_{WEST}$ wrapping fabrics display a characteristic anastomosing pattern and comprise coarse elongate fish of muscovite and biotite which are intergrown with fine prismatic / fibrous sillimanite and staurolite (e.g. samples SP 20, ON 87 725, TK 95 67, TK 94 159, TK 94 157). The $S3_{WEST}$ fabric which cross-cuts the variably pseudomorphed andalusites in high-strain regions is less well developed, showing an irregular spaced 'step-like' form, and is predominantly sillimanite / fibrolite-, staurolite-rich (fig. 3.15c). Sillimanite forms fine prismatic needles which show a strong preferred orientation, whereas fibrolite forms matted aggregates of fine needles which anastomose around grains of quartz and mica (fig. 3.15b). The quartz grains, both within the sillimanite / fibrolite-rich fabric, and within quartzofeldspathic layers show elongate lenticoid form (e.g. in samples SP 20, TK 95 108, ON 87 747a). These mineral assemblages commonly show evidence for subsequent recovery and recrystallisation into coarse polygonal quartz grains, which form type 2 ribbons in quartzofeldspathic domains (Boullier & Bouchez, 1978), and show rimming by fine sillimanite / fibrolite within pelitic domains (e.g. in samples TK 94 159, TK 94 157).

Relationship between kyanite and sillimanite / fibrolite

Key relationships between the development of kyanite and sillimanite / fibrolite are shown a) internally within andalusites where the crenulated S2 fabric is sliced-up by the intense $S3_{WEST}$ microfractures, and b) in the margins of the pseudomorphed andalusites which are wrapped by high-strain $S3_{WEST}$ (fig. 3.16). In places (e.g. sample TK 95 108), the sillimanite / fibrolite-, staurolite-rich fabric which cross-cuts the pseudomorphed andalusites appears to truncate the laths of kyanite (3.16a). In contrast, where kyanites are located in the rims of pseudomorphed andalusites (e.g. sample SP 20) they commonly show a subtle transition into fibrolite contained along the wrapping $S3_{WEST}$ fabric (fig. 3.16b). It is important to note however, that the transition of kyanite into prismatic sillimanite has not been observed. The above relationships appear to suggest that the absence of kyanite and the presence of sillimanite and fibrolite within wrapping $S3_{WEST}$ fabrics is at least in part deformationally controlled. Similar types of relationships have been described and discussed by

Fig. 3.15 Sillimanite / fibrolite-, staurolite-rich $S3_{WEST}$ fabrics; a) forming along microfractures cross-cutting andalusites; b) wrapping andalusite porphyroblasts; c) cross-cutting and wrapping andalusite (in RHS & LHS of photograph respectively) with coarse staurolite growth in andalusite strain shadows (field of view; 4.5mm).

a)

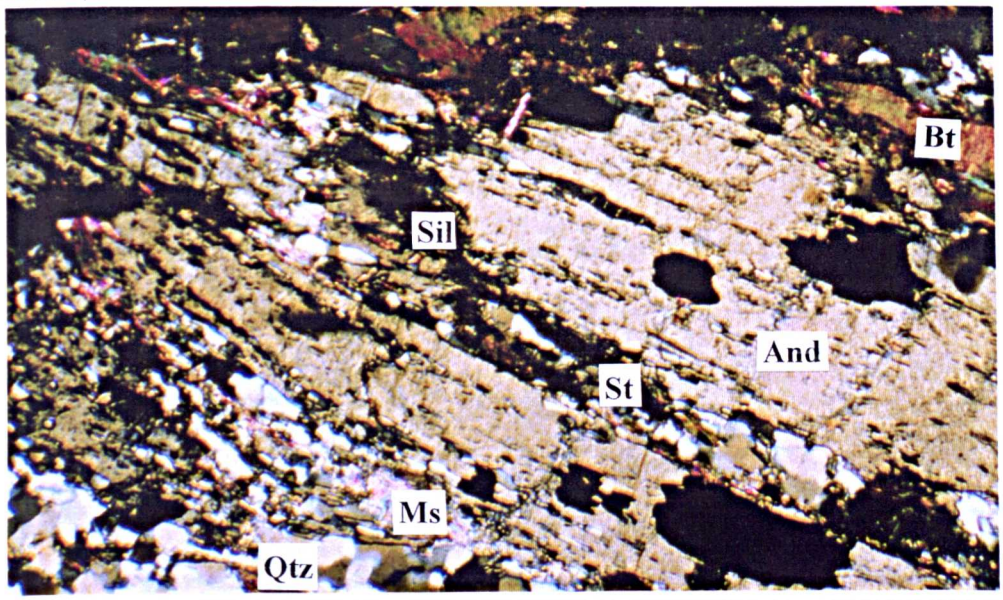

b)

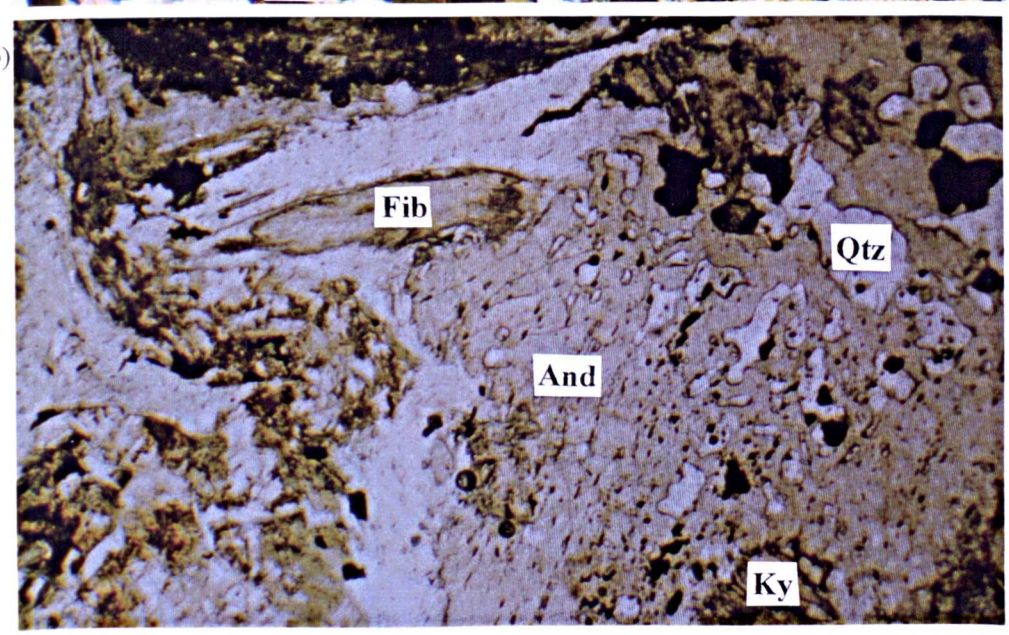

c)

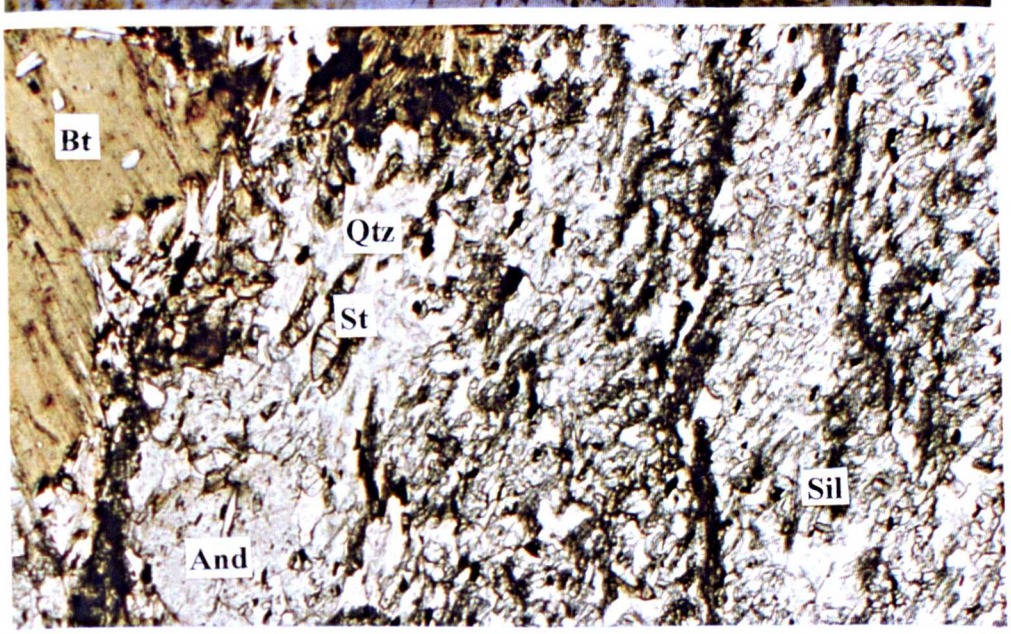

fibrolite within foliae and high-strain fields of rocks, and conclude the growth of fibrolite through a pressure-solution / local base-cation leaching of biotite.

Fig. 3.16 Sketch showing the relationship between the growth of kyanite and prismatic / fibrous sillimanite.

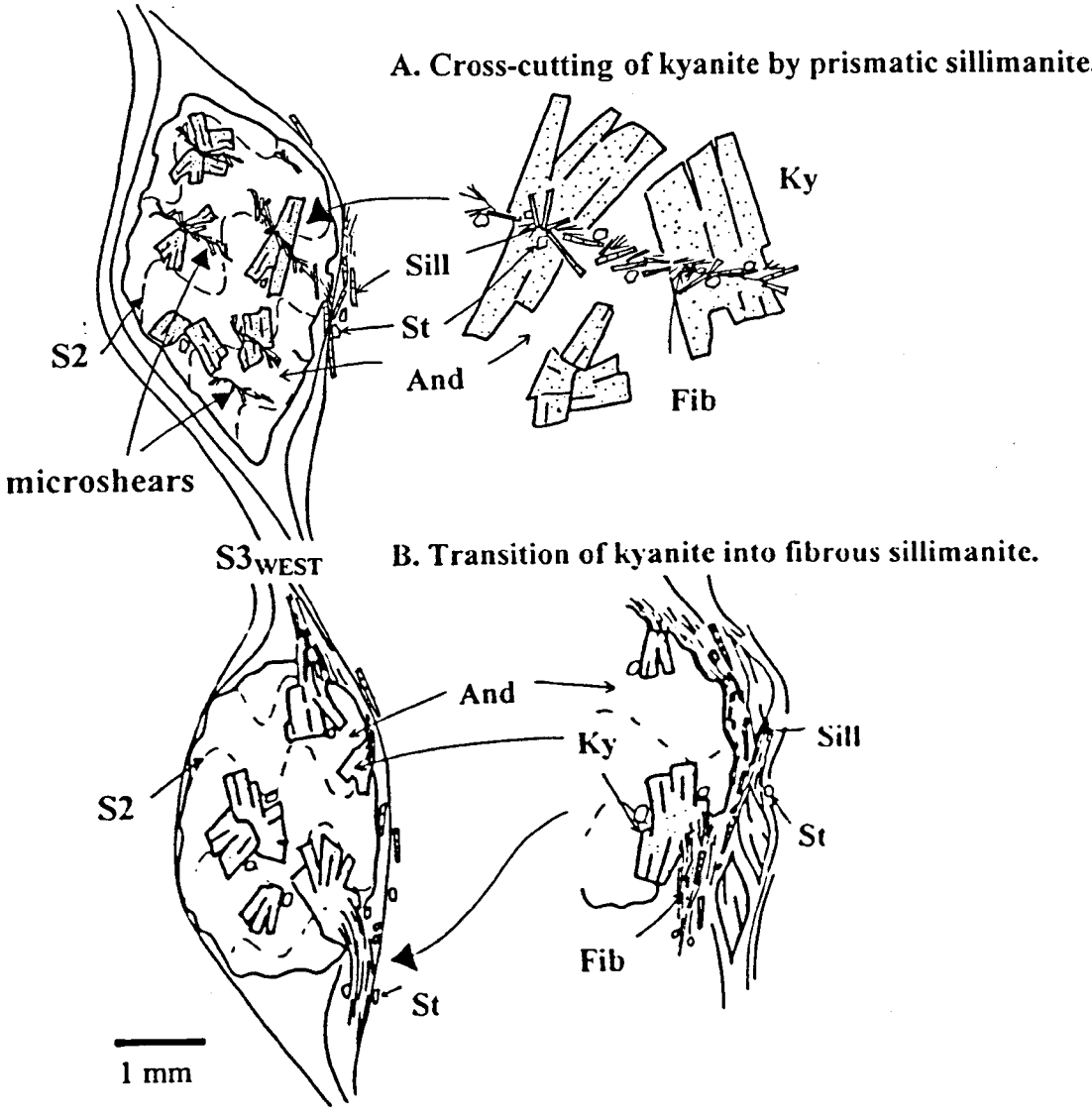

3.4.3 $D4_{WEST}$ retrogressive deformation

The effects of $D4_{WEST}$ retrogressive deformation are characterised by the development of penetrative closely-spaced (millimetre scale) fabrics ($S4_{WEST}$) which show non-planar, anastamosing form (fig. 3.17). The fabrics comprise variable amounts of muscovite, chlorite, garnet, quartz and plagioclase, epidote and opaques. The assemblages and microstructures formed during $D4_{WEST}$ are characterised locally by a variable biotite, muscovite and chlorite content, it is apparent however that the disappearance of biotite, and a decrease in muscovite and chlorite occurs at progressively lower grades.

Garnet forms idiomorphic to subidiomorphic grains (e.g. in sample TK 158, ON 87 725) which clearly cross-cut the biotite-, muscovite-, fibrolite-, staurolite-rich $S3_{WEST}$ fabrics in pelitic domains and are interpreted as retrogressive (fig. 3.17a & 3.18a). The garnets preserve a concentric pattern which is defined by quartz inclusions. The development of garnet in similar assemblages has been attributed to the breakdown of sillimanite and biotite (e.g. Thompson, 1976; Tracey & Dietsch, 1982). In staurolite and fibrolite-bearing, biotite-absent assemblages (e.g. TK 94 158, TK 94 167c, TK 94 164), garnet porphyroblasts deflect the chlorite and muscovite-rich $S4_{WEST}$ fabrics (interpreted as products of lower grade retrogressive deformation; similar retrogressive assemblages have been described by Hollocher, 1987). In lower grade assemblages (fig. 3.18b), muscovite forms elongate aggregates of fine to medium anastomosing grains which show the development of kink bands. Quartz forms subgrains and dynamically recrystallised neoblasts which were developed during retrogressive deformation. The presence of polygonal grain boundaries suggests that they underwent later recrystallisation. Plagioclase forms medium to coarse grains which show minor marginal recrystallisation. Chlorite forms fine to medium grained aggregates which occur as stacks around quartz grains and intergrown with muscovite. Epidote is abundant, forming medium to coarse subidiomorphic grains.

Fig. 3.17 Sketch showing the range of $S4_{WEST}$ retrogressive fabrics (showing decrease in grade); a) Bt-bearing fabric overprinted by Mn-rich garnet; b) Ms-, Chl-rich fabric wrapping Mn-rich garnet; c) Ms-, Chl-rich fabric with recrystallised quartz.

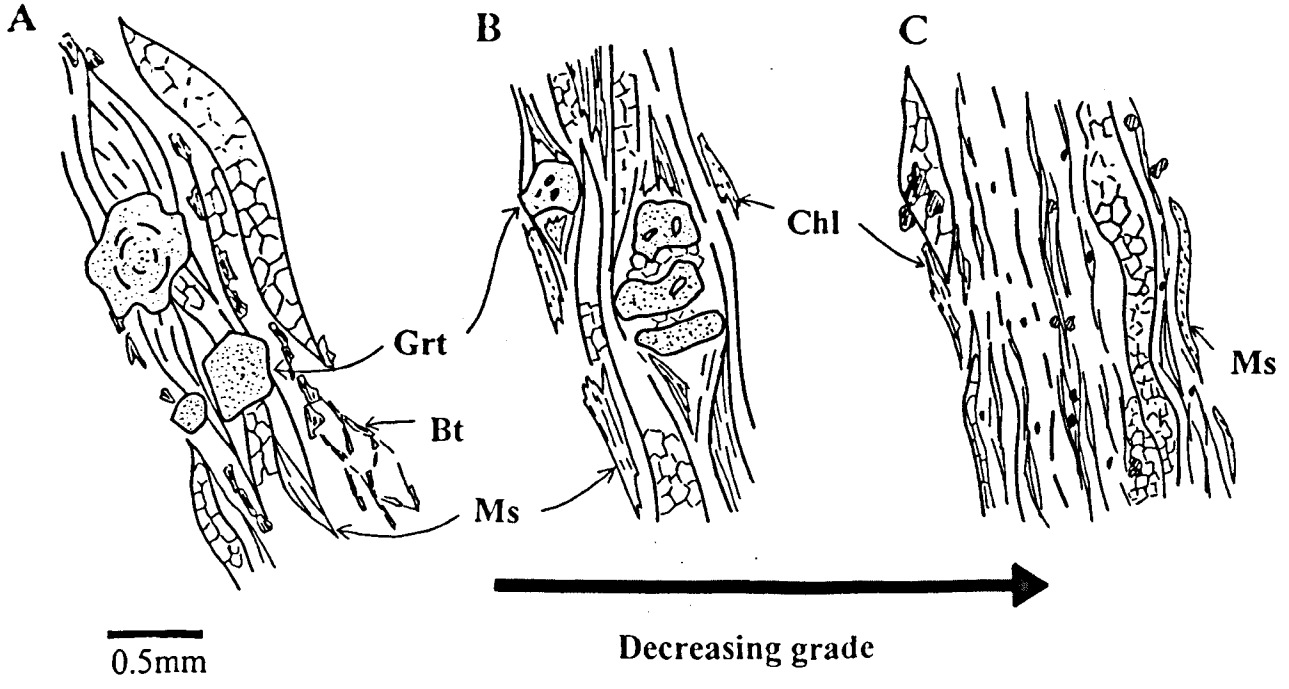

Fig. 3.18 $S4_{WEST}$ retrogressive fabrics; a) Grt porphyroblasts overprinting Bt-rich fabric; b) Ms-, Chl-rich platey fabric with $D4_{WEST}$ microfolds.

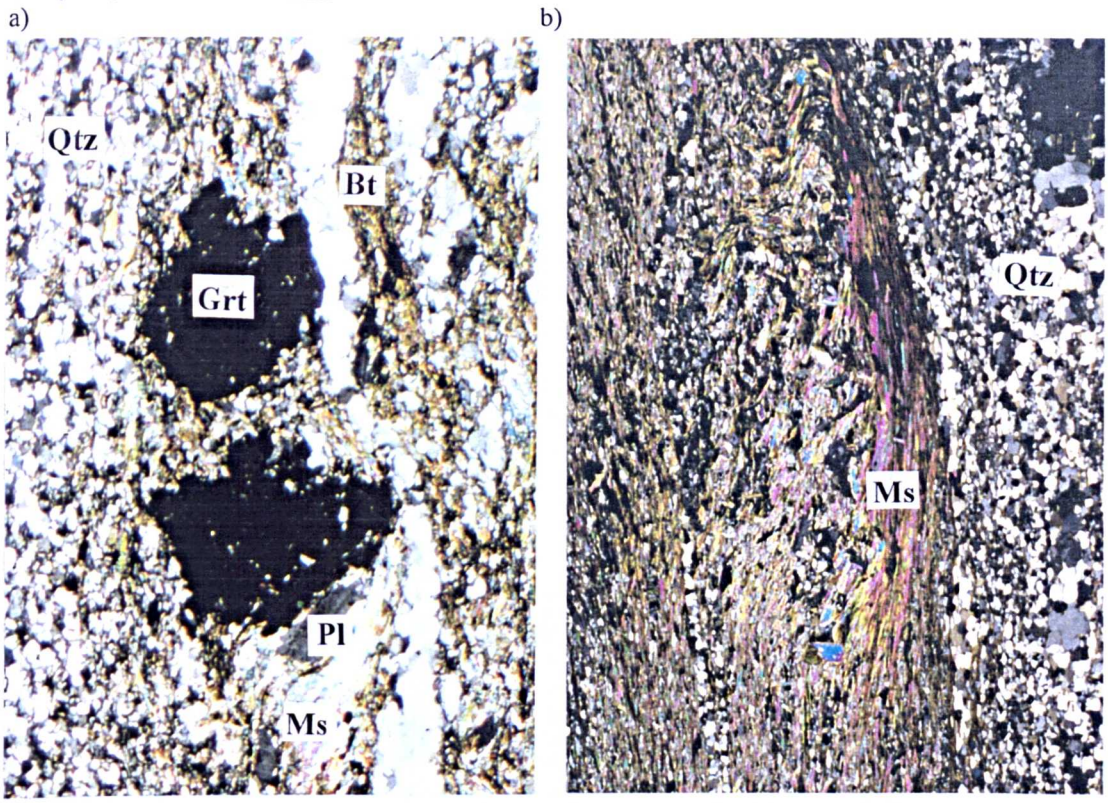

3.4.4 Contact metamorphic overprint

The contact metamorphosed metasediments adjacent to the Gander Lake Granite characteristically display a distinct coarse hornfelsed texture, pelitic lithologies show development of coarse (*c.* 2-mm scale) subidioblastic cordierite spots. The assemblages are biotite-rich, and quartzofeldspathic regions show a coarse granoblastic texture, biotite forms medium to coarse laths which clearly overprint steep $S3_{WEST}$ and crenulated S2 fabrics. Sample TK 154 (locality TCH 94 14) comprises the modal proportions cordierite 5%, biotite 5%, muscovite 13%, plagioclase 5%, quartz 70% and ilmenite 2%, and displays a coarse granoblastic texture. Subidioblastic cordierites are developed in the semi-pelitic regions where they clearly overprint the $S3_{WEST}$ pressure solution fabric, and show widespread evidence for pinitisation. Biotite forms fine to medium subidiomorphic grains which are intergrown with the quartz and commonly show replacement by chlorite.

Pelitic metasediments in the aureole of the Middle Brook Granite similarly show widespread development of a hornfelsed granoblastic texture and cordierite spots (fig. 3.19). Cordierite forms coarse xenomorphic poikiloblasts which overprint a muscovite-, chlorite-rich retrogressive fabric, and show total pinitisation. The hornfelsed assemblages comprise only small amounts of biotite. Sample TK 166a (locality, TCH 94 24) comprises muscovite 60%, biotite 10%, chlorite 8%, quartz 15%, plagioclase 5% and ilmenite 2%. Cordierite porphyroblasts are completely pseudomorphed by intergrowths of fine muscovite and sericite and clearly overprint chlorite-, muscovite-rich $S4_{WEST}$ retrogressive fabrics. Biotite forms subidiomorphic grains which are intergrown with quartzofeldspathic grains, quartz is abundant and forms coarse polygonal grains.

Fig. 3.19 Steep $S4_{WEST}$ platey fabric overprinted by large (1-2 mm scale) contact metamorphic porphyroblasts (field of view; 6.5 mm).

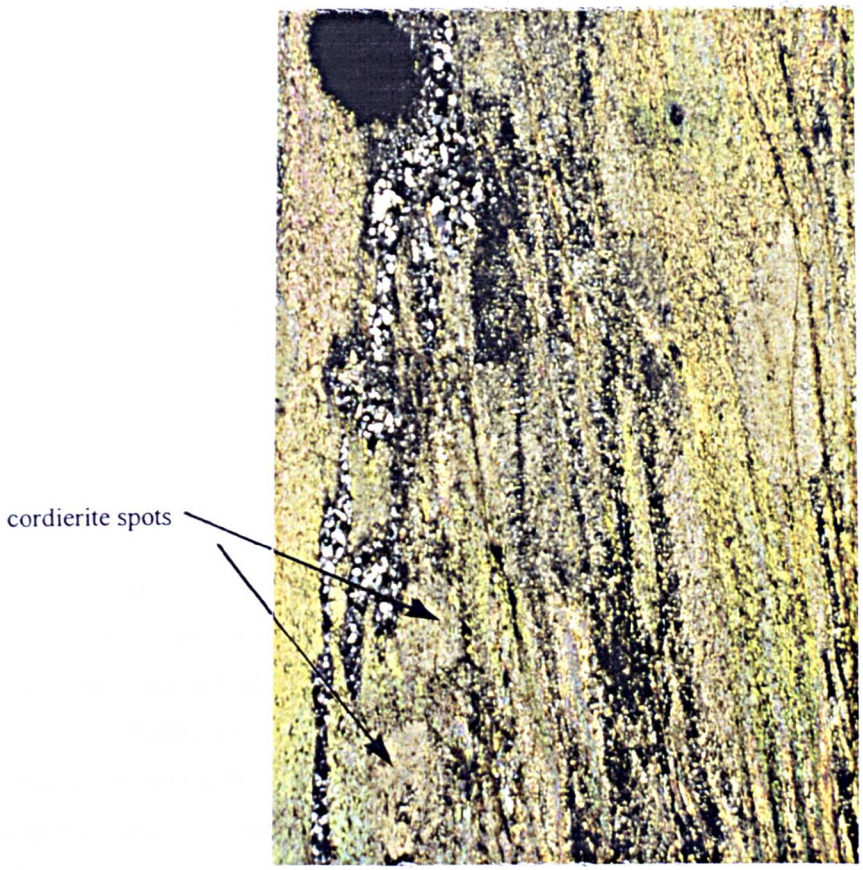

In the aureole of the Deadmans Bay Granite, metasediments similarly to those described above (adjacent to the Middle Brook Granite), show variable development of biotite, cordierite spots and andalusite porphyroblasts (e.g. locality WPSZ 3). The porphyroblasts clearly overprint the $S4_{WEST}$ micaceous pressure solution fabric. Sample TK 69 (locality WPSZ 3) comprises the following modal proportions, cordierite 8%, andalusite 4%, biotite 8%, chlorite 10%, muscovite 10%, quartz 40%, plagioclase 19% and ilmenite 1%. Both the cordierite and andalusite porphyroblasts occur within pelitic regions of S0-Sn. Cordierite grains are xenomorphic and poikilolitic with inclusions of quartz and biotite and show common marginal pinitisation wheras the andalusites form rare subidiomorphic grains. Biotite forms medium subidiomorphic grains which are intergrown with polygonal quartz and commonly show marginal alteration to chlorite.

3.5 Constraints on P-T conditions

3.5.1 Methodology

D2, $D3_{WEST}$ and $D4_{WEST}$ conditions of metamorphism within the domain have been investigated by the interpretation of the petrological-fabric relationships (previously described in section 3.4) in order

to establish mineral growth sequences and mineral forming reactions. The absence of suitable mineral assemblages excludes the use of geothermobarometry.

Fig. 3.20 Mineral reactions inferred within domain 2 assemblages.

Reaction:	Author	Reaction #
Cd[1] -rich Phen[2] + Chl → Cd-poor Phen + Chl (Al richer) + Bt	Hudson (1980)	R1
Chl + Ms → And + Bt + Qtz + H_2O	e.g. Williams (1994)	R2
Ms + Chl → St + Bt + Qtz + H_2O	Hoschek (1969)	R3
Ms + Kfs + Ab + Qtz + V → L	Thompson & Algor (1977)	R4
St + Qtz → Crd / Grt + Als + V	Bickle & Archibald (1984)	R5

3.5.2 D2

The S2 bearing sample TK 87 746b has been chosen for detailed microtextural and petrographic analysis in order to limit the conditions of relic D2. The sample is semi-pelitic and comprises the modal proportions, muscovite 35%, chlorite 10%, quartz 45% and plagioclase 10%. S2 forms a non-planar muscovite-rich foliation which anastomoses around quartz and plagioclase. Muscovite forms medium to coarse grained laths, quartz and plagioclase are fine to medium grained. Chlorite shows fine feathery form, and occurs intergrown within muscovite. Both quartz and plagioclase show evidence for marginal ductile recrystallisation and muscovite displays brittle kinking, plagioclase grains show local sericitisation.

The presence of muscovite, chlorite and the absence of biotite suggests assemblages record mid greenschist facies conditions. The conditions are constrained to below the biotite producing reaction R1 (fig. 3.20). The ductiley deformed nature of the plagioclase limits conditions to *c.* 450 °C (i.e. above the plagioclase brittle-ductile transition; e.g. Simpson, 1985; Tullis & Yund, 1987; Gapais, 1989).

3.5.3 Prograde $D3_{WEST}$

The detailed metamorphic conditions of progressive $D3_{WEST}$ are inferred from the results of detailed study of three key samples, ON 87 746b, TK 95 108 and TK 157 which display critical mineralogical relationships (previously described in section 3.4.2).

Sample ON 87 746b is from the south of Wing Pond and contains the following modal proportions; andalusite 20%, sillimanite / fibrolite 2%, staurolite 2%, biotite 10%, muscovite 25%, quartz 25%, plagioclase 9%, chlorite 5% and ilmenite 2%. The sample displays the relationship between growth of andalusite and early stages of $S3_{WEST}$ fabric development (fig. 3.9a). S2 fabric

[1] Cd=Celedonite
[2] Phen=Phengite

preserved in the sample is muscovite-, chlorite-rich whereas $S3_{WEST}$ is biotite-, andalusite-, sillimanite- and muscovite-rich. The andalusites contain inclusions of quartz and rare muscovite and biotite, muscovite grains display curved resorbed edges and are aligned parallel to quartz inclusions, whereas biotites commonly have sharp boundaries and cross-cut the inclusion trails.

Sample TK 95 108 is from the Trans Canada Railway section and shows the development of kyanite within andalusite porphyroblasts. The sample comprises the modal proportions, andalusite 10%, kyanite 15%, sillimanite / fibrolite 6%, staurolite 4%, biotite 13%, muscovite 25%, quartz 20%, plagioclase 5% and ilmenite 2%. Kyanite is extensively developed within the andalusites where it mimetically overgrows inclusion trails (fig. 3.14a), although is absent from the wrapping sillimanite-, fibrolite-rich $S3_{WEST}$ fabric. Staurolite is developed in association with kyanite, sillimanite and fibrolite. Kyanite grains within andalusites are cross-cut by sillimanite-, fibrolite-rich shears which are associated with high-strain $D3_{WEST}$.

Fig. 3.21 Representative mineral analyses for $S3_{WEST}$-bearing sample TK 157.

TK 94 157					
	Bt	Ms	Pl	St	And
	1	43	47	20	58
SiO2	34.77	44.31	60.17	26.91	34.28
TiO2	2.34	0.88	0.00	0.80	0.00
Al2O3	18.34	35.13	24.85	55.24	63.46
FeO	20.69	2.75	0.34	12.33	1.50
MnO	0.26	0.00	0.00	0.59	0.00
MgO	9.47	0.59	0.00	1.43	0.24
ZnO	0.00	0.00	0.00	0.00	0.00
CaO	0.00	0.00	5.76	0.00	0.00
Na2O	0.37	0.91	8.00	0.25	0.00
K2O	10.22	10.67	0.00	0.00	0.00
total	96.46	95.24	99.12	97.55	99.48
Cations per oxygens	*22*	*22*	*32*	*24*	*20*
Si	5.31	5.98	10.79	4.54	5.26
Al	3.30	5.59	5.25	10.99	11.48
Ti	0.27	0.09	0.00	0.10	0.00
Fe	2.64	0.31	0.05	1.74	0.19
Mn	0.03	0.00	0.00	0.08	0.00
Mg	2.16	0.12	0.00	0.36	0.05
Zn	0.00	0.00	0.00	0.00	0.00
Ca	0.00	0.00	1.11	0.00	0.00
Na	0.11	0.24	2.78	0.08	0.00
K	1.99	1.84	0.00	0.00	0.00
XMg	0.45				
XK	0.95				
XAn			0.28		
XAb			0.72		

Sample TK 157 displays minor development of kyanite within andalusites however is characterised by the presence of a highly evolved $S3_{WEST}$ fabric (types 5-6 modified after Bell &

Rubenach, 1983). The rock contains andalusite 15 %, kyanite 2 %, sillimanite 8 %, staurolite 4 %, biotite 25%, muscovite 15%, quartz 15%, plagioclase 15% and ilmenite 1%. The inclusions within the andalusites are composed of predominantly plagioclase, quartz and muscovite, plagioclase grains at their margins show a discrete concentric zonation against the andalusites. The $S3_{WEST}$ is anastomosing and comprises coarse fish of biotite and muscovite surrounded by sillimanite / fibrolite and staurolite. The andalusites are commonly cross-cut by a sillimanite-, fibrolite-, staurolite-rich shear fabric (also seen in sample TK 95 108), and in places are boudinaged along $S3_{WEST}$. The samples TK 95 108 and TK 157 contain evidence for mylonitic deformation shown by strained quartz grains which show evidence for partial recrystallisation, micas show evidence for kinking. For representative mineral compositions of $D3_{WEST}$ assemblages from sample TK 157 see fig. 3.21 and for full results Appendix A. Biotite has X_{Mg} values between 0.44 and 0.46, composition of plagioclase is X_{An} 0.28-0.29.

The absence of chlorite from the $S3_{WEST}$ fabrics, and the presence of resorbed muscovite inclusions within the andalusites, suggests that these phases were consumed during the development of andalusite. Textural relationships also show the presence of biotite along $S3_{WEST}$ in association with andalusite, and its absence from S2. The concentric zoned nature of the rare inclusions trails of plagioclase within andalusites (fig. 3.8c, sample TK 157) may suggest that their breakdown in part played a role in the production of andalusite. However, the majority of relationships suggest that andalusite was produced through the following continuous reaction:

$$Chl + Ms \rightarrow And + Bt + Qtz + H_2O \qquad (R2)$$

This andalusite producing reaction has previously been recognised in similar rocks (e.g. Rubenach, 1992; Williams, 1994). The development of staurolite within the chlorite-poor, biotite-rich $S3_{WEST}$ assemblages suggests that the production of staurolite occurred through the reaction:

$$Ms + Chl \rightarrow St + Bt + Qtz + H_2O \qquad (R3)$$

(Hoschek, 1969).

The association of staurolite with kyanite within the $D3_{WEST}$ assemblages provides evidence that the polymorphic transition of andalusite to kyanite occurred broadly synchronous with the development of staurolite. These relationships can only be reconciled with the aluminosilicate phase boundaries of Richardson *et al.* (1969), and the requirement that they occurred simultaneously limits prograde P-T conditions to *c.* 550 °C and 4.8 kbar (fig. 3.24). The absence of kyanite from the $S3_{WEST}$ wrapping fabrics together with the cross-cutting of kyanite by the sillimanite-rich shear fabric within pseudomorphed andalusites suggest that peak $D3_{WEST}$ occurred within the stability field of sillimanite (Richardson *et al.* 1969). The assemblages do not display evidence for partial melting therefore

peak conditions are constrained by the limits imposed by the kyanite → sillimanite phase boundary combined with the metapelitic solidus:

$$Ms + Kfs + Ab + Qtz + V \rightarrow L \qquad (R4)$$

(Thompson & Algor, 1977).

This places an upper limit on P-T conditions to *c.* 650 °C and 5.5 kbar (fig. 3.24), further constraint is given by the position of the staurolite-out reaction:

$$St + Qtz \rightarrow Crd / Grt + Als + V \qquad (R5)$$

(Bickle & Archibald, 1984).

Fig. 3.24 shows the reaction equilibria inferred from the $D3_{WEST}$ assemblages described above, which constrain the P-T conditions during progressive deformation.

3.5.4 Retrograde $D4_{WEST}$

A range of retrogressive assemblages have been analysed in order to assess the retrograde portion of the P-T path. Two garnet-bearing samples TK 158 and ON 87 725 were chosen for detailed microstructural and petrographic study.

Sample ON 87 725 is from the east shore of Wing Pond, and comprises the following modal proportions, garnet 3%, biotite 20%, muscovite 30%, chlorite 5%, quartz 35%, plagioclase 5%, ilmenite 1% and epidote 1%. The retrogressive biotite-, muscovite-rich $S4_{WEST}$ fabric is both overprinted and in places deflected by subidioblastic garnets (figs. 3.17 & 3.18). Sample TK 158 shows a similar assemblage but in contrast to sample ON 87 725 the $S4_{WEST}$ chlorite-, mica-rich fabric anastomoses around the subidioblastic garnets. Sample TK 158 is from the Trans Canada Highway section near Square Pond, and comprises the modal proportion, garnet 4%, biotite 10%, muscovite 5%, chlorite 10 %, quartz 45%, plagioclase 16%, ilmenite 4 % and epidote 6 %. In both samples, the biotite grains show evidence for kinking and marginal recrystallisation, and both quartz and plagioclase grains show evidence for marginal recrystallisation. Representative mineral analyses of assemblages are presented in fig. 3.22 and full analyses are in Appendix. A. Biotites are extensively retrogressed, unaltered grains in sample ON 87 725 have X_{Mg} values *c.* 0.43. The garnets are characterised by high X_{sps} values which range between 0.2 (in sample ON 87 725) and 0.45 (in sample TK 158). Plagioclase has X_{Ab} values of 0.85 and 0.62 in samples ON 87 725 and TK 125 respectively. Chlorite shows X_{Al} values of 0.9 and 0.33 and X_{Mg} values of 0.46 and 0.65 in samples ON 87 725 and TK 157 respectively. Epidote in sample TK 158 has Ps content *c.* 0.51.

Fig. 3.22 Representative mineral analyses for $S4_{WEST}$-bearing samples ON 87 725 and TK 158.

	Grt		Bt	Chl		Pl		Ep
	ON87725	TK158	ON87725	ON87725	TK158	ON87725	TK158	Tk158
Analysis:	1	1	1	25	9	23	27	15
SiO2	36.48	35.87	35.09	43.53	30.35	63.33	58.30	37.04
TiO2	0.23	0.00	1.93	0.53	0.92	0.11	0.00	0.00
Al2O3	20.70	20.39	17.93	32.07	18.50	22.67	26.56	21.20
FeO	31.36	18.84	21.00	2.72	18.17	0.36	0.00	15.84
MnO	8.84	20.81	0.25	0.00	0.46	0.00	0.00	0.18
MgO	2.33	2.41	9.03	1.31	18.98	0.00	0.00	0.00
ZnO	0.00	0.00	0.00	0.00	0.00	0.00	0.00	0.00
CaO	1.51	2.28	0.00	0.00	0.15	3.36	7.98	24.28
Na2O	0.00	0.00	0.40	0.90	0.40	10.59	7.15	0.00
K2O	0.00	0.00	9.88	10.48	0.98	0.07	0.00	0.00
total	101.45	100.60	95.51	91.54	88.91	98.27	99.99	98.54
Cations per O	*24*		*22*	*28*		*32*		*12.5*
Si	5.90	5.85	5.41	7.80	6.14	11.19	10.42	3.07
Al	3.95	3.92	3.26	6.77	4.41	4.72	5.60	2.07
Ti	0.00	0.00	0.22	0.07	0.00	0.01	0.00	0.00
Fe	4.24	2.57	2.71	0.41	3.07	0.05	0.00	1.10
Mn	1.21	2.87	0.03	0.00	0.08	0.00	0.00	0.01
Mg	0.56	0.59	2.07	0.35	5.72	0.00	0.00	0.00
Zn	0.00	0.00	0.00	0.00	0.00	0.00	0.00	0.00
Ca	0.26	0.40	0.00	0.00	0.03	0.64	1.53	2.15
Na	0.00	0.00	0.12	0.31	0.16	3.63	2.48	0.00
K	0.00	0.00	1.94	2.39	0.25	0.02	0.00	0.00
Xgrs	0.01	0.06						
Xsps	0.23	0.45						
Xprp	0.09	0.09						
Xalm	0.67	0.40						
XAn						0.15	0.38	
XAb						0.85	0.62	
XAl				0.90	0.33			
XMg	0.12	0.19	0.43	0.46	0.65			
XFe	0.88	0.81						
XK			0.94					
Ps								0.51

The presence of garnet, biotite and chlorite-bearing assemblages is indicative of upper greenschist facies conditions within the garnet zone *c.* 500-550 °C and 2 kbar (similar Barrovian assemblages have previously been extensively described e.g. Harte & Hudson, 1979). The Mn-rich nature of the garnets (shown by the high X_{sps} values) indicates that they are retrogressive in origin (e.g. Harte & Hudson, 1979), suggesting that these assemblages formed at lower mid-greenschist facies conditions. The chloritised nature of the mica margins suggests that assemblages also record retrogression at lower greenschist facies. The ductiley deformed nature of plagioclase indicates that assemblages formed at temperatures *c.* 450 °C above its brittle-ductile transition. The marginally recrystallised nature of the micas and the development of kink bands is also characteristic of deformation at mid to upper greenschist facies conditions (e.g. Simpson, 1985; Tullis & Yund, 1987; Gapais, 1989; Tribe, 1995).

Fig. 3.23 Summary of the sequence of mineral development during $D3_{WEST}$ and $D4_{WEST}$ in domain 2.

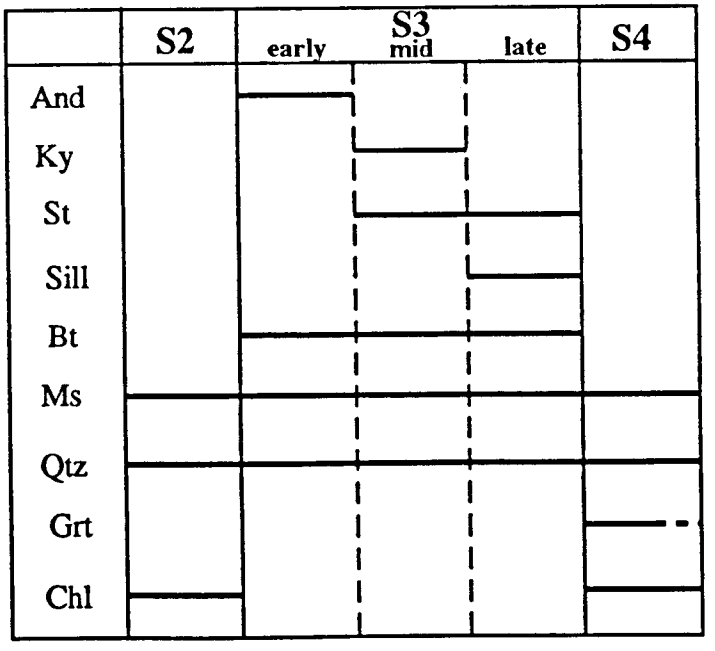

3.6 Constraints on timing of deformation and metamorphism

The flat-lying folds which deform S0-Sn and the S1 fabric are correlated with regional D2

Fig. 3.24 P-T-t-d evolution path for domain 2 from results of petrological studies.

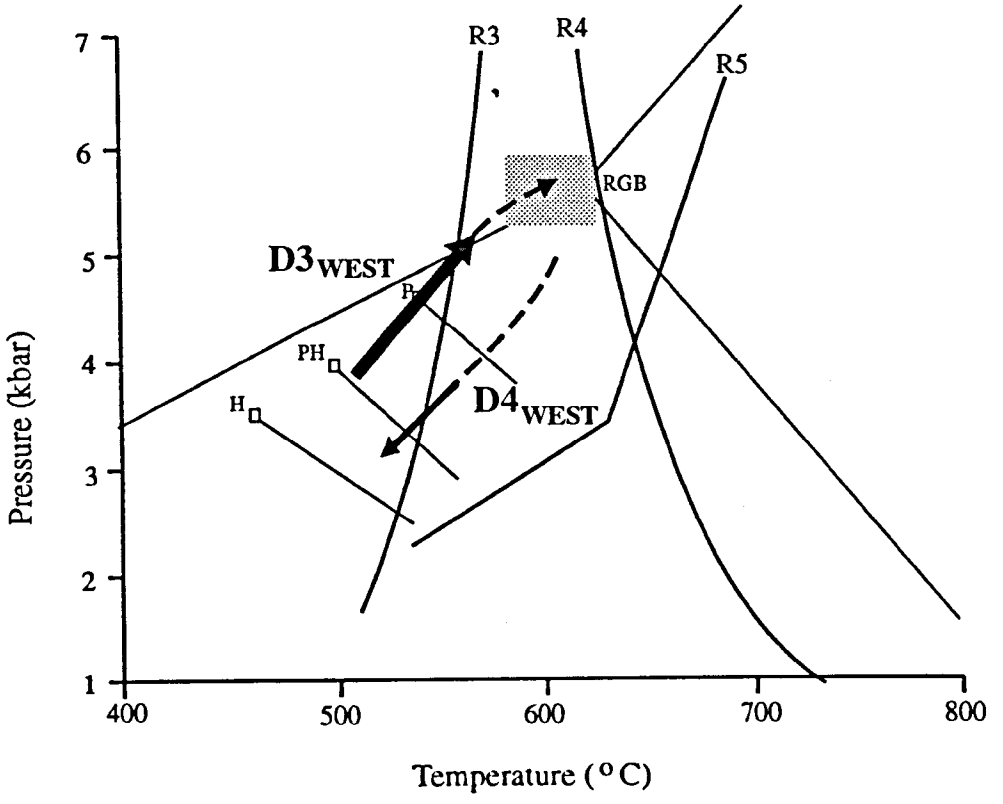

Shaded box shows peak P-T conditions. Reactions on grid; R3) St-in, Hoschek (1969); R4) metapelitic solidus, Thompson & Algor (1977); R5) St-out, Bickle & Archibald (1984). Al2SiO5 stability data; RGB, Richardson et al. (1969); H, Holdaway (1971); P & H, Pattison & Harte (1985); P, Pattison (1989).

deformation. D2 assemblages are deformed by $D3_{WEST}$ structures which form a series of upright folds with associated steep axial planar amphibolite facies fabrics. $D3_{WEST}$ assemblages are cross-cut in the west of the domain by the unfoliated Gander Lake Granite whose margins contain metasedimentary blocks, which display a deformed S2 pin-stripe fabric. Contact effects from the granite recrystallise metasediments in the aureole, producing a granoblastic hornfels texture and contact metamorphic spots (K-Ar dates on biotite give an age *c.* 360 Ma; compilation of Mandeville, see Kerr *et al.* 1994). In the north of the domain, the development of $S3_{WEST}$ fabrics is post-dated by intrusion of the unfoliated Deadmans Bay Granite which produces contact metamorphic spotting and hornfelsing of the assemblages. High precision U-Pb age data (on accessory zircon, monazite and titanite) from the Deadmans Bay Granite suggest an age of emplacement of *c.* 385 Ma (Dunning *et al. in prep.*). In the centre and east of the region, $D3_{WEST}$ assemblages are subordinately overprinted by steep $S4_{WEST}$ retrogressive fabrics. The timing of $D4_{WEST}$ retrogression clearly predates the intrusion of the largely unfoliated Middle Brook Granite which adjacent to its western margin produces recrystallisation, hornfelsing and contact metamorphic spotting of low-grade $S4_{WEST}$ fabrics. The Middle Brook Granite has traditionally been interpreted as a post-tectonic Devonian pluton (e.g. Blackwood, 1977;

Colman-Sadd *et al.* 1990) however preliminary U-Pb age data (on accessory zircon and titanite) from the Middle Brook Granite (Dunning *et al. in prep*) suggest an age of *c.* 427 Ma. ^{40}Ar / ^{39}Ar data (on muscovite) from Wing Pond Shear zone assemblages (O'Neill, 1991) has given values *c.* 429 Ma.

3.7 Summary

The northeast-southwest trending domain comprises a deformed assemblage of Gander Group metasediments, which are characterised by the development of prograde $D3_{WEST}$ fabrics which overprint regional D2 structures and fabrics, and are themselves overprinted by retrogressive $D4_{WEST}$ shear fabrics. Planar structures and fabrics in the domain are dominantly steep, whereas the subordinately developed mineral lineation is variably plunging.

$D3_{WEST}$ deformation has been focused into narrow (100m wide), high-strain zones, which broadly correspond to the more pelitic lithologies. The deformation is progressive in style and typified by the development of upright open folds which show evidence for refolding and interference. The associated steep axial planar fabrics are commonly mylonitic and display a predominantly sinistral sense of shear. The region is metamorphically complex, and is characterised by the development of the aluminosilicate polymorphs andalusite, kyanite and sillimanite within prograde $D3_{WEST}$ assemblages (fig. 3.23). Prograde assemblages record a clockwise prograde P-T path, passing from andalusite → kyanite → sillimanite grade and culminating in peak metamorphism *c.* 650 °C and 5.5 kbar (fig. 3.24). The timing of $D3_{WEST}$ post-dates the D2 obduction of Dunnage over the Gander Lake Subzone (dated as *c.* 470 Ma; Williams & Stevens, 1974; Williams, 1984; Colman-Sadd *et al.* 1992a).

Retrogression in domain 2 is characterised by the development of steep anastomosing $S4_{WEST}$ shear fabrics which locally transpose the limbs of $F3_{WEST}$ folds. These form the pervasive fabric in local narrow (2-15 metre wide) high-strain zones and in a kilometre wide high-strain tract in the east of the domain. The retrogressive fabrics show variable shear sense, and are predominantly dextral with a subhorizontal mineral lineation. The fabrics are characteristically micaceous, and of greenschist facies, assemblages locally show the development of Mn-rich garnet, however are typically muscovite-, chlorite-rich. Retrograde fabrics are overprinted by contact metamorphism from the Middle Brook Granite which is unfoliated, and has been variably interpreted as a post-tectonic Devonian (e.g. Blackwood, 1977; Colman-Sadd *et al.* 1990), and a Silurian (*c.* 427 Ma; Dunning *et al. in prep.*) pluton.

Chapter 4.

Domain 3: The Central Gander Metasedimentary Belt

Chapter 4. Domain 3: The Central Gander Metasedimentary Belt

4.1 Introduction

The Central Gander Metasedimentary Belt is a northeast-southwest trending tract (fig. 1.9), situated between the Wing Pond Shear Zone (domain 2) and the Eastern Gander Migmatite Belt (domain 4). The width of the domain is laterally variable measuring *c.* 7 km in the north, and a narrower 3-5 km in the south. The domain comprises variably deformed and metamorphosed Gander Group metasediments forming a continuous sequence which shows an eastward increase in structural complexity and metamorphic grade, and passes laterally into partially melted migmatites (Blackwood, 1978). The western margin of the domain is loosely defined by the absence of the steep mylonitic fabrics (of the adjacent domain 2), and the presence of low grade subhorizontal assemblages. The eastern margin of the domain is marked by the boundary between metasediments and the foliated North Pond Granite (Jayasinghe, 1978) in the north, and metasediments and migmatites in the south (Blackwood, 1978). This margin coincides with steep mylonitic northeast-southwest trending fabrics (Blackwood, 1978; Jayasinghe, 1978; Holdsworth, 1994a) which display an associated predominantly subhorizontal mineral lineation. The metasediments in the domain are bounded in the northeast by the unfoliated Deadmans Bay Granite.

The predominant composition of the Gander Group metasediments is semi-psammitic with intercalations and layers of garnet-bearing pelitic and semi-pelitic lithologies, and rare layers and lenses of calc-silicates (e.g. Blackwood, 1977, 1978). The characteristic rock type is a grey psammitic gneiss with a fine (1-3 mm scale) pin-stripe fabric (Square Pond Gneiss of Blackwood, 1977, 1978).

The aims of this chapter are to establish through field, microtextural and petrographic-fabric analysis, and the application of geothermobarometry, the conditions of prograde, peak and retrograde metamorphism in the domain and hence enable the construction of a P-T-t-d path.

4.2 Structure and metamorphism

The deformation within the region is heterogeneous (e.g. O'Neill, 1991) and shows an overall eastward increase in complexity and metamorphic grade, accompanied by the intensification of a regional subhorizontal northeast-southwest mineral lineation (Kennedy & McGonigal, 1972; Hanmer, 1981; O'Neill, 1991; Holdsworth, 1994a). Holdsworth (1994a) suggested that the regional structure is dominated by effects of progressive deformation which overprint regional D1/D2 structures and fabrics in the west and intensify eastwards, and noted the presence of localised high strain zones with northeast-southwest trending mylonitic fabrics in the east. D2 structures form flat-lying folds which display axial planar S2 fabrics. S2 forms a low grade pressure solution (pin-stripe) cleavage

(Kennedy & McGonigal, 1972; Hanmer, 1981; O'Neill, 1991; Holdsworth, 1994a). The overprinting progressive deformation (termed $D3_{EAST}$), forms upright folds in the west and close to tight structures in the east which became refolded during the deformation which gave rise to the northeast-southwest trending mineral lineation (Holdsworth, 1994a).

Prograde metamorphism in the region has produced sillimanite-bearing paragneissic metasediments which pass eastwards into migmatites of the adjacent domain 4, these show effects of progressive amphibolite facies deformation (e.g. Blackwood, 1978; Holdsworth, 1994a). The boundary between the paragneiss and migmatites ('the migmatite front', Blackwood, 1978) appears to correlate with a change in lithology of metasediments from dominantly psammitic to dominantly pelitic (e.g. Holdsworth, 1994a; D'Lemos & Holdsworth, 1995). Detailed field studies have shown however that the migmatite front is obscured by the presence of retrogressive ($D4_{EAST}$) high-strain zones where prograde ($D3_{EAST}$) folds and fabrics become totally transposed by steep micaceous fabrics. These zones display an intense subhorizontal regional mineral lineation, and are characterised by the development of micaceous platey sinistral shear fabrics comprising shear bands and σ-porphyroclasts (Holdsworth, 1994a). The eastwards increase in metamorphic grade of the $D3_{EAST}$ metasedimentary assemblages across the region is shown by a coarsening of grain size, the pervasive development of biotite, the local development of garnet and the development of sillimanite in the metasediments (e.g. Holdsworth, 1994a). The metasediments in domain 3 are locally cross-cut by metre scale, northeast-southwest trending dextral brittle faults.

Fig. 4.1 SE-NW section showing the structural characteristics across domain 3, NPG=North Pond Granite (from Holdsworth, 1994a).

Fig. 4.2 Locality / sample map for domain 3.

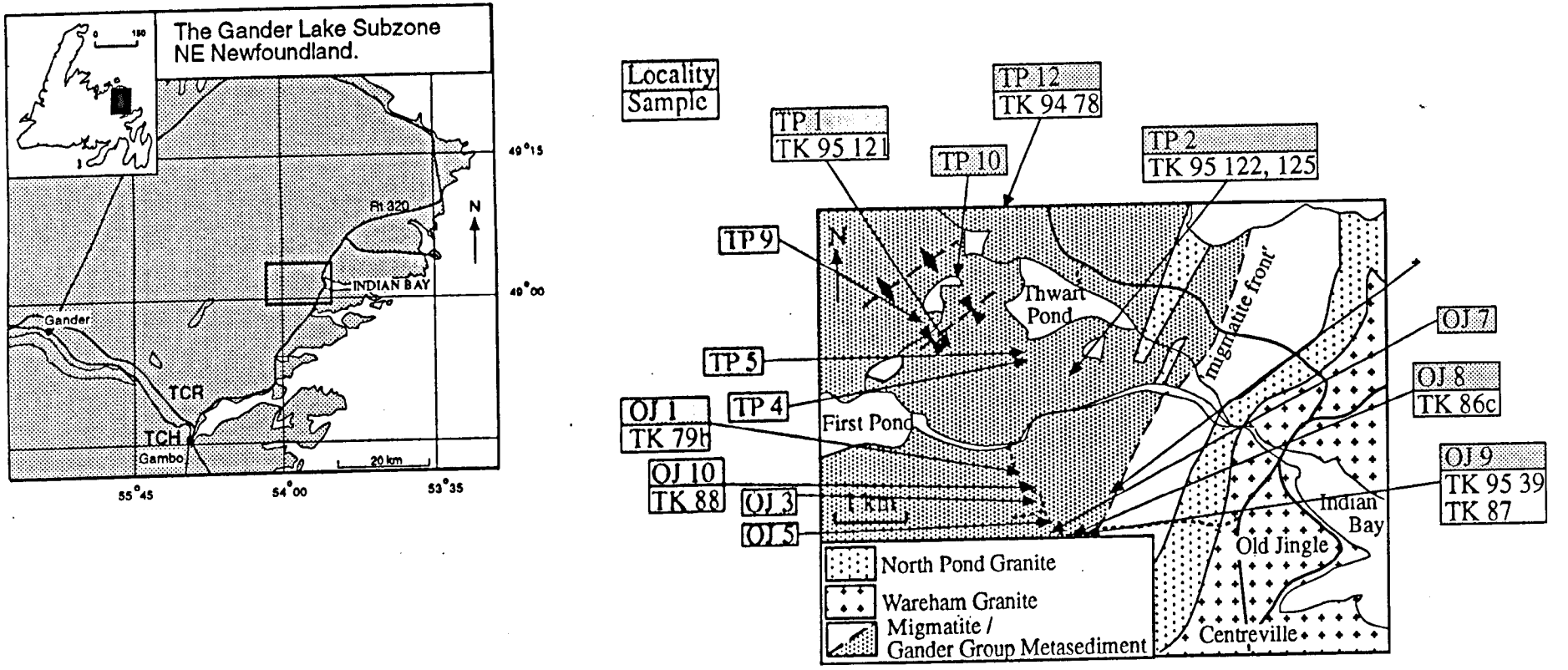

In this study, the relationships between deformation and metamorphism in the metasediments has been assessed by detailed field study along the key traverses at Thwart Pond and Old Jingle (fig. 4.2), combined with widespread petrologic study and geothermobarometric study of key assemblages. The field access into the northwest, southwest and south-central regions of the domain is poor and hence field relationships, including the relationship between metasediments and the Middle Brook and Deadmans Bay granites, are unconstrained.

4.3 Field relationships

In the west of the domain, discrete layers of S0-Sn fabric (corresponding to transposed bedding variation) which display a subparallel, fine S1 fabric are deformed by flat-lying easterly verging folds (fig. 4.1, loc. A). These folds are termed D2 and display development of an S2 axial planar pressure solution cleavage. Development of S2 is pervasive and S1 is only rarely preserved within its microlithons. The F2 folds are deformed in the west by upright open folds, deformation has locally produced refolding of F2 folds. The upright folds are termed $F3_{EAST}$ and display subordinate development of a steep axial planar $S3_{EAST}$ fabric (fig. 4.1, loc. B & C). The development of these fabrics intensifies eastwards where they thoroughly transpose pre-existing D2 structures. Prograde $D3_{EAST}$ fabrics are overprinted locally and in the eastern margin of the domain, by lower grade steep micaceous shear fabrics termed $S4_{EAST}$ (fig. 4.3).

Fig. 4.3 Microstructural field, and petrographic characteristics of prograde $S3_{EAST}$ and retrograde $S4_{EAST}$.

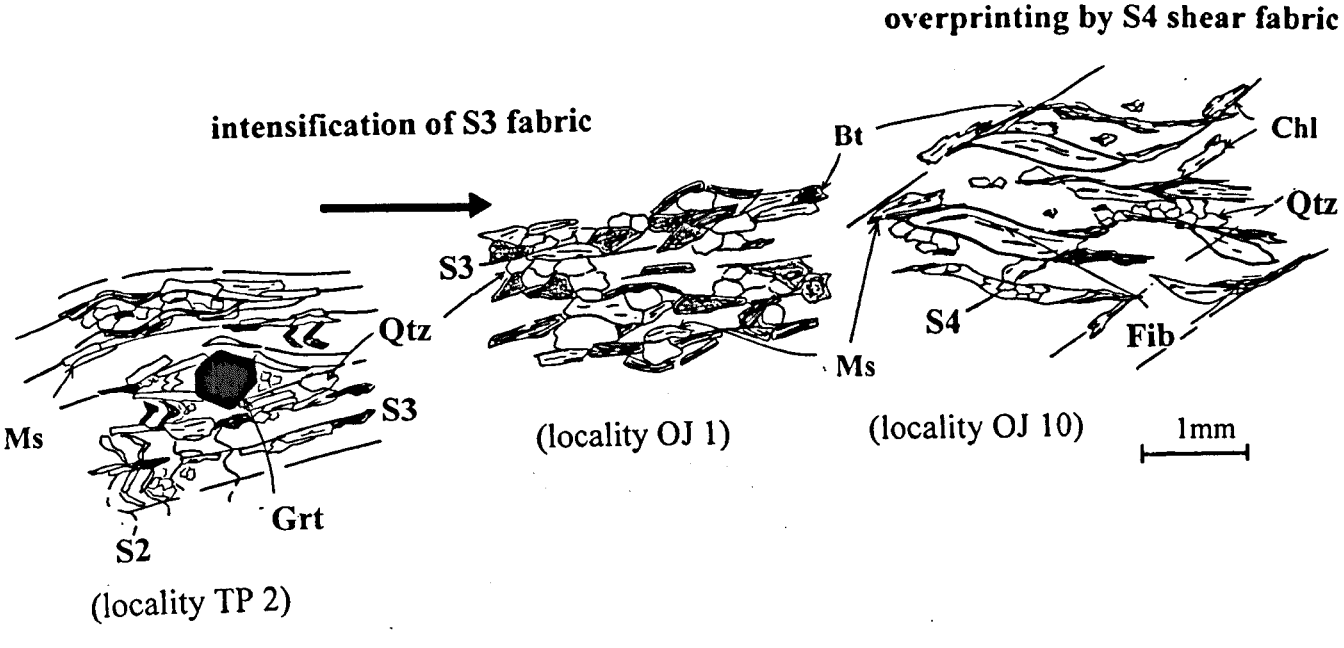

4.3.1 Pre-D2 structures and fabrics

The preservation of pre-D2 fabrics is rare being largely restricted to the west of the domain where rocks show limited effects of overprinting by $D3_{EAST}$ (fig. 4.1, loc. A). Northwest (*c.* 2 km) of Thwart Pond, psammitic metasediments in regions of low-strain D2 (locality TP 9) preserve (0.5-1m scale) relic cross-bedding (fig. 4.4). Bedding (1-50 cm scale) and fine scale bedding laminations (millimetre scale) are well defined (i.e. locality TP 1) by subtle mineralogical variation in mica and quartzofeldspathic mineral content. In regions of low $D3_{EAST}$ strain (i.e. localities TP 1, TP 9), local way-up criteria of metasediments is given both by fine (1-4 mm scale) graded bedding and cross-bedding. Further east where $D3_{EAST}$ strain increases, bedding structures become transposed into S0-Sn fabric forming centimetre to metre scale layers of discrete lithology. Transposed calc-silicate and pelitic beds (localities TP 2, TP 4 respectively) are observed southeast of Thwart Pond. Further east towards Old Jingle (i.e. localities OJ 3, OJ 5), highly transposed lithological bedding variation is evident and is characterised by psammitic (metre scale) and semi-pelitic and pelitic layers (0.25-1m scale) in gneissic metasediments. S1 forms a millimetre scale fabric, which is orientated subparallel to S0-Sn (fig. 4.8), and is defined by aligned intergrowths of muscovite and chlorite. S1 is poorly preserved within assemblages due to its transposition by the effects of overprinting D2 and $D3_{EAST}$ deformation.

Fig. 4.4 Relic cross-bedding in psammitic Gander Group metasediment.

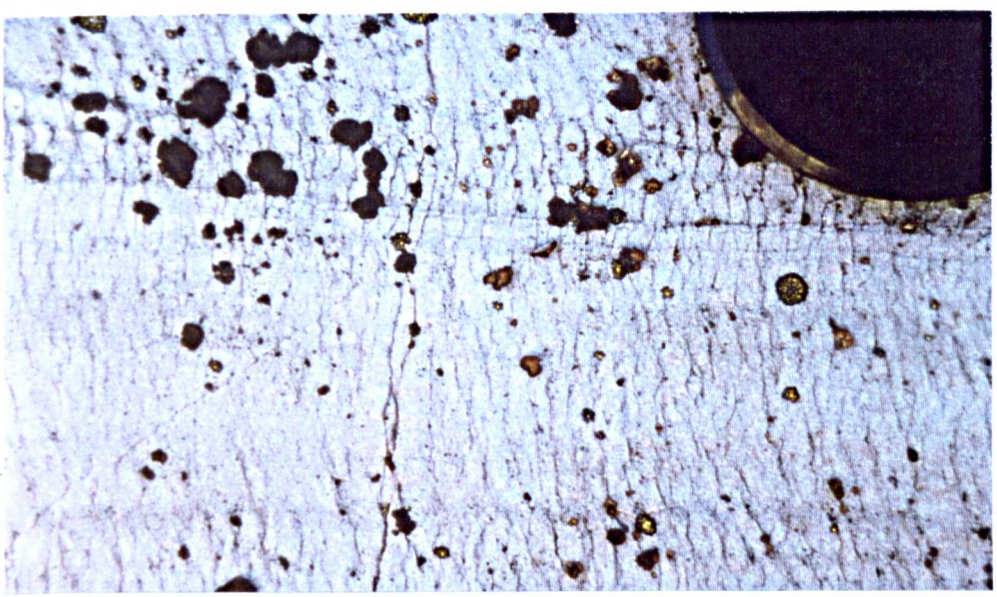

4.3.2 D2 deformation

The preservation of D2 structures and associated fabrics is similarly restricted to regions of low $D3_{EAST}$ strain observed in the west and central parts of the domain (fig. 4.1, loc. A), and preferentially occurs within psammitic and semi-psammitic lithologies. The folds deform a millimetre scale S1 fabric, and show pervasive development of a pressure solution axial planar fabric.

F2 folds and associated S2 locally occur northwest of Thwart Pond (locality TP 1) where they form flat-lying (metre scale) sheath-like structures (previously recognised by Holdsworth,

Fig. 4.5 $D3_{EAST}$ assemblages; a) steep $S3_{EAST}$ overprinting S2 pin stripe and transposed bedding S0-Sn; b) intensified $S3_{EAST}$ fabric in pelitic metasediment preserving intrafolial S2; c) sinistral $S3_{EAST}$ fabrics wrapping garnet-bearing calc-silicate pod (a: photo on side, left=up, b & c: plan view with left=north).

a)

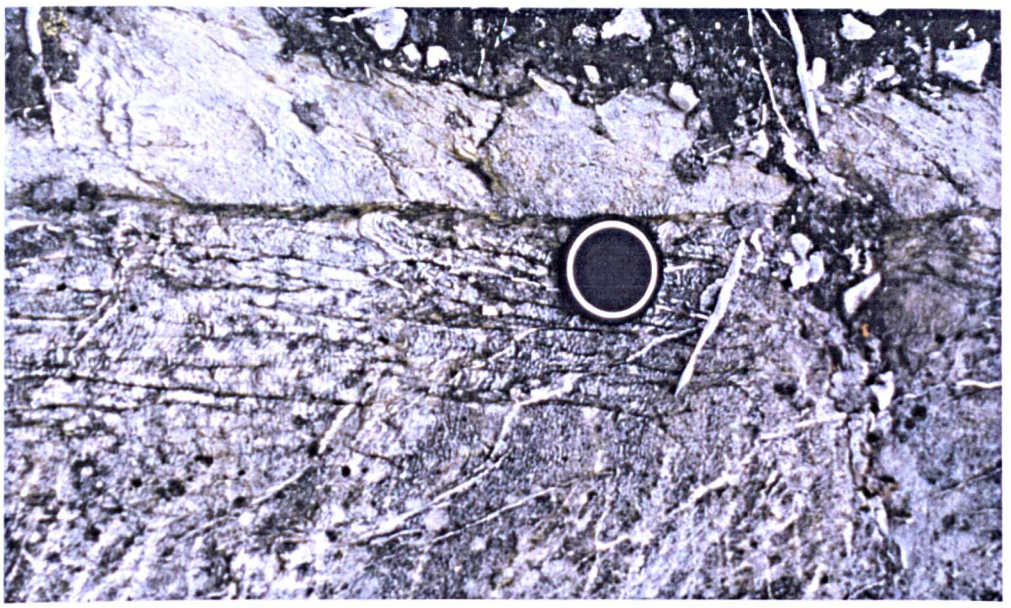

b)

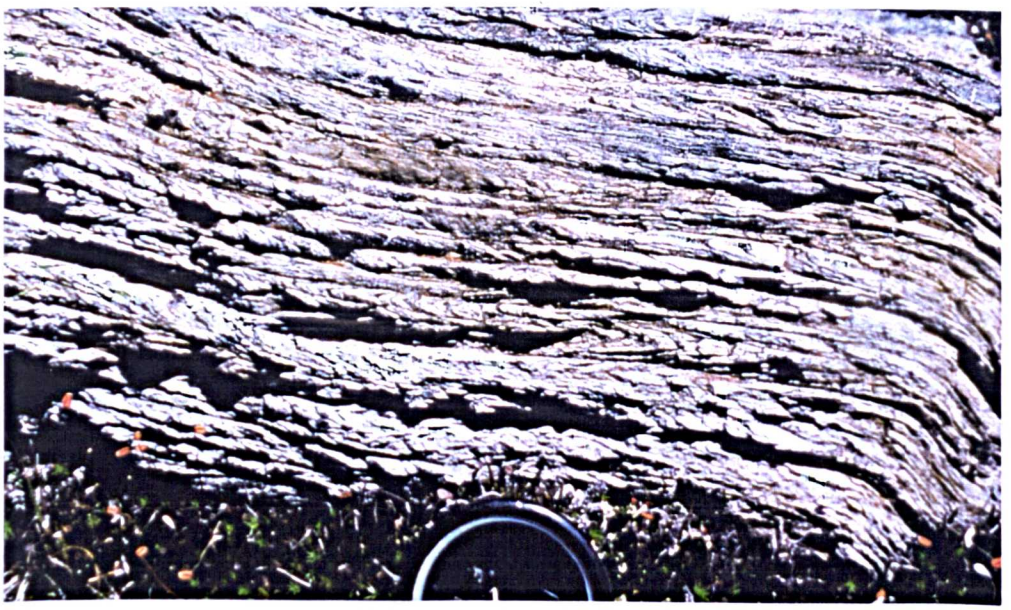

c)

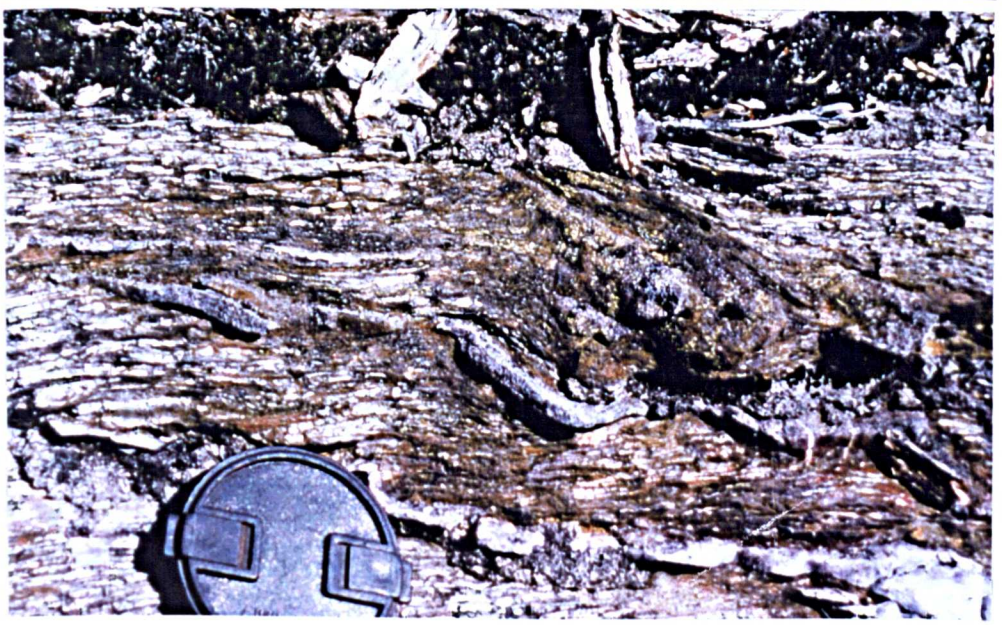

1994a) with a well developed axial planar S2 cleavage. S2 forms a closely spaced (1-3 mm) non-linear pressure solution cleavage which comprises mica-, chlorite-rich dark cleavage domains separated by pale quartzofeldspathic microlithons (fig. 4.8). Subordinate development of a northeast-southwest trending, subhorizontal mineral lineation occurs in association with D2 assemblages.

4.3.3 $D3_{EAST}$ deformation

Fig. 4.6 Detailed structural and petrographic characteristics of $D3_{EAST}$ in the Thwart Pond section (looking NE).

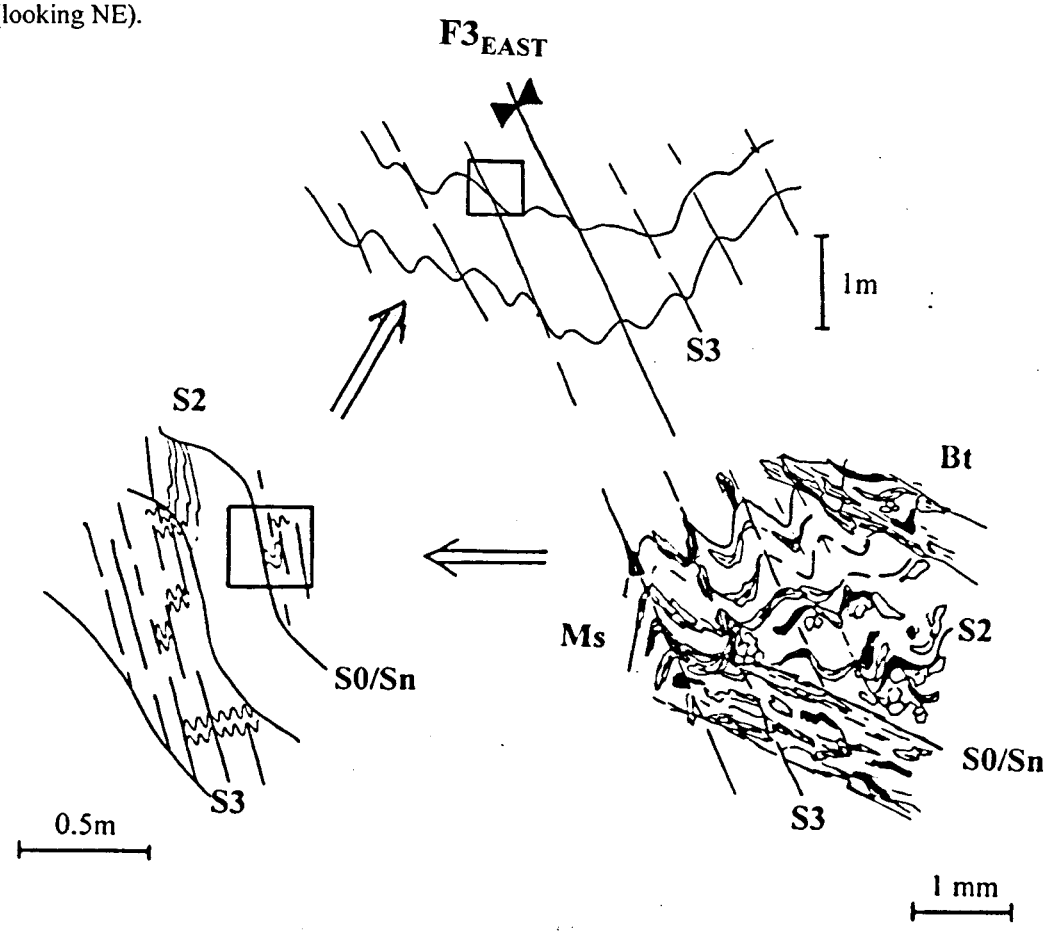

$D3_{EAST}$ structures and fabrics clearly overprint regional F2 folds forming a series of northeast-southwest trending open to tight upright folds (i.e. $F3_{EASTA}$, $F3_{EASTB}$) with variably well developed axial planar $S3_{EAST}$ fabrics. South of Thwart Pond where F2 folds are transposed by effects of $D3_{EAST}$, relic S2 fabric is preserved intrafolial to $S3_{EAST}$, the intersections between the S2 and $S3_{EAST}$ fabrics commonly form a complex herringbone cleavage patterns (fig. 4.5). In the west of the domain (southwest of Thwart Pond, localities TP 1, TP 10), $F3_{EAST}$ folds form large (10m scale) structures with subordinately developed axial planar $S3_{EAST}$ fabrics, locally the folds form (< metre scale) parasitic structures on the limbs of larger $F3_{EAST}$ structures (fig. 4.6). The cores of the folds commonly contain deformed pods and lenses of retrogressed metabasite (e.g. locality TP 10). Further east, effects of $D3_{EAST}$ become more intense as shown by a discrete tightening of folds into which are curvilinear about the regional northeast-southwest trending mineral lineation (previously

described by Holdsworth, 1994a). This is accompanied by the pervasive development of moderately to steeply southeast-dipping axial planar $S3_{EAST}$ (e.g. locality TP 2, TP 5). The western region of the Old Jingle section illustrates a continuing sequence of $D3_{EAST}$ intensification which is shown by the presence of a pervasive moderate to steep south-east dipping $S3_{EAST}$ fabric in interbanded pelites, psammites and rare metabasites (locality OJ 1).

$S3_{EAST}$ fabric (fig. 4.3) is typically non-planar, and forms a pervasive schistose (1-2 mm) fabric in pelites and semi-pelites, and a less pervasive pressure-solution pin-stripe (2-3 mm) cleavage in psammites. The fabric is defined by dark muscovite-, ± biotite-bearing cleavage domains which separate pale quartzofeldspathic microlithons. In the western and central regions of the domain (e.g. localities TP 1, TP 9), muscovite is the dominant phyllosilicate whereas further east (e.g. localities TP 5, OJ 1, OJ 3), it is accompanied by the development of biotite. The association of biotite ± muscovite with medium to coarse garnet porphyroblasts locally occurs in the central to eastern regions of the domain where garnets are clearly wrapped by the micaceous $S3_{EAST}$ fabric (fig. 4.5c). The garnet-rich horizons form discontinuous (2-10 m scale) layers and lenses which correspond to pelitic and semi-pelitic layers of S0-Sn (e.g. locality TP 2).

4.3.4 $D4_{EAST}$ deformation

Fig. 4.7 Sinistral $S4_{EAST}$ S - C shear fabrics in a) pelitic metasediment; b) North Pond Granite (plan views, a: right=NE, b: top RHS=NE).

a) b)

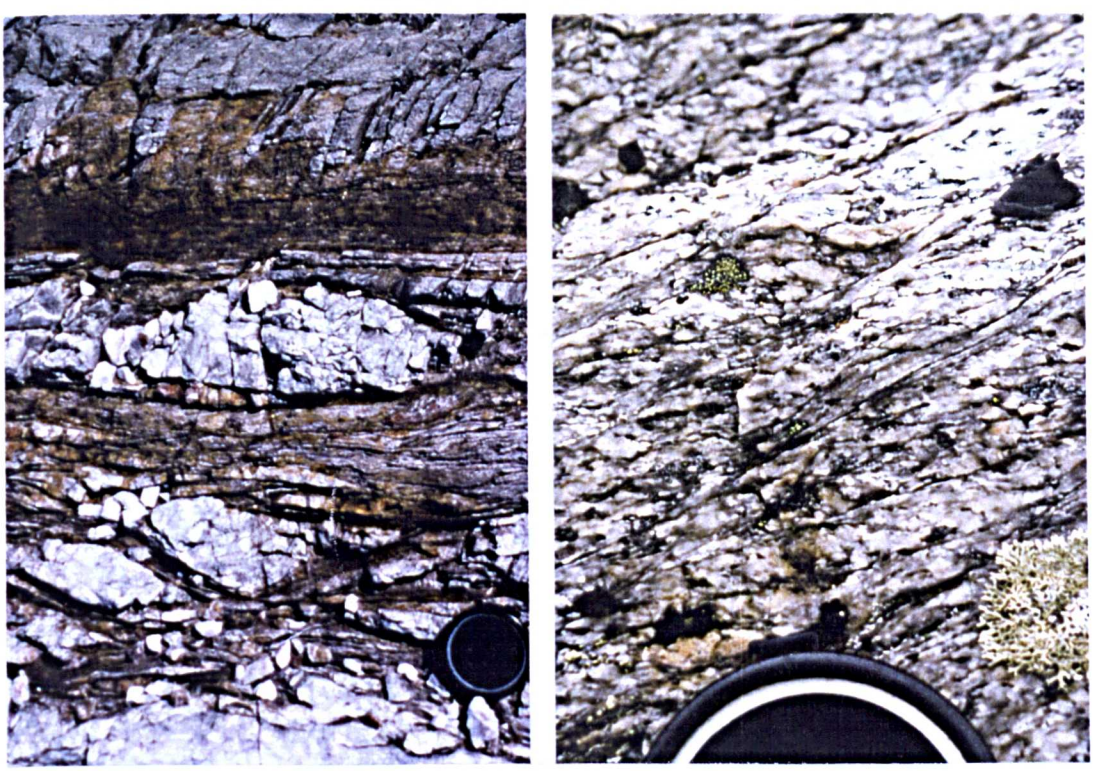

In the east of the domain, the prograde $D3_{EAST}$ assemblages are clearly transposed locally (e.g. localities OJ 3, OJ 5) and pervasively in a discrete 100m scale high-strain zone by micaceous retrogressive $S4_{EAST}$ shear fabrics (figs. 4.3 & 4.7). Effects of $D4_{EAST}$ retrogressive deformation are also contained within migmatites and both the North Pond and Wareham granites of the adjacent domain 4 (fig. 4.7b), forming a discrete (100-200m scale) northeast-southwest trending tract (seen at Old Jingle). $S4_{EAST}$ is the dominant fabric in the eastern margin of domain 3, being characterised by steep sinistral shear fabrics (e.g. localities OJ 7, OJ 10). Within the zones of $D4_{EAST}$ deformation, the pre-existing $S3_{EAST}$ foliation is thoroughly overprinted and destroyed, however, the highly transposed S0-Sn can still be recognised and is defined by discrete (centimetre to 0.5m-scale) layers of mica-rich and quartzofeldspathic mineralogy.

Associated with the $S4_{EAST}$ shear fabrics is a well developed subhorizontal mineral stretching lineation which is defined by intergrowths of aligned muscovite and chlorite The $S4_{EAST}$ fabrics form platey shear fabrics defined by 1-5 mm scale shear bands, the fabrics are predominantly defined by muscovite and biotite however in places show development of fibrolite. The shear bands wrap plagioclase σ-porphyroclasts which record a clear sinistral sense of shear.

4.4 Petrological descriptions

4.4.1 Pre-D2 structures and fabrics

Variably transposed lithological bedding variations are defined throughout the domain by distinct variations (centimetre to metre scale) in mica and quartzofeldspathic content (e.g. sample TK 95 121, locality TP 1). Bedding laminations (millimetre scale) are similarly defined by layers of dark fine to medium grained micas and pale coarse quartzofeldspathic grains. The micas show a clear preferential alignment which is subparallel to S0-Sn fabrics, and is interpreted to represent relic S1 fabric. Psammitic beds comprise quartz and plagioclase with minor muscovite and chlorite, and semi-pelitic and pelitic beds of predominately muscovite and chlorite. Calc-silicate lithologies are composed of variable amounts of biotite, muscovite, garnet, plagioclase, quartz, hornblende and opaques.

4.4.2 S2 fabric

S2 forms a well developed pressure solution cleavage which is composed of discrete quartzofeldspathic and micaceous domains (fig. 4.8). The trace of the fabric is accentuated by dark solution seams which contain pleochroic orange to brown coloured material and are planar to undulating in form. The Q domains of S2 comprise quartz, plagioclase, muscovite and chlorite and the M domains predominately of muscovite and chlorite with minor quartz (e.g. sample TK 95 121, locality TP 1). The microlithons of S2 are characterised by fine to medium intergrowths of quartz and plagioclase with coarse grains of quartz and plagioclase which are subidiomorphic, and display slight elongation subparallel to S2. Coarse quartz grains show undulose extinction and development of

internal subgrains. Cleavage domains contain minor amounts of coarse elongated quartz grains but characteristically show muscovite and chlorite grains deflected around the coarse quartz, with chlorite commonly forming stacks around the grains. In places the microlithons of the S2 fabric preserve a poorly defined crenulated relic S1 which forms a fine fabric defined by aligned muscovite and chlorite.

Fig. 4.8 S2 fabrics in a) psammitic metasediment showing discrete Q and M domains; b) semi-pelitic metasediment defined by pressure solution seams, S0-Sn defined by Chl-, Ms-rich layer and relic S1 by aligned Chl wrapping grains of Qtz (field of view; 4.5mm).

a)

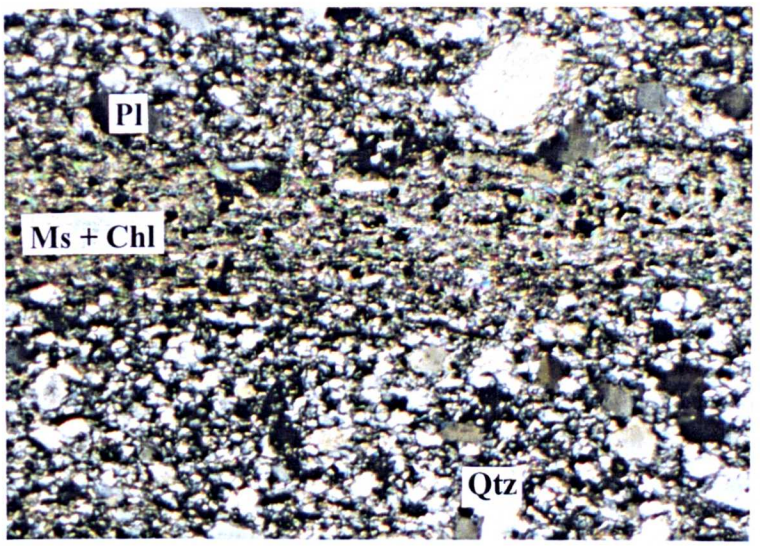

b)

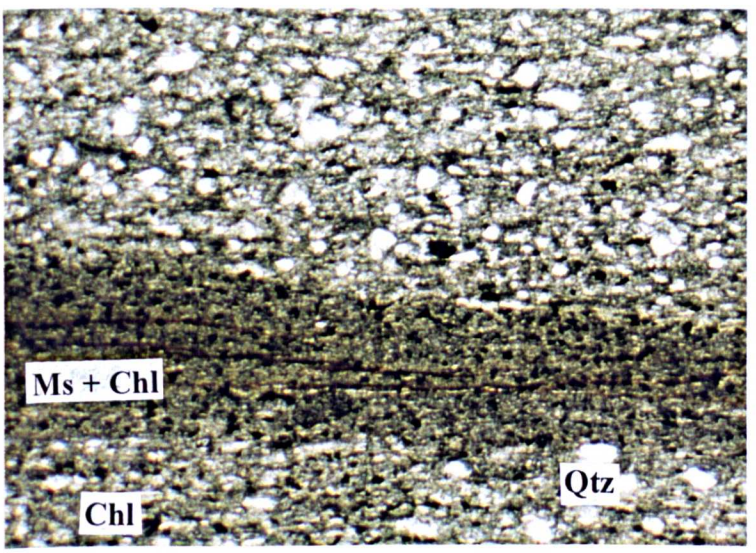

4.4.3 $S3_{EAST}$ fabric

In psammites, the $S3_{EAST}$ pressure solution pin-stripe fabric comprises Q domains which are predominately composed of quartz and muscovite and M domains of aligned muscovite and biotite, and is characterised by the presence of dark solution seams. In pelitic and semi-pelitic lithologies however (e.g. TK 95 122, TK 95 125, locality TP 2), $S3_{EAST}$ forms a spaced schistose foliation, this is

Fig. 4.9 Syn-kinematic garnets in $D3_{EAST}$ assemblages (TK 95 122); a) porphyroblasts deflecting Bt-, Ms-rich $S3_{EAST}$ showing inclusion-rich cores and asymmetric pressure shadows; b) sigmoidal-shaped inclusion trails of consistent form between individual porphyroblasts; c) sketch of garnet showing relationship between inclusion trails, $S3_{EAST}$ and pressure shadows (field of view for a = 6.5mm; b & c = 4.5mm).

a)

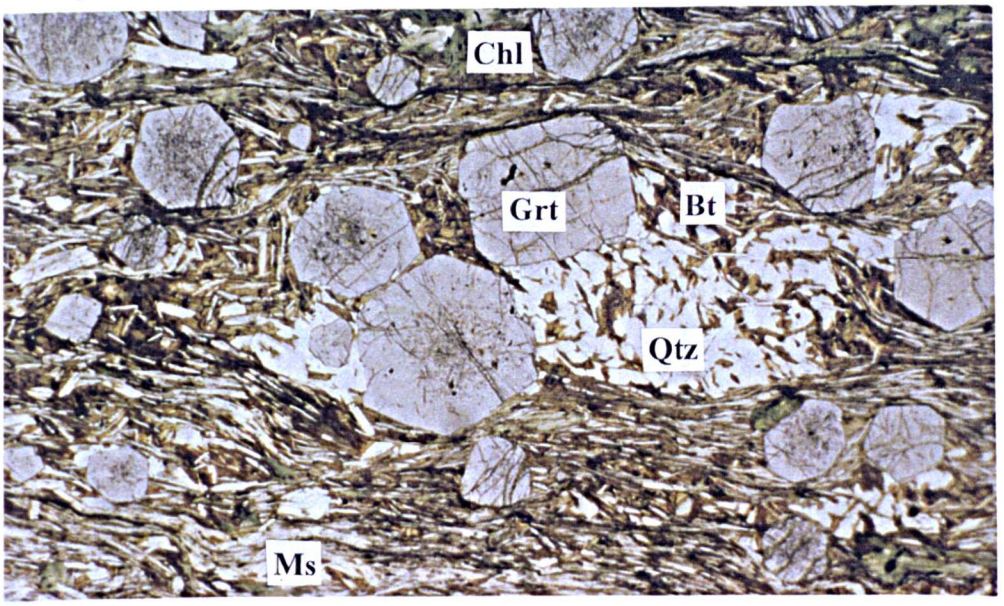

b)

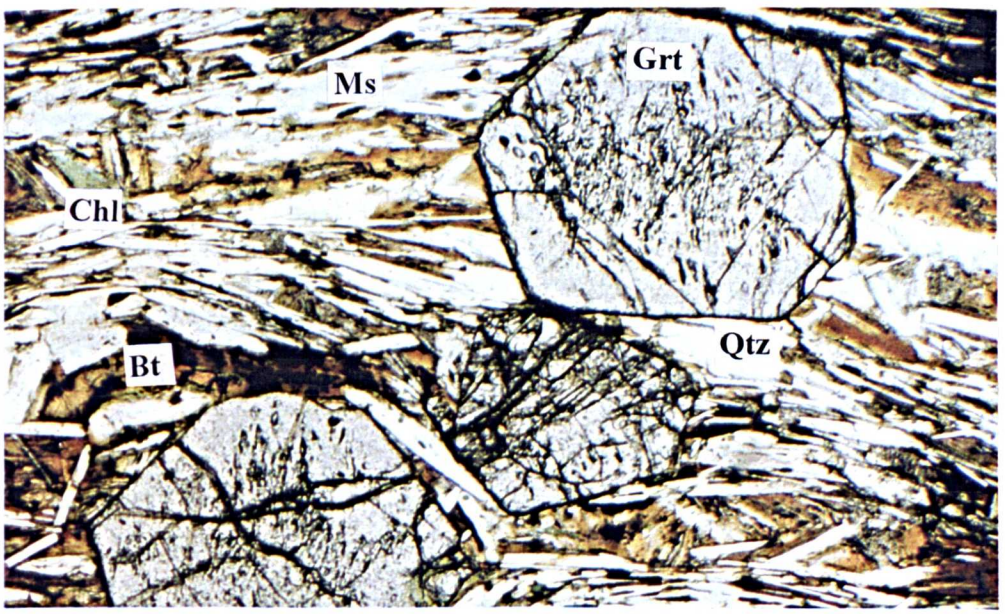

c)

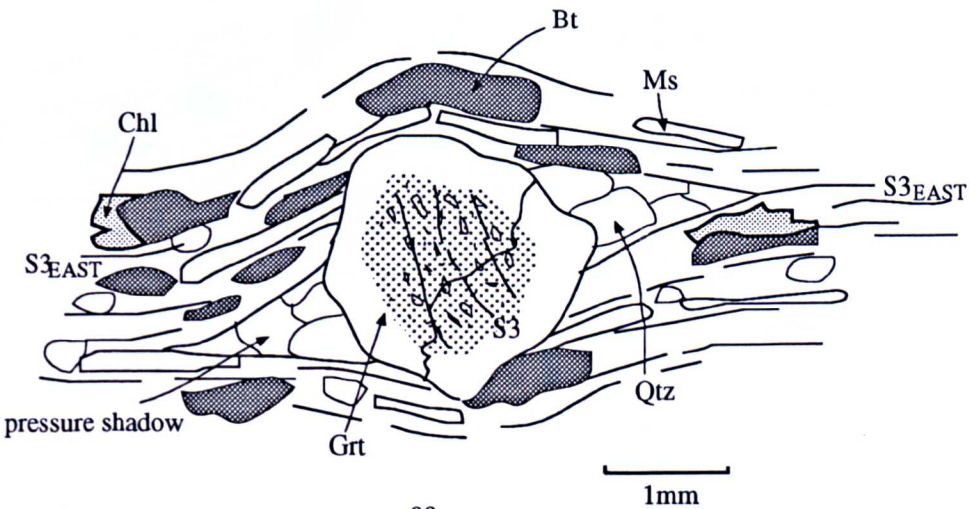

Fig. 4.10. Relationship between garnet and $S3_{EAST}$ in sample TK 95 125, a) complex inclusion trails and Bt-rich (Ms absent) $S3_{EAST}$ fabric, b) sketch showing relationship between the wrapping $S3_{EAST}$ fabric and inclusion trails (field of view for a = 2.5mm; b = 4.5mm).

a)

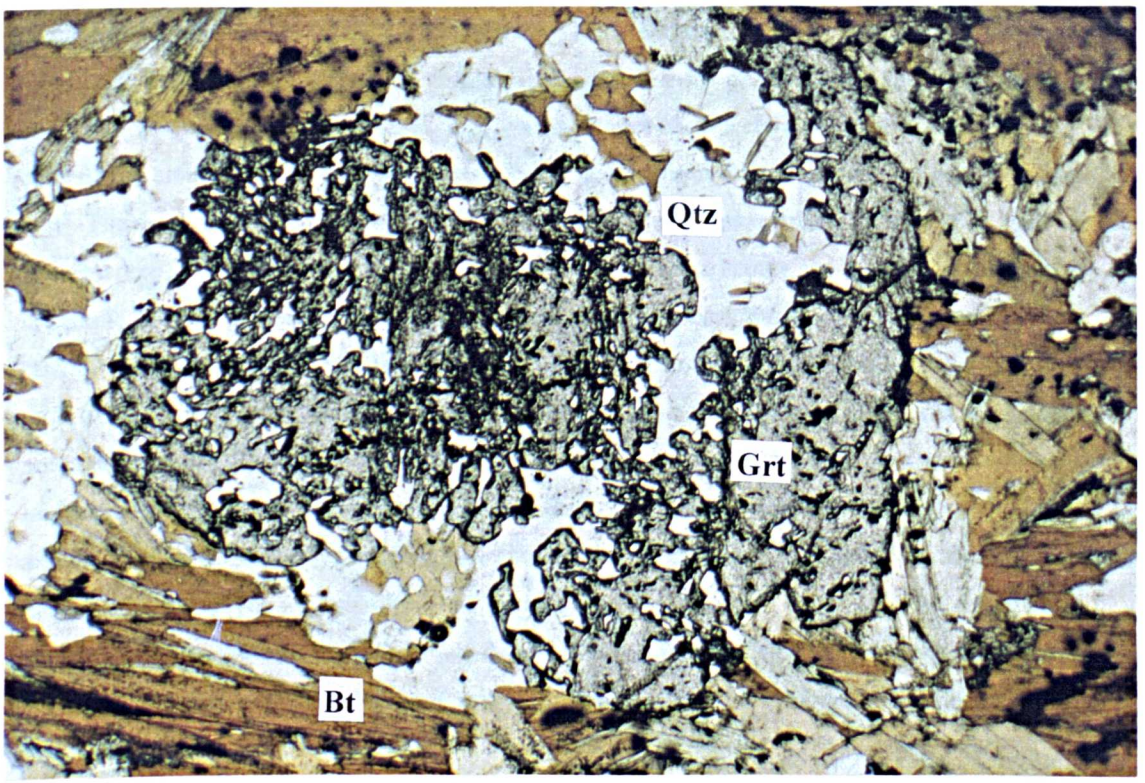

b)

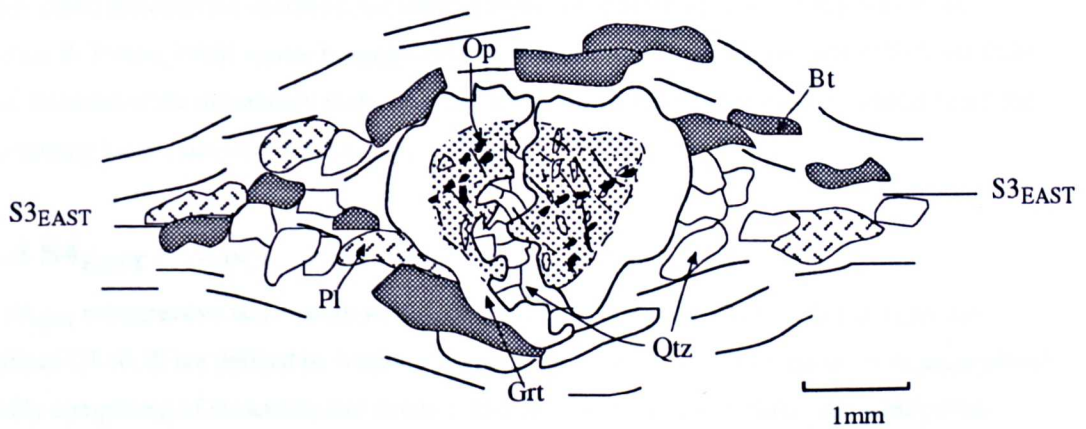

defined by discrete Q and M domains, and preserves a relic intrafolial crenulation cleavage which is defined by microfolds of intergrown coarse micas.

The composition of the $S3_{EAST}$ Q domains is consistently quartzofeldspathic, whereas the composition of M domains is laterally variable across the domain comprising variable amounts of muscovite, biotite, garnet, quartz, alkali feldspar, plagioclase and minor fibrous sillimanite (figs. 4.9 & 4.10). Eastwards across the domain, $S3_{EAST}$ assemblages show a clear decrease in muscovite content and an increase in biotite content, accompanied by the local development of garnet (in the east). The development of subidioblastic to idioblastic garnet porphyroblasts which deflect, and are in places wrapped by intergrown aligned laths of medium to coarse biotite and muscovite is illustrated in sample TK 95 122 (locality TP 2, fig. 4.9). Similar garnet porphyroblast-$S3_{EAST}$ fabric relationships are observed in sample TK 95 125 (fig. 4.10), however in contrast to sample TK 95 122, muscovite is absent from the assemblage. The majority of garnets contained within the $S3_{EAST}$ fabrics are poikiloblastic, showing the development of inclusions-rich cores, whereas rims are consistently inclusion-free (fig. 4.9a). The inclusions are commonly aligned in simple sigmoidally-shaped trails, and comprise predominantly of quartz, however rare biotite and opaque mineral inclusions are present (fig. 4.9b). The inclusion trails within the garnets (e.g. sample TK 95 122) are defined by preferentially orientated elliptical to lensoid shaped inclusions which are straight in the cores of the garnets, and curve in towards the fabric approaching the rims. In general, the orientation of the sigmoidal trails and their angular relationship with the matrix fabric (*c.* 120 °) appears to be consistent between individual garnets (fig. 4.9b).

The porphyroblast-fabric relationship between the garnets and the micaceous $S3_{EAST}$ fabric (e.g. samples TK 95 122 and TK 95 125) clearly show deflection of the anastomosing fabric around the garnet rims. The spatial relationship between the inclusions in the garnets and the matrix fabric however is unclear due to the inclusion-free nature of their rims. Porphyroblasts display asymmetrical strain shadows which comprise coarse recrystallised polygonal quartz grains and biotite which show a consistent shape and form between garnets. The origin of these types of sigmoidal inclusion trail has been much debated (e.g. Bell, 1985; Bell & Johnson, 1989; Bell *et al.* 1992; Passchier *et al.* 1992; Barker, 1994) although the characteristic features of the trails described above (summarised in Passchier & Trouw, 1996) appear to suggest a rotational (rather than an overgrowth of helicitic folds) origin. Because of the uncertainty in the origin of the inclusion trails in the garnets, a shear sense for the wrapping fabrics has not been inferred.

4.4.4 $S4_{EAST}$ fabric

The $S4_{EAST}$ retrogressive fabrics both within metasediments (localities OJ 1, 9, 38) and granites (localities OJ 10, 8) are defined by blastomylonitic fabrics and discrete shear bands, with shear planes variably comprising of muscovite and biotite ± fibrolite (fig.4.3 & 4.11). Deformed semi-pelitic metasedimentary assemblages display development of coarse anastomosing shear bands. The shear fabric is defined by biotite, intergrown with coarse laths of muscovite and fibrous sillimanite

(e.g. locality OJ 18) which wrap recrystallised quartz (showing evidence for recrystallisation into coarse polygonal grains) and coarse porphyroclasts of plagioclase (with recrystallised margins).

The $S4_{EAST}$ fabric within deformed granitic rocks is defined by a coarse shear fabric (e.g. samples TK 95 42, TK 95 52b and TK 94 88, localities OJ 28, 39, 10) which comprises medium to coarse biotite grains which wrap medium to coarse grains of plagioclase. In places, plagioclase forms coarse discrete porphyroclasts (e.g. sample TK 94 88) which show rare evidence for marginal ductile recrystallisation although the majority of plagioclase grains are strain-free (suggesting that rocks have undergone extensive recovery and recrystallisation). Quartz forms medium to coarse polygonal grains which in places shows grain size reduction in the shear bands. Blastomylonitic sample TK 95 50 (locality CV 14) comprises predominantly annealed quartz grains and rare plagioclase grains which show limited evidence for marginal ductile recrystallisation. The deformed biotite and muscovite grains show evidence for marginal recrystallisation and rare internal kinking.

Fig. 4.11 Coarse $S4_{EAST}$ sinistral S-C shear fabric in metasediment (field of view; 6.5mm).

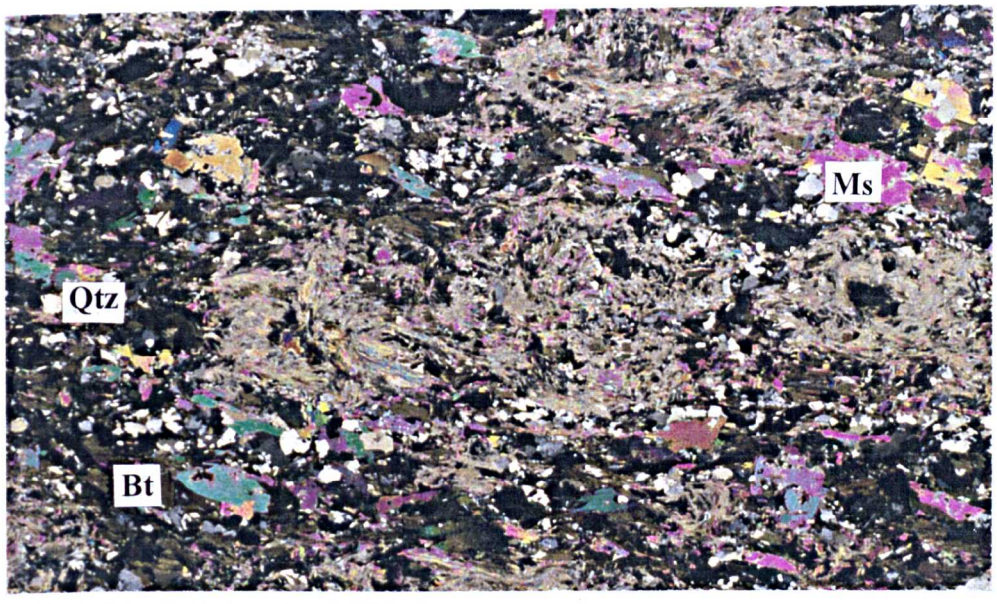

4.5 Constraints on P-T conditions

4.5.1 Methodology

D1, D2, $D3_{EAST}$ and $D4_{EAST}$ conditions of metamorphism within the domain have been investigated by detailed petrographic-fabric analysis of *c.* 35 samples from across the region, combined with microstructural and geothermobarometric studies of key assemblages. Garnet-biotite thermometry was applied to $D3_{EAST}$ garnet-bearing pelitic assemblage (TK 95 122) however geobarometric study of the garnet-bearing assemblages however was not possible due to the absence of thermobarometrically sensitive assemblages.

Fig. 4.12 Mineral reactions inferred within domain 3 assemblages.

Reaction:	Author:	Reaction #:
Cd[1] -rich Phen[2] + Chl → Cd-poor Phen + Chl (Al richer) + Bt	Hudson (1980)	R1
Chl + Ms + Qtz → Grt + Bt + H_2O	Powell & Holland (1990)	R6.
Ms + Chl → St + Bt + Qtz + H_2O	Hoschek (1969)	R3
Ms + Kfs + Ab + Qtz + V → L	Thompson & Algor (1977)	R4

4.5.2 D1/D2 assemblages

The mineralogical and petrographic relationships which typify D2 assemblages in the domain are highlighted in sample TK 94 78 (locality TP 12). This is a semi-pelitic sample from the west of the domain which comprises of muscovite 30 %, chlorite 15 %, quartz 35 % and plagioclase 20 %. S2 is the dominant fabric which is defined by intergrowths of fine grained mica and chlorite, and wraps elongate medium to coarse grains of quartz and plagioclase (fig. 4.8). Relic S1 fabric is rarely preserved intrafolial to S2, and is defined by elongate grains of muscovite and chlorite.

The abundance of chlorite and muscovite along the S2 (and the relic S1) fabric, and the absence of biotite within the assemblage constrains conditions of metamorphism to chlorite-bearing greenschist facies, and the low-T and -P side of the biotite producing reaction R1 (fig. 4.12). The flattening of the quartz and plagioclase is interpreted to be a product of low-grade, low-strain deformation (Soper & Barber, 1982; Law, 1986) of detrital grains.

4.5.3 Prograde $D3_{EAST}$

Two garnet-bearing metasediments TK 95 122 and TK 95 125 (locality TP 2) were chosen for petrographic analysis. In addition, detailed geothermobarometric determinations were carried out on sample TK 95 122. Geothermometry could not be applied to the garnet-bearing sample TK 95 125 due to the retrogressed nature of the biotites.

Both of the garnet-bearing samples are pelitic assemblages from within the metasedimentary sequence south of Thwart Pond (fig. 4.2). Sample TK 95 122 contains a biotite-, muscovite-rich $S3_{EAST}$ fabric which is deflected around garnet idioblasts (previously described in section 4.4.3), and comprises garnet 30 %, biotite 33 %, alkali feldspar 7 %, muscovite 15 %, quartz 10 %, chlorite 4 %, ilmenite < 1 % and zircon. In contrast to sample TK 95 122, $S3_{EAST}$ in sample TK 95 125 is muscovite absent and biotite-rich, and comprises garnet 10 %, biotite 25 %, epidote 3%, plagioclase 30 % quartz 25%, chlorite 5% ilmenite <1 % and apatite < 1%. For representative mineral analyses of

[1] Cd=celedonite
[2] Phen=phengite

Fig. 4.13 Zoning profile of garnet from sample TK 95 122.

	Garnet										
	rim				core						rim
	39	40	41	42	43	44	45	46	47	48	49
SiO2	36.32	36.47	36.01	36.07	35.78	35.87	36.00	36.33	35.94	35.82	36.01
TiO2	0.00	0.00	0.00	0.00	0.00	0.17	0.00	0 00	0.00	0.00	0.00
Al2O3	20.89	20.79	20.93	20.79	20.88	20.74	20.77	20.93	20.89	21.01	20.89
FeO	39.69	39.32	38.45	37.49	37.00	37.24	37.60	38.02	38.61	39.13	38.94
MnO	2.23	2.79	4.11	5.21	5.53	5.37	4.97	4.00	3.06	2.39	2.22
MgO	1.86	1.65	1.62	1.38	1.39	1.35	1.44	1.45	1.80	1.93	1.71
ZnO	0.00	0.00	0.00	0.00	0.00	0.00	0.00	0.00	0.00	0.00	0.00
CaO	2.51	2.66	2.70	2.58	2.60	2.60	2.65	2.86	2.60	2.56	2.74
Na2O	0.00	0.00	0.00	0.00	0.00	0.00	0.00	0.00	0.00	0.00	0.00
K2O	0.00	0.00	0.00	0.00	0.00	0.00	0.00	0.00	0.00	0.00	0.00
total.	103.50	103.68	103.82	103.52	103.18	103.34	103.43	103.59	102.90	102.84	102.51
	Cations per 24 oxygens										
Si	5.81	5.83	5.76	5.79	5.76	5.77	5.78	5 81	5.78	5.76	5.80
Al	3.94	3.91	3.95	3.93	3.97	3.93	3.93	3 95	3.96	3.98	3.97
Ti	0.00	0.00	0.00	0.00	0.00	0.02	0.00	0 00	0.00	0.00	0.00
Fe	5.31	5.25	5.15	5.03	4.99	5.01	5.05	5 08	5.20	5.27	5.25
Mn	0.30	0.38	0.56	0.71	0.75	0.73	0.68	0 54	0.42	0.33	0.30
Mg	0.44	0.39	0.39	0.33	0.33	0.32	0.34	0 35	0.43	0.46	0.41
Zn	0.00	0.00	0.00	0.00	0.00	0.00	0.00	0 00	0.00	0.00	0.00
Ca	0.43	0.46	0.46	0.44	0.45	0.45	0.46	0 49	0.45	0.44	0.47
Na	0.00	0.00	0.00	0.00	0.00	0.00	0.00	0.00	0.00	0.00	0.00
K	0.00	0.00	0.00	0.00	0.00	0.00	0.00	0.00	0.00	0.00	0.00
XMg	0.08	0.07	0.07	0.06	0.06	0.06	0.06	0.06	0.08	0.08	0.07
Xalm	0.81	0.81	0.78	0.77	0.76	0.77	0.78	0.79	0.80	0.81	0.82
Xsps	0.05	0.06	0.09	0.11	0.12	0.11	0.10	0 08	0.06	0.05	0.05
Xprp	0.07	0.06	0.06	0.05	0.05	0.05	0.05	0 05	0.07	0.07	0.06
Xgrs	0.07	0.07	0.07	0.07	0.07	0.07	0.07	0 08	0.07	0.07	0.07

both samples see fig. 4.14) and for full results Appendix A. Fig. 4.13 shows a zoning profile of garnet from sample TK 95 122, the garnet is essentially an almandine-rich variety (X_{Alm} 0.81-0.82) with minor components of grossular, spessartine and pyrope. The X_{Mg}^{Grt} values taken from garnet rims range from 0.07 to 0.08, cores preserve low X_{Mg}^{Grt} values of 0.06. A small amount of chemical zoning is evident within garnets which is characterised by an increase in X_{Alm} (0.06) and in X_{Sps} (0.07) and a decrease in X_{Prp} (0.02) content from the rim to the core, no zonation in X_{Grs} component exists. Biotites display a limited range in X_{Mg} values between 0.30 to 0.32, grains show no zoning against the adjacent garnets.

The composition of $D3_{EAST}$ metasediments is characterised by the absence of chlorite (minor retrogressive chlorite is present) and the development of biotite, the presence of muscovite is variable and the localised development of garnet in association with biotite ± muscovite occurs. These fabric assemblages suggest that garnet was produced through the reaction:

$$Chl + Ms + Qtz \rightarrow Grt + Bt + H_2O \qquad (R6)$$

(Powell & Holland, 1990).

The absence of staurolite within the assemblages suggests that conditions did not exceed those required for staurolite production, therefore constraining conditions to the low-P and -T side of the reaction:

$$Ms + Chl \rightarrow St + Bt + Qtz + H_2O \qquad (R3)$$

(Hoschek, 1969).

No evidence for partial melting within the rocks is seen which therefore limits conditions to the low-side of the H_2O saturated metapelitic solidus:

$$Ms + Kfs + Ab + Qtz + V \rightarrow L \qquad (R4)$$

(Thompson & Algor, 1977).

The mineral compositions used for geothermometry are presented in fig. 4.14. The garnet compositions were taken slightly away from the rim zones in order to avoid analysis of retrograde rims. Rims display lower X_{Mg} values which has been interpreted as a result of Fe-Mg exchange on cooling (e.g. Gibson & Bickle, 1994). Individual garnet-biotite pairs have been used for thermobarometric calculations rather than average compositions to avoid effects of local chemical equilibrium variation. The temperature estimates were made for P = 4 kbar which is the most likely pressure estimate based on the evidence from reaction equilibria (shown on fig. 4.16).

Fig. 4.14 Representative analysis of a garnet-biotite pair from sample TK 95 122.

Tk 95 122	Grt	Bt
anal. #	60	57
SiO2	35.81	33.37
TiO2	0.00	1.78
Al2O3	20.84	18.95
FeO	38.77	26.40
MnO	2.55	0.00
MgO	1.89	6.55
ZnO	0.00	0.00
CaO	2.61	0.00
Na2O	0.00	0.33
K2O	0.00	9.28
total	102.47	96.66
Cations per oxygens	*24*	*32*
Si	5.78	5.21
Ti	3.97	3.49
Al	0.00	0.21
Fe	5.23	3.44
Mn	0.35	0.00
Mg	0.45	1.52
Zn	0.00	0.00
Ca	0.45	0.00
Na	0.00	0.10
K	0.00	1.85
XMg	0.08	0.31
Xalm	0.81	
Xsps	0.05	
Xprp	0.07	
Xgrs	0.07	

A series of six calibrations of the garnet-biotite Fe-Mg exchange thermometer have been applied to the $D3_{EAST}$ assemblages (see Appendix B3 for details). There is a general lack of agreement about the accuracy of the calibrations, however, the experimentally derived calibration of Ferry & Spear (1978) which assumes ideal mixing between Fe and Mg is widely recognised to be the most reliable (e.g. Essene, 1982, Spear 1993). The calibration of Perchuk & Lavrent'eva (1983) which is based on recent experimental data, is similarly considered to be consistently reliable (e.g. Chipera & Perkins, 1988; Jones, 1988). The empirical calibration of Indares & Martignole (1985, based on the mixing model of Ganguly & Saxena, 1984) uses various correction factors which have been generated for specific rocks, hence authors suggest caution when applying their calibration, (Spear, 1993 found the calibration to give low results). The calibrations of Hodges & Spear (1982) and Ganguly & Saxena (1984) which apply specific garnet mixing models have been found to give excessive data spread, and petrographically inconsistent results (e.g. Chipera & Perkins, 1988; Jones, 1988; Spear, 1993; Gibson & Bickle, 1994). The model of Ferry & Spear (1978)[3] which

[3] Using Bermans (1990) garnet solution model

also uses a specific garnet mixing model has been found to be both reliable (e.g. Spear, 1993), and give unreasonably high estimates (e.g. Gibson & Bickle, 1994).

In this study the most reliable results of garnet-biotite geothermometry *c.* 600 °C (see fig. 4.15), were given by the calibrations of Ferry & Spear (1978), Perchuk & Lavrent'eva (1983) and Indares & Martignole (1985). These gave a similar range of values which are consistent with the observed mineral equilibria. The calibrations of Hodges & Spear (1982), Ganguly & Saxena (1984) and Ferry & Spear (1978)[3] consistently give higher estimates (fig. 4.15) *c.* 650 °C which is inconsistent with the petrography.

Fig. 4.15 Results of garnet-biotite geothermometry on sample TK 95 122.

Mineral pair (rim-rim)		T C (P = 4 kbar)					
Grt	Bt	F & S	H & S	G & S	P & L	I & M	F & S *
60	57	615	643	668	599	597	650
61	58	603	631	660	592	587	639
72	64	560	588	619	569	547	596
73	65	575	603	631	577	551	611
74	66	590	618	644	585	570	626
76	67	621	649	671	601	597	656
77	68	632	660	685	608	602	668
96	89	603	634	658	592	590	642
97	91	641	670	692	612	610	678
99	92	650	680	700	616	615	689
99	93	649	679	699	616	629	688
99	87	654	684	704	618	619	693
Mean		616	645	669	599	593	653
2Sd		62	62	56	32	52	64

Calibrations: F & S (Ferry & Spear, 1978); H & S (Hodges & Spear, 1982); G & S (Ganguly & Saxena, 1984; symmetrical garnet solution model); P & L (Perchuk & Lavrent'eva, 1983); F&S* (Ferry & Spear using Bermans 1990 correction model); I&M (Indares & Martingole, 1985).

Fig. 4.16 is a petrogenetic grid which shows the combined results of mineral equilibria and geothermobarometric study of the $S3_{EAST}$ garnet bearing assemblages, illustrating the prograde $D3_{EAST}$ path and the peak temperature conditions between 600 and 650 °C.

4.5.4 Retrograde $D4_{EAST}$

The deformed metasedimentary sample TK 95 39 (OJ 18) was chosen for detailed microstructural and petrographic analysis in order to assess the grade of retrogressive $D4_{EAST}$ deformation. The sample comprises biotite 35 %, muscovite 30%, quartz 18%, plagioclase 14%, fibrolite 2% and ilmenite 1%. The shear fabrics are defined by coarse intergrown laths of biotite and muscovite which

[3] Using Bermans (1990) garnet solution model

Fig. 4.16 P-T-t-d evolution path for domain 3 using combined results of mineral equilibria studies and geothermometry.

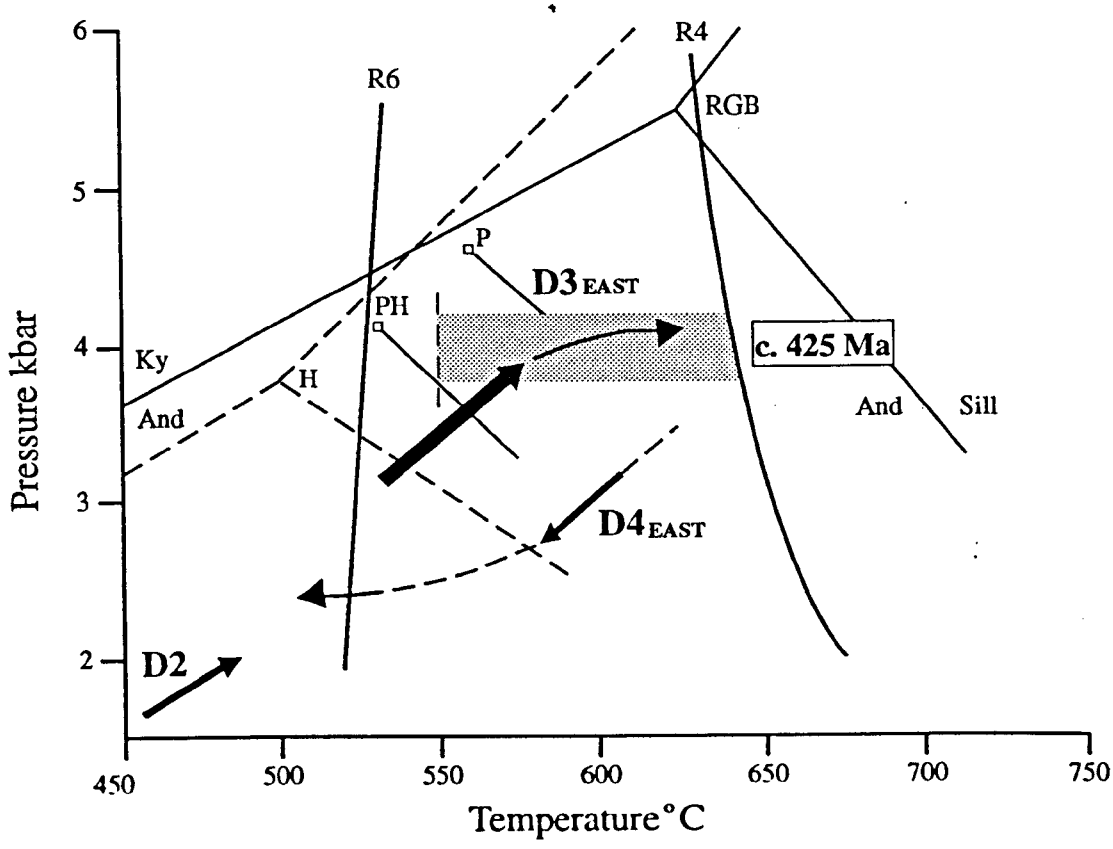

Shaded box shows results of Grt - Bt geothermometry at 4 kbar ((Ferry & Spear, 1978, Perchuk & Lavent'eva, 1983) for $S3_{EAST}$-bearing metapelite sample TK 95 122. Reactions on grid; R6) Grt-in, Powell & Holland (1990); R4) metapelitic solidus, Thompson & Algor (1977); Al_2SiO_5 stability data: RGB, Richardson et al. (1969); H, Holdaway (1971), PH, Pattison & Harte (1985), P, Pattison (1989).

display internal kinking and evidence for marginal recrystallisation. The muscovite forms fish which in places are intergrown with fibrolite, suggesting moderate to high (i.e. amphibolite facies) grades of deformation. Quartz forms medium to coarse grains which preserve evidence for ductile deformation and show widespread evidence of recrystallisation to polygonal grains. A significant grain size reduction of quartz is evident into the C-plane of the shear bands. Plagioclase forms coarse porphyroclasts which show evidence for widespread marginal ductile recrystallisation. The range of fabrics described above indicate that low amphibolite to upper greenschist facies conditions (see fig. 4.16) were achieved during deformation (e.g. Boullier & Bouchez, 1978; Simpson, 1985, 1990; Tullis & Yund, 1985; Gapais, 1989).

4.6 Timing constraints on deformation and metamorphism

The metasediments in domain 3 clearly preserve a relic lithological variation which has been deformed and transposed to form S0-Sn fabric, rare evidence for S1 fabric is preserved subparallel to S0-Sn. Both fabrics have undergone deformation by recumbent F2 folds with a well developed subhorizontal axial planar fabric. These folds display similar structural characteristics (e.g. deformation of fine S1 & eastward-directed vergence) to the flat-lying F2 folds of domain 1, which would sugest their origin during the eastwards thrusting of the Dunnage Zone over the Gander Lake Subzone (see section 2.6) *c.* 470 Ma (Williams & Stevens, 1974; Williams, 1984; Colman-Sadd, 1980, 1982; Colman-Sadd *et al.* 1992a).

Constraints on the relative timing of $D3_{EAST}$ is given by field relationships which show the overprinting and eastwards progressive deformation of D2 assemblages by upright $F3_{EAST}$ folds. The axial planar $S3_{EAST}$ fabric displays an eastwards intensification and increase in metamorphic grade into a gneissic fabric, which has been correlated (e.g. Holdsworth, 1994a) with the migmatitic fabric in the paragneisses of the adjacent domain 4. High precision U-Pb age dates (from accessory zircon and titanite) from the migmatites (in domain 4) suggest an age of *c.* 425 Ma (Dunning *et al. in prep*). Relative timing constraints on the $D4_{EAST}$ retrogression are provided in the metasediments by the overprinting of the prograde $D3_{EAST}$ assemblages by the micaceous $S4_{EAST}$ shear fabrics.

4.7 Summary

Domain 3 comprises variably deformed and metamorphosed Gander Group metasediments which record evidence for the deformation of relic S1 by F2 folds, which in turn have been progressively overprinted by the effects of $D3_{EAST}$ prograde deformation. High-grade $D3_{EAST}$ metasedimentary assemblages in the east are overprinted by steep $S4_{EAST}$ shear fabrics formed during retrogressive deformation.

The F2 folds are typically flat-lying in attitude with a well developed axial planar greenschist facies fabric, their preservation is restricted to metasediments in the west of the domain where they show variable effects of overprinting by $D3_{EAST}$. The D2 deformation has been correlated with the obduction of Dunnage over the Gander Lake Subzone (e.g. Williams & Stevens, 1974; Williams, 1984; Colman-Sadd, 1980, 1982; Colman-Sadd *et al.* 1992a).

$F3_{EAST}$ folds form upright structures in the west which show subordinate development of steep $S3_{EAST}$ axial planar fabrics. The $D3_{EAST}$ deformation intensifies eastwards shown by the tightening of folds and pervasive development of $S3_{EAST}$. The $S3_{EAST}$ assemblages display an eastward increase in grade and record regional prograde $D3_{EAST}$ metamorphism from biotite- to garnet-grade culminating in peak temperature conditions of *c.* 600-650 °C. Correlation of the $S3_{EAST}$ fabrics with the $S3_{EAST}$ migmatitic fabric in paragneisses of adjacent domain 4 suggests that the

metasediments record the prograde conditions pre- or syn-migmatisation (U-Pb age dates for the migmatites are *c.* 425 Ma; Dunning *et al. in prep*).

The $D4_{EAST}$ retrograde assemblages are characterised by low amphibolite to upper greenschist facies sinistral shear fabrics. These overprint $D3_{EAST}$ assemblages both in the east of domain 3 and in the west of the adjacent domain 4 within a 100m-scale high-strain zone. The retrogressive deformation is characterised by micaceous shear fabrics which are associated with an intense subhorizontal mineral lineation.

Chapter 5.

Domain 4: The Eastern Gander Migmatite Belt

Chapter 5. Domain 4: The Eastern Gander Migmatite Belt.

5.1 Introduction

The Eastern Gander Migmatite Belt is a northeast-southwest trending domain in the east of the Gander Lake Subzone (fig. 5.1) measuring 6 to 18 km by *c.* 50 km, which is located between the Central Gander Metasedimentary Belt (domain 3) and the Dover Fault Shear Zone (domain 5). The domain is an elongate belt which comprises predominately of sillimanite-bearing migmatites (Hare Bay Gneiss; Blackwood & Kennedy, 1975, Blackwood, 1977) and foliated granites (Strong *et al.* 1974; Jayasinghe & Berger, 1976; Blackwood, 1977; Jayasinghe, 1978; Holdsworth, 1991; O'Brien & Holdsworth, 1992). Minor volumes of orthogneiss and amphibolitic metabasite (included in Hare Bay Gneiss unit; Blackwood, 1977) are contained within the migmatites.

The western margin of the domain is gradational, marked in the north (e.g. Old Jingle) by the transition from non-migmatised paragneiss (Square Pond Gneiss of Blackwood, 1977) into migmatite. This margin coincides locally with steep sinistral lower amphibolite to upper greenschist facies fabrics ($S4_{EAST}$), the trace of which can be followed north to Windmill Bight, and southwards into the Fox Pond region. In the far south of the Gander Lake Subzone, the western margin of domain 4 (marked by the contact between the Middle Brook Granite and the Hare Bay Gneiss migmatites) is poorly exposed, and defined (e.g. in Lower Dark Cove) by steep brittle faults. The eastern margin of domain 4 is characterised by the presence of steep greenschist facies dextral fabrics (D5) which overprint predominately sinistral (e.g. Holdsworth, 1994a) higher grade fabrics (i.e. upper amphibolite grade $D3_{EAST}$ and mid amphibolite-upper greenschist facies $D4_{EAST}$) in the migmatites and foliated granites. The intensity of development of the low grade shear fabrics (S5) shows local variation, therefore the position of the eastern margin of the domain is only loosely constrained.

This chapter aims, through field, petrographic and geothermobarometric studies, to establish the conditions of, and characterise prograde and peak and retrograde metamorphism within the domain enabling construction of a P-T-t-d evolutionary path.

5.2 Structure and metamorphism

The rocks within the domain display northeast-to southwest trending fabrics which parallel those in the adjacent paragneissic metasediments (of domain 3), and the regional strike across the Gander Lake Subzone (fig. 1. 5). The migmatites preserve effects of $D3_{EAST}$ deformation and prograde metamorphism (correlated with $D3_{EAST}$ in the adjacent metasediments and previously termed 'early ductile deformation'; Holdsworth, 1991, 1994a) which is variably overprinted by lower grade ductile $D4_{EAST}$ retrogressive fabrics (previously termed 'late brittle structures'; Holdsworth, 1991, 1994a).

Fig. 5.1 Locality / sample map for Domain 4; a) Windmill Bight, b) Valleyfield.

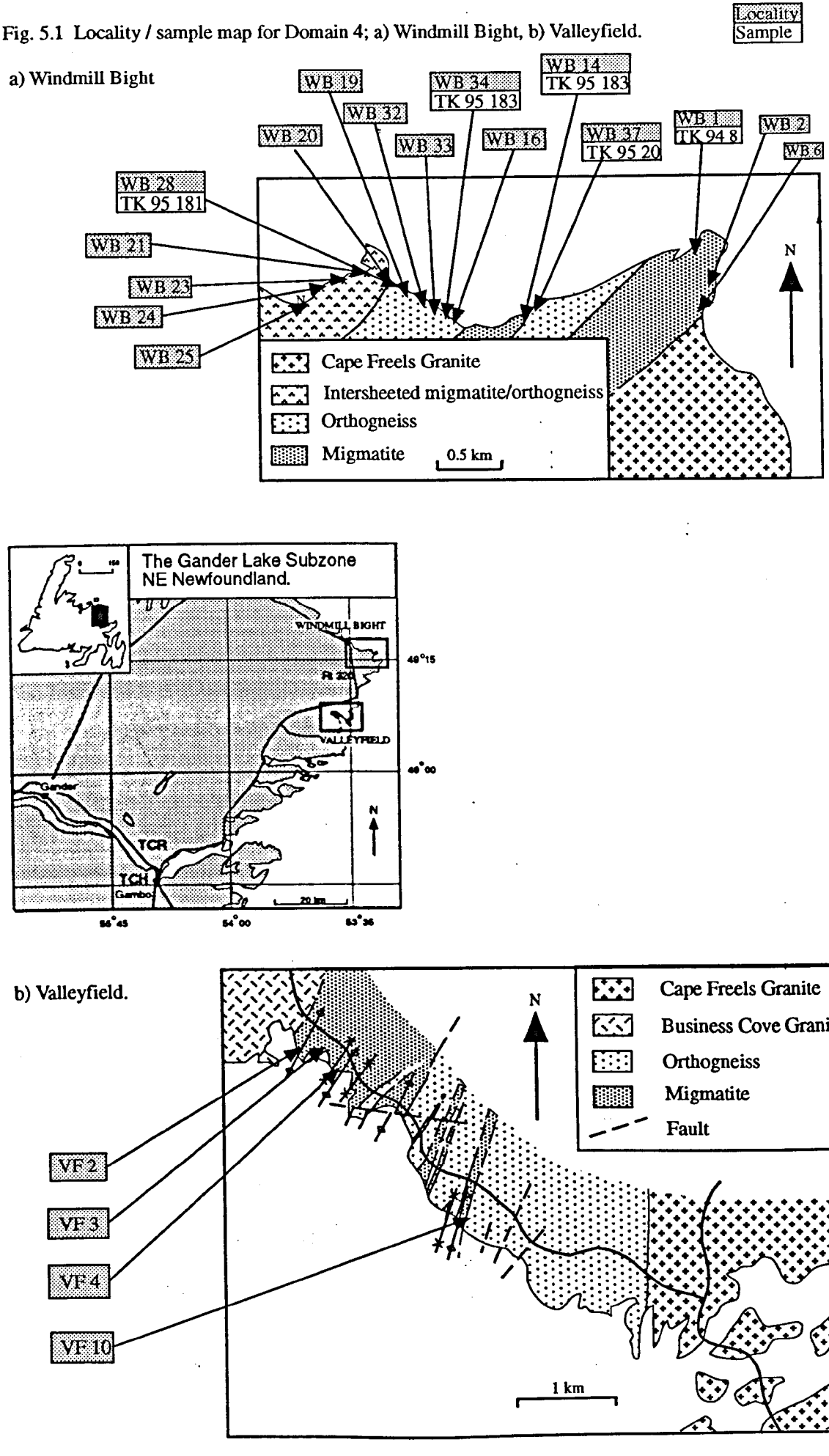

Fig. 5.2 Locality / sample map for Domain 4; a) Greenspond Road, b) Indian Bay

a) Greenspond Road

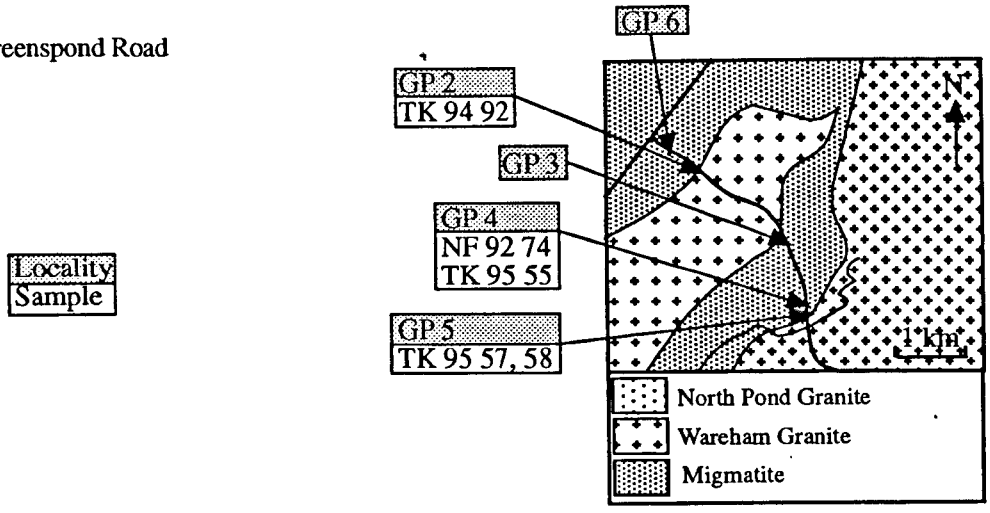

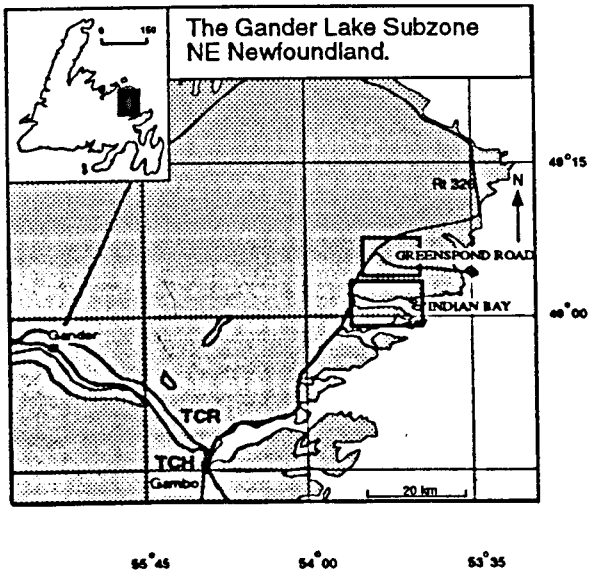

b) Indian Bay

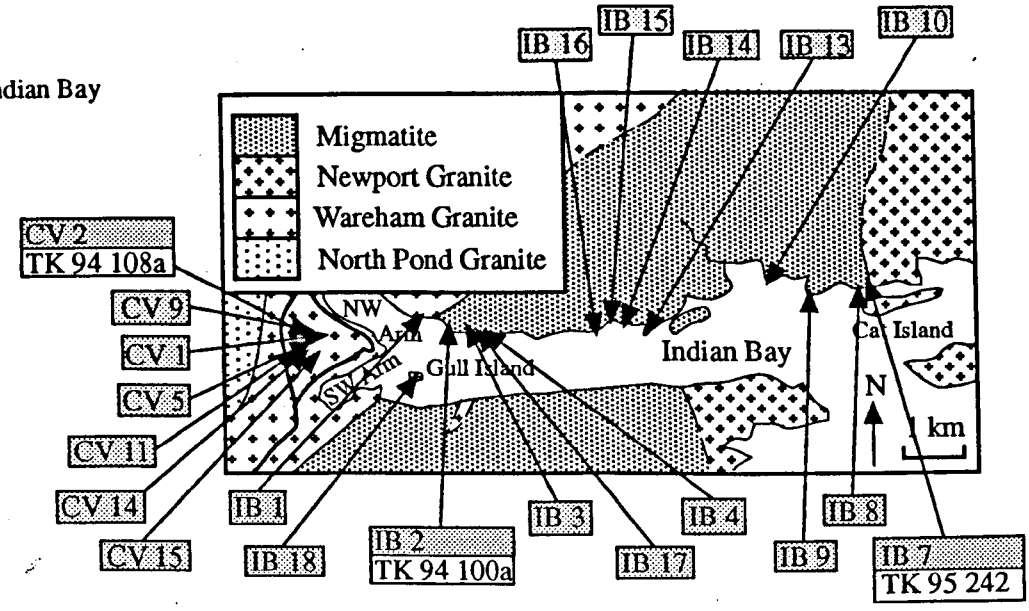

Fig. 5.3 Locality / sample map for Domain 4; a) Freshwater Bay, b) Trinity Gut

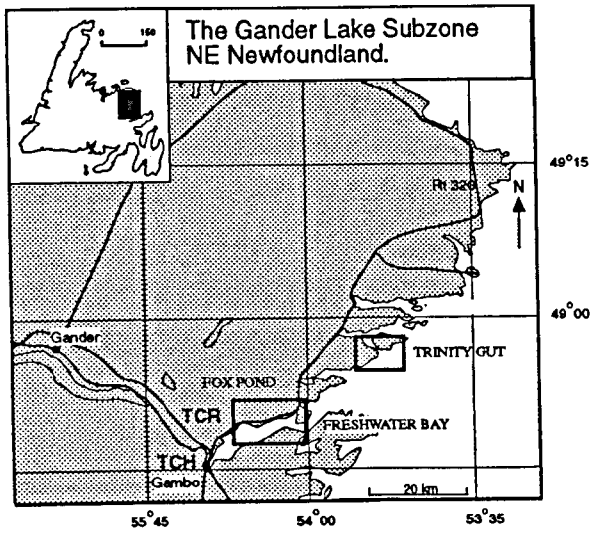

a) Freshwater Bay

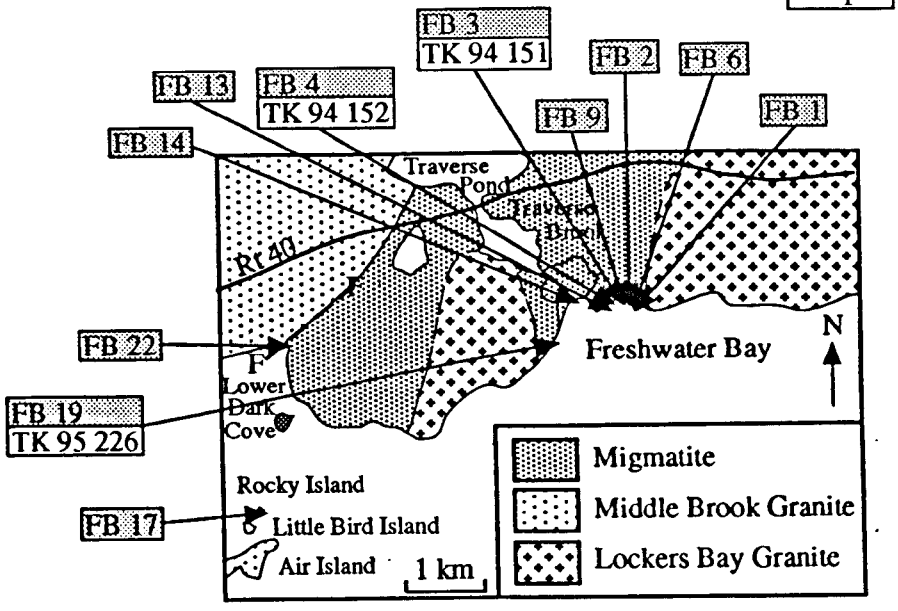

b) Trinity Gut

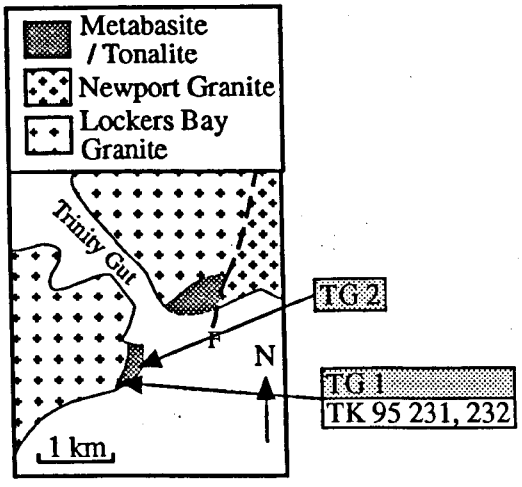

Fig. 5.4 Locality / sample map for Domain 4; Lockers Bay, Butlers Cove, Hare Bay

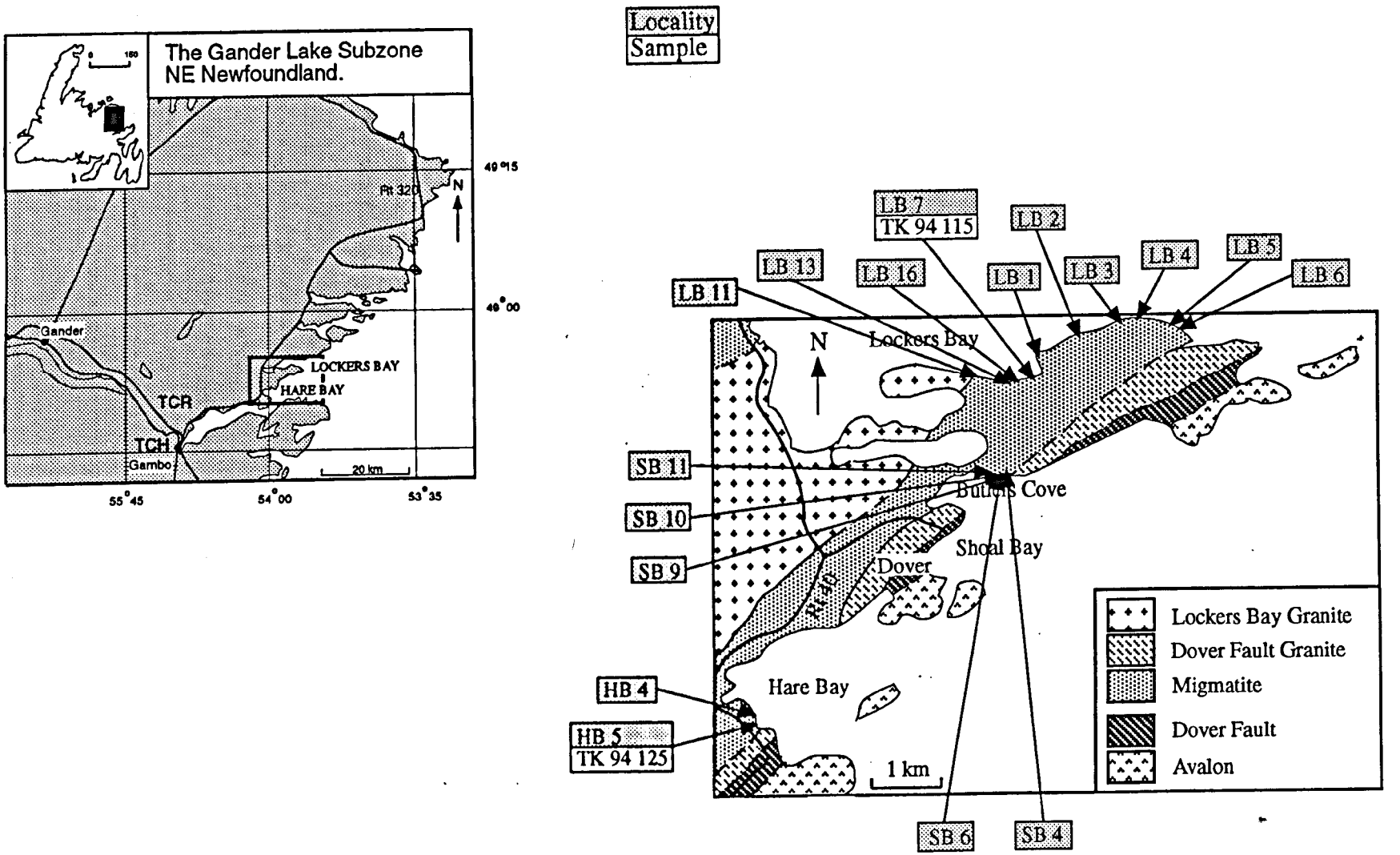

The grade of $D3_{EAST}$ deformation is upper amphibolite facies (Holdsworth, 1991, 1994a). $D3_{EAST}$ deforms Hare Bay Gneiss assemblages, and has been focused into the rheologically weaker, more mobilised migmatites forming sinistral shear bands and melt-filled shear pods. $D4_{EAST}$ shear fabrics are sinistral and form mid amphibolite to upper greenschist facies solid-state fabrics which overprint $S3_{EAST}$ assemblages in the migmatites and orthogneiss, and form the dominant fabric in the majority of the foliated granites (e.g. the Lockers Bay and Cape Freels granites; Holdsworth, 1991; O'Brien & Holdsworth, 1992, Holdsworth *et al.* 1993; Schofield *et al.* 1996).

Migmatite represents the main component of the Hare Bay Gneiss (Blackwood, 1977) which also includes paragneiss, metabasite and orthogneiss (see chapter 1). Holdsworth (1991, 1994a) differentiated types of migmatites on the basis of degree of partial melting from coherent 'soaked' migmatites through to thoroughly mobilised, schlieric-rich granites. The metabasite and orthogneiss components form sheets and pods within the migmatites, both of which preserve deformed amphibolite grade $S3_{EAST}$ fabrics. The paragneiss (which displays $S3_{EAST}$ fabric) forms rafts within migmatites and rarely within foliated granites, and is interpreted as representing metamorphosed Gander Group sediment which formed the host rock to early granitoid and mafic intrusions (now metamorphosed to orthogneiss and metabasite), and the precursor to the migmatites (Blackwood, 1978; Holdsworth, 1991). Evidence to suggest that the Gander Group metasediments and the Hare Bay Gneiss migmatites are part of a single succession showing differing degrees of metamorphism and deformation is given by the absence of an unconformity or tectonic break between the units, their close lithological similarities (e.g. Blackwood, 1978) and by their isotopic similarities (D'Lemos and Holdsworth, 1995). The transition from low-melt percent paragneiss into partially melted migmatite within the sequence is locally gradational (1-10m scale) hence indicating that the degree of partial melting may be protolith controlled (e.g. Holdsworth, 1994a; D'Lemos & Holdsworth, 1995).

5.3 Field relationships

5.3.1 Paragneiss

The distribution of paragneiss within the domain is restricted to the western region (i.e. Centreville, Old Jingle, Windmill Bight) of the migmatite belt, and rafts and cognate enclaves contained within higher melt percentage migmatites (e.g. Indian Bay, Freshwater Bay). Paragneiss is defined as a layered metasedimentary rock which contains discrete lithological variations and a metamorphic segregation, and which may contain small proportions of locally derived granitic melt. The structural characteristics of the paragneisses appear to be closely deformationally controlled, and related to $D3_{EAST}$ deformation. Types of paragneissic migmatite are loosely classified into 3 types on the basis of the degree of syn-anatexis deformation (fig. 5.5). In low strain regions type 1 paragneiss displays coherent open folds, whereas in higher-strain regions folds are tighter and transposed on the limbs by a solid-state micaceous fabrics, forming type 2 paragneiss. In high strain regions these transposition fabrics become mylonitic and totally overprint pre-existing fabrics to form type 3 paragneiss.

Fig 5.5 Schematic diagram showing the relationship between degree of syn-anatexis deformation and the percentage melt in migmatites, showing migmatite types 1 -12.

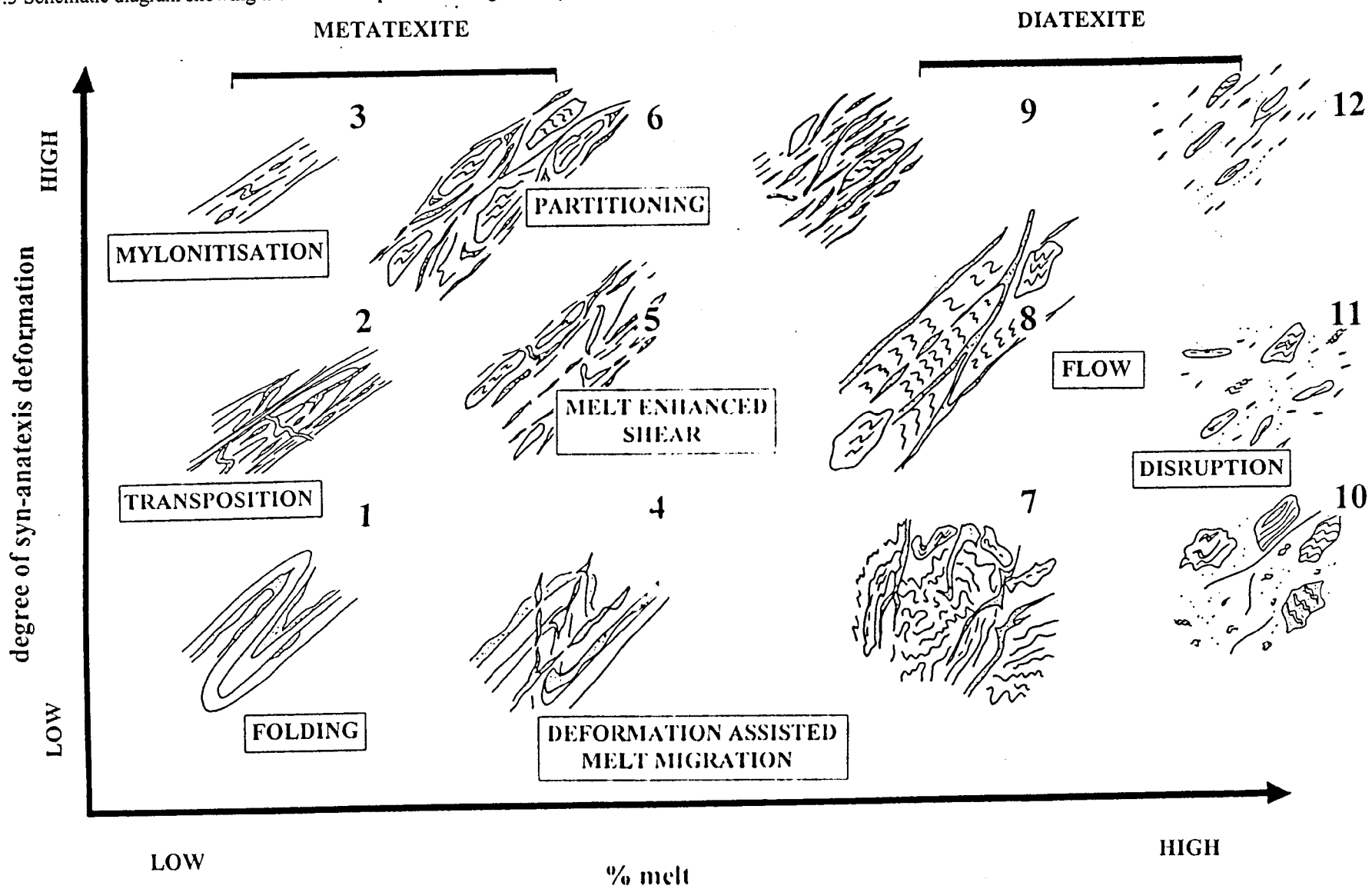

Fig. 5.6 Paragneissic migmatites, a) layered type 1 paragneiss showing minor insitu melting (right = up); b) type 2 folded paragneiss with local small-scale melt migration; c) transposed type 3 paragneiss.

a)

b)

c)

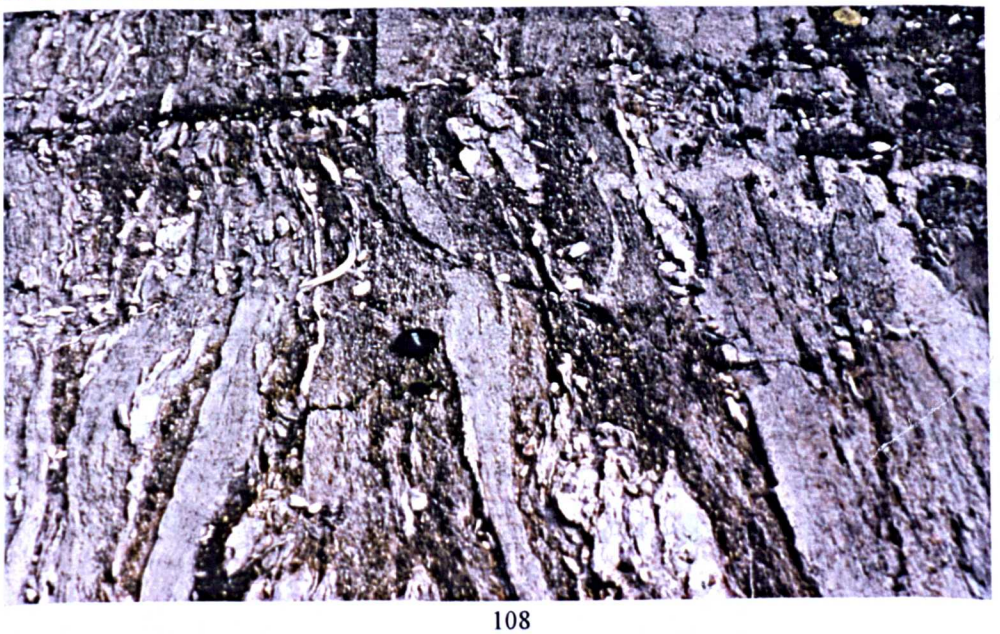

The weakening of low-melt percentage paragneisses (dominated by a granular framework) has been experimentally demonstrated by Miller *et al.* (1988), showing that their strength will decrease at high strains due to the breakdown of the solid grain supporting skeleton. Rushmer (1991, 1992) demonstrated this, and showed that at natural high strain rates, low fraction granite minimum melts may be expelled. Miller & McLellan (1986) have proposed that the layered fabric in low-melt percentage rocks deformed at high strains may be a product of layer-parallel shearing.

Type 1 paragneiss is displayed at Old-Jingle and Centreville (e.g. localities CV 11, 15) where it forms deformed screens within the Wareham Granite (described by Holdsworth, 1994a). The discrete large-scale layering (centimetre to 0.5 m scale) in the rocks is defined by mineralogical variation which represents transposed 'S0-Sn' bedding fabric (fig. 5.6a). The fine millimetre scale fabrics (corresponding to $S3_{EAST}$) are best developed within semi-pelitic and pelitic lithologies, formed sub-parallel to 'S0-Sn'. The fabrics represent gneissic segregations defined by pale Q and dark M domains which are saccharoidal, in places migmatitic, and contain small volumes of in situ melt. These migmatitic fabrics are termed 'Sm' (fig. 5.7). The psammitic lithologies display a coarse S0-Sn layering, however lack the presence of migmatitic segregations, these layers commonly preserve relic S2 fabric (intrafolial to $S3_{EAST}$) within the low strain zones of the more competent quartzofeldspathic lithologies. The limbs of type 2 folded paragneiss are transposed by schlieric to linear axial planar micaceous fabrics termed 'St' (e.g. locality CV 5, 9). Within type 3 paragneiss the transposition fabrics are pervasively developed, forming planar solid-state coarse (2-3 mm scale) shear fabrics.

M domains of the 'Sm' fabric in the paragneiss are characterised by the presence of biotite, muscovite and both prismatic and fibrous sillimanite (e.g. CV 1, 2, 14), in places coarse porphyroblasts of andalusite are present along the fabric (e.g. locality CV 2). The Q domains are predominately quartzofeldspathic in composition. The 'St' transposition fabrics display a similar mineralogy to 'Sm' migmatitic fabrics, being variably defined by biotite-, muscovite-, sillimanite- and fibrolite-rich M domains, and quartzofeldspathic Q domains.

5.3.2 Migmatite

Migmatite represents the most voluminous component of the Hare Bay Gneiss within the Gander Lake Subzone. The migmatites are 'mixed rocks' (Sederholm, 1907) which comprise light (leucosome) and dark (mesosome) components. There are a number of potential mechanisms which have been proposed for leucosome generation including partial melting of host rocks (e.g. Holmquist, 1921; Mehnert, 1968; Johannes, 1983, 1988), solid-state differentiation (e.g. Ashworth, 1985), introduction of alkali elements during metasomatism (Olsen, 1985), and the injection of granitic melt (e.g. Sederholm, 1907; Buddington, 1948). The Hare Bay Gneiss migmatites display a variety of field and petrographic features including the local transition from stromatic into schlieric migmatites and anatectic melt, and the presence of igneous textures (e.g. Vernon & Collins, 1988). These features suggest that leucocratic portions were generated through partial melting of the host

Fig. 5.7 Development of migmatitic fabrics.

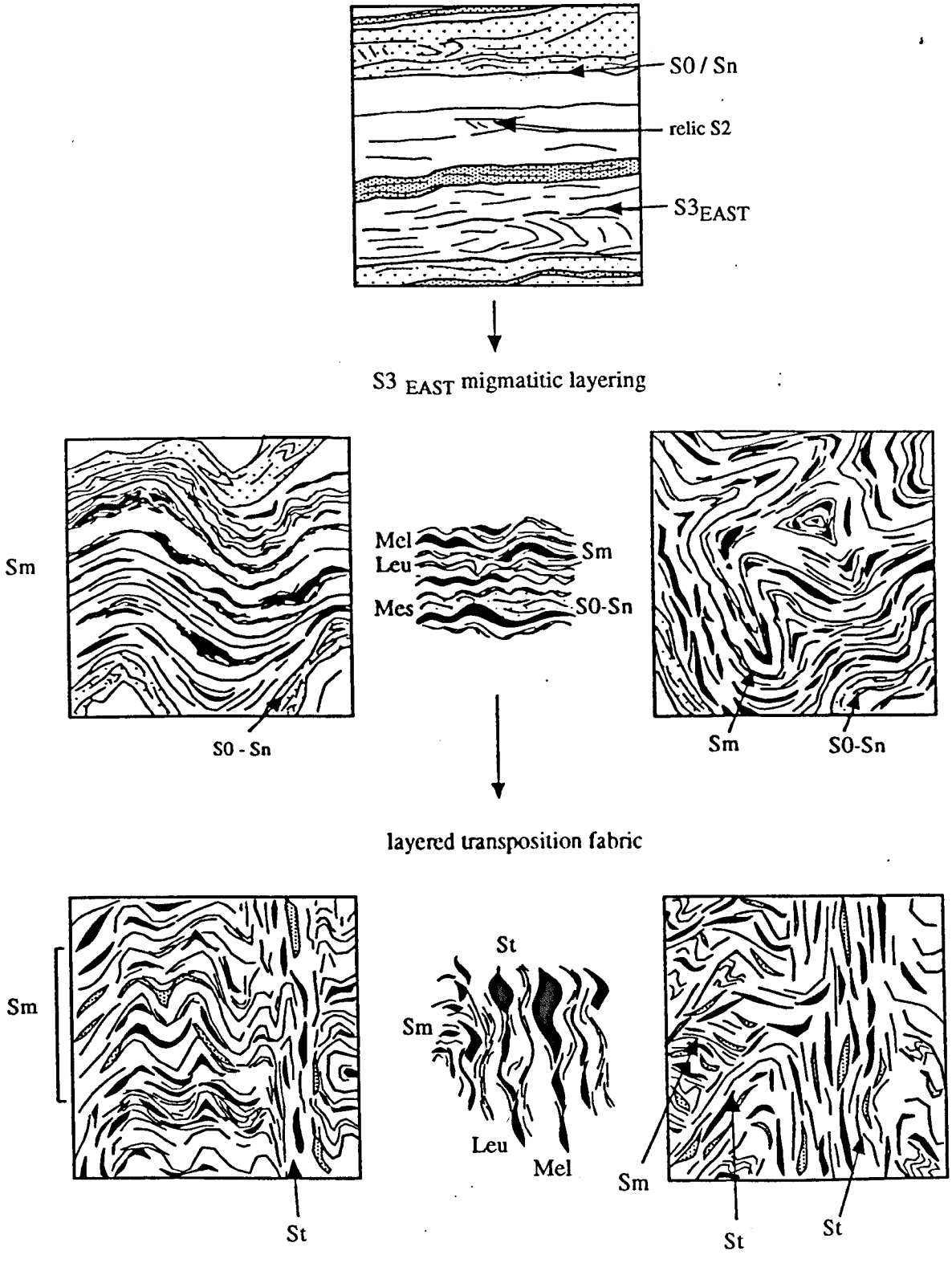

Fig. 5.8 Migmatitic fabrics, a) stromatic layering; b) schlieric transposition fabric; c) irregular schlieren forming nebulitic texture; d) schlieric fabric in anatectic granite.

a)

b)

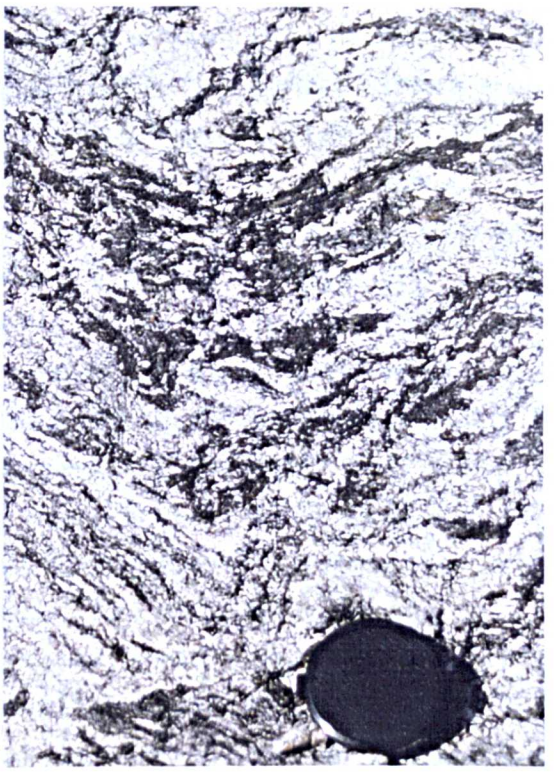

c)

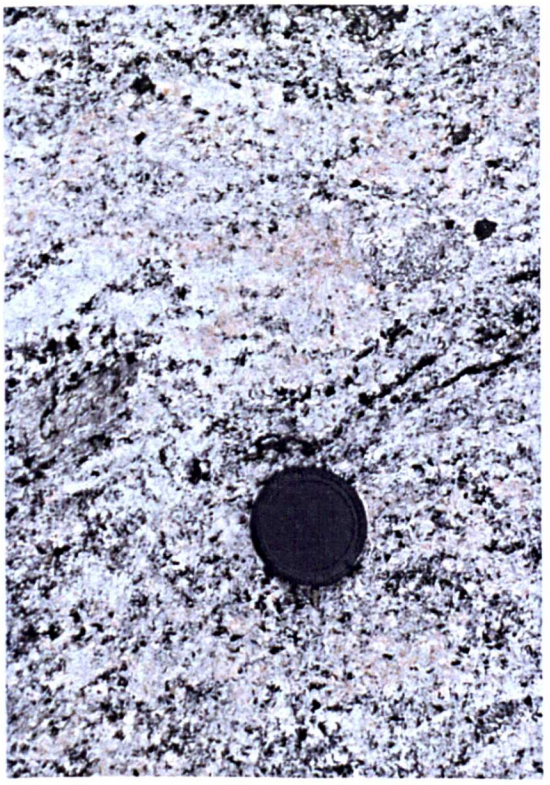

d)

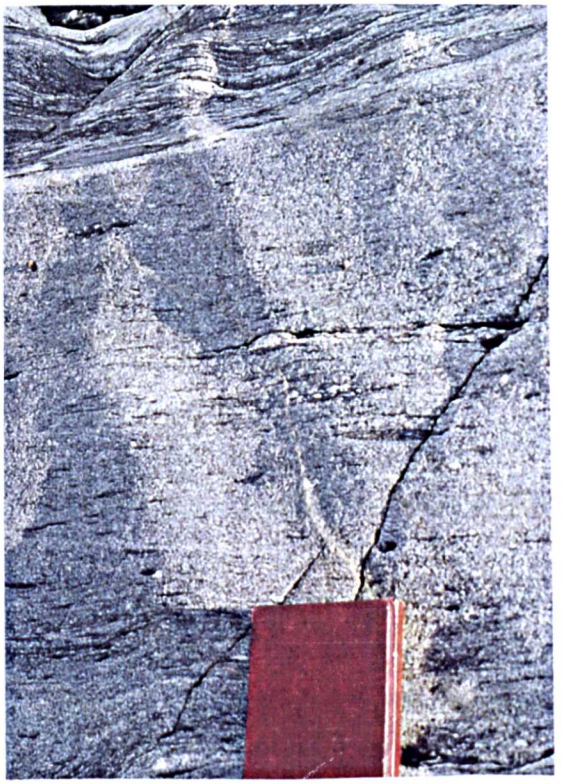

metasediments. The migmatites comprise varying proportions of partial melt (indicated by field observations of transgressive leucosome) which has enabled their broad classification into metatexite, inhomogeneous and homogeneous diatexite (using terminology of Brown, 1973). The migmatites form a wide variety of contrasting structural types (Mehnert, 1968) whose formation appears to be closely controlled by the effects of deformation-enhanced segregation (invoked by McLellan, 1988, 1989; Sawyer 1991; D'Lemos *et al.* 1992). The melt portion of migmatites becomes mobile at volumes exceeding the critical melt fraction by migration when melt forms a continuously connected phase (Maaloe, 1982). However melt migration is enhanced by deformation (Sawyer, 1991) which leads to the continuous 'squeezing out' of melt from the ductiley deforming melt-matrix below the critical values (Brown, 1994). This has led to a wide variety of migmatite types within the Hare Bay Gneiss migmatite sequence, which have been classified into specific types on the relationship of percentage partial melt compared to the degree of syn-anatexis deformation (fig. 5.5).

Stromatic migmatites are widely recognised to represent regular layers of granitic melt (termed layer-parallel leucosomes; Brown & Rushmer, *in press.*) separated by continuous selvages of residual minerals (termed melanosomes) which are related to pre-existing layers in host metasediments (e.g. Johannes, 1988; Brown *et al.* 1995), and represent the products of small-scale melt segregation (e.g. Brown, 1994; Brown *et al.* 1995). The stromatic layering within Hare Bay Gneiss migmatites is characterised by a coherent continuous migmatitic fabric 'Sm' (corresponding to the regional $S3_{EAST}$ fabric) which is orientated sub-parallel / parallel to transposed lithological variation 'S0-Sn' (fig. 5.8). The layered fabric comprises complementary biotite-rich melanosome and quartzofeldspathic leucosome (fig. 5.9a), the mesosome component of the migmatites displays a gneissic fabric (previously described in paragneiss, section 5.3.1). The higher melt percentage migmatites show the development of discontinuous schlieric fabrics which comprise biotite-rich layers and quartzofeldspathic granitic layers. These 'St' transposition fabrics represent products of disaggregation and realignment of the pre-existing Sm fabric. St fabrics commonly display similar forms to Sm fabrics therefore care is needed when interpreting the origin of layering within deformed migmatites. St forms the dominant layering in the migmatites in Lockers Bay, elsewhere i.e. in Indian Bay St is generally only locally developed in high-strain regions of the migmatites (fig. 5.9).

Metatexites with moderate degrees of melt percentage which have undergone low to moderate degrees of syn-anatexis deformation (types 4 & 5; localities FB 1, 10, IB 3, VF 3, 4, 10, IB 13, LB 1) and are inferred to have experienced only minor 'deformation assisted' melt migration (e.g. Sawyer, 1996). These migmatites preserve stromatic fabrics and in places show local melt migration into low strain zones such as boudin necks and fold hinges (fig. 5.9c), and the development of pinch and swell structures. At higher degrees of melt percentage and low strains, diatexites (type 7; localities LB 1, FB 13) display incoherent and chaotic fabrics. In contrast, migmatites with moderate to high percentage of melt which have experienced high degrees of syn-anatexis deformation display the development of heterogeneous melt migration resulting in focusing and subsequent enhancement of shearing. These effects are highlighted in 'dictyonitic' migmatites (type 8; localities LB 1, 2, SB

Fig. 5.9 Migmatites in Indian Bay, a) coherent 'type 4' layered metatexite; b) structurally incoherent folded 'type 4 / 7' migmatite; c) moderately deformed higher melt % 'type 5' metatexite with local melt migration and disruption of layering, d) schlieric inhomoneneous 'type 11' diatexite showing mixing with the megacrystic Wareham Granite.

a)

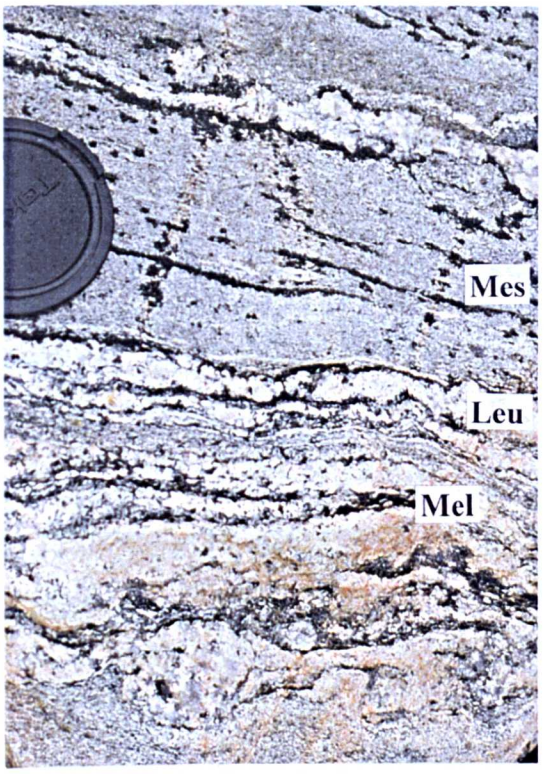

b)

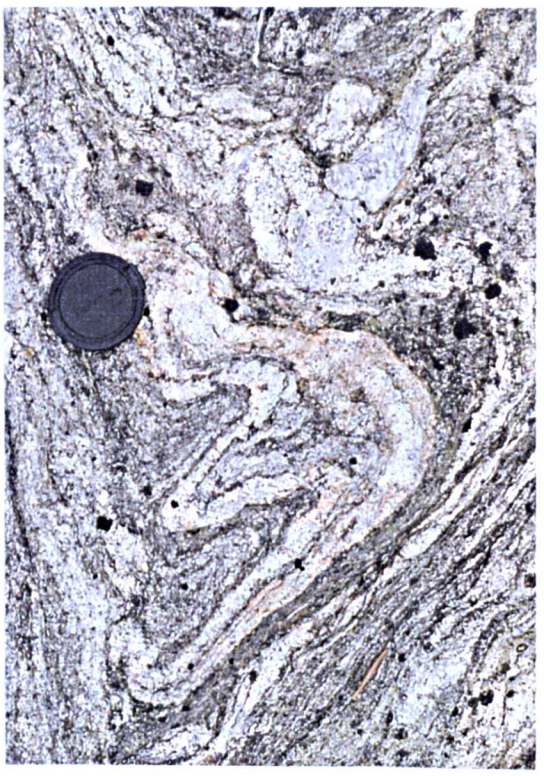

c)

d)

Fig. 5.10 Strain partitioning in migmatites forming a) dictyonitic shear fabric; b) melt-filled sinistral shear pods; c) foliated granitic sheets with minor biotite schlieren.

a)

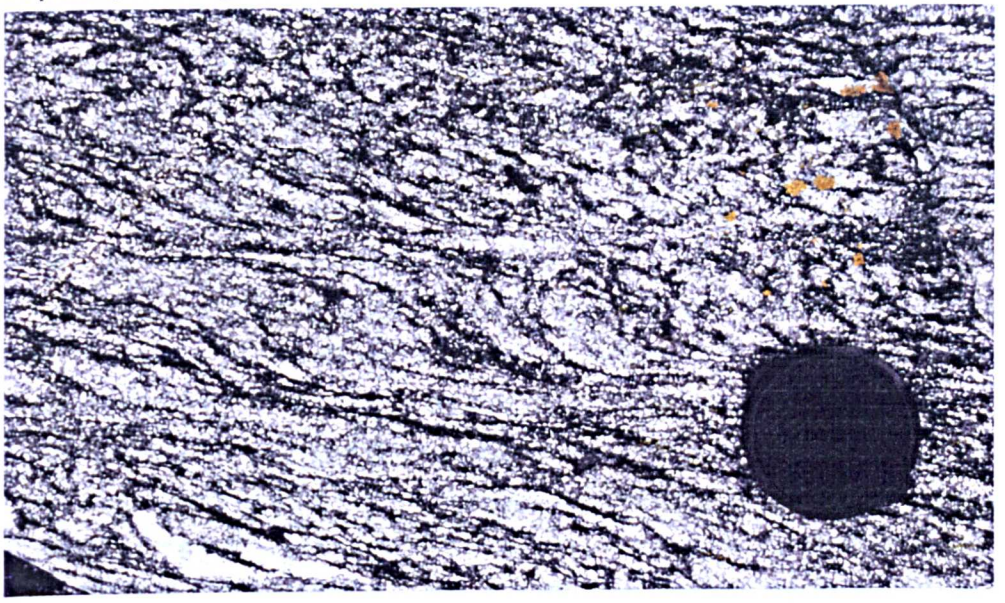

b)

c)

10, 11; fig 5.10a) and in migmatites which contain melt-filled (predominantly sinistral) shear pods (fig. 5.10b). Homogeneous diatexites (fig. 5.10 c) are the product of high degrees of partial melting, and form either localised unfoliated bodies within inhomogeneous diatexites at low degrees of syn-anatectic strain (type 10; localities IB 3, GP 3, 6) or foliated schlieric granitic bodies at higher degrees of strain (type 9 & 11; localities IB 8, 9, 10, FB 17).

The wide spectrum of migmatite types present within the Hare Bay Gneiss migmatite sequence is shown in Indian Bay (fig. 5.9) where rocks display locally variable amounts of melt percentage and syn-anatexis deformation. It is evident that the structure of the migmatites can vary over a 0.5 m scale therefore making correlations between outcrops difficult. The structure within stromatic migmatites is defined by folded layers of S0-Sn which display local disaggregation. Local melt migration into the hinge region of folds is evident (fig. 5.9b). Within moderate to high melt percent inhomogeneous diatexite, the S0-Sn layering has been largely destroyed, the rock comprises of isolated cognate blocks of psammitic paragneiss, stromatic metatexite and type 1 metabasite (e.g. localities IB 4, 8, 13) which are variably wrapped by non-linear schlieric (St) fabrics (fig. 5.9c). It is clear that the more structurally coherent folded migmatites are represented by those which comprise high proportions of psammitic S0-Sn layers. The intermingling of metatexites and diatexites can be seen on an outcrop scale (localities IB 14, 15) where the metatexite is invaded and broken up (fig. 5.8b & 5.9c), or bounded by schlieric inhomogeneous diatexite. The inhomogeneous diatexites are similarly invaded by (locality IB 13), or contain (locality IB 14, 16) homogeneous diatexite which forms diffuse pods of melt (centimetre to metre scale). No evidence is seen to suggest that large amounts of melt are generated from the melting of migmatites. In Freshwater Bay (localities FB 17), metre scale outcrops of homogeneous diatexite form discrete bodies and sheets (10-15 m scale) which intrude, and locally mingle with inhomogeneous migmatites (fig. 5.11) suggesting higher degrees of mobilisation. These migmatites are characterised by coarse biotite-rich restitic schlieren (fig. 5.9d) which show a strong preferential alignment.

In the western region of the migmatite belt (e.g. localities GP 2, IB 1, 17, 18) high melt percentage migmatites are clearly seen to mix and mingle with coarse alkali feldspar-rich megacrystic Wareham granite (fig. 5.9d). The migmatites commonly display a nebulitic texture characterised by coarse 'blebs' of alkali feldspar which are surrounded by clots (0.5-1 cm scale) of biotite and prismatic sillimanite (fig. 5.8c). On Gull Island (locality IB 18) the Wareham Granite clearly locally mixes with the mobilised migmatites to produce a 'hybrid' alkali feldspar-rich granitic melt, in general however, the migmatites do not display evidence for mixing with the foliated granites (e.g. the Cape Freels and Lockers Bay Granites).

The $D3_{EAST}$ migmatites throughout the domain show variable development of retrogressive $D4_{EAST}$ fabrics and assemblages. $S4_{EAST}$ forms a range of fabrics from mid amphibolite to upper greenschist facies which overprint $D3_{EAST}$ assemblages, and parallel similar grade solid-state fabrics in the foliated granitoids (e.g. the Cape Freels and Lockers Bay granites). $S4_{EAST}$ in the migmatites forms linear solid-state fabrics which are defined by aligned micaceous foliae and S-C shear bands. These are well illustrated in the migmatites located adjacent to the margin of the Lockers Bay Granite

Fig. 5.11 Map of island in Freshwater Bay (locality, FB 17) showing field relationships between types of migmatite and foliated granitoids.

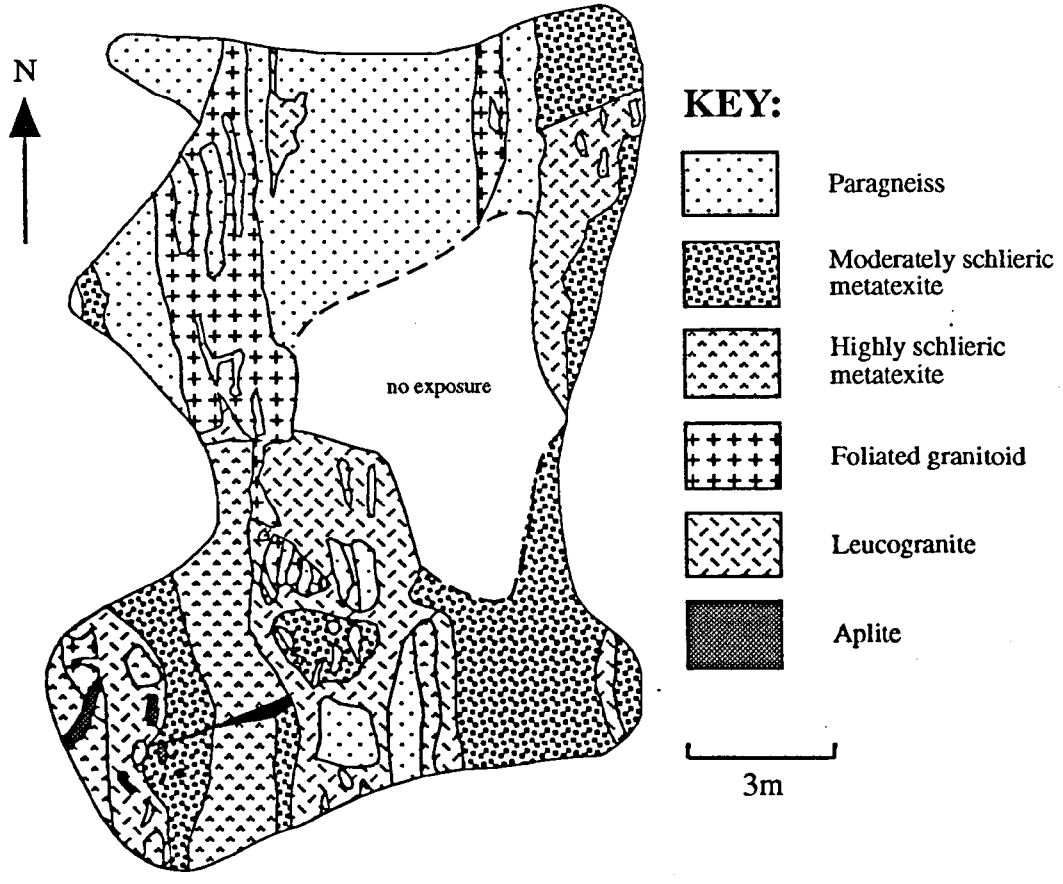

(localities LB 3, 11, 13, 16) and display a spectrum of micaceous lower amphibolite to upper greenschist facies shear fabrics, parallel to similar grade fabrics in the adjacent granite. Similarly, migmatites in the western margin of the Cape Freels Granite at Windmill Bight (localities WB 2, 14) display a variety of $S4_{EAST}$ S-C fabrics which are sinistral, and overprint $D3_{EAST}$ migmatitic assemblages. In places these retrogressive fabrics are contained in metre scale sinistral shear zones which anastomose around pods of $D3_{EAST}$ migmatite. Subordinate development of S5 phyllonitic shear fabrics (e.g. localities LB 4, WB 25) occurs within the migmatites, these fabrics are predominately dextral and are characterised by muscovite-rich greenschist facies S-C shear bands.

5.3.3 Metabasite

Metabasic rocks are commonly associated with felsic material, and occur throughout the Gander Lake Subzone. Three distinct types of metabasite are recognised which display contrasting distributions, field relationships and fabrics.

Type 1 metabasite occurs both within the migmatite and orthogneiss, and has been interpreted as representing mafic bodies which were intruded into the Gander Group metasediments early in the tectonic history of the region (Holdsworth, 1991). These metabasites may broadly correlate with the low grade metabasic intrusions which occur in greenschist facies Gander Group metasediments of domain 3 (O'Neill, 1991; Holdsworth, 1994a). The field relationships which suggest that the intrusion of type 1 metabasites occurred prior to, or during the main phase of $D3_{EAST}$ deformation, and prior to peak $D3_{EAST}$ include, 1) the presence of folds in the metabasic intrusions which are identical to amphibolite facies $D3_{EAST}$ structures in the migmatites and 2) the pervasive development of a fine (millimetre scale) amphibolite facies fabric in the metabasites which is parallel to the $S3_{EAST}$ migmatitic fabric. The type 1 metabasites display a range of disaggregation and boudinage structures. Bodies form both metre scale discontinuous sheets (e.g. localities IB 2, 14, WB 20) and isolated < metre scale rafts (e.g. localities FB 6, 17, IB 4, 8, 9, 10, 16). It is evident (e.g. in Indian Bay), that metabasite within low melt percentage and low strain metatexite forms sheets which display boudinage and local thickness variation (fig. 5.12a) and are laterally persistent (over 10's metres). In contrast, metabasite within high percentage melt diatexite (also in Indian Bay) forms isolated deformed pods (fig. 5.12b). In Freshwater Bay (e.g. localities FB 2, 3), type 1 metabasite forms deformed pods which display evidence for refolding during progressive $D3_{EAST}$ (fig. 5.12a) and the formation of new axial planar fabric defined by aligned amphiboles. The metabasites are in places spatially associated with variably deformed metadioritic bodies (e.g. HB 4, 5), also commonly associated with type 1 metabasite is a coarse to pegmatitic leucocratic granitic material (e.g. locality IB 4) which commonly surrounds, or is contained as veins within the bodies (fig. 5.12b).

The type 1 metabasites display subordinate development (e.g. localities LB 5, 6) of northeast-southwest trending micaceous platey shear fabrics which are in places actinolitic. The fabrics are anastomosing in form with an associated moderately plunging mineral lineation, and are attributed to $S4_{EAST}$ retrogression. A range of these types of fabrics are present within type 1 metabasites in the central region of Lockers Bay, and appear to be concentrated in the marginal zone of the Locker Bay Granite. The development of retrogressive fabrics in type 1 metabasite is also evident at Windmill Bight (locality WB 24) where assemblages are transposed by micaceous S-C shear bands which display a sinistral shear sense.

A second, more massive group of metabasites termed 'type 2' form intersheeted mafic to felsic complexes which occur predominately in the east of the domain, and are distributed in isolated zones in the vicinity of the Dover Fault (i.e. east of Lockers Bay, Shoal Bay, Trinity Gut and Freshwater Bay). Sheets (1-5 m in thickness) are orientated northeast to southwest, subparallel to the regional foliation. At Shoal Bay (e.g. localities SB 4, 6, 10) and Trinity Gut (e.g. localities TG 1, 2),

Fig. 5.12 Type 1 metabasite, a) folded ($F3_{EAST}$) pod within stromatic migmatite, b) angular block within inhomogeneous diatexite.

a)

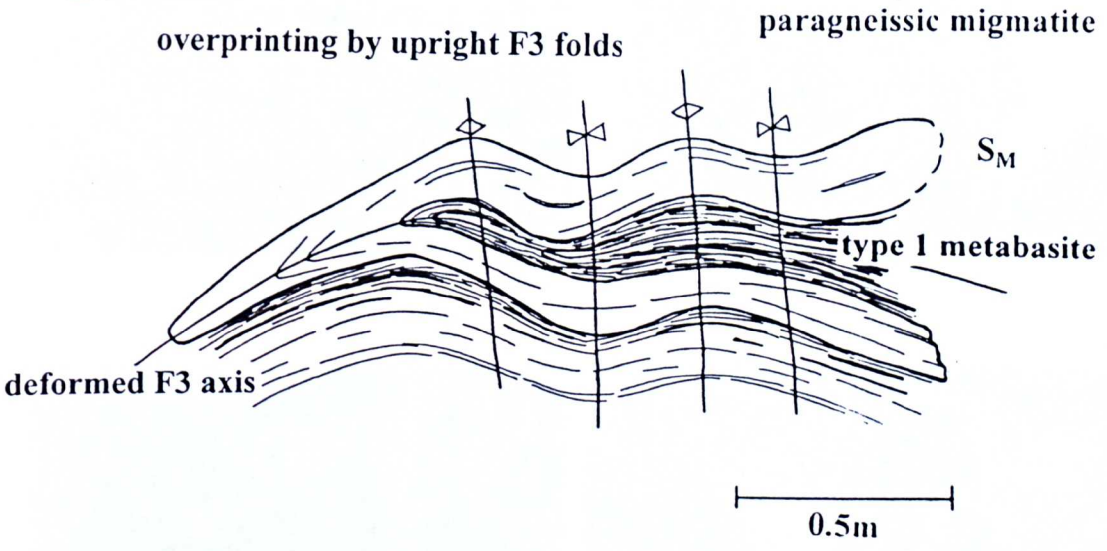

b)

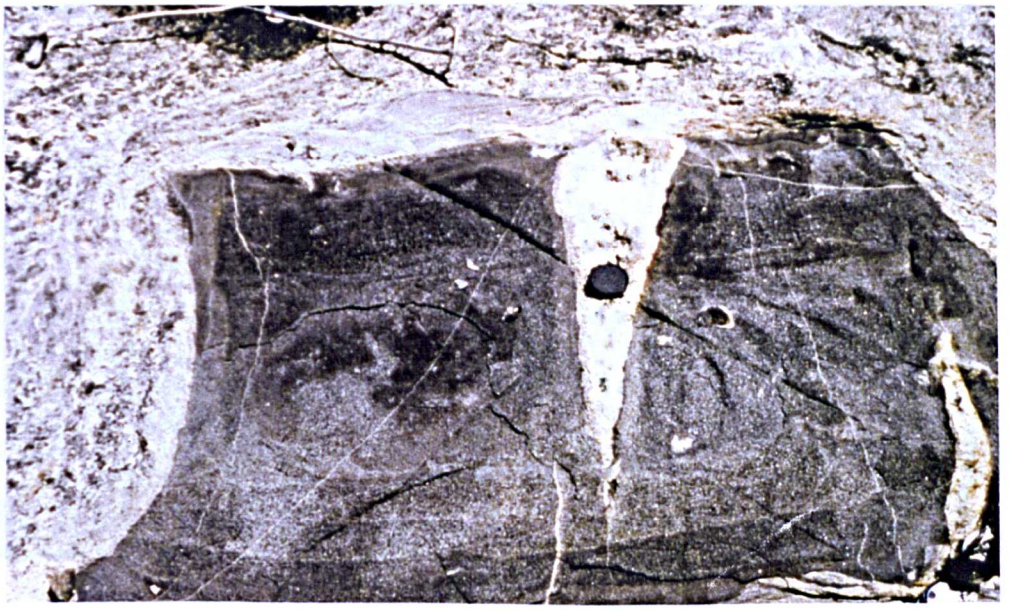

Fig. 5.13 Type 2 metabasic assemblages, a) fine amphibolitic layered metabasite with leucogranitic segregations; b) folded amphibolite facies layering with new transposition fabric; c) schlieric plagioclase-rich melt enclosing clinopyroxene-bearing pods; d) isolated metabasite pod in plagioclase-rich melt.

a)

b)

c)

d)

metabasites form metre scale sheets and deformed pods which are variably associated with sheets of foliated granite, metagabbro and schlieric plagioclase-rich granitoid (fig. 5.13). Type 2 metabasites display a pervasive fine amphibole-rich layered fabric which is deformed into tight to isoclinal folds (fig. 5.13b) and variably transposed on limbs by a planar fabric of similar grade and appearance. Both the folded and transposition fabrics commonly enclose elongate (2-10 cm) clinopyroxene-bearing pods (fig. 5.13c) which are characterised by their green colour and weathered appearance. Similar to the type 1 metabasites, type 2 metabasites are commonly associated with small volumes of coarse tonalitic to granitic material (fig. 5.13a.) contained both within anastomosing fine vein networks (e.g. localities SB 9), and larger scale veins which cross-cut the fabric within the bodies (fig. 5.13 c & d; e.g. localities SB 4, 6).

The regional structural correlation of fabrics within the type 2 metabasites and their field relationship with type 1 metabasite is unclear due to sheared (lower amphibolite to upper greenschist facies) contacts between type 2 metabasic complexes and the Hare Bay Gneiss assemblages. At Trinity Gut, the fabric in type 2 metabasite is cross-cut by foliated megacrystic granite of similar appearance to the Lockers Bay Granite. If this does in fact represent part of the Lockers Bay Granite, it would suggest that the metabasites were metamorphosed prior to its emplacement (dated as *c.* 417 Ma by high precision U-Pb on zircon and titanite; Dunning *et al. in prep*), possibly during $D3_{EAST}$. However, no direct evidence relates these granite sheets to the Lockers Bay Granite, therefore no link can be made between $D3_{EAST}$ and the structures and fabrics within the type 2 metabasites.

A third minor group of metabasite, termed 'type 3', forms bodies of gabbroic to dioritic composition within the foliated Lockers Bay Granite. The bodies contain lower amphibolite to greenschist facies deformation fabrics which are similar to those contained within the Lockers Bay Granite. The type 3 metabasites preserve magmatic and ductile recrystallisation fabrics, although lack the pervasive development of an upper amphibolite facies metamorphic fabric. These metabasites are interpreted to have been intruded into the domain synchronously with the Lockers Bay Granite (post-peak $D3_{EAST}$ and syn $D4_{EAST}$) *c.* 417 Ma (Dunning *et al. in prep*).

5.3.4 Orthogneiss

Orthogneiss comprises a series of tonalitic to granitic bodies which occur within a *c.* 10 km wide high grade zone adjacent to the Dover Fault and do not exhibit features consistent with a derivation from Hare Bay Gneiss migmatites. Previous classifications have included some orthogneiss as part of the Hare Bay Gneiss, and others as belonging to later intrusive suites (i.e. Blackwood, 1977; Hanmer, 1981; Holdsworth, 1994a). A complete textural gradation from folded granitic augen gneiss to mylonite, protomylonite and megacrystic granite protolith still preserved in shear-bounded, low-strain pods has been described at Valleyfield (Hanmer, 1981; Holdsworth, 1991). In places (e.g. locality IB 8, FB 9, 14), orthogneiss encloses deformed migmatite and type 1 metabasite, these rare orthogneisses (previously described by Blackwood, 1977) may be interpreted as granitic bodies emplaced post $D3_{EAST}$ and syn-early amphibolite facies $D4_{EAST}$.

A group of distinctive granite gneisses occurring at Cape Freels, Valleyfield and Freshwater Bay (figs. 5.1 & 5.3) displays a metamorphic fabric which is deformed by the $D3_{EAST}$, and is interpreted to represent the earliest and most strongly transposed part of the igneous suite in the domain (e.g. Holdsworth, 1994a). At Windmill Bight (e.g. localities WB 21, 32, 34), orthogneiss forms a granitic to tonalitic banded augen gneiss contained as sheets (< 50 m scale) within paragneiss and stromatic metatexite which are spatially associated with discontinuous pods (≤ metre scale), and coherent sheets (1-3 m scale) of type 1 metabasite. Contacts between the orthogneiss, metabasite and the host Hare Bay Gneiss are in general strongly transposed and sheared (e.g. locality VF 2) and original intrusive igneous relations are not preserved. An intrusive origin is, however suggested by the presence of deformed metasedimentary rafts within the orthogneiss (Schofield *et al.* 1996). At Valleyfield, orthogneiss forms metre scale bodies which are folded in association with paragneissic and stromatic migmatites (locality VF 1). The gneissic fabric in the orthogneiss is defined by a recrystallised metamorphic fabric comprising of Q and M domains, and characterised by partially or completely recrystallised alkali feldspars or plagioclase megacrysts which coalesce to form a L-S gneissosity. This fabric was variably deformed during progressive $D3_{EAST}$, and forms close to tight upright fold structures which commonly show attenuation on the limbs and transposition by new streaky gneissic fabric (e.g. locality WB 14, 19, VF 1). The orthogneisses display a range of grades of retrogressive $D4_{EAST}$ fabrics, these are well illustrated at Windmill Bight (e.g. localities WB 16, 20, 23, VF 1) where amphibolite-grade gneissic fabrics are locally deformed and overprinted in discrete lower amphibolite to greenschist-facies shear zones (fig. 5.38c). The $S4_{EAST}$ fabrics form coarse S-C micaceous shear fabrics which overprint the $D3_{EAST}$ gneissic fabrics.

5.4 Petrological descriptions

5.4.1 Paragneiss

Paragneiss comprises discrete layers of micaceous and quartzofeldspathic-rich mineralogy which show a variety of prograde and retrograde assemblages (formed during $D3_{EAST}$ and $D4_{EAST}$ - D5 respectively). M domains comprise of variable amounts of biotite (α = straw yellow, $\beta = \gamma$ = brown-green), andalusite, fibrolite / prismatic sillimanite, muscovite, chlorite, ilmenite, rutile and hercynite. Q domains are composed predominately of quartz, plagioclase and alkali feldspar.

At Centreville (fig. 5.2c), $S3_{EAST}$ is a gneissic segregation which is defined by a Q-M layered fabric comprising dark biotite-, andalusite / sillimanite-rich domains which separate pale quartzofeldspathic domains (e.g. sample Tk 108a, locality CV 2). The andalusite forms large porphyroblasts within the fabric (fig. 5. 15a), and contains fine inclusions of ilmenite and hercynite, the cores of the andalusites display a distinct pink pleochroism. The presence of prismatic sillimanite along $S3_{EAST}$ is rare, although at Windmill Bight (sample TK 95 20, locality WB 14) paragneiss shows an $S3_{EAST}$ Q-M fabric with M domains defined by coarse biotite, prismatic sillimanite and fibrous sillimanite. The muscovite and chlorite associated with these fabrics replaces the margins of the biotite and andalusite and is clearly retrogressive, however, minor amounts of prograde muscovite

are present and form fine to medium subidiomorphic grains whose margins show evidence for instability. The absence of prograde muscovite, and the presence of minor melt segregations along $S3_{EAST}$ suggests that assemblages are a product of prograde muscovite dehydration melting operating in the stability fields of andalusite / sillimanite by the following reaction:

Ms + Qtz → Als + Kfs + melt (R7a)

(Chatterjee & Johannes, 1974).

Fig. 5.14 Mineral reactions inferred for assemblages in domain 4.

Reaction:	Author	Reaction #:
Ms + Qtz → Als + Kfs + L	Chatterjee & Johannes (1974)	R7a
Ms + Qtz → And + Kfs + L	(as above)	R7b
Bt + And + Qtz → Crd + Kfs + L	Holdaway & Lee (1977)	R8a
Bt + Sill + Qtz → Crd + Kfs + L	(as above)	R8b
Ms + Kfs + Ab + Qtz + V → L	Thompson & Algor (1977)	R4
Hbl + Pl → Hbl + Pl + cpx ± Fe-Ti oxides + H_2O	Spear (1981)	R9
oxidised mafic phases + Sph → reduced mafic phases + Ilm + O_2	(as above)	R10
basalt wet solidus	Yoder & Tilley (1962)	R11
oligoclase-in	Maruyama *et al.* (1983)	R12
two plagioclase stability	(as above)	R13
Ca-Amp solidus	Begin (1992)	R14

The development of $S4_{EAST}$ retrogressive fabrics which overprint $D3_{EAST}$ assemblages is seen in paragneiss at Old-Jingle (sample TK 94 108, locality CV 2). Biotite-rich $S3_{EAST}$ domains show development of cross-cutting medium to coarse muscovite. Andalusites display marginal replacement and overprinting by intergrowths of coarse muscovite containing both prismatic, and fibrous sillimanite. Similar textural relationships are seen in the paragneiss at Windmill Bight where overprinting of the $S3_{EAST}$ biotite-rich fabric during $D4_{EAST}$ has formed assemblages of intergrown dynamically recrystallised white mica, fibrous and prismatic sillimanite which is cross-cut by coarse muscovite. The fibrolite forms radiating bundles and matted intergrowths within muscovite-rich fabric (fig. 5.15b), and forms anastomosing foliae around quartz and feldspars (sample TK 95 20, locality WB 14). The muscovite foliae preserve limbs of tight to isoclinal microfolds (thought to represent residual crenulation folds). Prismatic sillimanite forms bladed crystals with marginal alteration to aggregates of white mica. Similarly, alkali feldspar commonly displays marginal alteration to fine muscovite. The association of crenulated foliae of fibrolite with muscovite in medium to high grade schists has been widely documented (e.g. Vernon, 1987), and has been

Fig. 5.15 Paragneissic fabrics, a) sillimanite / fibrolite pseudomorphs of andalusite in folded paragneiss; b) $S3_{EAST}$ fabric defined by anastomosing biotite-, muscovite-rich layers (field of view of b; 6.5mm).

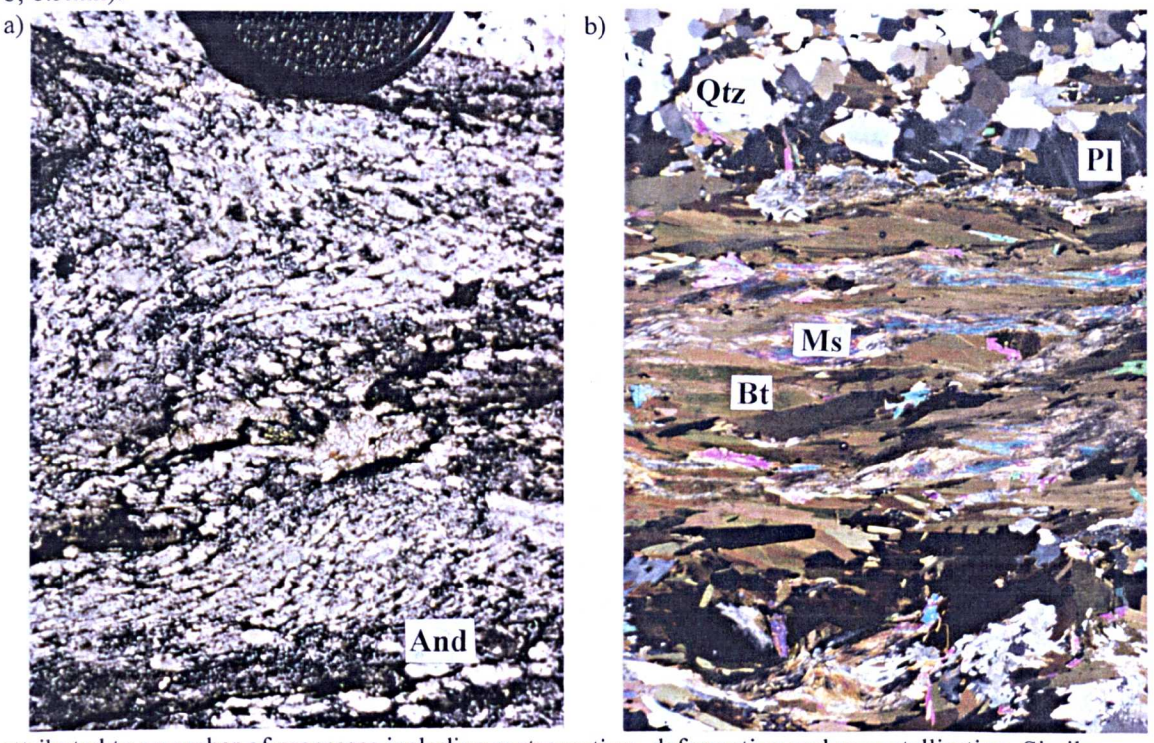

attributed to a number of processes including metsomatism, deformation and recrystallisation. Similar assemblages and textures have been previously described by Jones (1994) and interpreted as the product of reaction reversals. The $D4_{EAST}$ assemblages and textures described above are similarly interpreted as being the product of subsolidus reversal of reaction R7a (fig. 5.14). This reaction may be operating in either the sillimanite field (Richardson *et al.* 1969) or metastable overstepping into the andalusite field (e.g. Salje, 1986; Wintsch & Andrews, 1988; Kerrick, 1990).

Fig. 5.16 $S4_{EAST}$ sinistral shear fabrics, a) S-C′ fabric in paragneiss; b) amphibolite-grade blastomylonite with coarse biotite and muscovite fish (field of view, a; 8mm, b; 4.5mm).

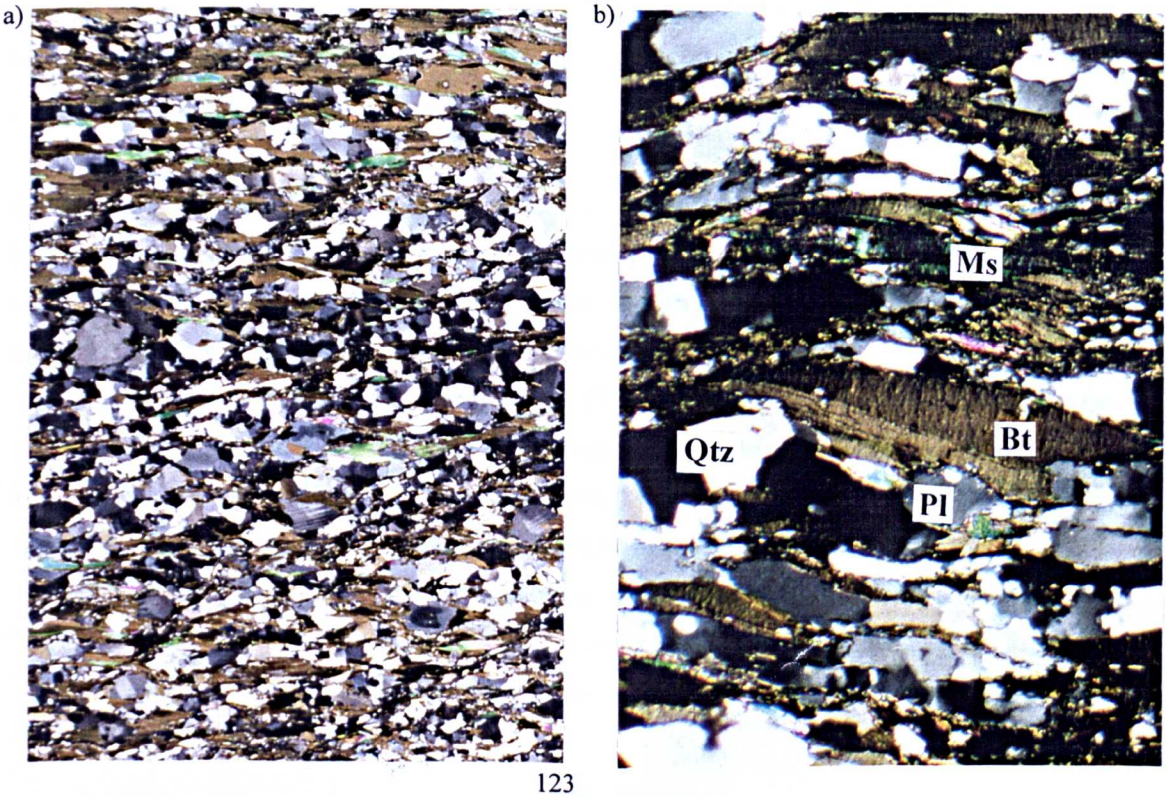

5.4.2 Migmatite

Migmatites within the Gander Lake Subzone exhibit a range of mineralogical assemblages and reactions related to prograde and retrograde metamorphism (formed during $D3_{EAST}$ $D4_{EAST}$ - D5 respectively). Biotite (α = straw yellow, $\beta = \gamma$ = brown - green) is the predominant melanosome component of the migmatites. The composition of the leucocratic portion is highly variable between migmatites, comprising different proportions of cordierite, andalusite, fibrolite / prismatic sillimanite, alkali feldspar, plagioclase, quartz, biotite (α = straw yellow, $\beta = \gamma$ = brown - green), muscovite, ilmenite, hercynite and apatite. Mesosome portions generally comprise variable amounts of biotite (α = straw yellow, $\beta = \gamma$ = brown - green), quartz, plagioclase, muscovite, ilmenite and rutile.

In the west of the domain at Greenspond Road (fig. 5.2), leucocratic components of migmatites (e.g. samples NF 92 74, TK 95 55, locality GP 4, sample TK 95 58, locality 5) are characterised by the development of andalusite porphyroblasts intergrown with cordierite, alkali feldspar and quartz (e.g. figs. 5.17 & 5.18). Andalusite forms subidiomorphic porphyroblasts which contain inclusions of biotite, quartz, hercynite and ilmenite. All inclusions display subidiomorphic to xenomorphic form (fig. 5.18a). Andalusite commonly shows skeletal form (figs. 5.17a, b, c & 5.18b) with lobate margins. The rims of andalusites commonly contain prismatic and fibrous sillimanite (which also form inclusions within surrounding quartz). The cordierite forms subidiomorphic grains which are intergrown with coarse alkali feldspar, biotite and quartz. Both cordierite and alkali feldspar commonly contain xenomorphic inclusions of biotite and quartz (figs. 5.17b & 5.18a, b). The textures described above suggest that andalusite, biotite and quartz were unstable phases which were being consumed by growth of cordierite, alkali feldspar and sillimanite / fibrolite. These relationships are interpreted to be products of biotite dehydration melting through the following reaction (forming minor amount of both prismatic and fibrous sillimanite as additional reaction products):

$$Bt + And + Qtz \rightarrow Crd + Kfs + melt \qquad (R8a)$$

(Holdaway & Lee, 1977).

Similar assemblages and textures attributed to biotite dehydration melting (e.g. R8a, fig. 5.14) have been widely documented (e.g. Jamieson, 1984; Pereira & Bea, 1994). Jamieson (1984) described the breakdown of andalusite in association with the biotite dehydration melting reaction to produce cordierite, alkali feldspar and excess sillimanite (as described above).

Migmatite types 4 to 8 (fig. 5.5;e.g. sample TK 94 92, locality GP 2) are characterised by the presence of abundant sillimanite forming matted intergrowths with biotite, the margins of the intergrowths show feathery form and are surrounded by xenomorphic quartz (fig. 5.19). The quartzofeldspathic portion of migmatites is characterised by the presence of cordierite and alkali feldspar. Cordierite is subidiomorphic to xenomorphic and contains fine to medium inclusions of biotite, sillimanite / fibrolite, quartz and rare fine inclusions of hercynite and ilmenite (figs. 5.19b & 5.21a, b). Alkali feldspar forms coarse subidiomorphic grains with inclusions of quartz, sillimanite

Fig. 5.17 Petrographic relationships in andalusite-, cordierite-, sillimanite-bearing migmatite NF 92 74 (scale bar = 1mm) showing a) And-, Crd-rich melt portion with Sil as additional reaction product, b) And-, Crd-, Kfs-rich melt, c) breakdown of And and Bt, d) replacement of And by intergrowth of Ms and Sil / Fib, e) pinitisation of Crd, f) inclusions of Bt and Qtz in Kfs and relict And.

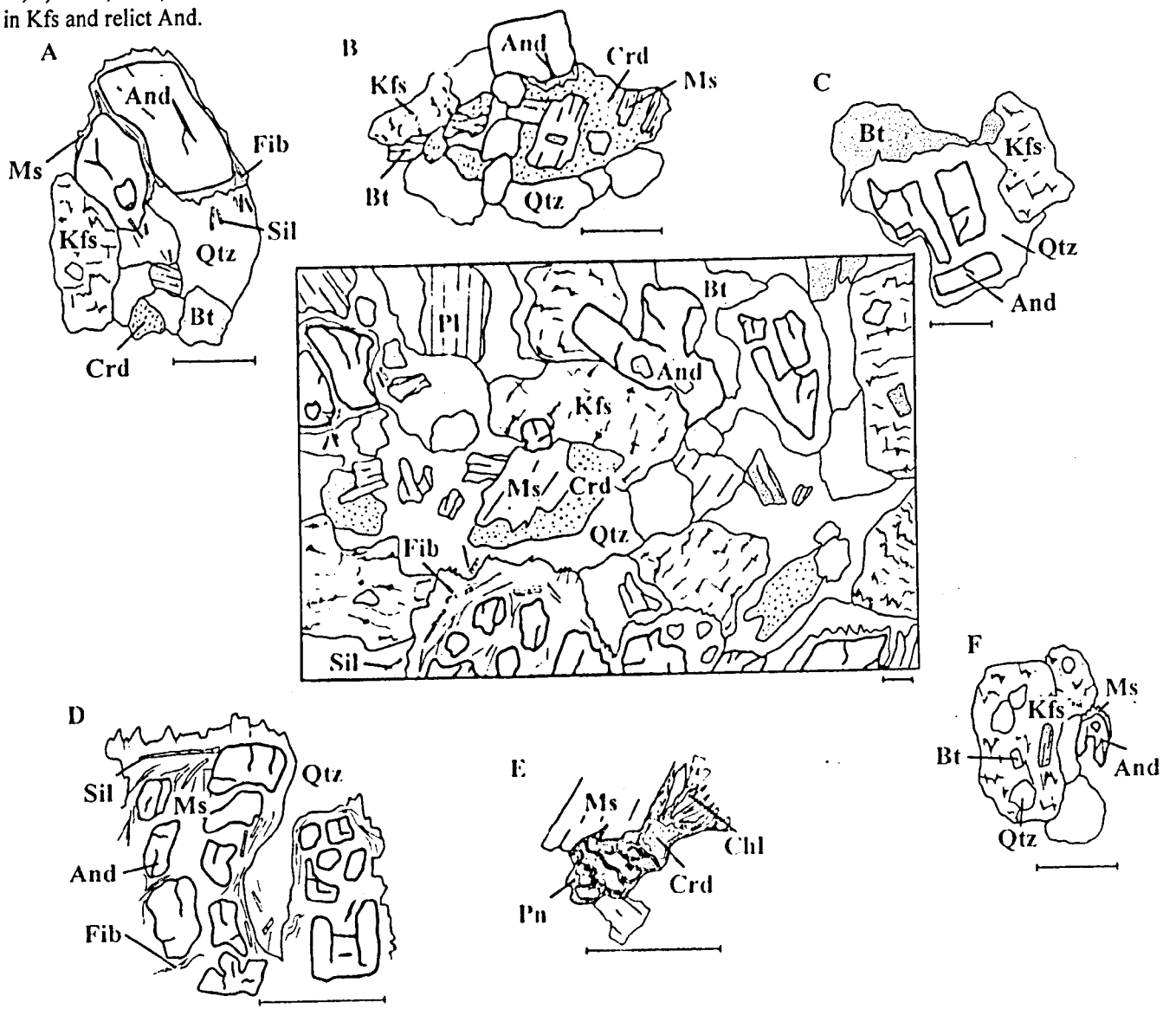

Fig. 5.18 Andalusite-bearing leucosome assemblages of migmatites (NF 92 74), a) andalusite porphyroblast with inclusions of coarse biotite and rare hercynite rimmed by cordierite; b) andalusite, cordierite, alkali feldspar assemblage showing breakdown of andalusite; c) marginal replacement of andalusite by intergrowth of coarse muscovite and fibrolite (field of view; 3.5mm).

a)

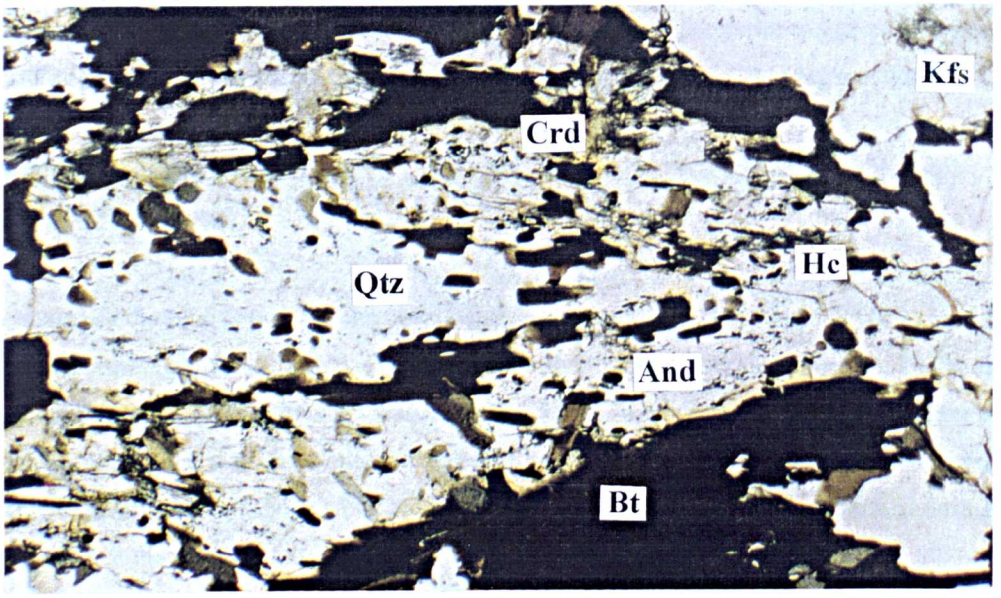

b)

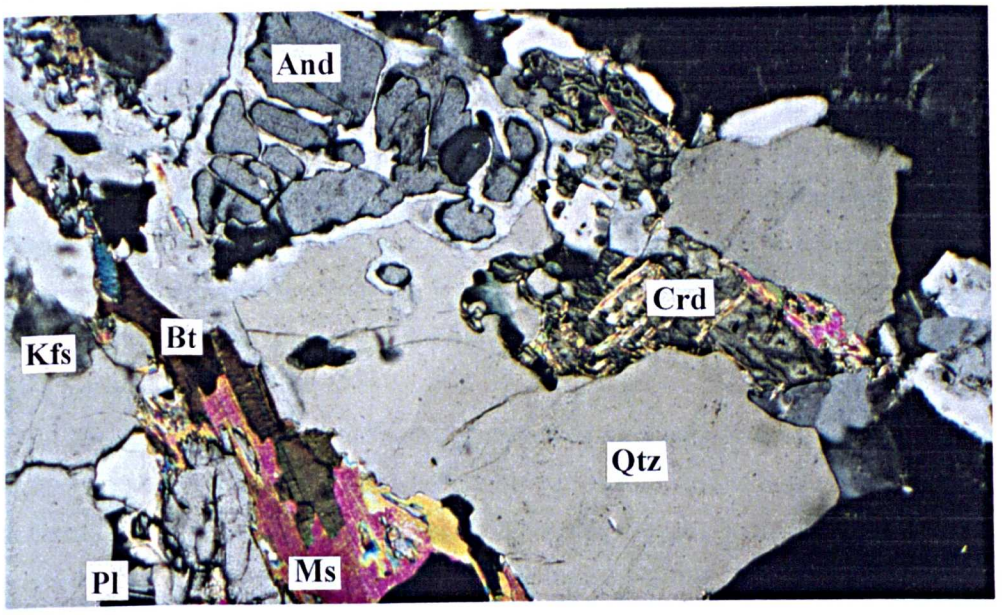

c)

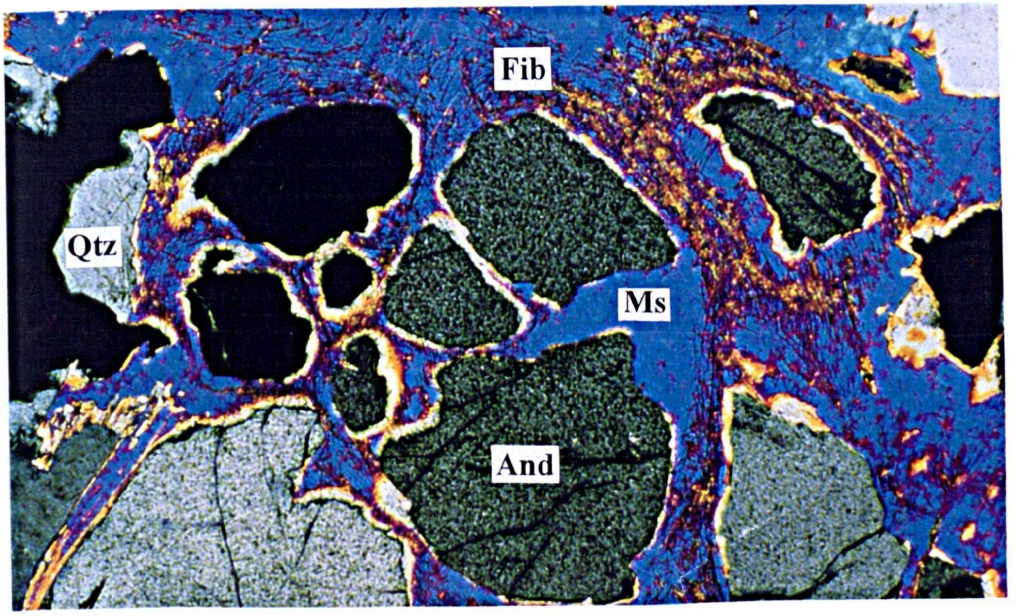

and biotite (fig. 5.19c). The assemblages and textures described above suggest that biotite, sillimanite and quartz are unstable and being consumed during the growth of cordierite and alkali feldspar, and are interpreted as a product of biotite dehydration melting through the following reaction:

$$Bt + Sill + Qtz \rightarrow Crd + Kfs + melt \qquad (R8b)$$

(Holdaway & Lee, 1977).

The quartzofeldspathic portions of the metatexites (e.g. sample TK 94 92, locality GP 2) contain rare relict andalusites (fig. 5.19d) which are intergrown with biotite, cordierite and quartz. The andalusites display xenomorphic form with abundant subidiomorphic to xenomorphic inclusions of biotite and quartz and rare fine grained hercynite. Textures are similar to those previously described in andalusite bearing migmatite (sample NF 92 74, locality GP 4), and are interpreted to have formed during biotite dehydration in the andalusite stability field (by the reaction R8a, fig. 5.14).

Migmatites in the east of the domain (i.e. Trinity , Lockers Bay, Butlers Cove and Freshwater Bay) are characterised by presence of coarse biotite-, sillimanite-rich intergrowths and cordierite-, alkali feldspar-bearing quartzofeldspathic portions (fig. 5. 20), these assemblages do not contain evidence for relict andalusite (e.g. sample TK 94 115, locality LB 7). Cordierite forms coarse subidiomorphic to xenomorphic grains associated with medium to coarse grained biotite and quartz, and contains medium inclusions of biotite and quartz, and fine inclusions of sillimanite, fibrolite, ilmenite and rare hercynite (figs. 5.20 a, b & 5.21a). The above assemblages and textures are interpreted to have formed (similarly to those in sample TK 94 92) through biotite dehydration melting (reaction R8b, fig. 5.14).

$S4_{EAST}$ shear fabrics in the migmatites are defined by biotite-, muscovite-rich layers which wrap quartz and feldspars, and display evidence for recrystallisation and minor kinking. Quartz forms both types 2 and 3 ribbons (Boullier & Bouchez, 1978) and commonly shows a decrease in subgrain size into the C-plane. The feldspars display evidence for recrystallisation. Alkali feldspar porphyroclasts show marginal recrystallisation and development of myrmekite (interpreted as strain induced, e.g. Simpson, 1985). In lower strain regions of $D4_{EAST}$, migmatites display development of a recrystallised texture which is defined by medium to coarse interlocking polygonal grains of quartz and development of coarse polygonal subgrains within cordierite porphyroblasts (fig. 5.20). The polygonal grain boundaries and 120° junctions (in both cordierite and quartz), are characterised by the development of fine needles of prismatic sillimanite and fibrolite, and in places by fine intergrowths of fibrolite and biotite (fig. 5.20d) and are interpreted as products of late-stage recrystallisation of the rocks. Low grade upper greenschist facies $D4_{EAST}$ is characterised by the development of coarse muscovite which cross-cuts $D3_{EAST}$ assemblages in the migmatites. Muscovite forms medium to coarse subidiomorphic laths which are intergrown with quartz ± sillimanite / fibrolite (figs. 5.18d & 5.19f). Similar relationships (previously described in the paragneiss in 5.2.1) are displayed on the margins of andalusites (e.g. samples NF 92 74, TK 94 92, localities GP 4, 2),

Fig. 5.19 Petrographic relationships in andalusite-, cordierite-, sillimanite-bearing migmatite TK 94 92 (scale bar = 1mm) showing, a) intergrowth of Bt, Sil and Qtz, b) Crd with inclusions of Sil, Hc and Ilm, intergrown with Bt, c) Kfs with inclusions of Qtz and Bt, d) relict And (with inclusions of Hc and Bt), intergrown with Bt and minor Crd intergrown with Qtz and Sil, e) breakdown of Bt to Chl and Rt, f) retrogressive Ms (associated with Fib / Sil) replacing Bt.

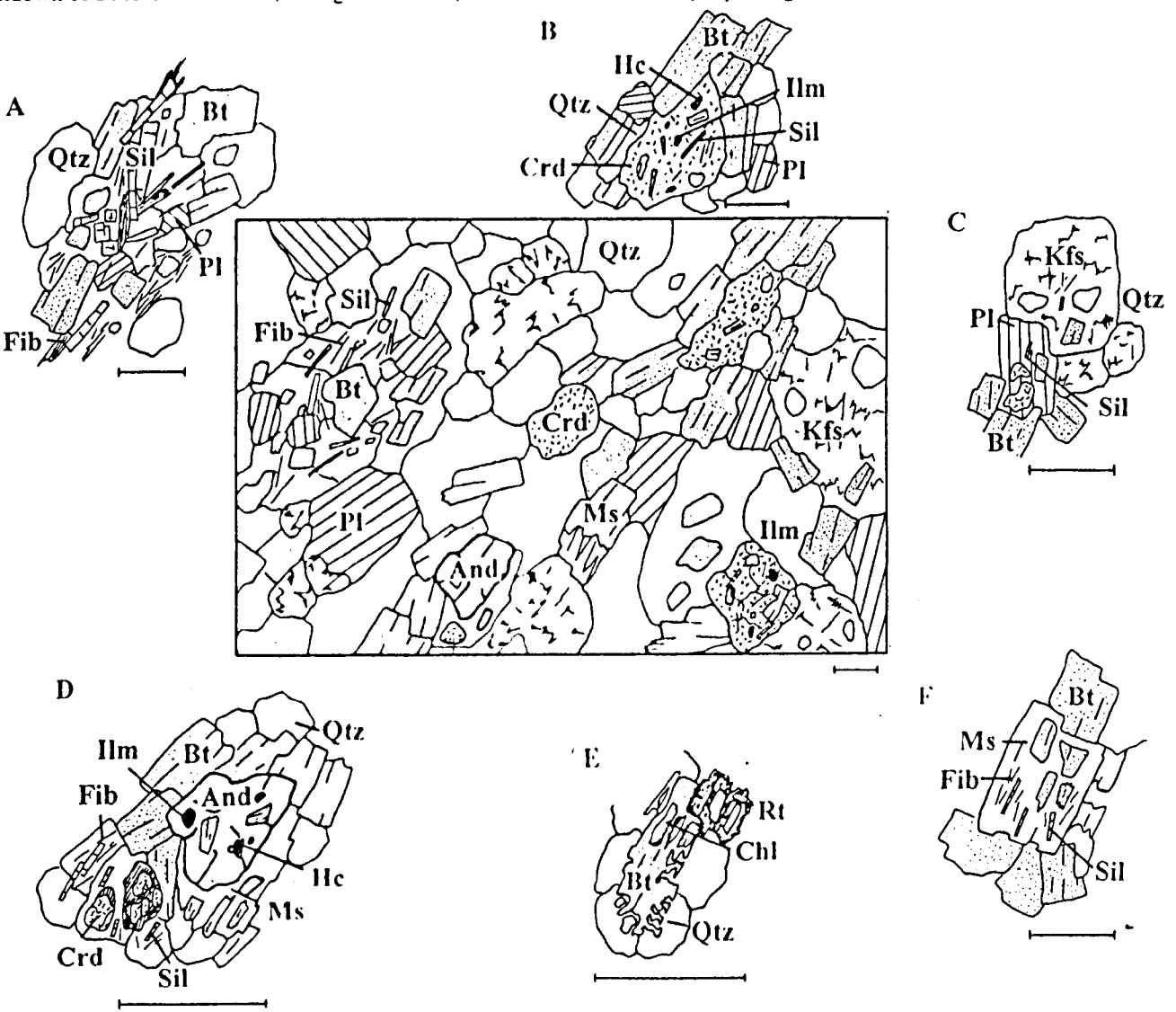

Fig. 5.20 Petrographic relationships in cordierite-, sillimanite-bearing migmatite TK 94 115 (scale bar = 1mm) showing, a) Crd with inclusions of Bt, Sil & Ilm, b) Crd intergrown with Bt and Ilm, c) pinitisation of Crd and replacement by coarse Ms, d) polygonal recrystallised grain boundaries with development of minor Fib.

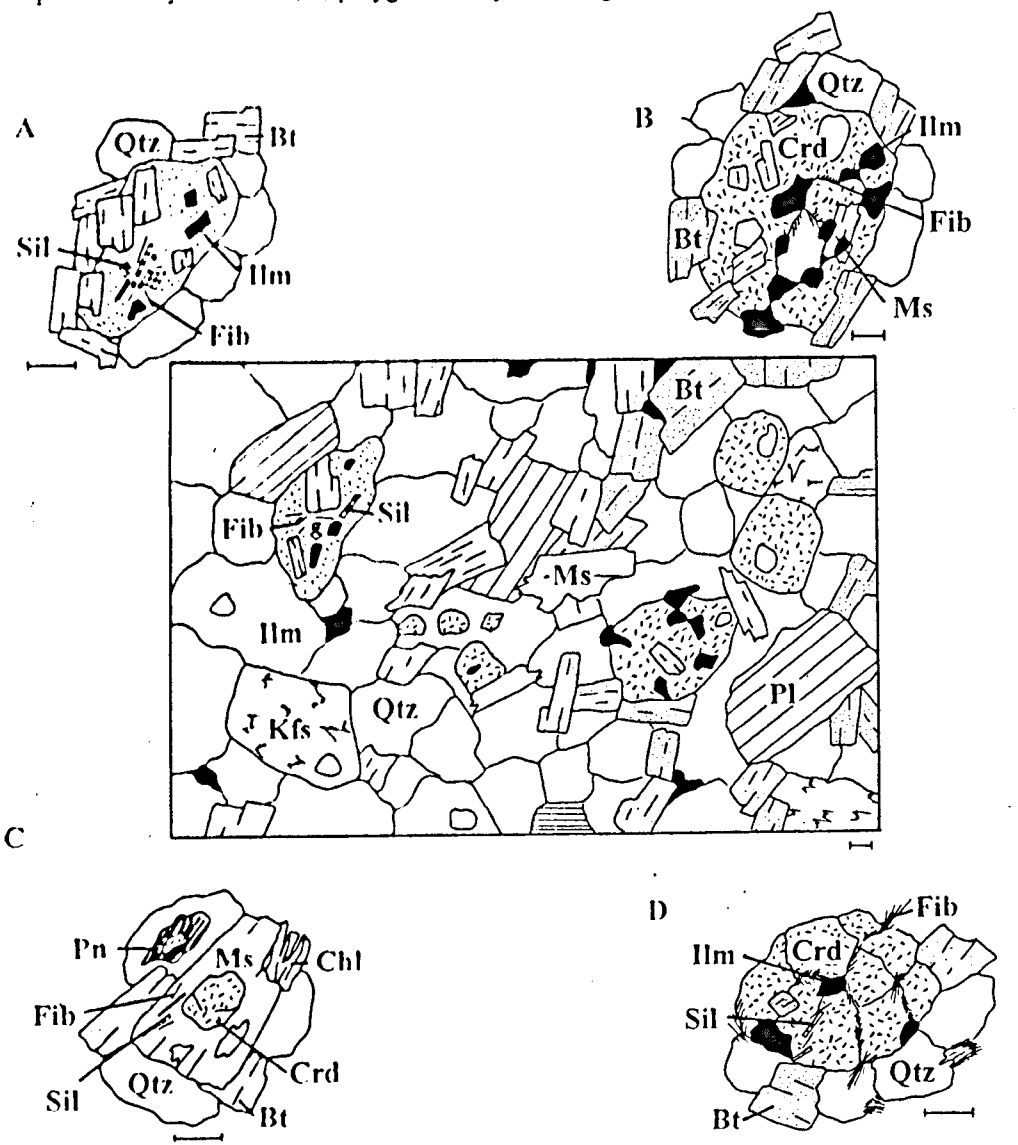

Fig. 5.21 Sillimanite-, cordierite-bearing migmatites, a) development of cordierite with inclusions of embayed biotite on melanosome margin (Tk 94 92); b) cordierite porphyroblast in leucosome, schlieric portion comprises intergrowth of biotite and fibrolite / sillimanite (Tk 94 92); c) stromatic migmatite (Tk 94 115) with sillimanite / fibrolite-, biotite-rich melanosome (field of view; 3.5mm).

a)

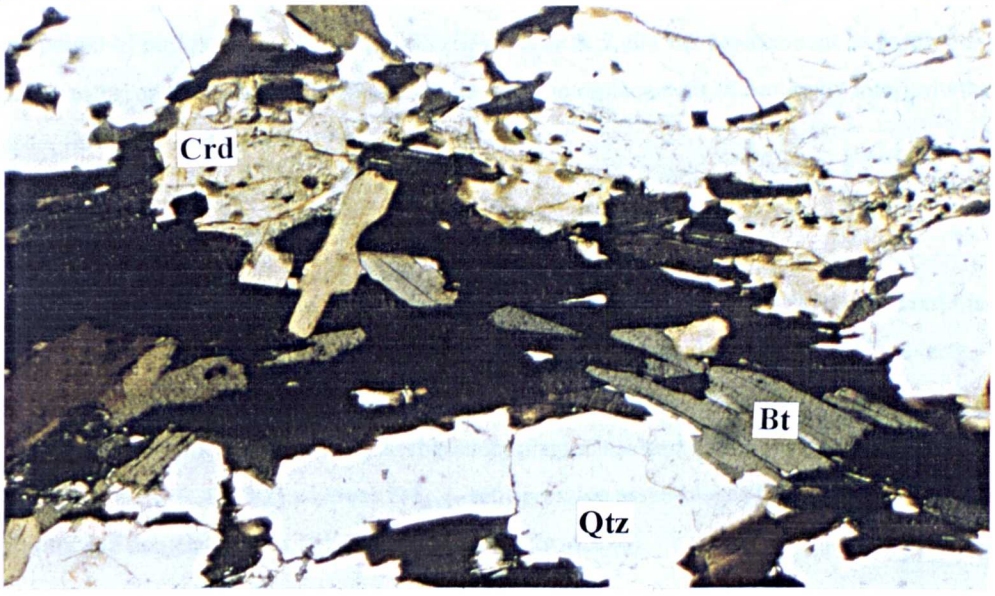

b)

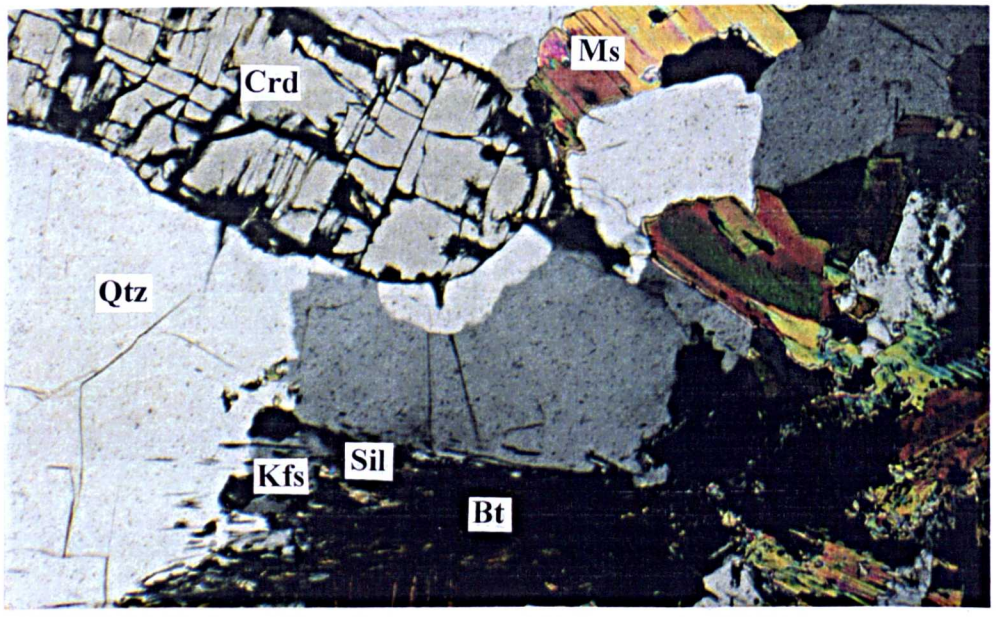

c)

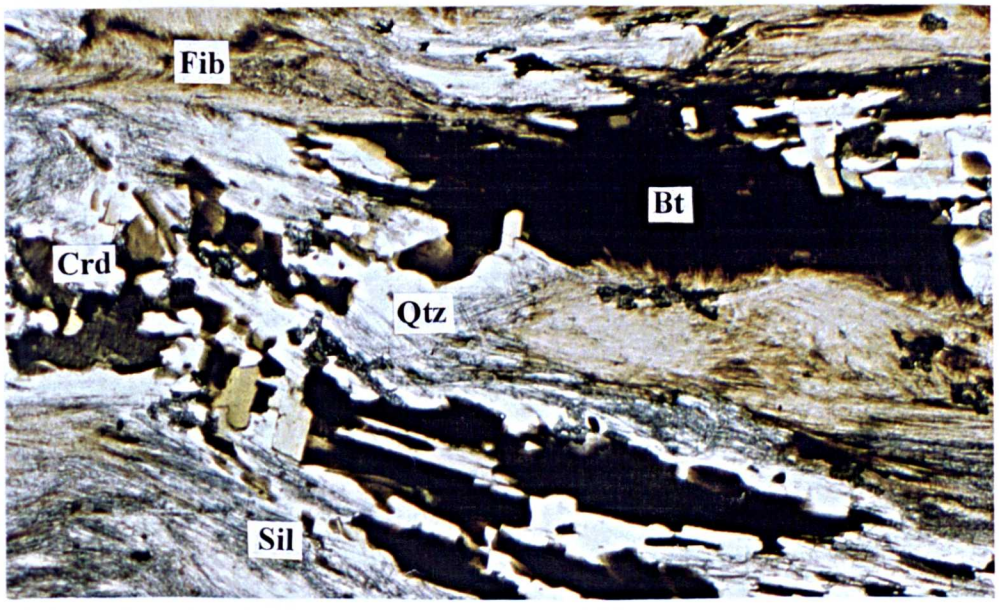

and are interpreted as products of the reversal of reaction R7a (fig. 5.14) during retrogressive $D4_{EAST}$.

Late-stage retrogressive alteration of migmatitic assemblages is widespread and shown by the development of pinitised rims to cordierites (figs. 5.17e & 5.20), the replacement of cordierite by feathery intergrowths of chlorite and muscovite, and the replacement of biotite by intergrowths of coarse chlorite, fine rutile and ilmenite (fig. 5.19e).

5.4.3 Metabasite

The type 1 metabasites display a range of prograde and retrogressive assemblages and textures (formed during $D3_{EAST}$ and $D4_{EAST}$ respectively) and comprise variable amounts of amphibole, quartz, plagioclase, biotite ± epidote, sericite, chlorite, rutile, apatite and opaques. $S3_{EAST}$ forms a penetrative fabric (fig. 5.22a) which is defined by hornblende, plagioclase and quartz (samples TK 94 151, 152, 100a, localities FB 3, 4, IB 2) whereas $D4_{EAST}$ retrogressive assemblages (TK 94 125, locality HB 5), are actinolitic and associated with chlorite and epidote (fig. 5.22b).

Fig. 5.22 Type 1 metabasites; a) $S3_{EAST}$ bearing assemblage, hornblendes display relic igneous brown cores; b) retrogressed $D4_{EAST}$ assemblage of actinolitic amphibole (field of view; 3.5mm).

a)

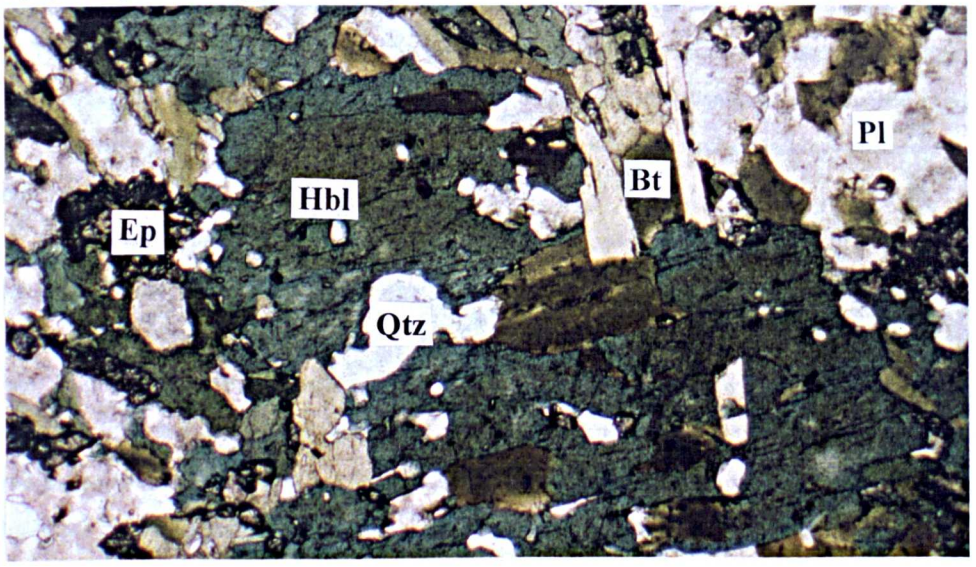

b)

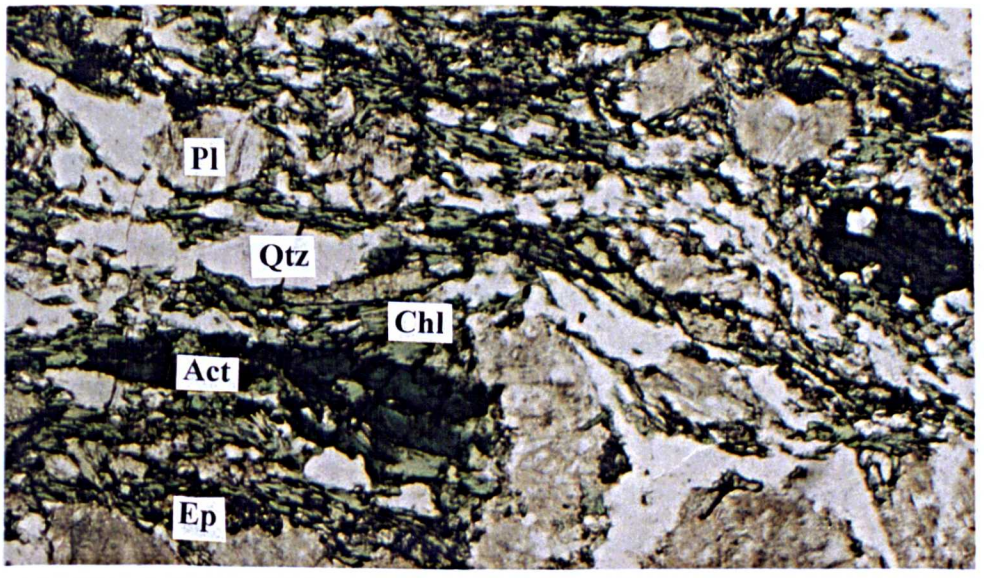

Amphibole (α = pale green - pale brown, β = olive green, γ = dark green - brown) forms medium to coarse preferentially aligned idiomorphic grains which define the $S3_{EAST}$ fabric. Grains commonly show compositional zoning with brown-green colour variation from tschermakitic-core to magnesio-hornblende-rims (fig. 5.22a). The brown cores are interpreted to have formed at high-temperature and to be igneous in origin (e.g. Jamieson, 1981). Plagioclase (An_{50-60}) and quartz form a mosaic of medium to coarse subidiomorphic to xenomorphic grains which interlock with amphibole grains. Dioritic type 1 metabasites (e.g. sample TK 94 151, locality FB 3) comprise lesser amounts of amphibole which forms coarse grains intergrown with biotite, plagioclase and quartz. The amphibole grains are subidiomorphic, forming rare poikiloblastic idiomorphs with inclusions of quartz, plagioclase, biotite and apatite. Biotite is developed in association with the aligned amphiboles along $S3_{EAST}$, quartz and plagioclase form medium to coarse inclusion free grains.

Retrogressive alteration of the type 1 metabasites (e.g. sample TK 94 125, locality HB 5) includes development of actinolitic and high Si magnesio-hornblende amphiboles, coarse subidioblastic biotite, chlorite and epidote (fig. 5.22b). Hornblendes display a pale green colour (α = pale green, β = pale yellow - green γ = pale green), and in places rim, or completely replace pre-existing brown tschermakitic-/ high Si magnesio-hornblende. The rims of the amphiboles display alteration to feathery intergrowths of biotite and chlorite in association with medium subidiomorphic grains of epidote. Plagioclase forms xenomorphic grains of which are oligoclase to andesine in composition (An_{28-40}) and commonly show patchy sericitic alteration. Chlorite and epidote are subordinately developed in the assemblages.

The type 2 metabasites (e.g. samples TK 95 226, 231, localities FB 19, TG 1) display a medium to coarse penetrative fabric which is defined by amphibolitic and quartzofeldspathic layers (fig. 5.23). The assemblages comprise variable amounts of amphibole, clinopyroxene, biotite, plagioclase, quartz ± epidote, chlorite, muscovite, apatite and ilmenite. Amphiboles (α = pale green - pale brown, β = olive green, γ = dark green - brown) are predominantly tshermakitic-hornblendes, forming fine to coarse idiomorphic grains which show a preferential alignment (fig. 5.23a). Amphibole-rich layers comprise predominately of interlocking coarse hornblende in contrast to quartz-rich layers in which amphiboles are fine to medium grained. Quartz-rich layers comprise interlocking amphibole, quartz, plagioclase (An_{25-60}) commonly forming a granoblastic texture.

Type 2 metabasites (e.g. sample TK 95 226, locality FB 19) are characterised by the presence of pods which comprise poikioblastic clinopyroxene grains (diopside) intergrown with coarse granoblastic grains of quartz and plagioclase (fig. 5.23b & c). The cores of the pods contain coarse interlocking plagioclase whereas the rims comprise coarse interlocking clinopyroxene (e.g. sample TK 95 232, locality TG 1). The margins of the clinopyroxene grains are typically embayed and show curved form. Grains contain abundant fine to medium xenomorphic inclusions of plagioclase, quartz and lesser amounts of subidiomorphic amphibole and biotite (α = straw yellow, β = γ = red-brown). Amphibole and biotite inclusions show xenomorphic form, their embayed margins suggest instability and breakdown. Biotite grains are common around the margins of pods intergrown with quartz and plagioclase. Biotites show curved to lobate grain boundaries. The assemblages forming the pods show igneous textures

Fig. 5.23 Type 2 metabasites showing, a) deformed amphibolite grade fabric and development of transposition fabric; b) clinopyroxene-, plagioclase-bearing melt pod; c) clinopyroxene poikiloblasts intergrown with plagioclase (field of view for a; 5mm, b; 8mm, c; 3.5mm).

a)

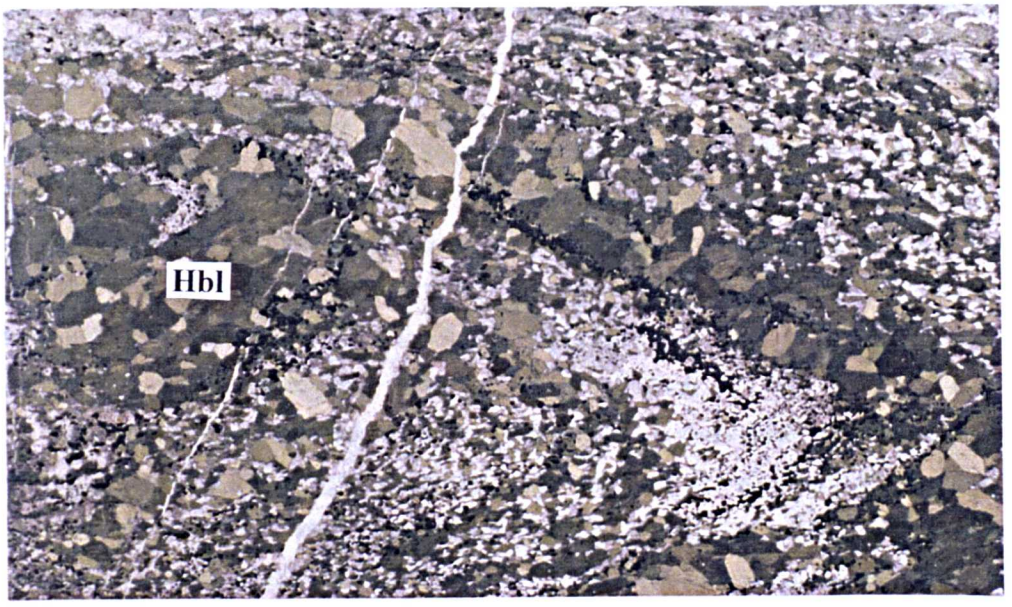

b)

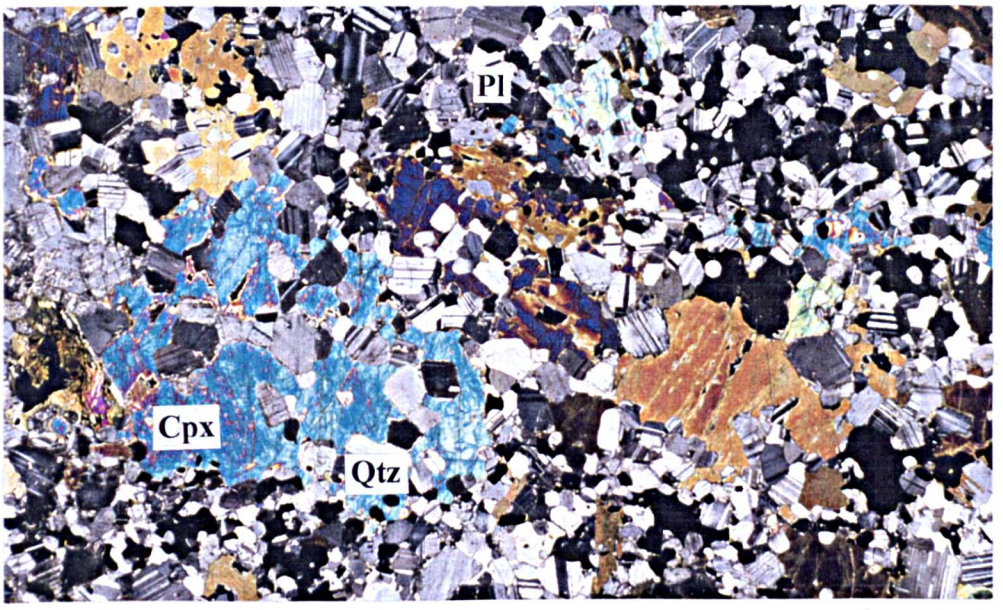

c)

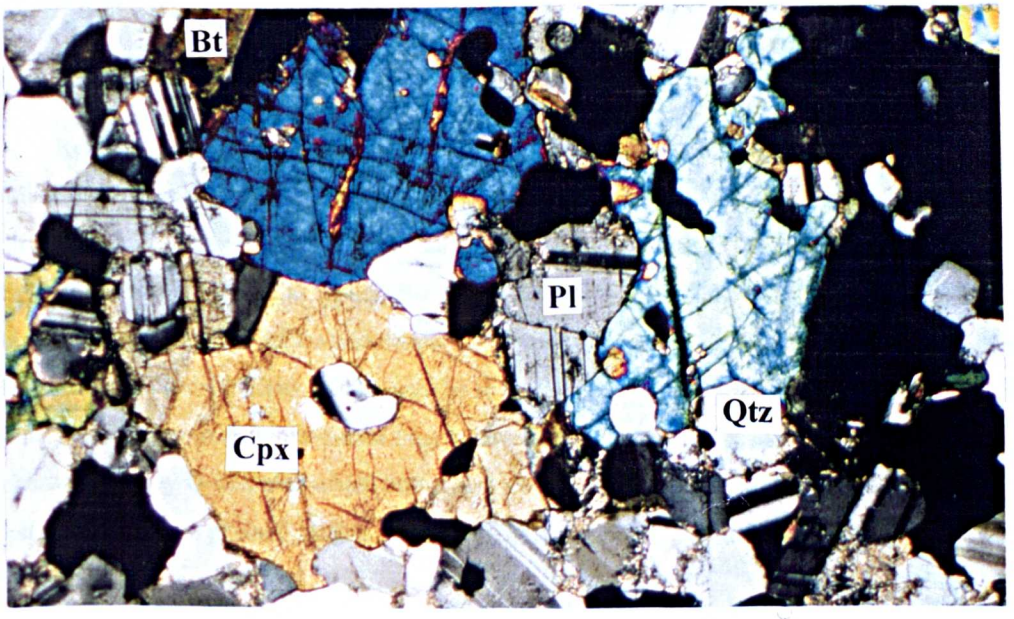

consistent with their crystallisation from a melt, which include subophitic and ophitic texture in the clinopyroxenes, and symplectic intergrowths between clinopyroxene, plagioclase and quartz on the margins of the clinopyroxene grains.

The amphibole-rich transposition fabric in type 2 metabasite at Trinity Gut (e.g. localities TG 1, 2), although slightly coarser, shows the same assemblage, textures and grade as the folded amphibolite facies fabric described above. The transposition fabric forms preferentially on limbs of microfolds (fig. 5.23a), and in places is defined by clinopyroxene. Clinopyroxenes along these fabrics form fine to medium idioblastic grains developed on the rims of coarse clinopyroxene poikiloblasts, and are granoblastically intergrown with plagioclase and quartz (fig. 5.23b & c).

Effects of retrogressive alteration of type 2 metabasites include the marginal replacement of the tschermakitic-hornblendes by magnesio-hornblende, and the marginal replacement of clinopyroxene grains by actinolitic-to tschermakitic-hornblende (e.g. sample TK 95 232, locality TG 1). Subordinate marginal replacement of amphibole grains by biotite is also evident, as well as widespread replacement of clinopyroxene-, plagioclase-bearing pods by coarse intergrowths of epidote.

5.4.4 Orthogneiss

The Q-M layered fabric in orthogneiss (2-4 mm) comprises variable amounts of biotite, quartz, plagioclase, alkali feldspar ± muscovite, chlorite, garnet, ilmenite, apatite, zircon and rutile. The Q domains associated with $S3_{EAST}$ are characterised by augen and discontinuous lenses of alkali feldspar (e.g. samples TK 95 181, 183, localities WB 28, 34) which variably comprise both single coarse grains, and interlocking coarse grain aggregates. The grains show stringer perthitic texture and strain induced twins, their margins are variably recrystallised and are commonly intergrown with fine to medium quartz and plagioclase ($An_{10\text{-}90}$). Augen, which comprise plagioclase grains are less common and display xenomorphic form, minor marginal recrystallisation and development of internal kink bands. Quartz forms type 2 ribbons (Boullier & Bouchez, 1978) which comprise a mosaic of subgrains. M domains associated with $S3_{EAST}$ are characterised by intergrowths of aligned biotite (α = straw yellow, $\beta = \gamma$ = red-brown), grains are medium to coarse with straight to curved margins, and commonly display internal kink bands.

Retrogressed orthogneisses (e.g. at Windmill Bight) are characterised by a range of $S4_{EAST}$ amphibolite to greenschist facies fabrics and assemblages. The $D4_{EAST}$ fabric (e.g. in sample TK 95 184, locality WB 37) is characterised by Q-domains which comprise medium to coarse alkali feldspar porphyroclasts contained within type 3 (Boullier & Bouchez, 1978) quartz ribbons, plagioclase forms a medium grained recrystallised mosaic. M-domains associated with $S4_{EAST}$ shear fabric are characterised by the presence of recrystallised biotite and the subordinate development of muscovite. Lower amphibolite to upper greenschist-facies $S4_{EAST}$ retrogressive fabrics (e.g. sample TK 94 8, locality WB 1) are characterised by Q-domains which comprise type 4 quartz ribbons (Boullier & Bouchez, 1978) and recrystallised medium grained plagioclase, and show subordinate development of

idioblastic garnet. M-domains are characterised by muscovite and marginally recrystallised biotite, which show subordinate marginal replacement by feathery intergrowths of chlorite, ilmenite and rutile.

5.5 Geothermobarometry

5.5.1 Methodology

Methods used to investigate prograde, peak and retrograde metamorphic conditions (during $D3_{EAST}$ and $D4_{EAST}$ respectively) in domain 4 include petrographic determination (using published petrogenetic grids), and the application of various published calibrations of geothermobarometers to thermobarometrically sensitive mineral assemblages. The absence of garnets within the migmatite assemblages eliminates the use of many of the published exchange geothermobarometers.

Conditions of prograde metamorphism (during $D3_{EAST}$) can be constrained by interpretation of petrographic analysis and mineral reaction textures. Two approaches have been taken in an attempt to quantify the P-T conditions. Firstly, the composition of cordierite, in biotite-, cordierite-bearing migmatites has been used as a geobarometer (using the method of Holdaway & Lee, 1977 based on the X_{Mg} value of cordierite coexisting with quartz, plagioclase, aluminosilicate, biotite and melt). Second, various calibrations of the amphibole-plagioclase geothermometer (Spear, 1980; Blundy & Holland, 1990 and Holland & Blundy, 1994) have been applied to type 1 metabasites. These calibrations were also applied to type 2 metabasites as well as the clinopyroxene-plagioclase-quartz geobarometer (Ellis, 1980), in order to investigate the P-T conditions of their formation (the interpretation of which depends on the interpretation of field relationships, see section 5.3.3).

Conditions of retrogressive metamorphism (during $D4_{EAST}$) can be loosely constrained by petrographic and microstructural mineral-fabric analysis of the migmatites and type 1 metabasites (e.g. Boullier & Bouchez, 1978; Simpson, 1985; Tullis & Yund, 1987; Gapais, 1989). The approaches used to quantify conditions include the application of the Spear (1980) calibration of the amphibole-plagioclase geothermometer, and the Plyusnina (1982) amphibole-plagioclase (experimentally calibrated) geothermobarometer to $S4_{EAST}$ bearing type 1 metabasites. The mineral equilibria in low-grade amphibole- and plagioclase-bearing assemblages (Maruyama *et al.* 1983; Begin, 1992) have been used to place further limits on the conditions.

5.5.2 Prograde $D3_{EAST}$

Petrographic analysis of the low-melt percentage paragneissic migmatite (sample TK 95 108a, locality CV 2) from a metapelitic screen contained within the western margin of the Wareham Granite (*c.* 100m east of the 'migmatite front') at Centreville enables investigation of prograde conditions during $D3_{EAST}$.

The rock contains the following mineral modal proportions, andalusite 2 %, fibrous sillimanite 8 %, biotite 20 %, muscovite 27 %, plagioclase 5 %, quartz 35 %, hercynite < 1 %, chlorite 1 % and ilmenite < 1 %. The dominant fabric is $S3_{EAST}$ which is a fine migmatitic layering defined predominately by biotite, muscovite, andalusite and fibrous sillimanite. Pseudomorphing of the andalusite grains present

along the $S3_{EAST}$ fabric by matted intergrowths of fibrous and sillimanite, which are intergrown with coarse muscovite is common (fig. 5.18c). Evidence to suggest that the leucocratic portion of the rocks represents minor volume of in situ melt is shown in the field by the localised migration of leucocratic portion to fold hinges (fig. 5.9b). The presence of prograde muscovite grains (along $S3_{EAST}$) is rare, where present they exibit evidence for instability and breakdown (see section 5.5.1), suggesting that melting in these rocks formed through the muscovite dehydration reaction:

$$Ms + Qtz \rightarrow And + Kfs + melt \qquad (R7b)$$

(Chatterjee & Johannes, 1974).

The above petrographic relationships are best reconciled with the aluminosilicate phase boundaries of Richardson *et al.* (1969).

Further information on prograde $D3_{EAST}$ is given by the petrographic analysis of biotite-, andalusite-, cordierite-bearing migmatites (samples NF 92 74, TK 94 92d, TK 95 57, 242, localities GP 4, 2, 5, IB 7) combined with results of cordierite geobarometry (on sample TK 94 92) from the migmatitic sequence at Greenspond Road and Indian Bay. The migmatites contain the assemblage andalusite 5 %, sillimanite 3 %, biotite 35 %, alkali feldspar 14 %, cordierite 2 %, plagioclase 12 %, muscovite 8 %, quartz 20 %, ilmenite < 1 % and minor hercynite. Representative mineral analyses from sample TK 94 92d are shown in fig. 5.25, full results are given in Appendix A. Cordierite has an X_{Mg} value between 0.56 and 0.58, the X_{Mg} content of biotite range between 0.36 to 0.38. Petrographic and textural relationships including the skeletal appearance of andalusite and biotite (suggesting their instability), the presence of cordierite and alkali feldspar and the absence of prograde muscovite (see above) suggest that melting occurred through the following biotite dehydration melting reaction:

$$Bt + And + Qtz \rightarrow Crd + Kfs + melt \qquad (R8a)$$

(Holdaway & Lee, 1977).

Petrographic grid constraints including the presence of andalusite-bearing neosome and absence of prograde muscovite limits the conditions to below the intersection of the andalusite / sillimanite boundary (Richardson *et al.* 1969), above the metapelitic solidus (R4, fig. 5.14), and above the muscovite-out reaction (R7, fig. 5.14). Geobarometric constraint on the peak conditions for sample TK 94 92 (from the Greenspond Road area) is given by results of cordierite geobarometry (Holdaway & Lee, 1977) which suggests pressures *c.* 3.5 ± 0.4 kbar. The combined results of petrographic and geobarometric analysis for these prograde $D3_{EAST}$ assemblages are displayed on a petrogenetic grid (fig. 5.24), showing the proposed path for prograde $D3_{EAST}$ migmatisation and the local peak conditions (fig. 5.24, box A) of migmatisation *c.* 675 °C and 3.5 kbar.

Fig. 5.24 Petrogenetic grid showing prograde and peak conditions in migmatites in domain 4 formed during $D3_{EAST}$.

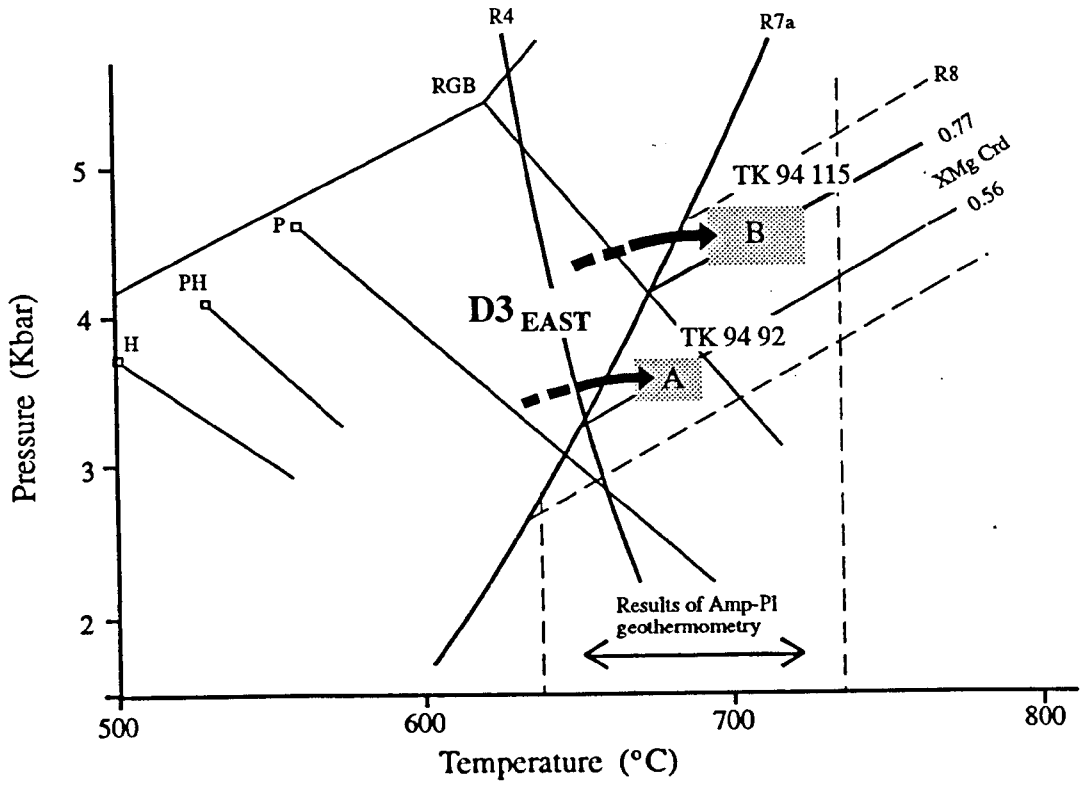

Shaded boxes A & B show P-T estimates from samples TK 94 92 & TK 94 115 respectively. Reactions on grid, R7a) Chatterjee & Johannes (1974), R4) metapelitic solidus; Thompson & Algor (1977). R8) Holdaway & Lee (1977). Al_2SiO_5 data, H; Holdaway (1977), RGB; Richardson *et al.* (1969), PH; Pattison & Harte (1985). P; Pattison (1989). Results of amphibole- plagioclase geothermometry (Spear, 1980) are from $S3_{EAST}$-bearing type 1 metabasite sample TK 94 151.

5.5.3 Peak $D3_{EAST}$ migmatisation

Assessment of overall peak $D3_{EAST}$ conditions of migmatisation in the domain is enabled by petrographic analysis and interpretation of reaction textures, combined with results of geothermobarometry. Both biotite-, cordierite-, sillimanite-bearing migmatite (sample TK 94 115, locality LB 7) and type 1 metabasite (sample TK 94 151, locality FB 3) were analysed. Field relationships show that both assemblages record high-grade fabrics and assemblages formed during $D3_{EAST}$ (see section 5.3.2, 5.3.3).

The migmatite sample contains biotite 10 %, cordierite 9 %, prismatic sillimanite 2 %, fibrous sillimanite 1 %, alkali feldspar 25%, plagioclase 10 %, quartz 35 %, muscovite 5 %, ilmenite 2 % and chlorite 1%. Representative mineral analyses from sample TK 94 115 are given in fig. 5.15, and full results are shown in Appendix A. X_{Mg} values of cordierite range between 0.76 to 0.77. Plagioclase is oligoclase in composition with X_{An} values between 0.16 and 0.23, alkali feldspar has X_{Or} value c. 0.81.

Fig. 5.25 Representative mineral analysis from $S3_{EAST}$-bearing migmatite samples TK 94 92d and TK 94 115.

	Bt	Crd		Pl		Kfs
	Tk94 92d	Tk9492d	Tk94 115	Tk94 92d	Tk94115	Tk9492d
	19	3	3	8	3	4
SiO2	34.14	46.99	48.12	62.48	60.97	64.38
TiO2	2.66	0	0	0	0	0.21
Al2O3	19.11	33.28	33.78	23.15	23.93	19.08
FeO	22.56	9.28	5.6	0	0	0
MnO	0.38	0.85	0.69	0	0	0
MgO	7.25	7.09	9.87	0	0	0
ZnO	0	0	0	0	0	0
CaO	0	0	0	0	5.22	0
Na2O	0	0.55	0	10.08	9.62	1.88
K2O	10.29	0	0	0.24	0.15	14.37
total	96.39	98.04	98.06	100.03	99.89	99.92
Cations per oxygens	*22*	*18*			*32*	
Si	5.27	4.91	4.92	11.10	10.88	11.85
Al	3.47	4.10	4.07	4.85	5.04	4.14
Ti	0.31	0.00	0.00	0.00	0.00	0.03
Fe	2.91	0.81	0.48	0.00	0.00	0.00
Mn	0.05	0.08	0.06	0.00	0.00	0.00
Mg	1.67	1.10	1.50	0.00	0.00	0.00
Zn	0.00	0.00	0.00	0.00	0.00	0.00
Ca	0.00	0.00	0.00	0.78	1.00	0.00
Na	0.00	0.11	0.00	3.47	3.33	0.67
K	2.02	0.00	0.00	0.05	0.03	3.38
XMg	0.36					
XK	1.00					
XAn				0.16	0.18	
XAb				0.83	0.81	
XOr						0.83
XMg		0.58	0.76			

The melt portion of the migmatite is characterised by the presence of cordierite and alkali feldspar. Textures including the presence of subidiomorphic biotite and prismatic sillimanite within cordierite grains (see section 5.4.2) suggest that melting occurred through biotite dehydration:

Bt + Sill + Qtz → Crd + Kfs + melt (R8b)

(Holdaway & Lee, 1977).

The presence of melt, and the absence of prograde muscovite within the assemblages constrains P-T conditions to the high-temperature side of the metapelitic solidus (R4, fig. 5.14), and the high-temperature side of the muscovite-out reaction (R7b, fig. 5.14). Geobarometric constraint (fig. 5.25, box B) is given by results of cordierite geobarometry (Holdaway & Lee, 1977) which suggests pressure conditions of *c.* 4.5 ± 0.4 kbar.

Type 1 metabasite (sample TK 94 151, locality FWB 3) is from the core of a $D3_{EAST}$ folded metabasic pod. The $S3_{EAST}$ fabric is defined by hornblende which is in local equilibrium with plagioclase (see section 5.4.3). The sample comprises hornblende 35 %, plagioclase 27 %, quartz 8 %,

Fig. 5.26 Leake (1978) nomenclature diagram of representative amphibole analyses from type 1 metabasic samples a) TK 94 151 and b) TK 94 125.

Amphibole analysis determined on the basis of 23 oxygens. Formula recalculated to include Fe^{3+}. MH = magnesio-hornblende, TSH HBL = tschermakitic-hornblende, TSH = tschermakite, AH = actinolitic-hornblende.

biotite 15 % and epidote 15 %. For representative geochemical mineral analyses, see fig. 5.27, and for full results see Appendix A. The composition of the amphiboles (fig. 5. 26) plots on the boundary between the magnesio-, and tschermakitic-hornblende fields, Mg / (Mg + Fe2+) values range between 0.73 and 0.79, and Al (IV) values between 6.27 and 6.56. The composition of plagioclase is andesine to labradorite with X_{An} values between 0.49 and 0.59.

Fig. 5.27 Representative amphibole-plagioclase mineral pair analysis for $S3_{EAST}$-bearing type 1 metabasite.

Tk 94 151			
	Amp (r)		Pl (c)
	26		36
SiO2	44.92		54.97
TiO2	1.42		0
Al2O3	10.75		28.79
FeO	15.86		0
MnO	0.32		0
MgO	11.42		0
CaO	11.95		10.39
Na2O	1.47		5.72
K2O	0.54		0
Total	98.65		99.87
Cations	*23*		*32*
Si	6.45	Si	9.91
Al - IV	1.55	Al	6.12
Al - VI	0.27	Ti	0
Fe3+	1.16	Fe	0
Ti	0.16	Mn	0
Mg	2.45	Mg	0
Ni	0	Zn	0
Fe2+	0.75	Ca	2.01
Mn	0.04	Na	2.00
Ca	0.19	K	0
Fe2+			
Mn		XAn	0.5
Ca	1.65	XAb	0.5
Na	0.35		
Ca			
Na	0.06		
K	0.1		
SUM	15.18		
Mg #	0.77		

Petrographic constraints on the conditions of metamorphism recorded by the $S3_{EAST}$ bearing type 1 metabasites is given by the absence of clinopyroxene and melt textures within assemblages, suggesting that they formed on the low-T, low-P side of both the clinopyroxene-in reaction (R9, fig. 5.14) and the basalt wet solidus (R11, fig. 5.14). A range of temperature estimates were given by the various calibrations of the amphibole-plagioclase geothermometer (fig. 5.28). The calibration of Spear (1980) yielded estimates averaging 685 °C (n = 10, 2S.D. = 48 °C), which is consistent with the observed petrographic assemblages and experimental phase relations (shown on fig. 5.37). The calibrations of Blundy & Holland (1990) and Holland & Blundy (1994) gave unreasonably high estimates (B & H; 874 °C, n = 10, 2S.D = 58 °C; H & B, 777 °C, n = 10, 2S.D. = 24°C), which are clearly incompatible with petrographic phase relations (i.e. yield temperatures above the basalt wet solidus and clinopyroxene-in reaction). The reliability of the different calibrations is unclear, although in agreement with the results above, Mengel & Rivers (1991)

obtained best estimates on similar assemblages using the Spear (1980) calibration, and obtained erroneously high estimates using the Blundy & Holland (1990) calibration.

Fig 5.37 is a composite metapelitic and basic petrographic grid, showing the combined results of petrographic and geothermobarometric analysis of assemblages, and summarising the prograde path and peak P-T conditions (*c.* 725 °C and 4.5 kbar) during $D3_{EAST}$.

Fig. 5.28 Results of amphibole-plagioclase geothermometry on $S3_{EAST}$-bearing type 1 metabasite sample TK 94 151.

mineral pair			Temp (P = 4 kbar)		
Amp	Pl	core / rim	S	B & H	H & B
8	2	c - c	677	857	789
9	3	r - r	685	850	771
14	17	r - r	729	903	767
14	18	r - c	709	858	761
23	22	c - c	684	853	801
24	21	r - r	673	864	779
25	33	r - r	688	919	780
25	36	r - c	681	921	777
26	36	r - c	685	871	781
30	36	c - c	637	843	765
Mean			685	874	777
2Sd			48	58	24

S = Spear (1980); B & H = Blundy & Holland (1990);
H & B = Holland & Blundy (1994).

5.5.4 Metamorphic conditions of type 2 metabasite

Investigation of the P-T conditions recorded by type 2 metabasites was enabled by petrographic analysis of sample TK 95 226 (locality FB 19) from a metabasic dyke situated within orthogneiss at Freshwater Bay, and of samples TK 95 232 and TK 95 231 (locality TG 1) from the metabasic sequence at Trinity Gut. Petrographic observations were combined with geothermetric analysis of samples TK 95 226 and TK 95 232, and geobarometric analysis of TK 95 226 and TK 95 231.

The metabasites show the presence of melt pods which comprise equilibrium assemblages of hornblende, plagioclase, clinopyroxene and quartz (see section 5.4.3). The amphibole facies fabric is defined by aligned hornblende, plagioclase and quartz. Sample TK 95 226 is characterised by the presence of large poikiloblasts of clinopyroxene, and contains the following modal proportions clinopyroxene 25 %, hornblende 30 %, biotite 6 %, plagioclase 25 %, quartz 10 % and ilmenite 4 %. Amphiboles are calcic in composition, and plot on the tschermakite-/magnesio-hornblende boundary (fig. 5.29). The composition of clinopyroxene is diopside (fig. 5.30a). Plagioclase is labradorite in composition with X_{An} values between 0.56 and 0.64. Representative mineral analyses are shown in fig. 5.31, and full results given in Appendix A. The samples TK 95 232 and TK 95 231 are characterised by the presence of elongate clinopyroxene-bearing pods and lenses, orientated

Fig. 2.29 Leake (1978) nomenclature diagram of representative amphibole analysis from type 2 metabasite samples, TK 95 226, TK 95 231 &TK 95 232.

Fig. 5.30 Composition & classification of representative clinopyroxene analyses (Morimoto et al. 1988) from type 2 metabasite samples, a) TK 95 226, b) TK 95 232.

Fig. 5.31 Representative amphibole-plagioclase mineral pair analyses for type 2 metabasite samples TK 95 226, TK 95 232 and TK 95 231.

	Amp (r)		Pl (r)		Amp (r)		Pl (r)		Amp (r)		Pl (r)	
	Tk 95 226				Tk 95 232				Tk 95 231			
	62		75		21		29		28		37	
SiO2	44.74		53.87		44.96		62.55		43.37		61.32	
TiO2	1.48		0.00		1.12		0.00		0.96		0.00	
Al2O3	9.30		30.59		8.69		24.20		11.13		24.97	
Cr2O3	0.00		0.00		0.00		0.00		0.00		0.00	
FeO	18.38		0.30		19.49		0.37		17.25		0.25	
MnO	0.30		0.00		0.33		0.00		0.35		0.00	
MgO	10.50		0.00		9.79		0.00		10.54		0.00	
ZnO	0.00		0.00		0.00		0.00		0.00		0.00	
CaO	12.61		11.81		12.74		4.80		12.36		5.70	
Na2O	1.05		5.10		1.51		8.83		1.65		8.39	
K2O	0.97		0.14		0.43		0.00		0.43		0.00	
total	99.33		101.81		99.06		100.75		98.04		100.62	
cations	*23*		*32*		*23*		*32*		*23*		*32*	
Si	6.55	Si	9.59	Si	6.62	Si	11.00	Si	6.36	Si	10.83	
Al - IV	1.45	Al	6.42	Al - IV	1.38	Al	5.02	Al - IV	1.64	Al	5.20	
Al - VI	0.16	Ti	0.00	Al - VI	0.13	Ti	0.00	Al - VI	0.29	Ti	0.00	
Fe3+	0.74	Fe	0.04	Fe3+	0.81	Fe	0.05	Fe3+	0.97	Fe	0.04	
Ti	0.16	Mn	0.00	Ti	0.12	Mn	0.00	Ti	0.11	Mn	0.00	
Cr	0	Mg	0.00	Cr	0.00	Mg	0.00	Cr	0.00	Mg	0.00	
Mg	2.29	Zn	0.00	Mg	2.15	Zn	0.00	Mg	2.31	Zn	0.00	
Ni	0	Ca	2.25	Ni	0.00	Ca	0.90	Ni	0.00	Ca	1.08	
Fe2+	1.51	Na	1.76	Fe2+	1.58	Na	3.01	Fe2+	1.14	Na	2.87	
Mn	0.04	K	0.03	Mn	0.04	K	0.00	Mn	0.04	K	0.00	
Ca	0.1			Ca	0.17			Ca	0.14			
Fe2+		XAn	0.56	Fe2+		XAn	0.23	Fe2+		XAn	0.27	
Mn		XAb	0.44	Mn		XAb	0.77	Mn		XAb	0.73	
Ca	1.88			Ca	1.84			Ca	1.80			
Na	0.12			Na	0.16			Na	0.20			
Ca				Ca				Ca				
Na	0.18			Na	0.27			Na	0.27			
K	0.18			K	0.08			K	0.08			
XMg	0.6			XMg	0.58			XMg	0.67			

parallel to the amphibolite facies fabric. Amphibole-rich portions comprise the following modal proportions; hornblende 40 %, plagioclase 25%, quartz 30%, epidote 5% and ilmenite, whilst clinopyroxene-bearing pods comprise clinopyroxene 75 %, hornblende 4 %, plagioclase 10 %, quartz 8 % and epidote 3 %. Representative mineral analyses are shown in fig. 5.31, and full results given in Appendix A. Amphiboles are calcic in composition (fig. 5.29), those from sample TK 95 231 plot in the tschermakite-hornblende field whereas those from TK 95 232 plot on the magnesio-,/ tschermakite-hornblende boundary. The composition of clinopyroxene is diopside (fig. 5.30b). Plagioclase in both samples is oligoclase with X_{An} values between 0.23 and 0.29.

Petrographic constraints on conditions of metamorphism are provided by clinopyroxene-bearing melt pods and the absence of titanite within assemblages. This limits the conditions to the high-T, -P side of the clinopyroxene-in reaction R9, the basalt wet solidus R11, and the titanite-in reaction R10 (figs. 5.14 & 5.33). A range of temperature estimates were obtained from various calibrations of the amphibole-plagioclase geothermometer (fig. 5.32). The combined results of mineral equilibria and geothermobarometric study of type 2 metabasic assemblages are shown on the petrogenetic grid, fig. 5.33. The calibration of Holland & Blundy (1994) yields average estimates of 822 °C (n = 5, 2S.D. = 62°C) and 756 °C (n = 10, 2S.D. = 44 °C) for samples TK 95 226 and TK 95 232 respectively which are broadly consistent with the observed qualitative results from petrographic analysis. Higher mean estimates of 1002 °C (n = 5, 2S.D. = 180 °C) for sample TK 95 226, and lower mean estimates of 735 °C (n = 10, 2S.D = 48 °C) for sample TK 95 232, were obtained from the Blundy & Holland (1990) calibration which are less compatible with the observed phase relationships as compared to the calibration of Holland & Blundy, (1994). Erroneously low estimates of 587 °C (n = 5, 2S.D. = 22 °C) and 495 °C (n = 10, 2S.D. = 30 °C) were given by the Spear (1980) calibration for samples TK 95 226 and TK 95 232 respectively, such estimates are incompatible with equilibria and phase relations (i.e. presence of clinopyroxene-bearing melt pods). Previous work by Burton & O' Nions (1994), similarly found the Blundy & Holland (1990) calibration to yield the most accurate results when applied to their high grade assemblages. The results obtained in this study by the application of the clinopyroxene-plagioclase-quartz geobarometer (Ellis, 1980) were unreasonably low, (*c.* 0.5-1kbar), and have hence been disregarded.

Fig. 5.32 Results of amphibole-plagioclase geothermometry on type 2 metabasites

a) Clinopyroxene-bearing sample TK 95 226.

Mineral pair (rim-rim)		Temp C (P = 4 Kbar)		
Amp	Pl	S	B & H	H & B
62	75	576	865	822
63	71	595	1021	820
66	75	574	989	818
67	76	594	1116	782
69	77	596	1018	868
Mean		587	1002	822
2Sd		22	180	62

b) Clinopyroxene-bearing sample TK 95 231.

Mineral pair (rim-rim)		Temp C (P = 4 kbar)		
Amp	Pl	S	B & H	H & B
4	16	526	827	768
7	19	538	791	750
8	20	520	786	766
23	32	541	798	799
26	35	532	806	771
28	37	530	703	758
29	38	535	796	767
Mean		532	787	768
2Sd		7	78	30

c) Sample TK 95 232.

Mineral pair (rim-rim)		temp C (P = 4 Kbar)		
Amp	Pl	S	B & H	H & B
1	2	509	765	763
11	3	505	771	761
18	10	497	730	722
19	27	471	725	716
20	28	473	703	751
21	29	505	733	776
23	31	500	712	774
24	32	492	740	782
71	78	514	760	761
72	79	482	710	752
Mean		495	735	756
2Sd		30	48	44

S = Spear (1980); B & H = Blundy & Holland (1990);
H & B = Holland & Blundy (1994).

Fig. 5.33 Petrogenetic grid for type 2 metabasites within domain 4.

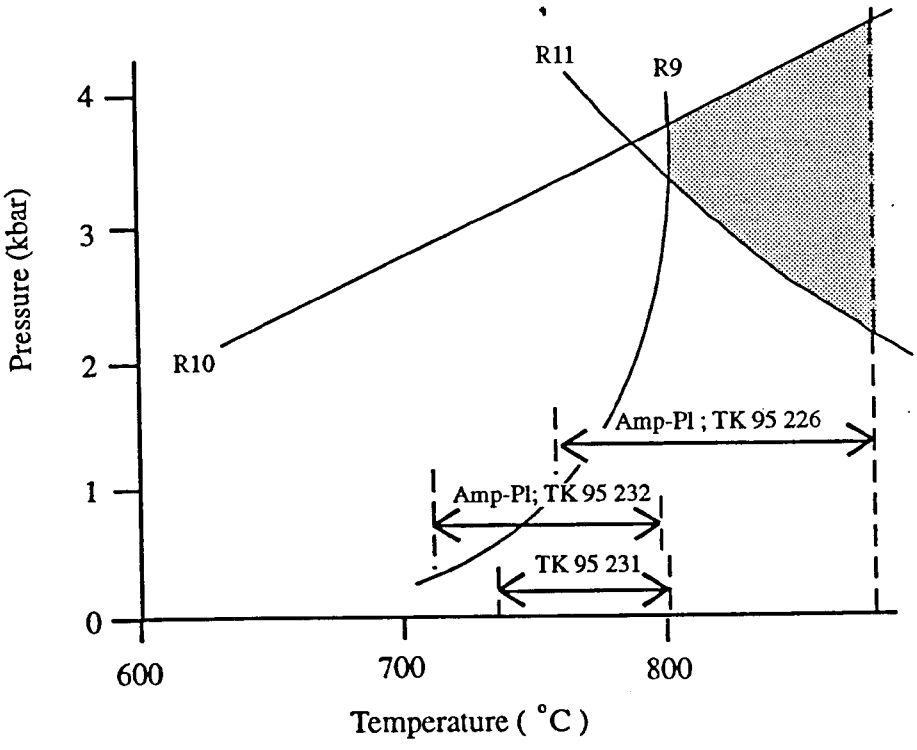

Results of amphibole - plagioclase geothermometry (Holland & Blundy, 1994) from samples TK 95 232, TK 95 231 and TK 95 226. Shaded box shows combined results of mineral equilibria and geothermometry from sample TK 95 226. Reactions on grid; R10; sphene-in, R9; clinopyroxene-in (Spear, 1981) & R11; basalt wet solidus (Yoder & Tilley, 1962).

5.5.5 $D4_{EAST}$ retrogression

Investigation of the conditions of metamorphism during $D4_{EAST}$ using petrographic and microstructural analysis has been undertaken on a range of retrogressed migmatites (e.g. samples TK 94 15, TK 94 110b, TK 95 26, localities WB 6, LB 2, WB 20). These results have been combined with further petrographic study and geothermobarometric study of the $D4_{EAST}$ retrogressed type 1 metabasite (sample TK 94 125, locality HB 5).

The $S4_{EAST}$ fabric in migmatites is characterised by aligned grains of biotite and muscovite which separate quartzofeldspathic layers. Sample TK 95 110b comprises the following modal proportions, biotite 11 %, muscovite 15 %, plagioclase 33 %, quartz 35 %, chlorite 5 % and ilmenite 1 %. Quartzofeldspathic layers comprise both type 2 and type 3 quartz ribbons, and subidiomorphic feldspars. Feldspars show evidence for marginal ductile recrystallisation, quartz shows a grain size reduction into the C-plane of the shear bands. Micas display evidence for kinking and marginal recrystallisation. The microstructures described above which characterise the $D4_{EAST}$ migmatitic

assemblages have been interpreted (e.g. Boullier & Bouchez, 1978; Simpson, 1985; Tullis & Yund, 1987; Gapais, 1989) to form at lower amphibolite,to upper greenschist facies conditions.

The $S4_{EAST}$ fabric in retrogressed type 1 metabasites is defined predominately by grains of aligned green actinolite (α = pale green, β = pale yellow-green γ = pale green) and plagioclase (fig. 5.22b). The cores of the amphiboles are commonly brown coloured and thought to represent relic igneous composition (see section 5.4.3). Sample TK 94 125 comprises the modal proportions, amphibole 20 %, plagioclase 35 %, quartz 5 %, biotite 15%, chlorite 10% and epidote 15%. Representative mineral analyses are shown on fig. 5.34, and full results are given in Appendix A.

Fig. 5.34 Representative mineral pair analysis for $S4_{EAST}$-bearing type 1 metabasite sample TK 94 125.

	Amp (r)		Pl (r)
	Tk 94 125		
	34		29
SiO2	48.21		58.12
TiO2	0.33		0.00
Al2O3	6.99		27.05
FeO	15.61		0.00
MnO	0.44		0.00
MgO	12.24		0.00
CaO	13.05		8.33
Na2O	0.84		6.91
K2O	0.27		0 00
Total	97.98		100.41
Cations	*23*		*32*
Si	7.01	Si	10.35
Al - IV	0.99	Al	5.68
Al - VI	0.21	Ti	0.00
Fe3+	0.69	Fe	0.00
Ti	0.04	Mn	0.00
Mg	2.65	Mg	0.00
Ni	0.00	Ca	1.59
Fe2+	1.21	Na	2.39
Mn	0.05	K	0.00
Ca	0.15		
Fe2+		XAn	0.40
Mn		XAb	0.60
Ca	1.88		
Na	0.12		
Ca			
Na	0.12		
K	0.05		
SUM	15.17		
Mg #	0.69		

Amphiboles are calcic with compositions plotting in the tschermakite-, magnesio- and actinolite-hornblende fields (fig. 5.26b). Plagioclase is andesine to oligoclase in composition, and comprises X_{An} values of 0.4 to 0.28. Epidote has Ps content ranging between 0.37 to 0.38. The X_{Al} value of chlorite ranges between 0.29 and 0.38, and the X_{Mg} content is between 0.53 and 0.58. It is

important to note that the range in compositions of hornblende and plagioclase in the $D4_{EAST}$ assemblages may suggest that the rocks have undergone heterogeneous retrogression and re-equilibration.

Fig. 5.35 Experimental hornblende-plagioclase geothermobarometer (Plyusnina, 1982) for Type 1 metabasite sample TK 94 125: X_{An} of plagioclase, plotted against total Al content of amphibole.

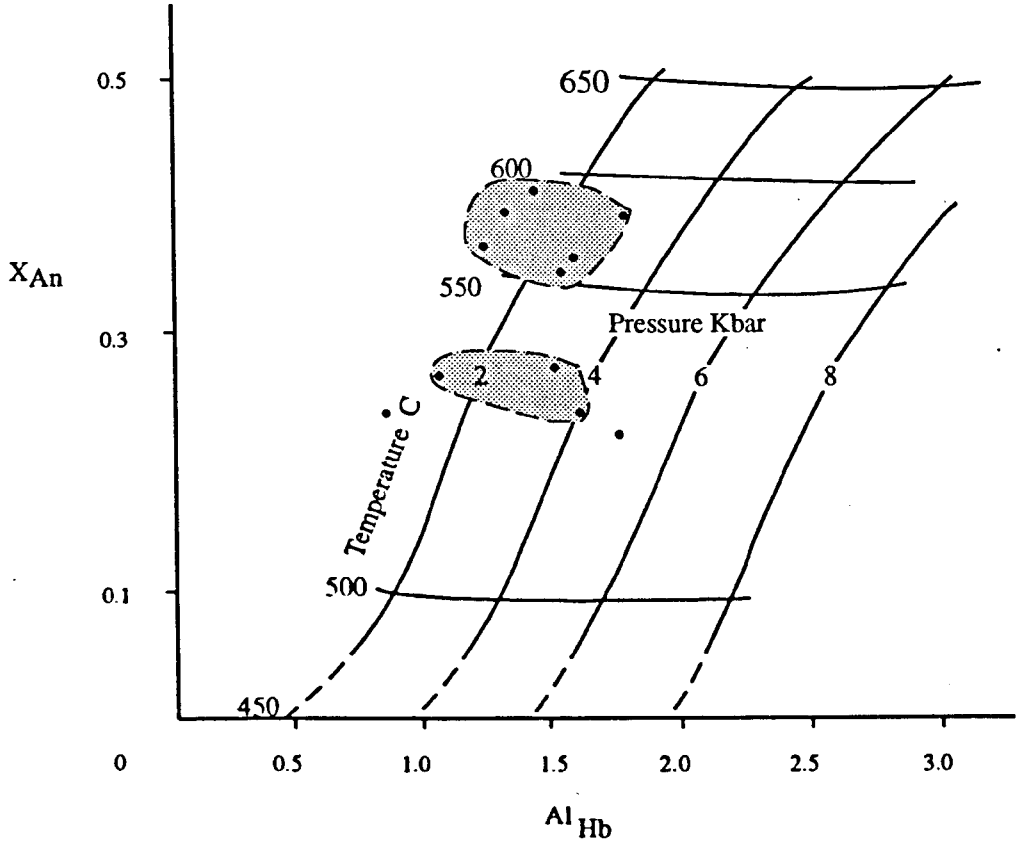

The presence of coexisting oligoclase and actinolite sets an upper pressure limit of *c.* 4 kbar for the assemblage (Maruyama *et al.* 1983) and places assemblages to the high-temperature, low-pressure side of the oligoclase-in reaction R12 (fig. 5.14). Results of the Spear (1980) calibration of the amphibole-plagioclase geothermometer give an average temperature value of 539 °C (n = 11, 2S.D. = 54 °C), the Plyusnina (1982) calibration gives a similar average of 554 °C (n = 11, 2S.D = 64 °C). The pressure estimates from Plyusnina (1982) are variable between 4.8 and < 2 kbar. Temperature results given by the Blundy & Holland (1990) and Holland & Blundy (1994) calibrations are unreasonably high, and incompatible with the observed phase assemblages hence have been disregarded. The effects of heterogeneous retrogression during $D4_{EAST}$ described above is demonstrated by the data where, low temperature estimates (Spear, 1980) are obtained from actinolitic-oligoclase pairs (e.g. Amp # 41, Pl # 47) and generally higher estimates from magnesio-hornblende, andesine pairs (e.g. Amp # 15, Pl # 19). The results of combined mineral equilibria and geothermobarometric studies of $S4_{EAST}$ assemblages are shown on fig. 5.37.

Fig. 5.36 Results of geothemometry on $S4_{EAST}$-bearing type 1 metabasite sample TK 94 125.

mineral pair		T C (P = 4 kbar)		P Kbar
		Spear	Plyusnina	
Amp	Plag			
1	6	576	511	3.9
11	12a	554	567	< 2
13	17	517	569	2.5
15	19	586	558	2.4
22	23	553	505	4.8
34	29	535	581	< 2
37	32	508	583	3
38	33	541	583	<2
41	47	507	521	<2
58	63	511	592	< 2
59	64	545	528	3.1
Mean		539	554	
2Sd		54	64	

Estimates from Spear (1980); Plyusnina (1982).

5.6 Timing constraints on metamorphism

The field relationships of the paragneissic screens within the Wareham Granite at Centreville and Old-Jingle, show the migmatitic fabric in the paragneiss being deformed into upright folds and variably transposed by a steep axial planar fabric. This folded migmatitic fabric can be laterally traced into, and has previously been correlated with (e.g. Holdsworth, 1994a) the steep $S3_{EAST}$ fabric in metasediments of the adjacent domain 3.

The foliated granitoids within domain 4 show characteristics of emplacement syn-regional high grade deformation (Hanmer, 1981; Holdsworth & O'Brien, 1993; Schofield *et al.* 1996). The granites fulfil widely recognised criteria for a syn-tectonic origin (after Hutton, 1988; Paterson *et al.* 1989; Ingram & Hutton, 1994; Tribe & D'Lemos, 1996), which include the overall, 1) development of predominately northeast-southwest trending fabrics which parallel the regional structure; 2) elongate shape of the plutons which is concordant with regional structures; 3) presence of a continuum of magmatic through to high-temperature solid-state fabrics; 4) the difference in foliation strain pattern developed within the pluton (grain scale S-C fabrics) and host rock (heterogeneous foliations) and 5) the development of syn-tectonic porphyroblasts within the granite contact aureole (fig. 5.38b). In domain 4 these criteria are locally displayed in the western margin of the Cape Freels Granite, shown by preservation of a range of magmatic to high-temperature solid-state syn $D4_{EAST}$ fabrics in the granite, and complex refolding and moderate-temperature overprinting of solid-state fabric in aureole migmatites (Schofield *et al.* 1996).

The majority of the granites (e.g. the Cape Freels and Lockers Bay granites) contain pervasive, mid to lower amphibolite facies $S4_{EAST}$ fabrics (fig. 5.38a) which are non-pervasively developed within the surrounding migmatites (e.g. Schofield *et al.* 1996). Tribe & D'Lemos (1994)

suggested that (due to their cooling to regional ambient conditions in considerable shorter time periods than overall periods of deformation), syn-tectonic plutons will display down-temperature fabrics which are biased to the thermal conditions of the host rocks. This suggests therefore, that the foliated granites in domain 4 were emplaced post peak metamorphism ($D3_{EAST}$), and syn-lower grade retrogressive deformation ($D4_{EAST}$).

In contrast to the majority of the foliated syn-tectonic granites in the domain, the Wareham Granite records predominately magmatic and high grade solid-state fabrics, does not contain a pervasive solid-state fabric and is seen to mix with migmatitic assemblages (see section 5.3.2). These relationships suggest that the Wareham Granite was emplaced syn-$D3_{EAST}$, therefore making it slightly older than the other foliated granites. The subordinate development of $S4_{EAST}$ fabrics in both the Wareham granite and the migmatites illustrates that strain partitioning of $D4_{EAST}$ deformation occurred (e.g. D'Lemos *et al.* 1997). Preliminary high precision U-Pb data (on zircon and monazite) suggests an age for the migmatites of *c.* 425 Ma and an age of *c.* 417 Ma (on zircon and titanite) for the Cape Freels and Lockers Bay foliated megacrystic granites (Dunning *et al. in prep*). No age data exists for the Wareham Granite.

Fig. 5.37 Summary P-T-t-d path for domain 4 shown on composite (pelitic and basic) petrogenetic grid showing results of geothermometry.

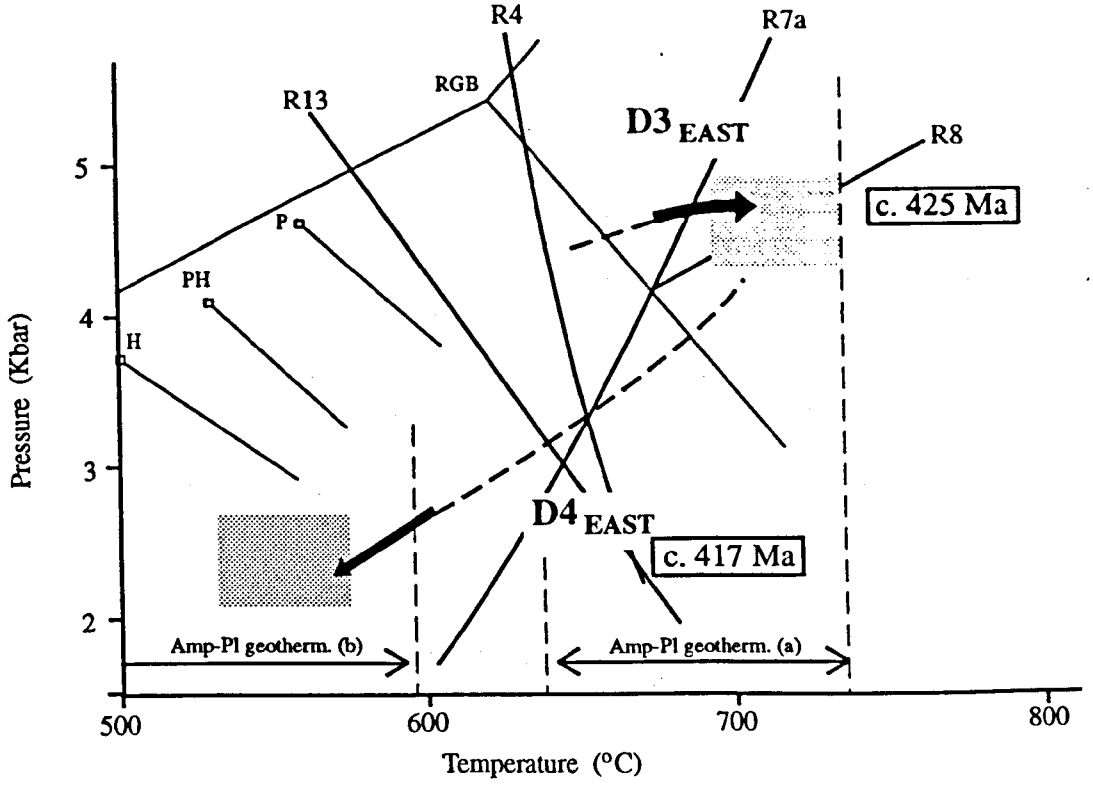

Reactions on grid; R7a) Chatterjee & Johannes (1974); R4) metapelitic solidus, Thompson & Algor (1977); R8) Holdaway & Lee (1977); R 13) Ca-amp solvus, Begun (1992). Al2SiO5 data; H, Holdaway (1977), RGB, Richardson et al. (1969), PH, Pattison & Harte (1985), P, Pattison (1989. Amp-Pl geothermometry results of Spear (1980) for a) sample TK 94 151, b) TK 94 125.

Fig. 5.38 a) Sinistral mid-amphibolite facies $S4_{EAST}$ fabric in the syn-tectonic Lockers Bay Granite; b) Contact related Crd-rich nodules in the metamorphic aureole of the Cape Freels Granite.

a)

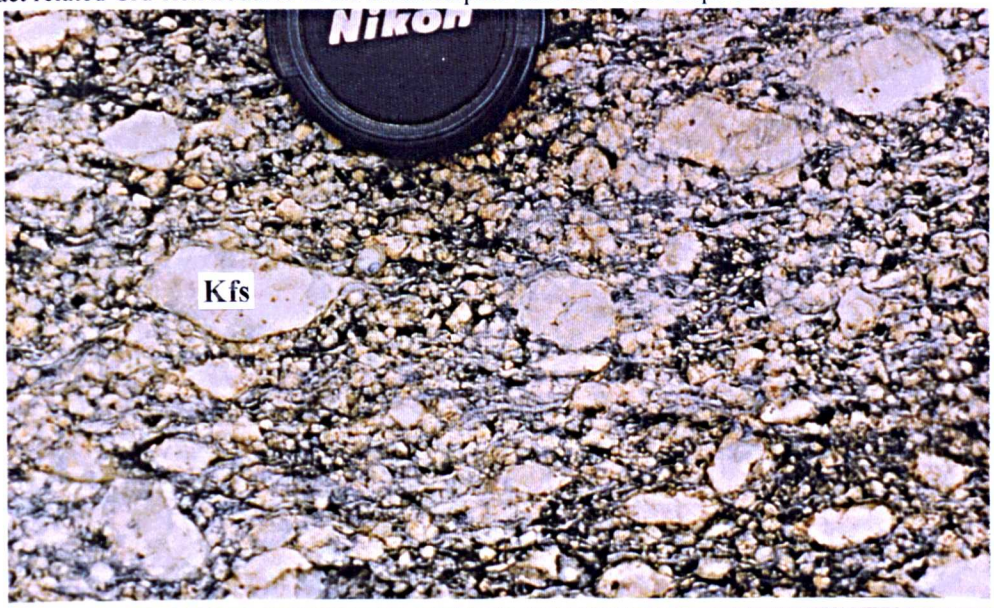

b)

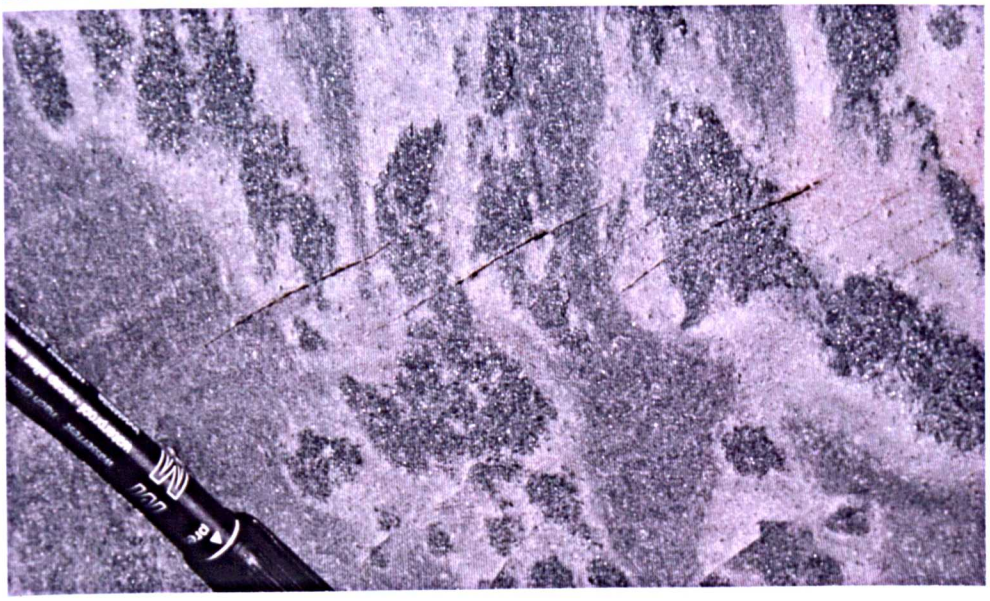

5.7 Summary

Domain 4 comprises a deformed assemblage of migmatite, orthogneiss, metabasite and foliated granite which show variable preservation of prograde, peak and retrograde fabrics. The domain is characterised by a clockwise form of P-T-t-d path (fig.5.37). The migmatites, orthogneisses and type 1 metabasites preserve effects of $D3_{EAST}$ which are locally overprinted by sinistral $S4_{EAST}$ shear fabrics, forming the dominant foliation in the majority of syn-tectonic granites. Locally $D4_{EAST}$ structures and fabrics are overprinted by low grade D5 fabrics, and cross-cut by brittle D6 faults. The effects of progressive $D3_{EAST}$, which was predominately sinistral, include refolding and the development of chaotic folds in the amphibolite facies migmatites. The retrograde deformation is characterised by a range of amphibolite to greenschist facies sinistral ($D4_{EAST}$), and greenschist facies dextral (D5) fabrics.

The metamorphic conditions during prograde $D3_{EAST}$ deformation are recorded by paragneiss (forming as screens within the Wareham Granite) which show minor amounts of melt, formed through muscovite dehydration melting (R7b, fig. 5.14). The majority of the migmatites are characterised by higher melt proportions which formed by biotite dehydration melting (e.g. R8a, R8b, fig. 5.14), these are cordierite- and sillimanite-bearing, and record peak conditions for $D3_{EAST}$ of *c.* 725 °C and 4.5 kbar. The high grade migmatites have been isotopically dated as *c.* 425 Ma (by U-Pb on zircon and monazite; Dunning *et al. in prep*). Anomalously high temperature conditions of *c.* 800 °C are recorded locally within the east of the domain by clinopyroxene-bearing type 2 metabasites, although their structural, and metamorphic relationships with respect to other deformation (i.e.$D3_{EAST}$) within the domain is unconstrained

The majority of the foliated granites (e.g. the Lockers Bay and Cape Freels granites) record steep sinistral, mid-low amphibolite to upper greenschist facies fabrics which parallel the $S4_{EAST}$ fabrics in the migmatites. The granites display criteria for a syn-tectonic origin, and are interpreted to have been emplaced into the region post-peak metamorphism and during ($D4_{EAST}$) retrogressive deformation, although the Wareham granite, which displays evidence for mixing with migmatites is interpreted to have been emplaced slightly earlier (syn-$D3_{EAST}$). The Lockers Bay and Cape Freels granites have been isotopically dated as *c.* 417 Ma (by U-Pb on zircon and titanite; Dunning *et al. in prep*).

Chapter 6.

Domain 5: The Dover Fault Shear Zone

Chapter 6. Domain 5: The Dover Fault Shear Zone

6.1 Introduction

The Dover Fault Shear Zone lies parallel to the Dover Fault (Yonce, 1970; Blackwood & Kennedy, 1975; Holdsworth, 1991), forming a north-northeast to northeast-southwest orientated high strain (and low grade) tract in the east of the Gander Lake Subzone (fig. 1.9). The domain marks the surface expression of the Gander-Avalon margin and structures and fabrics related to movement along this boundary can be correlated either side of the Dover Fault (Holdsworth & O'Brien, 1993). The domain is *c.* 2 km wide (Holdsworth, 1994a) although the extent of the retrogressive fabrics which characterise the region are laterally variable, ranging between 0.5 and 2 km. The domain preserves dextral, D5 ductile (previously termed, late ductile fabrics; Holdsworth, 1991), and D6 brittle (previously termed, late-brittle structures; Holdsworth, 1991) deformation which overprint effects of sinistral $D4_{EAST}$ deformation.

Fig. 6.1 Geological map of the Hare Bay-Dover Region, Bonavista Bay showing sample localities. Localities 1, 2 & 3 represent sites where the Gander - Avalon boundary is marked by a ductile (late ductile of Holdsworth, 1991) D5 fault (diagram modified after Holdsworth, 1991).

The Dover Fault Shear Zone has been the subject of extensive previous research (e.g. Holdsworth 1991; O'Brien & Holdsworth, 1992; Holdsworth 1994a) which has established its field, microstructural and kinematic characteristics. This chapter aims to briefly build upon these observations by using results of field and microstructural analyses in order to establish, the grade and timing of the ductile and brittle deformation (D5-D6), and the form of the retrograde P-T-t-d evolutionary path within the Gander Lake Subzone.

6.2 Structure and metamorphism

6.2.1 Introduction

The outer region of domain 5 is characterised by anastomosing networks of steeply dipping phyllonitic Hare Bay Gneiss and Dover Fault Granite in shear zones which are associated with a subvertical mylonitic foliation and a gently plunging mineral lineation (O'Brien & Holdsworth, 1992). Approaching the Dover Fault, rocks become progressively more epidote and chlorite-rich preserving grain-size reduction fabrics and are cross cut by metre scale brittle dextral faults.

Fig. 6.2 Steeply dipping, northeast - southwest trending brittle dextral fault representing a splay off the main Dover Fault (looking north).

D5 ductile fabrics in the mylonites display dynamic recrystallisation textures associated with a range of predominantly dextral, greenschist to sub-greenschist facies fabrics, although rare evidence for sinistral D5 fabrics is seen at the western margin of the Cape Freels Granite and further south at Maccles Lake (fig. 6.3; Dickson, 1974; Hanmer, 1981; O'Brien & Holdsworth, 1992; Holdsworth *et al.* 1993). D5 brittle structures form complex systems of steeply-dipping faults. The intensity of D5 and D6 deformation increases eastwards within the domain, until adjacent to the Dover Fault most earlier $D4_{EAST}$ structures are obliterated (O'Brien & Holdsworth, 1992).

Fig. 6.3 Map showing sample localities and the positioning of D5 shear zones ('late ductile dextral and sinistral shear zones' of Holdsworth, 1991) and D6 brittle faults ('late brittle faults' of Holdsworth, 1991; diagram modified after Holdsworth, 1994a).

6.2.2 D5 ductile structures and fabrics

The ductile D5 structures (figs. 6.3 & 6.5) are best preserved in the region of the Gander-Avalon boundary between the TCH and Maccles Lake, to both the north and south within the domain, they are less well preserved and disrupted by later D6 brittle faults (Holdsworth, 1991). The distribution and geometry of D5 ductile fabrics in the domain are characterised by a set of minor structures including, sheath folds, shear bands and antithetic sinistral shears (fig. 6.4). D5 dextral structures are characterised by presence of open to tight curvilinear folds of the mylonitic fabric which display dextral vergence (fig. 6.5c), hinges lie at high angles to the lineation (O'Brien & Holdsworth, 1992) and are overprinted by axial planar S5 (fig. 6.5a). Other characteristics are the

presence of dextral shear bands and σ-porphyroblasts, and development of antithetic sinistral faults in thin competent horizons. The sheared rocks are medium to fine grained with regular planar foliation and commonly contain elongate lenses and layers composed of finer-grained material. Ultramylonitic regions (0.5-1 m scale) are common, preserving straight internal layering (fig. 6.5b). D5 structures in the Dover Fault Granite are characterised by the presence of plagioclase and alkali feldspar σ-type porphyroclasts, wrapped by fine grained micas (fig. 6.6b). D5 fabrics in Hare Bay Gneiss migmatites (fig. 6.6a) are characterised by plagioclase and quartz σ-type porphyroclasts which are wrapped by abundant micas and chlorite. S5 forms mylonitic fabrics in the orthogneiss which comprise, coarse plagioclase σ-type porphyroclasts and fine to medium mica-fish.

Fig. 6.4 3D summary of minor structures associated with the D5 ('late ductile' dextral shear zones; diagram from O'Brien & Holdsworth, 1992).

6.2.3 D6 brittle structures and fabrics

The development of D6 dextral brittle faults in the region is concentrated in the vicinity of the present day Dover Fault and Cape Freels 'late ductile'(Holdsworth, 1991) shear zones (figs. 6.1 & 6.3). Faults exhibit shallowly plunging slickenfibres indicative of strike-slip displacement (Holdsworth, 1991), and occur on both small (centimetre to metre) and large (> 10m) scale. Small scale structures include conjugate sets of dextral and sinistral steeply dipping to subvertical faults, and brittle kink and box folds of variable plunge (O'Brien & Holdsworth, 1992).

Fig. 6.5 Effects of dextral D5 deformation, a) coarse S5 S-C shear fabric in migmatite, b) mylonitic S5, c) brittle dextrally-verging D5 fold.

a)

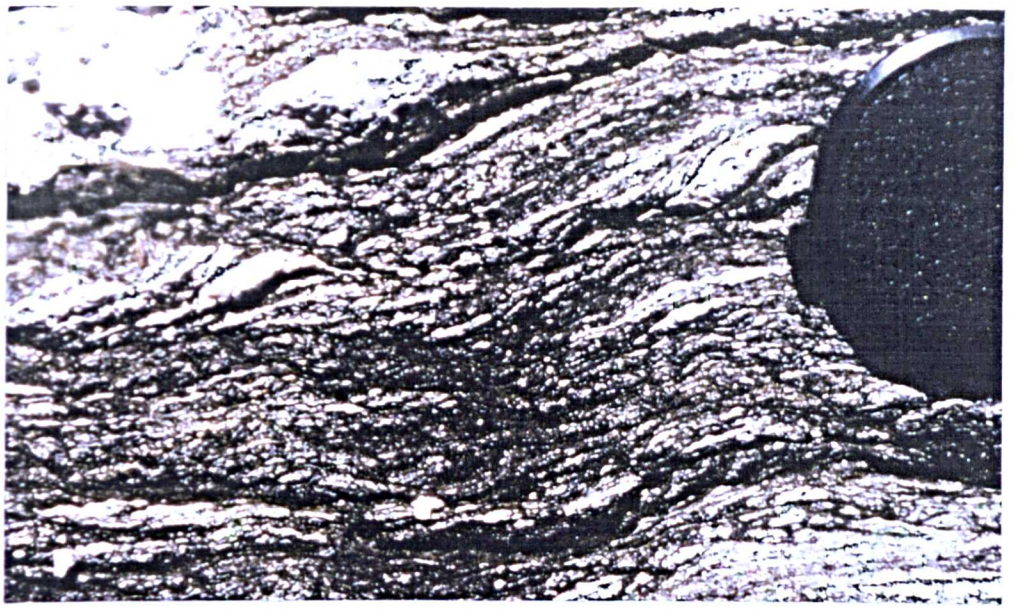

b)

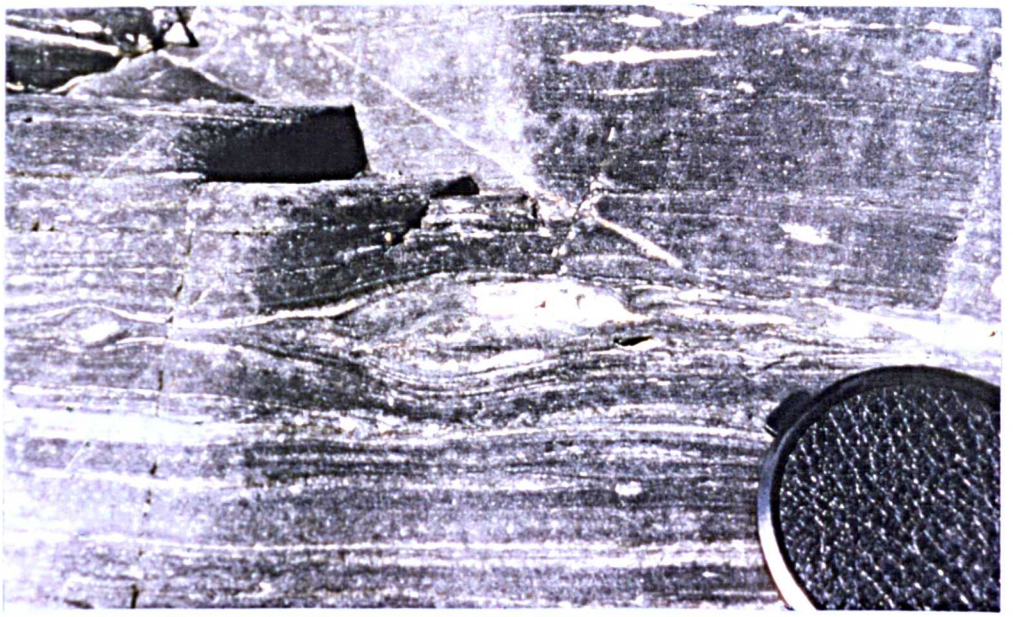

c)

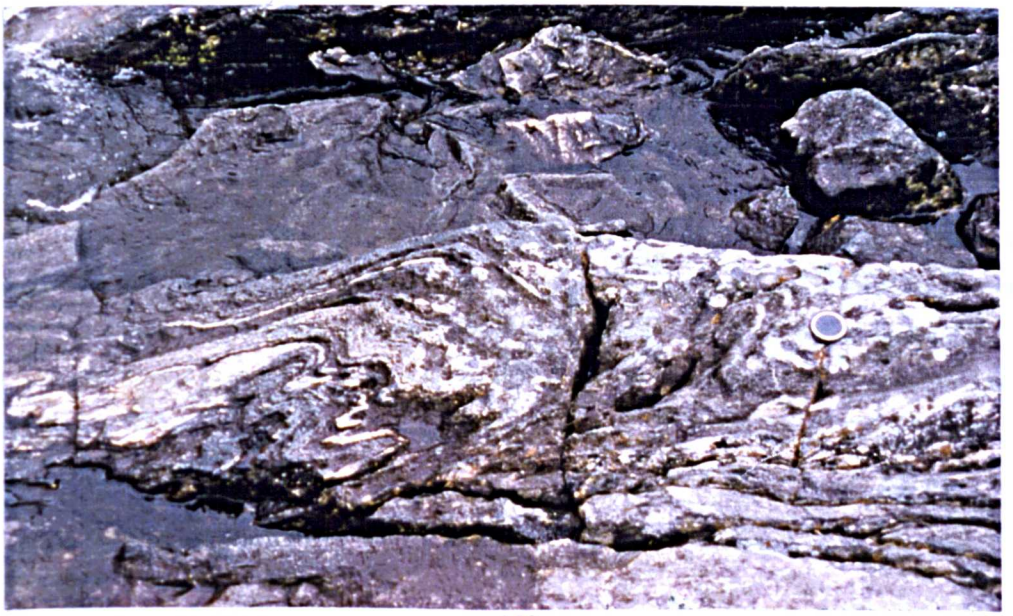

The presence of D6 brittle structures have been interpreted to indicate shortening at high angles, and extension subparallel to the regional foliation which allowed extension along the Gander-Avalon boundary as a consequence of accommodation of overall shortening (O'Brien & Holdsworth, 1992). Large scale brittle faults, although rarely exposed are commonly inferred from geological offsets, present-day topographic features (Holdsworth, 1991), or by the presence of narrow veins (< centimetre scale) of epidote cataclasite, or broader zones (< 50 m) of breccia. Large scale faults (fig. 6.2) appear to be associated with movements along the northeast-trending master Dover Fault, and are characterised by three predominant fault orientations and displacement senses (i.e. east to north-northeast = dextral; northeast = dextral and north to north-northeast = sinistral; Holdsworth, 1991). These fault orientations are thought to correspond to R, P and R' shears (sensu Tchalenko, 1970). In places D6 fault arrays are thought to define rotating fault blocks typical of brittle strike-slip deformation zones (Holdsworth, 1991).

6.3 Microtextural and metamorphic analysis

6.3.1 D5 ductile structures and fabrics

Mylonitic Dover Fault Granite (e.g. sample ML 10b) contains a layered fabric comprising predominantly of quartz and plagioclase which display crystal plastic deformation, and show evidence for crystal plastic recovery (fig. 6.6b). Porphyroclasts of plagioclase are abundant, forming dextrally sheared σ-type grains with subidiomorphic form. Porphyroclasts display curved edges, partial marginal recrystallisation, and show the development of internal kink bands. D5 fabric within orthogneiss is characterised by the abundance of alkali feldspar porphyroclasts (e.g. FB 20, FB 5 & FB 15b) which show limited incipient, and marginal recrystallisation. Within mylonitic orthogneiss and migmatite (e.g. ML 10a), fine to medium grained mica-fish are abundant, both wrapping porphyroclasts, and within the coarse S-C shear bands (fig. 6.6a).

Migmatitic sample ML 10a is from the D5 deformed sequence at Maccles Lake, and comprises plagioclase 35%, quartz 40%, muscovite 12%, biotite 8%, chlorite 4% and ilmenite 1%. The micas commonly show development of internal kink bands, chlorite forms fine grain aggregates which wrap porphyroclasts, and form stacks around quartz. The quartz forms fine to coarse subidiomorphic to xenomorphic subgrains which show internal xenomorphic subgrain development and commonly form type 2 ribbons (Boullier & Bouchez, 1978). The plagioclase grains, wrapped by the micaceous shear fabric, display evidence for marginal recrystallisation. The assemblages and microtextures described above including, the ductiley deformed nature of plagioclase, the marginally recrystallised nature of the micas and development of internal kink bands in the micas are characteristic of mid to upper greenschist facies conditions above the brittle-ductile transition of plagioclase *c.* 450 °C (e.g. Simpson, 1985; Tullis & Yund, 1987; Gapais, 1989; Tribe, 1995).

Fig. 6.6 Micaceous dextral D5 shear fabrics in a) deformed Hare Bay Gneiss Migmatite and b) Dover Fault Granite (field of view = 2.5mm).

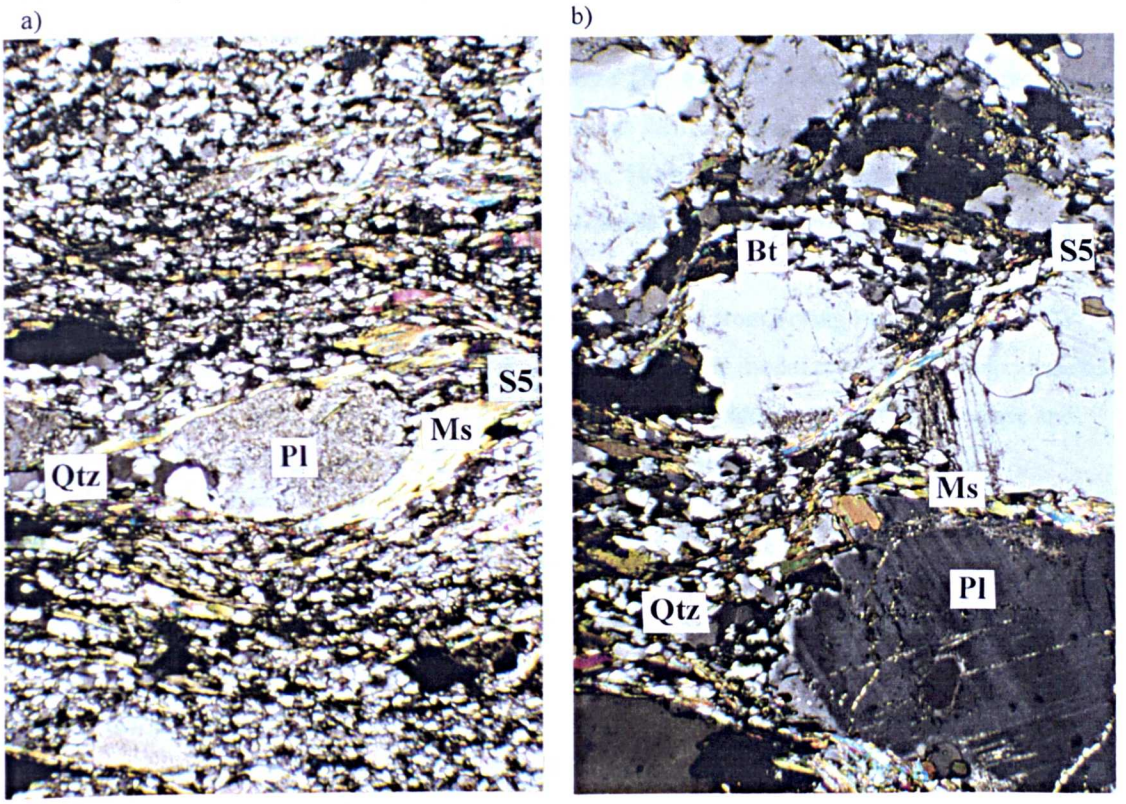

6.3.2 D6 brittle structures and fabrics

Fig. 6.7 Brittle D6 fabrics in sample FP 3 showing brittley deformed plagioclase and quartz porphyroclasts (field of view = 6.5mm).

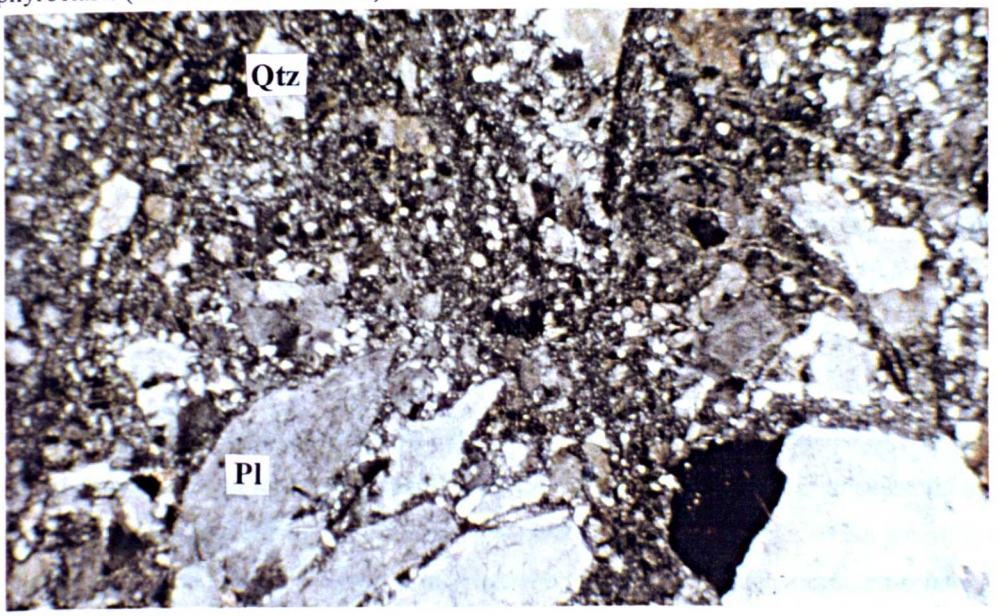

D6 assemblages (e.g. SB 24a) which preserve ductile-brittle mineral transitions display evidence for recrystallised quartz and brittley deformed feldspars, although the majority of D6 assemblages (FP 1, FP 3) show brittle behaviour of both quartz and feldspar (fig. 6.7). D6 assemblages are characterised by the presence of feathery chlorite and muscovite which form fine grains showing development of brittle kink bands, and fine grained sericitic aggregates. The minerals assemblages display intense

D6 assemblages (e.g. SB 24a) which preserve ductile-brittle mineral transitions display evidence for recrystallised quartz and brittley deformed feldspars, although the majority of D6 assemblages (FP 1, FP 3) show brittle behaviour of both quartz and feldspar (fig. 6.7). D6 assemblages are characterised by the presence of feathery chlorite and muscovite which form fine grains showing development of brittle kink bands, and fine grained sericitic aggregates. The minerals assemblages display intense brecciation, and are characterised by the presence of fine to coarse fragments which comprise sericitised plagioclase, alkali feldspar and quartz.

Sample FP 3 represents D6 deformed Newport Granite from Frying Pan Island (fig. 6.3) which displays brittle dextral fabrics, and comprises the following modal proportions, plagioclase 45 %, muscovite 12 %, quartz 30 %, chlorite 5 %, calcite 4 % and epidote 4 %. Both plagioclase and quartz form porphyroclasts which are fractured and variably sericitised.

6.4 Timing constraints on deformation

Ductile lower greenschist facies D5 fabrics are dextral and overprint mid to low amphibolite facies $S4_{EAST}$ sinistral fabrics. The field relationships in the adjacent domain 4, which show that $S4_{EAST}$ fabrics form the dominant foliation in the majority of the Silurian syn-tectonic granites (e.g. the Cape Freels Granite, dated by high precision U-Pb methods as *c.* 417 Ma; Dunning *et al. in prep*), suggest that the overprinting D5 deformation occurred post *c.* 417 Ma. The cross-cutting of S5 assemblages by the undeformed Newport Granite suggests that D5 occurred prior to its emplacement. The Newport Granite is interpreted as a Devonian post-tectonic pluton (e.g. Colman-Sadd *et al.* 1990). High precision U-Pb dates (on zircon, monazite & titanite) suggest an age of *c.* 385 Ma (Dunning *et al. in prep*). The lower to sub-greenschist facies D6 brittle fabrics cross-cut, and brittley deform the Newport Granite (D'Lemos *et al.* 1995) suggesting that they formed post its emplacement. The brittle fabrics are reportedly (Dallmeyer *et al.* 1983; Tuach, 1987) cross-cut further south in the Gander Lake Subzone by the Ackley Granite (dated using $^{40}Ar/^{39}Ar$ as *c.* 378 Ma; Kontak, 1988).

6.5 Summary

The Dover Fault Shear Zone (domain 5) is a steep narrow high-strain zone situated adjacent to the Dover Fault, which preserves predominately dextral shear fabrics which overprint sinistral $S4_{EAST}$ fabrics. The domain is characterised by the development of ductile D5 fabrics which are overprinted by ductile-brittle, and brittle D6 fabrics associated with steep predominately northeast-southwest trending brittle faults.

D5 deformation is characterised by the development of dextrally verging folds and coarse micaceous greenschist facies retrogressive fabrics. D6 is characterised by sub-greenschist facies, predominantly dextral brittle deformation, which forms shear fabrics and steep faults. Associated with D6 are subhorizontal slickenfibres related to movement along the present day Dover Fault. The

timing of D5 deformation occurred pre-emplacement of the Newport Granite (dated as *c.* 385 Ma; Dunning *et al. in prep*) whereas the brittle D6 deformation occurred post its emplacement, but pre-emplacement of the Ackley Granite (dated as *c.* 378 Ma; Kontak, 1988).

Chapter 7.

Conclusions

Chapter 7. Conclusions

7.1 Introduction

The Gander lake Subzone has been subdivided into five domains each of which preserves distinct structural characteristics and mineral assemblages, summarised in fig. 7.1. This chapter reviews each domain and attempts to correlate structures between zones (fig 7.2) in order to derive an overall tectonothermal evolution for the region.

7.2 Methods and principles of correlation

A number of possible methods exist by which to correlate the structural and metamorphic episodes across a region which include;

1) the chronological labelling of structures and related fabrics within individual geological blocks (e.g. D1, D2...) followed by their direct correlation between blocks,

2) the use of specific time markers, e.g. unconformities, intrusions, to correlate rocks and structures of the same age between different units,

3) the linking of different structures which formed at similar metamorphic grade. e.g. high grade / low grade events.

In general, a combination of the above methods is applied during correlation in order to avoid the potential pitfalls of correlating by individual methods. Problems may be encountered if different blocks, a) did not undergo all of the same deformational events, b) were at different structural levels or c) were located at different places therefore record different events. In this study, care has been taken to avoid such pitfalls, in particular structures have only been directly correlated where the field relationships show their comparable labelling (i.e. F2, F3...), style and metamorphic grade. Timing relationships (both relative and absolute) were established using a combination of field relationships and ages from radiometrically dated intrusions (shown in fig. 7.3).

7.3 Summary of structural assemblages in the Gander Lake Subzone

7.3.1 Domain 1

Throughout the domain, relic bedding is well preserved, defined by discrete mineralogical variations in quartzofeldspathic mineral, and mica content. A variably well preserved, millimetre scale low-grade fabric forms subparallel to the bedding. Both bedding and the millimetre scale fabric are deformed by subhorizontal, easterly-verging folds which show pervasive development of a muscovite - chlorite axial planar pressure solution fabric.

Fig. 7.1 Summary of the relative order of structural events and metamorphic characteristics (post deposition) in different domains within the Gander Lake Subzone, showing possible correlations between different domains, see text for details (n.b. excluding local deformation in domain 1).

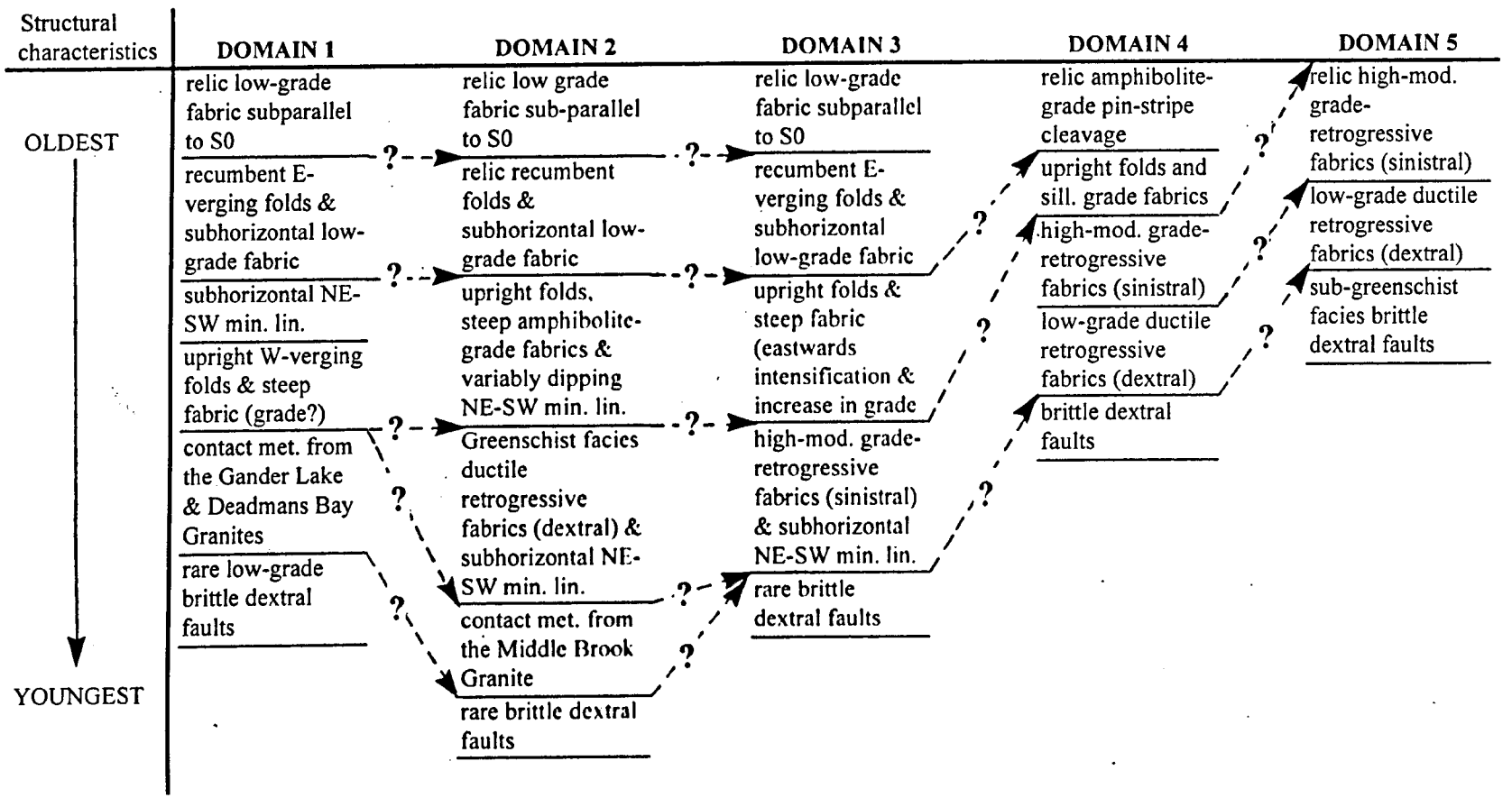

The subhorizontal elements in domain 1 are overprinted in the central and eastern regions by upright folds with steep axial planar fabrics and an associated subhorizontal northeast-southwest trending mineral lineation, and locally in the east by tight recumbent folds. The upright folds form westward-verging, open to close structures, the axial planar fabrics form a pin-stripe pressure solution cleavage. Upright folds and fabrics are locally cross-cut, and contact metamorphosed by the undeformed Gander Lake Granite which has produced hornfelsing and cordierite / andalusite spotting. The tight recumbent folds are westward-verging, deform the subhorizontal mineral lineation and show subordinate development of a muscovite-chlorite greenschist facies fabric. Their relationship with the Gander Lake Granite is unknown. Rocks throughout the domain are locally cross-cut by northeast-southwest trending brittle dextral faults.

In summary, the metapelites of domain 1 record a greenschist facies prograde mineral sequence characterised by east-verging recumbent folds which are overprinted by upright, and recumbent west-verging folds.

7.3.2 Domain 2

Domain 2, the Wing Pond Shear Zone, is characterised by upright structures with associated amphibolite facies fabrics which deform low grade fabrics, and are themselves locally overprinted by retrograde shear fabrics. Throughout the domain, transposed bedding is defined by subtle variations in quartzofeldspathic and micaceous composition in metasediments.

The upright structures form open to tight symmetrical folds with associated steep axial planar fabrics and a variably dipping northeast-southwest trending mineral lineation. The predominate sense of shear in the region is sinistral. The steep fabrics are characterised by the subsolidus prograde mineral sequence andalusite → kyanite → sillimanite, accompanied by the development of staurolite. The upright structures show an eastward tightening and refolding of folds and transposition by steep prograde fabrics, suggesting that the deformation was progressive in style.

Retrogressive greenschist facies fabrics which locally cross-cut, and pervasively overprint the prograde structures in the east of the domain are predominantly dextral, and associated with a northeast-southwest subhorizontal mineral lineation. The fabrics are characterised by a range of lower amphibolite to greenschist facies assemblages which comprise Mn-rich garnet, mica and chlorite. Adjacent to the western margin of the unfoliated Middle Brook Granite in the east of the domain, retrograde fabrics are overprinted by contact metamorphic hornfelsing and cordierite spots. Similarly, in the north of the domain, retrograde assemblages are overprinted by contact effects from the non-foliated Deadmans Bay Granite. Both prograde and retrograde mineral assemblages are subordinately cross-cut throughout the domain by northeast-southwest trending metre scale brittle dextral faults.

The P-T path preserved by rocks within domain 2 is clockwise in form. The early greenschist facies portion of the path is recorded by the relic recumbent structures. Subsequent prograde andalusite → kyanite, and peak sillimanite grade conditions of *c.* 650 °C and 5.5 kbar are

recorded by the steep fabrics associated with the upright structures. The retrograde portion of the path is recorded by steep, micaceous shear fabrics which overprint the prograde assemblages, and are predominately dextral.

7.3.3. Domain 3

Domain 3 is characterised by upright structures which refold low grade recumbent structures in the west, and are themselves overprinted in the east by retrograde, steep sinistral fabrics. Relic cross-bedding and cross-laminations are preserved in the west of the domain and transposed bedding, defined by layers of discrete quartzofeldspathic and micaceous lithology is evident throughout the domain. The relic recumbent folds are easterly-verging, and show development of a low grade subhorizontal axial planar pin-stripe cleavage, and a rare intrafolial chlorite-muscovite (millimetre scale) fabric.

The upright folds show development of steep, axial planar fabrics which are subordinately developed in the west and become pervasive eastwards as the deformation intensifies. Intensification is accompanied by the development of a northeast-southwest trending mineral lineation, and an increase in metamorphic grade shown by development of biotite (replacing muscovite) as the dominant phyllosilicate, and the local development of syn-kinematic garnet. Steep retrograde fabrics thoroughly transpose prograde assemblages in the east of the domain and are characterised by lower amphibolite to upper greenschist facies micaceous shear fabrics and a pervasive, northeast-southwest trending mineral lineation. Rocks within the domain are locally cross-cut by northeast-southwest trending brittle dextral faults.

The P-T path recorded by metapelites of domain 3 is clockwise in form. The prograde portion is characterised by greenschist facies conditions and eastward-verging recumbent folds. Subsequent prograde and peak amphibolite facies conditions *c.* 600 °C are recorded by progressively deformed upright structures and steep fabrics. The post-peak, retrograde metamorphic path is characterised by steep sinistral shear fabrics of lower amphibolite to upper greenschist facies conditions.

7.3.4 Domain 4

Domain 4 comprises paragneissic migmatites, orthogneiss, syn-tectonic granite and two main types of metabasite which display steep amphibolite facies prograde fabrics, and are locally overprinted by lower-grade retrogressive shear fabrics.

Throughout the domain, transposed bedding is defined by discrete psammitic and pelitic layers in paragneissic migmatites. Paragneissic migmatites in the west contain an andalusite-sillimanite migmatitic fabric which is deformed by the upright symmetrical folds. In places a pin-stripe cleavage is preserved intrafolial to the migmatitic fabric. Amphibolite-facies fabrics in orthogneiss and type 1 metabasites (contained within the migmatites) are similarly deformed by

upright folds. Further east, cordierite and sillimanite-bearing migmatites are characterised by higher melt percentages, show effects of progressive-style deformation, and locally mix with the megacrystic Wareham Granite. Focusing of the deformation has produced incoherent structures in the migmatites characterised by chaotic folds and complex fold interference patterns, local transposition of the migmatitic fabrics and local development of melt-filled sinistral shear pods. In the east of domain 4 anomalously high temperature conditions are recorded by type 2 metabasites which are in tectonic contact with the migmatites, and display an intensely folded and transposed clinopyroxene-bearing fabric.

Migmatites are subordinately overprinted by lower grade northeast-southwest trending steep shear fabrics which form the dominant fabric in the majority of the foliated syn-tectonic granites. The fabrics formed during mid amphibolite to upper greenschist facies metamorphism and display a sinistral sense of shear. Locally within the east of the domain, the sinistral retrogressive fabrics are overprinted by greenschist facies dextral shear fabrics. Overprinting of rocks by northeast-southwest trending dextral brittle faults occurs subordinately throughout the domain.

Domain 4 records a clockwise P-T path. Prograde and peak conditions of *c.* 750 °C and 4.5 kbar (i.e. low-pressure, high-temperature) are recorded by the migmatites and the type 1 metabasites. Intrusion of granites occurred post-peak migmatisation during sinistral mid amphibolite facies deformation, and was followed by greenschist facies dextral shearing.

7.3.5 Domain 5

Domain 5 comprises retrograde structures and fabrics which overprint, and thoroughly transpose pre-existing prograde fabrics. The region is dominated by steep, dextral ductile fabrics which are muscovite and chlorite-rich, overprint higher grade sinistral shear fabrics, and are pervasively developed adjacent to the Dover Fault. The ductile fabrics are locally overprinted by brittle fabrics associated with metre scale brittle dextral faults, also dextral and muscovite and chlorite-rich. The ductile dextral fabrics are locally cross-cut by the non-foliated Newport Granite, which is itself cross-cut by the brittle deformation fabrics. The Ackley Granite reportedly cross-cuts brittle fabrics further south in the domain.

Domain 5 preserves the retrograde portion of a P-T path, characterised by initial sinistral shearing which has been overprinted by dextral greenschist facies ductile, and brittle deformation respectively.

Fig. 7.2 Summary of the deformational features within domains 1-5 of the Gander Lake Subzone (excluding local deformation in domain 1), note possible correlation between deformation in the west and east is problematic, see text for discussion.

	Domain 1	Domain 2	Domain 3	Domain 4	Domain 5
D1	relic low-grade S1 fabric	rare relic low-grade S1 fabric	relic low-grade S1 fabric	structures largely overprinted	structures obliterated
D2	recumbent F2 folds & axial planar greenschist facies S2 fabric	relic F2 folds and greenschist facies S2 fabric	recumbent F2 folds and axial planar greenschist facies S2 fabric, NE-SW sub-horizontal min. lin.		
$D3_{WEST}$	upright $F3_{WEST}$ folds & steep $S3_{WEST}$ fabric, grade?	pervasive upright $F3_{WEST}$ folds & amphibolite facies steep $S3_{WEST}$ fabric, variable plunge of NE-SW min. lin.			
$D3_{EAST}$			upright $F3_{EAST}$ folds, steep amphibolite facies $S3_{EAST}$ fabric	upright $F3_{EAST}$ folds, $S3_{EAST}$ sillimanite grade migmatitic fabrics	structures obliterated
$D4_{WEST}$		steep greenschist facies $S4_{WEST}$ fabric (dextral), NE-SW sub-horizontal min. lin.			
$D4_{EAST}$			steep amphibolite-greenschist facies $S4_{EAST}$ fabric (sinistral), NE-SW sub-horizontal min. lin.	steep amphibolite-greenschist facies $S4_{EAST}$ fabric (sinistral), NE-SW sub-horizontal min. lin.	rare relic greenschist facies $S4_{EAST}$ fabric (sinistral)
D5				local steep greenschist facies S5 ductile fabric (dextral)	D5 folds and steep S5 ductile fabric (dextral)
D6	rare brittle D6 fabrics	rare brittle D6 fabrics	rare brittle D6 fabrics	rare brittle D6 fabrics	brittle D6 fabrics

7.4 Correlation of deformational events across the Gander Lake Subzone

7.4.1 D1

The earliest structural element to be recognised is the greenschist facies, S1 fabric, orientated subparallel to bedding and preserved both in domains 1 and 3 (and locally in domain 2). F1 structures are not preserved at outcrop but their presence is inferred by structural fold-facing studies which show that observed folds which deform S1 occur on the limbs of pre-existing larger structures.

Fig. 7.3 Summary of the timing constraints of deformation events within the Gander Lake Subzone.

Def. event	Relative timing	Possible absolute timing ?
D1	pre-obduction	> 470 Ma[1] ?
D2	syn-obduction	Ordovician; c. 470 Ma[1]?
$D3_{WEST}$	pre-Middle Brook Granite emplacement	Silurian; either i) > 427 Ma[2] or ii)pre-Devonian[3] ?
$D3_{EAST}$	syn-migmatisation & emplacement of the Wareham Granite	Silurian, *c.* 425 Ma[2]
$D4_{WEST}$	pre-Middle Brook Granite emplacement	Silurian; either i) > 427 Ma or ii)pre-Devonian?
$D4_{EAST}$	syn-emplacement of the syn-tectonic Cape Freels and Lockers Bay Granites	Silurian; c. 417 Ma[2]
D5	pre-emplacement of the Newport Granite	> 385 Ma[2]
D6	post-emplacement of the Newport Granite pre-emplacement of the Ackley Granite	< 385 Ma[2] > 378 Ma[4]

7.4.2 D2

The pervasive deformation of the millimetre scale, low grade S1 fabric in domain 1 by recumbent easterly-verging folds associated with greenschist facies flat-lying fabrics is considered to relate to D2 deformation. Similarly, the relic recumbent folds in domain 2 with intrafolial S1 are interpreted as D2. The recumbent folds are of similar form and style both in domains 1 and 3, therefore in domain 3 are also correlated with D2. Folds are accompanied by the pervasive development of axial planar low grade fabrics (S2). Previous studies (e.g. Williams & Stevens, 1974; Williams 1984; Colman-Sadd *et*

[1] Williams & Stevens, 1974; Williams, 1984; Colman-Sadd *et al.* 1992a
[2] Dunning *et al. in prep*
[3] Colman-Sadd *et al.* 1990
[4] Kontak, 1988.

al. 1992a) suggest that the form of the east-verging F2 structures is consistent with their development during eastward obduction and thrusting of the ophiolitic Dunnage Zone over the Gander Zone.

7.4.3 D3

Greenschist facies, recumbent D2 structures in domains 1 and 2 are deformed by northeast-southwest trending upright folds considered to relate to $D3_{WEST}$ deformation. In domain 3, recumbent D2 structures are deformed by upright folds which also deform migmatites of domain 4 and are termed $D3_{EAST}$. The recumbent folds which deform flat-lying S2 fabrics in domain 1 are not observed elsewhere, their relationship to upright $F3_{WEST}$ folds is uncertain, and hence they are termed $D3_{LOCAL}$.

When considering the relationship between, and possible correlation between $D3_{WEST}$ and $D3_{EAST}$ events, structural, metamorphic and geochronological data must be assessed. Similarities between $D3_{WEST}$ and $D3_{EAST}$ deformation include the, 1) northeast-southwest orientation of associated structures, 2) development of a northeast-southwest trending mineral lineation, 3) upright form of folds and steep dip of axial planar fabrics, 4) progressive style of the predominantly sinistral deformation and, 5) the overall eastwards increase in metamorphic grade. Significant differences exist between the $D3_{WEST}$ and $D3_{EAST}$ structures, the most obvious being the form of their prograde metamorphic paths (fig. 7.4) and their peak metamorphic conditions.

The metamorphic assemblage of $D3_{WEST}$ is characterised by subsolidus, andalusite, kyanite, sillimanite and staurolite-rich metasediments. Rocks record the prograde sequence andalusite → kyanite → sillimanite and peak conditions of *c.* 650 °C and 5.5 kbar. A characteristic feature of the $D3_{WEST}$ metamorphic assemblages is the preservation of the prograde reaction andalusite → kyanite. Although this transition has been documented in other metamorphic belts (e.g. Hollister, 1969; Crawford & Mark, 1982; Baker, 1987), it is uncommon. The observed reaction andalusite → sillimanite is, however well documented in metamorphic belts and typical of Barrovian-type metamorphism (e.g. Miyashiro, 1961). In contrast the $D3_{EAST}$ metamorphic assemblages are characterised by biotite → garnet-bearing metasediments and andalusite → sillimanite-bearing migmatites. Peak conditions for $D3_{EAST}$ of *c.* 700 °C and 4.5 kbar are recorded by migmatitic assemblages. A similarity in the peak pressure conditions recorded by the $D3_{WEST}$ and $D3_{EAST}$ metamorphic assemblages is evident although there is no evidence in the migmatites for relict kyanite suggesting that the prograde path of $D3_{EAST}$ passed below the aluminosilicate triple point (the aluminosilicate triple point of Richardson et al. 1969 best fits the observed petrography and geothermobarometric estimates for both $D3_{WEST}$ and $D3_{EAST}$ metamorphic assemblages).

In order to asses the possible relationship between the $D3_{WEST}$ and $D3_{EAST}$ deformation relative time constraints are needed. These are provided by critical field relationships between the non-foliated Middle Brook Granite and the surrounding rocks. In the south of the Gander Lake Subzone the Middle Brook Granite separates the $D3_{WEST}$ metasediments of domain 2 and the $D3_{EAST}$ migmatites of domain 4. Field relationships at the western margin of the Middle Brook Granite show a thermal overprinting of retrogressed $D3_{WEST}$ rocks (of domain 2) giving evidence of its post $D3_{WEST}$

Fig. 7.4 Summary P-T-t-d evolution paths for Domains 1-5 of the Gander Lake Subzone.

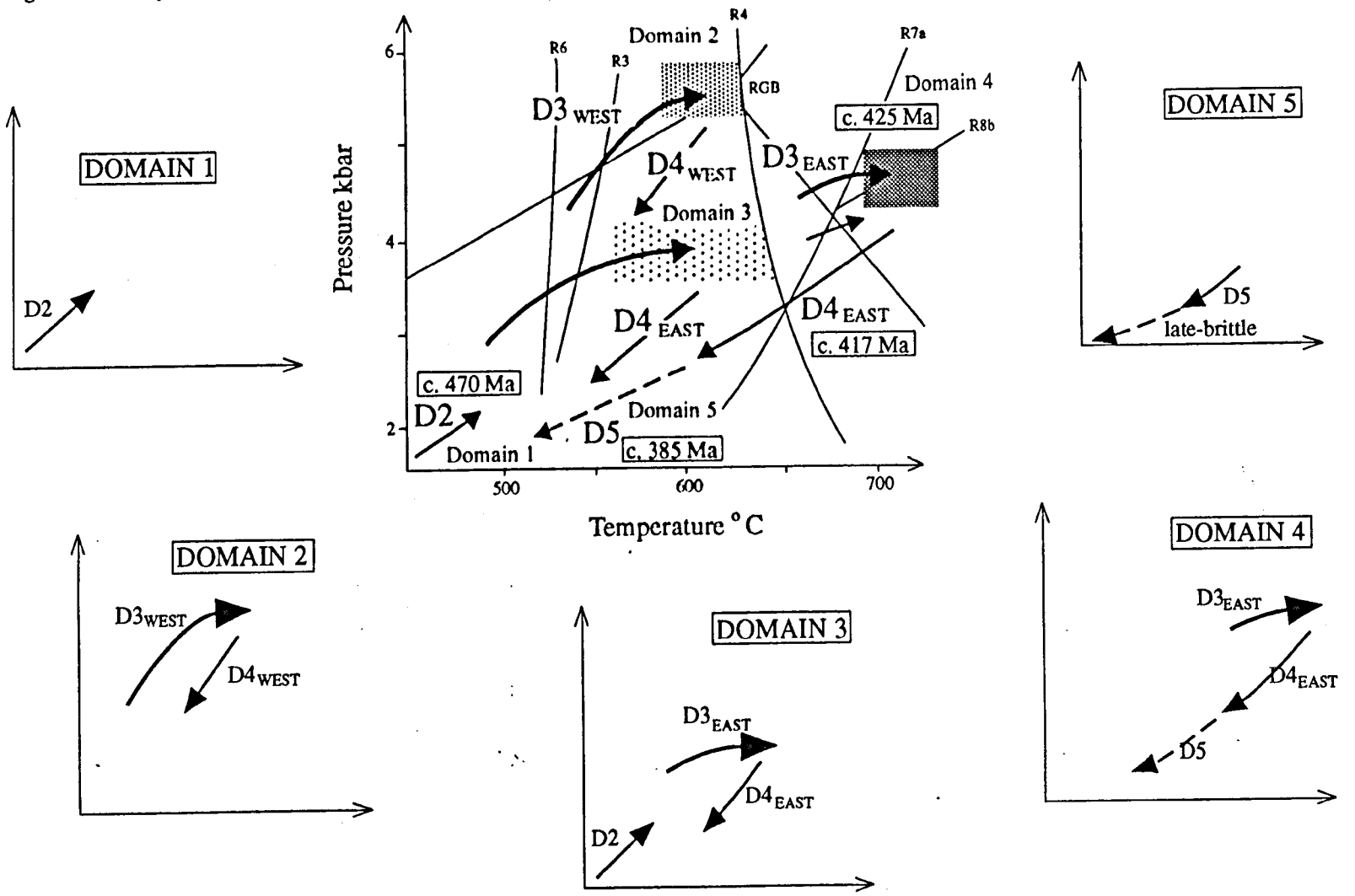

Al_2SiO_5 data from Richardson et al. (1969), reactions: R3)St-in, Hoschek (1969); R4) Thompson & Algor (1977); R6) Grt-in, Powell & Holland (1990); R7a) Chatterjee & Johannes (1974); R8a) Holdaway & Lee (1977).

emplacement. Field relationships at the eastern margin of the Middle Brook Granite (with domain 4) are unclear being obscured by late-stage brittle faults which juxtapose the Middle Brook Granite against the migmatites. The field relationship between emplacement of the granite and formation of the migmatites is therefore unknown. U-Pb age data from the Middle Brook Granite (Dunning *et al. in prep*) gives an age of *c.* 427 Ma which would suggest that $D3_{WEST}$ occurred prior to this date. In contrast U-Pb age data for the migmatites (Dunning *et al. in prep*) gives an age of *c.* 425 Ma suggesting that the $D3_{EAST}$ migmatisation event post-dated $D3_{WEST}$. The age obtained from the Middle Brook Granite is brought into question by its previous classification as a 'post-tectonic' Devonian pluton (e.g. Colman-Sadd *et al.* 1990), this interpretation being made on the basis of field mapping in particular by the undeformed nature and similarity to other isotopically dated Devonian plutons in the region. In the absence of the U-Pb age data, Holdsworth (1994b) argued that the upright structures within the Gander Lake Subzone (i.e. $D3_{WEST}$ and $D3_{EAST}$) formed during the same event and explained the anomalous high pressure metamorphic assemblages (in domain 2) by the rheologically / fluid controlled focusing of strain.

The combination of field, structural and metamorphic data in the aluminosilicate-bearing metasediments (of domain 2) and the migmatites (of domain 4) and isotopic age data from the Middle Brook Granite indicates that $D3_{WEST}$ and $D3_{EAST}$ are of different age and represent separate deformational events implying that the Gander Lake Subzone underwent two phases of progressive Silurian deformation and associated prograde metamorphism.

7.4.4 D4

Overprinting of $D3_{WEST}$ by steep northeast-southwest trending retrogressive micaceous fabrics occurs in the east of domain 2. These are considered to relate to $D4_{WEST}$. Similarly, overprinting of $D3_{EAST}$ structures by steep, retrogressive fabrics (also northeast-southwest trending) which occurs in domains 3 and 4 is considered to relate to $D4_{EAST}$.

The $D4_{WEST}$ and $D4_{EAST}$ fabrics share a number of characteristics including their retrogressive nature, micaceous assemblage, northeast-southwest orientation, steep attitude and associated northeast-southwest trending mineral lineation. Significant differences include their kinematics and metamorphic grade (fig. 7.4). $D4_{WEST}$ fabrics are predominantly dextral and of greenschist facies whereas $D4_{EAST}$ fabrics are sinistral and of lower amphibolite to upper greenschist facies.

Relative timing constraints on $D4_{WEST}$ are provided by the overprinting field relationships of the Middle Brook Granite at its western margin (with domain 2) indicating that $D4_{WEST}$ retrogression pre-dated emplacement of the Middle Brook Granite. Field relationships in domain 4 illustrate that the northeast-southwest trending $D4_{EAST}$ fabric in the migmatites (which overprints $D3_{EAST}$ fabrics) parallels the dominant foliation within the syn-tectonic granites (e.g. Lockers Bay and Cape Freels). Information on the absolute timing relationship between $D4_{WEST}$ and $D4_{EAST}$ is given by isotopic U-

Pb age dates of *c.* 427 Ma for the Middle Brook (discussed above in section 7.4.3) and *c.* 417 Ma for the Lockers Bay and Cape Freels Granites suggesting that $D4_{WEST}$ is slightly older than $D4_{EAST}$.

In the absence of the U-Pb data, the $D4_{WEST}$ and $D4_{EAST}$ retrogressive fabrics could represent the same D4 retrogressive event (due to their similar grade and field characteristics). The combination of field and geochronologic data, however, (discussed above), appears to suggest that the $D4_{WEST}$ retrogression pre-dates the $D4_{EAST}$ retrogression and that these episodes are temporally separate.

7.4.5 D5

Lower amphibolite to upper greenschist facies northeast-southwest trending $D4_{EAST}$ sinistral fabrics ($S4_{EAST}$) are locally overprinted within domain 4 by northeast-southwest trending greenschist facies dextral ductile fabrics thought to relate to D5. Similar northeast-southwest trending greenschist facies dextral fabrics (also overprinting higher grade sinistral fabrics) termed D5 are pervasively developed in domain 5 adjacent to the Dover Fault. The D5 fabrics, although preserving a different sense of shear, appear to represent a down grade continuation of the $D4_{EAST}$ retrogressive deformation. Time constraints on D5 (fig. 7.3) are given by field relationships which show their cross-cutting by the Devonian Newport Granite (dated as *c.* 385 Ma, Dunning *et al. in prep.*) indicating that D5 deformation pre-dated its emplacement.

7.4.6 D6

In domain 5, S5 dextral fabrics are locally overprinted by dextral brittle fabrics associated with northeast-southwest trending faults related to D6 deformation. Similar brittle fabrics associated with northeast-southwest trending dextral faults occur subordinately throughout the Gander Lake Subzone and are thought to be associated with late-stage movement along the Dover Fault. Timing constraints are given (fig. 7.3) by field relationships which suggest that D6 post-dates emplacement of the Newport Granite *c.* 385 Ma (Dunning *et al. in prep*) and pre-dates emplacement of the Ackley Granite *c.* 378 Ma (Kontak, 1988).

7.5 Summary of structures within the Gander Lake Subzone

The Gander Lake Subzone has been subjected to a number of phases of regional deformation, classified as D1-D6 (summarised in fig. 7.2). The D1 event, preserved in metasediments (in domains 1, 2 & 3) occurred at greenschist facies and formed a characteristic S1 fabric, although F1 folds have not been observed. The greenschist facies D2 event deforms S1 fabrics (in domains 1, 2 & 3), and is characterised by recumbent, easterly-verging F2 folds. D2 is considered to be related to the eastward obduction of the Dunnage Zone over the Gander Zone at *c.* 470 Ma.

The D2 structures in domains 1 & 2 are deformed by $D3_{WEST}$ structures and those in domains 3 and 4 by upright $D3_{EAST}$ structures. Both the $D3_{WEST}$ and $D3_{EAST}$ deformations show a progressive style and predominately sinistral shear sense indicators. Structures are characterised by upright, northeast-southwest trending folds with steep amphibolite facies prograde fabrics and an associated northeast-southwest trending mineral lineation. $D3_{WEST}$ is characterised by the prograde sequence andalusite → kyanite → sillimanite, the timing of which is constrained to pre-emplacement of the Middle Brook Granite (dated by U-Pb zircon methods as *c.* 427 Ma; Dunning *et al. in prep.* and previously classified as Devonian; Colman-Sadd *et al.* 1990). $D3_{EAST}$ is characterised by the prograde transition biotite→ garnet in metasediments and andalusite → sillimanite in migmatites which preserve high-temperature, low-pressure peak conditions. The timing of peak $D3_{EAST}$ is constrained to syn-migmatisation (*c.* 425 Ma) and pre-emplacement of the syn-tectonic granites (*c.* 417 Ma).

Effects of $D4_{WEST}$ retrogressive deformation overprint $D3_{WEST}$ structures (in domain 2) and are characterised by, steep northeast-southwest trending greenschist facies fabrics, a northeast-southwest trending mineral lineation and are predominantly dextral. Timing of $D4_{WEST}$ is constrained to pre-emplacement of the Middle Brook Granite (dated as *c.* 427 Ma and previously termed Devonian; see above). Effects of $D4_{EAST}$ retrogression overprint $D3_{EAST}$ structures (in domains 3 & 4), and are characterised by steep northeast-southwest trending sinistral fabrics (amphibolite to greenschist facies) and a northeast-southwest trending mineral lineation. Timing of $D4_{EAST}$ is synchronous with emplacement of foliated syn-tectonic granites in domain 4 (e.g. the Cape Freels & Lockers Bay Granites) which are dated as *c.* 417 Ma. D5 retrogressive deformation overprints $D4_{EAST}$ (in domain 5), forming northeast-southwest trending, steep greenschist facies dextral fabrics. Effects of D6 are concentrated in the vicinity of the Dover Fault, being characterised by greenschist facies brittle dextral fabrics and associated with northeast-southwest trending faults.

7.6 Possible causes of metamorphism

7.6.1 Low grade metasediments (of domains 1, 2 and 3)

The chlorite and muscovite-bearing metasediments (occurring throughout domain 1, and in the west of domains 2 and 3) are characterised by low metamorphic grade (fig. 7.4). The easterly verging flat-lying folds which deform these rocks are thought to have been formed by eastward thrusting of the Dunnage Zone over the Gander Zone during the Ordovician (*c.* 470 Ma; e.g. Williams & Stevens, 1974; Williams, 1984; Colman-Sadd *et al.* 1992a). The weak metamorphism associated with the flat-lying folds suggests that the Gander Lake Subzone was situated away from the main centre of deformation, possibly forming at shallow depth (*c.* 5 km) within a pile of stacked nappes.

7.6.2 Domain 2; the Wing Pond Shear Zone

The prograde sequence andalusite → kyanite → sillimanite recorded in metapelites of domain 2 (the Wing Pond Shear Zone) demonstrates a clockwise P-T-t-d metamorphic path (shown by initial

pressure increase closely followed by increasing temperature). Although the clockwise form of the path is consistent with the evolution of regional metamorphic belts, it is extremely rare for the early prograde andalusite → kyanite transition to be observed (England & Thompson, 1984).

A characteristic feature of the metamorphism in domain 2 is the abrupt increase in metamorphic grade which occurs over 1-2 km. The upright form of the $D3_{WEST}$ structures and the variable attitude of associated mineral lineations are consistent with their formation during compression and may record bulk inhomogeneous shortening (e.g. Bell & Johnson, 1989). Sinistral shear sense indicators suggest that there was an element of sinistral transpression accompanying the shortening. The localised increase in the intensity of the deformation in domain 2 suggests that strain was focused into the region which may have produced rheological weakening, this would also account for the focusing of $D4_{WEST}$ retrogressive deformation into the region.

The presence of the prograde andalusite → kyanite transition in domain 2 has important implications when considering a tectonic model for the evolution of the region. The andalusite → kyanite transition is interpreted to record an initial pressure increase during $D3_{WEST}$ tectonic thickening. This is consistent with the abundance of compressional structures in the region however field evidence for steep mineral lineations, which could be related to thrusting are absent. Other examples (although rare) of the prograde andalusite → kyanite transition in metamorphic belts have been documented and variably interpreted. Hollister (1969) considered the andalusite → kyanite transition as resulting from the metastable transition of andalusite to kyanite in the kyanite stability field, whereas Crawford & Mark (1982), in common with other authors (e.g. Baker, 1987; Kerrick, 1990) explain the prograde andalusite → kyanite mineral transition due to the occurrence of tectonic thickening. In contrast to many other documented examples, the aluminosilicate metamorphic assemblages of domain 2 formed during a single progressive deformational event rather than during a high pressure overprint of earlier low pressure assemblages. Crawford & Mark (1982) observed the transition andalusite → kyanite in south-east Pennsylvania and interpreted it as resulting from the overprinting of a regional high temperature and low pressure event by a second more widespread high temperature, moderate pressure event. An analogy of the metamorphism in domain 2 may be the metamorphic transition preserved in rocks to the west of the Portsoy-Duchray lineament (of the eastern Dalradian of Scotland). The transition of andalusite → kyanite in these rocks has been interpreted (Baker, 1987) as resulting from thrusting during low pressure Buchan metamorphism. The transition of kyanite → sillimanite preserved in the region is a common feature of metamorphic belts (e.g. England & Thompson, 1984) and in this study is consistent with thermal relaxation following thickening.

The Wing Pond Shear Zone contains only minor amounts of igneous intrusive bodies although gravity surveys in the region (Miller, 1988) show the presence of a high density northeast-southwest trending belt directly coinciding with the trace of the domain. This may suggest the presence of more ultramafics at depth which could be of importance when considering the possible causes of siting of the anomalous metamorphic belt, an alternative is that the region is underlain by

inherently weak basement. Another possibility is that the focusing of the $D3_{WEST}$ deformation occurred due to lithologically controlled partitioning into the predominately semi-pelitic and pelitic metasediments which dominate the region.

7.6.3 Migmatites

The prograde andalusite → sillimanite (And - Sill facies series) which culminated in low-pressure, high-temperature (LP/HT) conditions and migmatisation within the Gander Lake Subzone is characteristic of LP/HT belts (Miyashiro, 1961, 1973). The conditions recorded in the migmatites of the Gander Lake Subzone, indicate the presence of an above average crustal geothermal gradient of *c.* 50 °C/km. It is possible that the migmatites do not preserve the peak pressure conditions, which may have been eradicated by thermal relaxation following crustal shortening.

LP/HT metamorphism is not restricted to a specific tectonic setting, and has been documented in both regions of compression (e.g. Mary Kathleen Fold Belt: Reinhardt, 1992; Maine: Lux *et al.* 1986; De Yoreo *et al.* 1989a), and extension (e.g. Pyrenees: Wickham & Oxburgh, 1985, 1986). A characteristic features of these belts (also seen in the Gander Lake Subzone), is the abundance of peraluminous granites and the presence of the highest grade of metamorphism adjacent to plutons. Various causes of elevated temperatures in the crust have been proposed including, 1) high basal heat flow from upwelling mantle due to rifting (Wickham & Oxburgh, 1985), 2) lithospheric stretching and upward displacement of the lithosphere-asthenosphere boundary (Sandiford & Powell, 1986), 3) advected heat from either felsic or basic magmatic intrusions (De Yoreo *et al.* 1989b; Barton & Hanson, 1989) and 4) lithosphere delamination (Looseveld, 1989; Looseveld & Etheridge, 1990; van Staal & Fyffe, 1991; van Staal & De Roo, 1995).

The LP/HT belt of the Gander Lake Subzone, interpreted to have formed during compressive 'Acadian' deformation shares features similar to those formed during the same event further south in the Appalachian orogen (e.g. in Maine and New England; Lux *et al.* 1986; De Yoreo *et al.* 1989b). Similarities in the regions include the presence of a steep metamorphic transition over a relatively short distances (*c.* 25 km in the Gander Lake Subzone), the prograde And - Sill facies series, and the abundance of granitic magmas. The metamorphic P-T-t paths calculated for such compressional orogens (assuming purely conductive heat transfer) predict an upward shift in the crustal steady-state geotherm into high-pressure P-T conditions, and predict the crossing of the andalusite and sillimanite stability fields during exhumation and thermal relaxation (England & Thompson, 1984). Consequently, models suggest that under normal conditions, LP/HT metamorphism should not occur simultaneously with crustal shortening (e.g. Reinhardt, 1992) and would require an additional heat source (England & Thompson, 1984).

The common abundance of peraluminous granites in many of the compressional LP/HT belts has been used to explain the anomalous prograde And - Sill facies series metamorphism, suggesting that their intrusion increased the temperature of the upper crust. Lux *et al.* (1986) proposed that in western Maine the heat source for LP/HT metamorphism consisted of a series of sill-

like granitic bodies (emplaced at low-angles) resulting in a regional scale 'thermal contact' metamorphism. Similar interpretations have been made by Rothstein & Hoisch (1994) who concluded that in southeast California, LP/HT conditions resulted from short lived magmatic events involving rapid emplacement of multiple intrusions. These effects have been extensively modelled and show that in fact, the prograde And → Sill transition can be predicted (e.g. Lux *et al.* 1986). The intrusion of basic or intermediate magmas has been proposed (e.g. Steele & Price, 1985) in other regions, to explain the presence of high temperatures at shallow crustal levels. The model of Flood & Vernon (1978), predicts LP/HT conditions, whereby metamorphic zones and migmatitic envelopes are dragged upwards with the granite plutons (also described by Jones & Brown, 1990), this however would produce a low-pressure overprint of earlier higher pressure assemblages, for which there is no direct evidence in the migmatites of the Gander Lake Subzone.

The formation of intrusions within individual LP/HT belts has been variably attributed to lower crustal melting (e.g. western Maine: Lux *et al.* 1986) and mantle melting (e.g. Omeo Metamorphic Complex southeast Australia: Morand, 1990), in addition Huppert & Sparks (1988) model mantle melting which triggers crustal melting. With respect to the Gander Lake Subzone, the model of Lux *et al.* (1986) may explain the association of LP/HT migmatites in association with flat-lying sheets of the Wareham Granite, although in contrast to those described in the model, migmatites in the Gander Lake Subzone do not appear to directly envelope the individual plutons. Moreover, many of the intrusions (e.g. the Cape Freels, Lockers Bay, Newport and Deadmans Bay Granites) clearly post-date peak migmatisation. It is possible that other early plutons similar to the Wareham Granite, were intruded through the region, or occur at depth. Results of isotopic studies (D'Lemos & Holdsworth, 1995) show the granitic magmas in the Gander Lake Subzone to be lower crustal derived with input from the both the mantle and upper crust. The presence of only small volumes of mafic intrusions (type 1) associated with the migmatites in the Gander Lake Subzone appears to preclude their contribution as a source of local excess heat, although it is feasible that such bodies are present at depth. Another possibility is that the anomalous high temperature type 2 metabasites (with unknown field relationships with respect to the migmatites) may have supplied additional heat flux to the region.

An alternative model for attaining high temperature conditions in regions of compression (e.g. the Mary Kathleen Fold Belt; Reinhardt, 1992 and the Mount Isa Inlier; Rubenach, 1992) involves the removal of lithospheric mantle which brings the crust closer to the hot asthenosphere during simultaneous convective thinning of the lower lithosphere, and thickening of the crust (Looseveld & Etheridge, 1990). The abnormally high geothermal gradient produced in the lower crust would induce substantial partial melting, as seen within the Gander Lake Subzone, and syn-metamorphic granite plutonism. The model however predicts a 'delay' of the thermal event with respect to deformation which is non-consistent with field observations. This led to the suggestion (e.g. Reinhardt, 1992; Rubenach, 1992) that the LP/HT conditions may be due to the effects of earlier extensional deformational events in the crust (similar to those proposed for the Slave province,

Canada; Thompson, 1989) although no evidence for early extension is observed within the Gander Zone.

It has been suggested (e.g. Rubenach, 1992), that the heat-producing elements K, U and Th within granites may be an additional contributing factor to the overall thermal budget within LP/HT belts. This mechanism has been shown (e.g. Looseveld, 1989) to produce elevated temperatures adjacent to thick sheets of granite, although in general (i.e. for narrower bodies), the granites are required to be enriched in the heat-producing elements. Another proposed heating mechanism is the advective transfer of heat by fluids (e.g. Chamberlain & England, 1985) but is considered in itself, unlikely to explain widespread LP/HT metamorphism (e.g. De Yoreo *et al.* 1991).

To conclude, the LP/HT migmatite belt of the Gander Lake Subzone is characterised by the presence of abundant granitic, and small volumes of mafic material. In the absence of a definite single heat source, it is suggested that the LP/HT conditions of metamorphism resulted from a combination of crustal thickening and advected heat from granitic intrusions with possible additional heat input from mafic intrusions and internal heating. Future detailed geochemical analysis of the intrusions in the region would help to establish their source, and hence may provide information on their possible input to the excess heat, in addition, geophysical gravity surveys may identify the presence of other granitic or mafic intrusions present at depth.

7.7 Overall tectonic model

The Gander Lake Subzone, experienced low grade metamorphism associated with the mid Ordovician Penobscottian obduction event, but is dominated by effects of subsequent deformation and metamorphism associated with the late Ordovician to Silurian 'Salinic' orogeny. The initial focusing (fig. 7.5a) of Silurian compressive regional deformation (shown by polymorphic transition andalusite → kyanite into domain 2, fig. 7.4) and subsequent lower grade localised dextral transpressive deformation (fig. 7.5b) was followed by rheologically controlled partitioning of sinistral deformation into LP/HT migmatites and foliated granites (of domain 4; fig. 7.5c). The partitioning of deformation within the Gander Lake Subzone hence displays a definite eastward shift over time. Subsequent Silurian and Devonian retrogressive deformation within the Gander Lake Subzone (fig. 7.5d) was concentrated along the Gander-Avalon boundary and shows a change from sinistral to dextral transpression. Exhumation accompanied both sinistral and dextral transpressive motions, resulting in a change of ambient metamorphic grade from amphibolite to greenschist facies through the Silurian to Devonian.

It is widely accepted (e.g. van de Pluijm *et al.* 1990; 1995; Hibbard, 1994; van Staal, 1994) that the protracted deformational history preserved within the Appalachians resulted from multiple collisional events during the Ordovician to Silurian and Devonian (fig. 7.6). The timing, kinematics, metamorphic grade and deformational style of these events varies along the strike of the orogen, and can be explained by interaction of irregular plate margins (e.g. Stockmal *et al.* 1986), and in particular, by promontory-promontory type collision (e.g. Lin *et al.* 1994). The geometry of the

Fig. 7.5 Summary schematic diagram showing regionally important events within the Gander Zone of NE Newfoundland.
A) Tectonic thickening of crust (accompanied by sinistral transpression) in domain 2.
B) Localised dextral retrogressive deformation.
C) Eastward shift in the focus of deformation (post intrusion of the Middle Brook Granite, c. 427 Ma) and development of a high grade sinistral shear zone (containing migmatites, c.425 Ma and syn-tectonic granites, c.417 Ma).
D) Development of a retrogressive dextral high-strain zone juxtaposing high grade Gander Zone rocks against low grade Avalon rocks across the ductile-brittle Dover Fault (possibly overlapping with emplacement of the Newport Granite, c. 385 Ma).

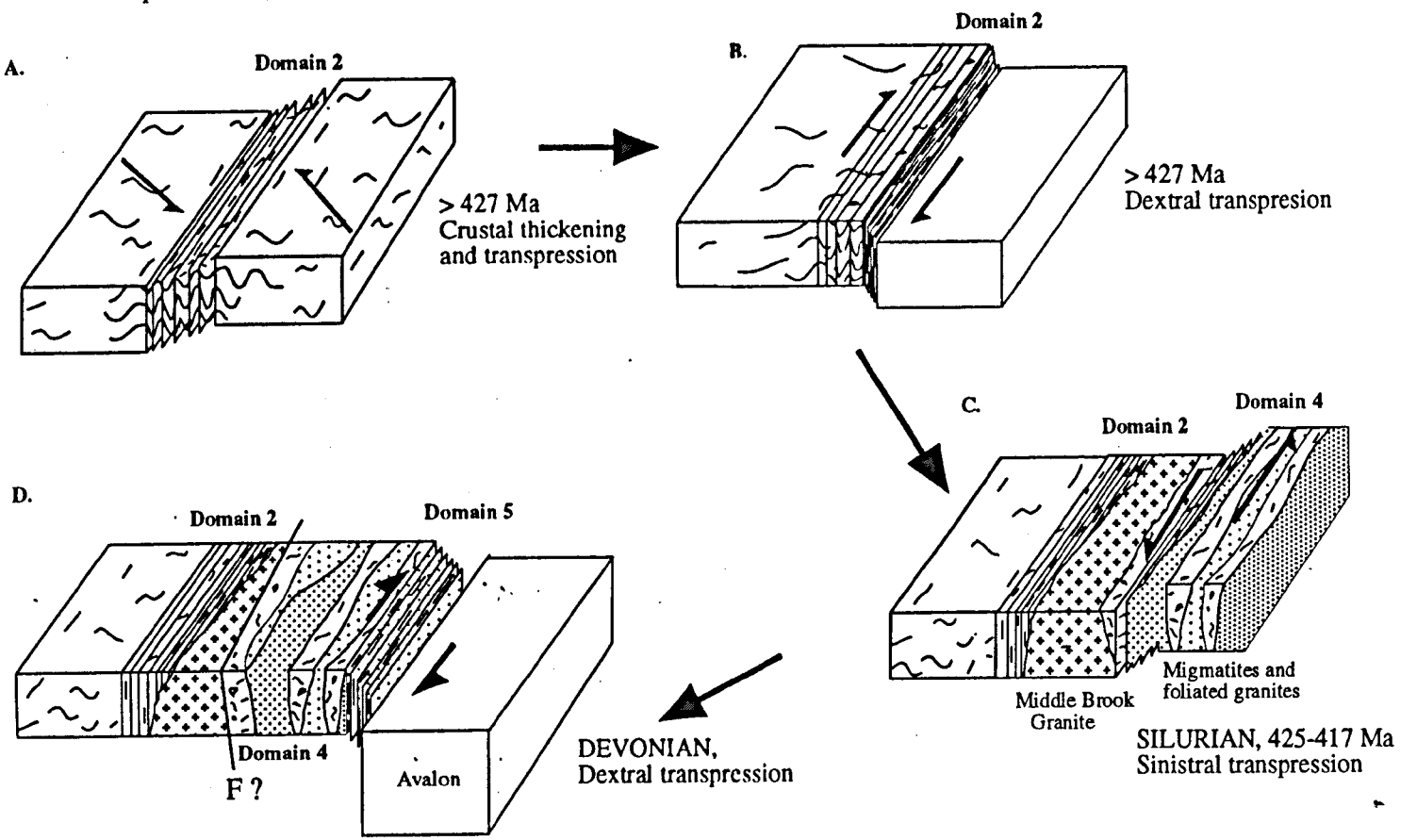

Fig. 7.6 Summary of Acadian deformation for the northern and Newfoundland Appalachians; A. Early Acadian (Ord-Sil); B. Classic Acadian (Dev); modified after Hibbard, 1994, CMB=Central Mobile Belt).

western margin of the Appalachians shows a z-shaped flexure across the Gulf of St. Lawrence (representing the Precambrian transform-rift configuration of the Iapetus), comprising the Quebec re-entrant and the St. Lawrence promontory. This promontory-re-entrant geometry was inherited further west in the orogen after subsequent arc-continent collision, leading to a similar shaped pattern on the western margin of Newfoundland (fig. 7.6) marked by the Cabot promontory and the Hermitage re-entrant (Williams, 1979).

The interaction of the Central Mobile Belt and Avalon is recorded heterogeneously throughout the Appalachian belt and is known as the Acadian event (e.g. Hibbard, 1994). Southwest Newfoundland and Cape Breton Island display a narrower, more intensely deformed belt of Silurian Acadian deformation with respect to other parts of the orogen, in particular, with respect to the study area in northeast Newfoundland. Specific to the southeast of Newfoundland are predominately high pressure, thrust-controlled compressional structures, as opposed to the lower pressure, transpressive structures in the northeast of Newfoundland. The Hermitage Flexure (fig. 7.6a), is a southwest extension of the Dover Fault characterised by intense Silurian shortening along asymmetric, north-verging folds and thrusts (O'Brien *et al.* 1991). The shortening was accommodated along east-northeast trending imbricate thrusts (the Bay d'Est and Cinq Cerf Faults), and was followed by Devonian, westward directed thrusting (e.g. of the Clam Bank Group; Cawood, 1993, fig. 7.6b). The Cape Ray Fault (fig. 7.6a), in the southwest corner of Newfoundland, is an orogen parallel, westward extension of the Hermitage Flexure dominated by Silurian westward-verging thrusts (e.g. O'Brien *et al.* 1991; Lin, 1992), in places, northeast trending segments of the fault, display Silurian sinistral transpressional structures, overprinted by late-Silurian to Devonian dextral fabrics (Dube *et al.* 1992). Comparable kinematic patterns and variations are evident further south in the orogen, e.g. in Cape Breton Island, New Brunswick and Maine (Hibbard, 1994), and evidence from the Brunswick subduction complex (van Staal & De Roo, 1995) suggests that during the Acadian, the region underwent Late Silurian sinistral transpression which changed through extensional collapse, into dextral transpression in the Early to Middle Devonian (fig. 7.6b).

The differences in Silurian Acadian deformational styles, in particular within Newfoundland, suggests that initial continental collision was orthogonal. The switch in kinematics from sinistral to dextral in the Acadian recognised along the Appalachian orogen (e.g. Hibbard, 1994), and also within other parts of the north European Caledonides (e.g. Soper et al. 1992), appears to be consistently Devonian in age, between *c.* 413 / 385 Ma. Such a widespread feature, is attributed to lithospheric plate scale processes between Laurentia and Avalon, and can be placed within the broader context of the Appalachian-Caledonide orogen (e.g. Soper *et al.* 1992; Hibbard, 1994). The synchronous switch of deformation from predominantly sinistral / compressive to dextral has been interpreted to reflect an abrupt reorganisation of Palaeozoic plates, related to the interactions of Laurentia, Baltica and Avalon at an apparent triple junction (Soper *et al.* 1987, 1992). It is important to note however that within the Gander Zone an episode of dextral transpression (in domain 2) appears to have occurred prior to much of the high grade sinistral transpression deformation (in domain 4). This kinematic pattern is

not consistent with the sinistral → dextral motion observed elsewhere in Newfoundland and the Appalachians as a whole although critical to this timing relationship is the isotopic age date of the Middle Brook Granite which post-dates dextral retrograde fabrics.

7.8 Final conclusions

Taken as a whole, the Gander Zone shows an increasing intensity of deformation and grade of metamorphism towards its eastern boundary with the Avalon Zone. The Gander Lake Subzone contains two, kilometre scale high-strain zones; domain 2 (the Wing Pond Shear Zone) and domain 4 (the Eastern Gander Migmatite Belt) which preserve high grades of metamorphism and localised strain partitioning, in particular transpressive deformation. The high-strain zones both show progressive deformation and a clockwise P-T-t-d path, although in detail their metamorphic histories and peak metamorphic conditions differ. The rocks of domain 2 preserve the prograde transition andalusite → kyanite → sillimanite whereas the migmatites in domain 4 preserve the prograde sequence andalusite → sillimanite. The andalusite → kyanite prograde transition in domain 2 is interpreted to have formed (pre. *c.* 427 Ma) during tectonic thickening. Low pressure, high temperature migmatisation (in domain 4) is interpreted to have occurred during slightly later (*c.* 425 Ma) synchronous with granite magmatism. Strain localisation into these zones may relate to the presence of mafic bodies and / or zones with an inherent basement weakness. An additional important factor controlling strain localisation within domain 4 appears to have been the presence of large volumes of igneous intrusions which were generated during sinistral transpressional thickening adjacent to the Gander-Avalon boundary.

The overall P-T-t-d paths within the Gander Zone record Silurian crustal thickening and heating during oblique continental collision. Reactivation in the Devonian removed the presumed easterly portion of the Gander Zone, resulting in exhumation and the juxtapositioning of high grade Gander Zone rocks against low grade rocks of the Avalon Zone across the ductile-brittle Dover Fault.

ASHWORTH, 1985. Migmatites. Blackie, New York.

BAIRD, D.M., MOORE, J.G.G., SCOTT, H.S. & WALKER, W. 1951. Reconnaissance geology of east central Newfoundland between Sir Charles Hamilton Sound and Bay d' Espoir. *Department of Natural Resources, Mineral Exploration Division, Newfoundland Geological Survey*, unpublished report.

BAKER, A.J. 1987. Models for the tectonothermal evolution of the eastern Dalradian of Scotland. *Journal of Metamorphic Geology*, **5**, 101-118.

BARKER, A.J. 1994. Interpretation of porphyroblast inclusion trails: limitations imposed by growth kinetics and strain rates. *Journal of metamorphic Geology*, **12**, 681-694.

BARR, S.M., RAESIDE, R.P., MILLER, B.V. & WHITE, C.E., 1995. Terrane evolution and accretion in Cape Breton Island, Nova Scotia. *In*. HIBBARD, J.P., VAN STALL, C.R. & CAWOOD, P.A., EDS., Current Perspectives in the Appalachian-Caledonian Orogen: Geological Association of Canada, Special Paper **41**, 283-301.

BARTON, M.D. & HANSON, R.B. 1989. Magmatism and the development of low-pressure metamorphic belts: implications from the western United States and thermal modelling. *Geological Society of America Bulletin*, **101**, 1051-1065.

BELL, T.H. 1981. Foliation development: the contribution, geometry and significance of progressive bulk inhomogeneous shortening. *Tectonophysics*, **75**, 273-296.

— 1985. Deformation partitioning and porphyroblast rotation in metamorphic rocks: a radical re-interpretation. *Journal of Metamorphic Geology*, **3**, 109-118.

— & RUBENACH, M.J. 1983. Sequential porphyroblast growth and crenulation cleavage development during progressive deformation. *Tectonophysics*, **92**, 171-194.

— & JOHNSON, S.E. 1989. Porphyroblast inclusion trails: the key to orogenesis. *Journal of Metamorphic Geology*, 7, 279-310.

—, RUBENACH, M.J. & FLEMMING, P.D.1986. Porphyroblast nucleation, growth and dissolution in regional metamorphic rocks as a function of deformation partitioning during foliation development. *Journal of Metamorphic Geology*, **4**, 37-67.

—, JOHNSON, S.E., DAVIS, B., FORDE, A., HAYWARD, N. & WILKINS, C. 1992. Porphyroblast inclusion trail orientation data: eppure non son girate! *Journal of Metamorphic Geology*, **10**, 295-307.

BERMAN, R.G. 1990. Mixing properties of Ca-Mg-Fe-Mn garnets. *American Mineralogist*, **75**, 3-4, 328-344.

BICKLE, M.J. & ARCHIBALD, N.J. 1984. Chloritoid and staurolite stability: Implications for metamorphism in the Archaean Yilgarn Block, Western Australia. *Journal of Metamorphic Geology*, **2**, 179-203.

BLACKWOOD, R.F. 1976. *The relationship between the Gander and Avalon Zones in the Bonavista Bay region, Newfoundland.* Msc thesis, Memorial University of Newfoundland, St. Johns.

— 1977. *Geology of the east half of the Gambo (2D/16) map area and the northwest portion of the St. Brendan's (2C/13) map area, Newfoundland.* Newfoundland Mineral Development Division, Report **77-5**.

— 1978. Northern Gander Zone, Newfoundland. *In*: Current Research, Newfoundland Department of Mines and Energy, Report **78-1**, 72-79.

— 1980. Geology of the Gander (west) area (2D/15), Newfoundland. *In* Current Research, Newfoundland Department of Mines and Energy, Mineral Development Division, Report **81-10**, 50-56.

— 1982. *Geology of the Gander Lake (2D/15) and Gander River (2E/2) area.* Newfoundland Department of Mines and Energy, Mineral Development Division, Report **82-4**.

— & KENNEDY, M.J. 1975. The Dover Fault: western boundary of the Avalon Zone in northeastern Newfoundland. *Canadian Journal of Earth Sciences*, **12**, 320-325.

BLENKINSOP, J., CUCMAN, P.F. & BELL, K.T., 1976. Age relationships along the Hermitage Bay-Dover Fault System, Newfoundlannd. *Nature*, **262**, 377-378.

BLUNDY, J.D., HOLLAND, T.J.B., 1990. Calcic amphibole equilibria and a new amphibole-plagioclase geothermometer. *Contributions to Mineralogy and Petrology*, **104**, 208-224.

BOULLIER, A.M. & BOUCHEZ, J.L. 1978. Le quartz en rubans dans les mylonites: *Bulletin de la Société Géologique de France*, **7**, 253-262.

BROWN, M, 1973. The definition of Metatexis, Diatexis and Migmatite. *Proceedings of the Geologists Association*, **84**, 371-82.

— 1993. P-T-t evolution of orogenic belts and the causes of regional metamorphism. *Journal of the Geological Society, London*, **150**, 227-241.

— 1994. The generation, segregation, ascent and emplacemnt of granite magma: the migmatite-to-crustally-derived granite connection in thickened orogens. *Earth Science Reviews*, **36**, 83-130.

—, RUSHMER, T. & SAWYER, E. 1995. Introduction to special section: Mechanisms and consequences of melt segregation from crustal protoliths. *Journal of Geophysical Research*, **100**, 15, 551-63.

— & RUSHMER, T, *in press*. The role of deformation in the movement of granitic melt: views from the laboratory and the field. *Mineralogical Society*

BURTON K.B. & O' NIONS, 1990. The timescale and mechanism of granulite formation at Kurunegala, Sri Lanka. *Contributions to Mineralogy and Petrology*, **106**, 66-89.

BUDDINGTON, 1948. Origin of granitic rocks of the northwest Adirondacks (New York). In.GILLULY, J. *Origin of Granite*. Geological Society of America, Boulder, CO, U.S.A.

CARON, A. & WILLIAMS, P.F. 1988A. The multistage development of the Dover Fault Shear Zone in Northeastern Newfoundland: the late stages. *Geological Association of Canada-Mineralogical Association of Canada-Canadian Society of Petroleum Geologists, Joint Annual General Meeting, Program with Absrtacts*, **13**, A17.

—, P.F., 1988B. The kinematic indicators of the Love Cove Group in Northeastern Newfoundland. *Geological Association of Canada-Mineralogical Association of Canada-Canadian Society of Petroleum Geologists Joint Annual General Meeting, Program with Abstracts*, **13**, A17.

CAWOOD, P.A. 1993. Acadian orogeny in west Newfoundland: definition, character and significance. *In*: ROY, D. & SKEHAN, J. (EDS). *The Acadian Orogeny*: Geologogical Society of America Special Paper, **275**, 135-152.

—, VAN GOOL, J.A.M. & DUNNING, G.R. 1995. Collisional tectonics along the Laurentian margin of the Newfoundland Appalachians. *In*. HIBBARD, J.P., VAN STALL, C.R. & CAWOOD, P.A., EDS., *Current Perspectives in the Appalachian-Caledonian Orogen*: Geological Association of Canada, Special Paper **41**, 283-301.

CHAMBERLAIN C.P. & ENGLAND, P.C. 1985. The thermal history of the Merrimack Synclinorium in the northern Appalachians. *Journal of Geology*, **93**, 593-602.

CHATTERJEE, N.D.& JOHANNES, W. 1974. Thermal stability and standard thermodynamic properties of synthetic $2M_1$ muscovite $KAl_2(AlSi_3O_{10}(OH)_2)$. *Contributions to Mineralogy and Petrology*, 48, 89-114.

CHIPERA, S.J. & PERKINS D. 1988. Evaluation of biotite-garnet geothermometers: Application to the English River sunprovince, Ontario. *Contributions to Mineralogy and Petrology*, **98**, 40-48.

COLMAN-SADD, S.P. 1980. Geology of south-central Newfoundland and evolution of the eastern margin of Iapetus. *American Journal of Science*, **280**, 991-1017.

— 1982. Two-stage continental collision and plate driving forces. *Tectonophysics*, **90**, 263-282.

— & SWINDEN, H.S. 1984. A tectonic window in central Newfoundland? Geological evidence that the Appalachian Dunnage Zone is allochthonous. *Canadian Journal of Earth Sciences*, **21**, 1349-1367.

—, HAYES, J.P. & KNIGHT, I. (Compilers). 1990. *Geology of the island of Newfoundland.* Newfoundland Department of Mines and Energy, Geological Survey Branch, Map **90-01**.

—, S.P., DUNNING, G.R. & DEC, T. 1992A, Dunnage-Gander relationships and Ordovician Orogeny in central Newfoundland: a sediment provenance and U-Pb age study. *American Journal of Science*, **292**, 317-355.

—, S.P., STONE, P., SWINDEN, H.S. & BARNES, R.P. 1992b, Parallel geological development in the Dunnage Zone of Newfoundland and the Lower Palaeozoic terranes of southern Scotland: an assessment. *Transactions of the Royal Society of Edinburgh*, **83**, 571-594.

CRAWFORD, M L. & MARK, L. 1982. Evidence from metamorphic rocks for overthrusting. Pennsylvania Piedmont, U.S.A. *Canadian Mineralogist*, **20**, 333-347.

— & HOLLISTER, L.S. 1984. Thermal and tectonic processes in an orogenic belt. *Jounal of the Geological Society of America*, **16**, 478-479.

CURRIE, K.L. & PAJARI, G.E. 1977. Igneous and and metamorphic rocks between Rocky Ray and Ragged Harbour, northeastern Newfoundland. *In Report of Activities, Part A*. Geological Survey of Canada, **77-1A**, 341-346.

—, —, & PICKERILL, R.K. 1979. Tectonostratigraphic problems in the Carmenville area, northeastern Newfoundland. *In Current Research, Part A*. Geological Survey of Canada, **79 1A**, 71-76.

DALLMEYER, R.D., BLACKWOOD, R.F. & ODOM, A.L. 1981. Age and origin of the Dover Fault: tectonic boundary between the Gander and Avalon Zones of the northeastern Newfoundland Appalachians. *Canadian Journal of Earth Sciences*, **18**, 1431-1442.

— HUSSEY, E.M., O'BRIEN, S.J. & O'DRISCOLL, C.F. 1983. Chronology of tectonothermal activity in the Western Avalon Zone of the Newfoundland Appalachians. *Canadian Journal of Earth Sciences*, **20**, 355-363.

DEWEY, J.F. & BIRD, J.M. 1970, Mountain belts and the new global tectonics. *In*. COX, A. (ED) *Plate Tectonics and Geomagnetic Reversals*. W.H. Freeman & Co. , San Francisco, 610-631.

DE YOREO, J.J., LUX, D.R. & GUIDOTTI, C.V. 1989a. The role of crustal anatexis and magma migration in the thermal evolution of regions of thickened continental crust. *In*. DALY, J.S., CLIFF, R.A. & YARDLEY, B.W., EDS., *Evolution of Metamorphic Belts*, Geological Society Special Publication, **43**, 187-202. Blackwell Scientific Publications; Oxford.

—, —, — & OSBERG, P.H. 1989b. The Acadian thermal history of western Maine. *Journal of Metamorphic Geology*, 7, 169-190.

—, —, — . 1991. Thermal modelling in low-pressure/ high-temperature metamorphic belts. Tectonophysics, 188, 209-238.

DICKSON, W.L. 1974. *The general geology and geochemistry of the granitoid rocks of the northern Gander Lake belt*. M.Sc. thesis, Memorial University, St. Johns, Newfoundland.

D'LEMOS, R.S. SCHOFIELD, D.I., HOLDSWORTH, R.E & KING, T.K. 1997. Deep crustal and local rheological controls on siting and reactivation of fault and shear zones, northeastern Newfoundland. *Journal of the Geological Society of London*, **154**, 117-121.

—, BROWN, M. & STRACHAN, R.A. 1992. Granite magma generation, ascent and emplacement within a transpressional orogen. *Journal of the Geological Society of London*, **149**, 487-490.

— & HOLDSWORTH R.A. 1995. Samarium-Neodymium Isotopic Characteristics of the Northeastern Gander Zone, Newfoundland Appalachians. *in:* HIBBARD, J.P., VAN STAAL, C.R.,AND CAWOOD, P.A. (EDS) *Current Perspectives in the Appalachian-Caledonian Orogen*, Geological Association of Canada, Special Paper **41**. 239-252.

—, TRIBE, I.R. & PEMBROKE, J.W. 1995. Emplacement and construction of Devonian 'posttectonic' granites, northeast Newfoundland Appalachians. *Current Research Newfoundland Department of Natural Resources Geological Survey Report* 95-1, 221-235.

DUBE, B., LAUZIERE, K. & TREMBLAY, A. 1992. Structural geology of a crustal scale fault zone: The Cape Ray Fault zone coastal section, southwestern Newfoundland. In: *Current Research,* Part D: Geological Survey of Canada, **92D**, 199-209.

DUNNING, G.R., O'BRIEN, S.J., COLMAN-SADD, S.P., BLACKWOOD, R.F., DICKSON, W.L., O'NEILL, P & KROGH, T.E. 1990. Silurian orogeny in the Newfoundland Appalachians. *Journal of Geology*, 98, 895-913.

—, O'BRIEN, S.J., HOLDSWORTH, R.E. & TUCKER, R.D. *In prep.* U-Pb Geochronology of Igneous and metamorphic rocks associated with the Gander-Avalon Zone Boundary, Northeastern Newfoundland Appalachians.

ELLIS, D. J. 1980. Osumilite-Sapphirine-Quartz Granulites from Enderby Land, Antarctica: P-T conditions of metamorphism, implications for Garnet-Cordierite equilibria and the evolution of the deep crust. *Contributions to Mineralogy and Petrography*, **74**, 201-210.

ENGLAND, P. & THOMPSON, A.B. 1984. Pressure-temperature-time paths of regional metamorphism I. Heat transfer during the evolution of regions of thickened continental crust. *Journal of Petrology*, **25**, 4, 894-928.

ERNST W.G. 1977. Tectonics and prograde versus retrograde P-T trajectories of high-pressure metamorphic belts. *Rendiconti Soc Italia Mineral Petrol*, **33**, 191-220.

ESSENE, E.J. 1982. Geologic thermomometry in barometry. *In*: FERRY J.M.(ED). *Characterisation of metamorphism through mineral equilibria*, 153-206. Reviews in Mineralogy, 10, Mineralogical Society of America, Washington, D.C.

— 1989. The current status of thermobarometry in metamorphic rocks. *In*: DALY J.S., CLIFF R.A. & YARDLEY, B.W.D., (EDS). *Evolution of Metamorphic Belts*, 1-44. Blackwell Scientific Publications, Oxford.

FERRY, J.M. & SPEAR, F.S. 1978. Experimental calibration of the partitioning of Fe and Mg between biotite and garnet. *Contributions to Mineralogy and Petrology*, **66**, 113-117.

FLOOD, R.H. & VERNON, R.H. 1978. The Cooma Granodiorite, Australia: an example of in situ crustal anatexis? *Geology*, **6**, 81-84.

FRYER, B.J., KERR, A., JENNER, G.A., & LONGSTAFFE, F.J. 1992. Probing the crust with plutons: Regional isotopic geochemistry of granitoid intrusions across insular Newfoundland. *In: Current Research.* Newfoundland Department of Mines and Energy, Geological Survey Branch, Report **92-1**, 119-139.

GANGULY, J. & SAXENA, S.K. 1984. Mixing properties of aluminosilicate garnets: constraints from natural and experimental data, and applications to geothermobarometry. *American Mineralogist*, **69**, 88-97.

GAPAIS, D. 1989. Shear structures within deformed granites: Mechanical and thermal indicators. *Geology*, **17**, 1144-1147.

GEOLOGICAL SURVEY OF CANADA. 1968a. Aeromagnetic map, Gander, Newfoundland 2D/16. *Geophysics Paper*, **179**.

GIBSON, R.L. & BICKLE, M.J. 1994. Thermobarometric constraints on the conditions of metamorphism in the Canigou massif, Pyrenees: implications for Hercynian geothermal gradients. *Journal of the Geological Society, London*, **151**, 987-997.

HANMER, S. 1981. Tectonic significance of the northeastern Gander zone, Newfoundland: an Acadian ductile shear zone. *Canadian Journal of Earth Sciences*, **18**, 120-135.

HARTE, B. & HUDSON N.F.C. 1979. Pelite facies series and the temperatures and pressures of Dalradian metamorphism in E. Scotland. *In: The Caledonides of the British Isles Reviewed*, Geological Society of London Special Publication, 8, 323-337.

HEPBURN, J.C., DUNNING, G.R. & HON, R. 1995. Geochronology and regional tectonic implications of Silurian deformation in the Nashoba Terrane, Southeast New England. *In.* HIBBARD, J.P., VAN STALL, C.R. & CAWOOD, P.A., EDS., *Current Perspectives in the Appalachian-Caledonian Orogen*: Geological Association of Canada, Special Paper **41**, 283-301.

HIBBARD, J. 1994. Kinematics of Acadian deformation in the Northern and Newfoundland Appalachians. *Journal of Geology*, **102**, 215-228.

HODGES, K.V. & SPEAR, F.S. 1982. Geothermometry, geobarometry and the Al_2SiO_5 triple point at Mt. Moosilauke, New Hampshire. *American Mineralogist*, **67**, 1118-1134.

HOLDAWAY, M.J. 1971. Stability of andalusite and the aluminum silicate phase diagram. *American Journal of Science*, **271**, 97-131.

— & LEE, S.M. 1977. Fe-Mg cordierite stability in high-grade pelitic rocks based on experimental, theoretical, and natural observations. *Contributions to Mineralogy and Petrology*, **63**, 175-198.

HOLDSWORTH, R.E. 1991. The geology and structure of the Gander-Avalon boundary zone in northeastern Newfoundland. *In: Current Research*, Newfoundland Department of Mines and Energy, Report **91-1**, 109-126.

— 1994a. Structural evolution of the Gander-Avalon terrane boundary: a reactivated transpression zone in the NE Newfoundland Appalachians. *Journal of the Geological Society of London*, **151**, 629-646.

— 1994b. The consequences and possible causes of deformation partitioning in the Gander Lake Subzone, NE Newfoundland. *New perspectives in the Appalachian-Caledonian Orogen*, Geological Association of Canada, NUNA Meeting, Abstract with programs.

— & O'BRIEN, S.J. 1993. A reconnaissance structural study along the Gander-Avalon Zone boundary between Terra Nova lake and the Ackley granite, Newfoundland. *In: Current Research*, Newfoundland Department of Mines and Energy, Report **93-1**, 229-237.

—, D'LEMOS, R.S., MCERLEAN, M.A. & O'BRIEN, S.J. 1993. Deformation of the Cape Freels Granite related to dextral displacements along the Dover Fault, northeast Newfoundland. *In: Current Research*, Newfoundland Department of Mines and Energy, Report **93-1**, 221-228.

HOLLAND, T. & BLUNDY, J. 1994. Non-ideal interactions in calcic amphiboles and their bearing on amphibole-plagioclase thermometry. *Contributions to Mineralogy and Petrology*, **116**, 433-447.

HOLLISTER, L.S. 1969. Metastable paragenetic sequence of andalusite, kyanite and sillimanite, Kwoiek area, British Columbia. *American Journal of Science*, **267**, 352-370.

— & CRAWFORD, M.C. 1986. Melt-enhanced deformation: a major tectonic process. *Geology* **14**, 558-561.

HOLLOCHER, K. 1987. Systematic retrograde metamorphism of sillimanite-staurolite schists, New Salem area, Massachusetts. *Geological Society of America Bulletin*, **98**, 621-634.

HOLMQUIST, P. J. 1921. Typen und Nomenklatur der Adergesteine. *Geol. Foren, Stockholm Forh*, **43**,191-631.

HOSCHEK, G. 1969. The stability of staurolite and chloritoid and their significance in metamorphism of pelitic rocks. *Contributions to Mineralogy and Petrology*, **22**, 208-232.

HUDSON, N.F.C. 1980. Regional Metamorphism of some Dalradian Pelites in the Buchan Area, N.E. Scotland. *Contributions to Mineralogy and Petrology*, **73**, 39-51.

HUGHES,C.J. 1970. The late Precambrian Avalonian Orogeny in Avalon, southeast Newfoundland. *American Journal of Science*, **258**, 183-190.

HUPPERT, H.E. & SPARKS, S.J. 1988. The generation of granitic magmas by intrusion of basalt into continental crust. *Journal of Petrology*, **29**, 599-624.

HUTCHINSON, R.D. 1962. Cambrian stratigraphy and trilobite faunas of southeastern Newfoundland. *Geological Survey of Canada Bulletin*, **35**.

HUTTON, D.H.W. 1988. Granite emplacement mechanisms and tectonic controls: inferences from deformation studies. *Transactions of the Royal Society of Edinburgh: Earth Sciences*, **79**, 245-255.

INDARES, A. & MARTIGNOLE, J. 1985. Biotite-garnet geothermometry in the granulite facies: the influence of Ti and Al in biotite. *American Mineralogist*, **70**, 272-278.

INGRAM, G.M. & HUTTON, D.H.W. 1994. The Great Tonalite Sill: Emplacement into a contractional shear zone and implications for Late Cretaceous to early Eocene tectonics in southeastern Alaska and British Columbia. *Bulletin of the Geological Society of America* , **106**, 715-728.

JAMIESON, R.A. 1981. Metamorphism during opiolite emplacement-the petrology of the St. Anthony Complex. *Journal of Petrology*, **22**, 387-449.

— 1984. Low pressure cordierite-bearing migmatites from Kelly's Mountain, Nove Scotia. *Contributions to Mineralogy and Petrology*, **86**, 309-320.

JAYASINGHE, N.R. 1976. *Geology of the Wesleyville area, Newfoundland.* M.Sc Thesis, Memorial University of Newfoundland, St. Johns.

— 1978. *Geology of the Wesleyville (2F/4) and the Musgrave Harbour east (2F/5) map areas, Newfoundland*. Newfoundland Departments of Mines and Energy, Mineral Development Division, Report **78-8.**

— & BERGER, A.R. 1976. On the plutonic evolution of the Wesleyville area, Bonavista Bay, Newfoundland. *Canadian Journal of Earth Sciences*, **13**, 1560-1570.

JENNESS, S.E. 1954. *Geology of the Gander River Ultrabasic Belt, Newfoundland.* Unpublished Ph.D. thesis, Yale University, New Haven.

— 1957. *Gander Lake (east half), Newfoundland*. Geological Survey of Canada, Map **5-1957**.

— 1958. *Geology of the Gander River Ultrabasic Belt, Newfoundland*, Geological Survey of Newfoundland, Report **11**.

— 1963. *Terra Nova and Bonavista map areas, Newfoundland*. Geological Survey of Canada, Memoir, **327**.

JOHANNES, W. 1983. On the origin of stromatic (layered) migmatites. *In:* ATHERTON, M. P. & GRIBBLE, C.D. (EDS), *Migmatites, melting and metamorphism*, Shiva, Nantwich, 234-248.

— 1988. What controls partial melting in migmatites? *Journal of Metamorphic Geology*, **6**, 451-465.

— & GUPTA, L.N., 1982. Origin and evolution of a migmatite. *Contributions to Mineralogy and Petrology*, **79**, 114-123.

JONES, K.A. 1988. The metamorphic petrology of the Southern Brittany Migmatite Belt, France. *PhD thesis*, Kingston Polytechnic, U.K.

— 1994. Progressive metamorphism in crustal-scale shear zone: an example form the Leon region, north-west Brittany, France. *Journal of Metamorphic Geology*, **12**, 69-88.

—, & BROWN, M. 1990. High temperature 'clockwise' P-T paths and melting in the development of regional migmatites: An example from Southern Brittany, France. Journal of Metamorphic *Geology*, **8**, 551-578.

KARLSTROM, K.E., MILLER, C.F., KINGSBURY, J.A. & WOODEN, J.L. 1993. Pluton emplacement along an active ductile thrust zone, Piute Mountains, southeast California: Interaction between deformational and solidification processes. *Bulletin of the Geological Society of America*, **105**, 213-230.

KEEN, C.E., KEEN, M.J., NICHOLS, B., REID, I., STOCKMAL, G.S., COLMAN-SADD, S.P., O'BRIEN, S.J., MILLER, H., QUINLAN, G., WILLIAMS, H. AND WRIGHT, J.A. 1986. Deep seismic reflection profile across the northern Appalachians. *Geology*, **14**, 141-145.

KENNEDY M.J. & McGONICAL M.H. 1972. The Gander Lake and Davidsville groups of northeastern Newfoundland: new data and geotectonic implications. *Canadian Journal of Earth Sciences*, **9**, 452-459.

KERR, A., DICKSON, W.L., HAYES, J.P. AND FRYER, B.J. 1993. Devonian postorogenic granites on the southeastern margin of the Newfoundland Appalachians: a review of geology, geochemistry, petrogenesis and mineral potential. *In: Current Research*, Newfoundland Department of Mines and Energy, Report **93-1**, 239-278.

—, JENNER, G.A. & FRYER, B.J. 1994. Sm-Nd isotopic geochemistry of Precambrian to Paleozoic granitoid suites and the deep-crustal structure of the southeast margin of the Newfoundland Appalachians. *Canadian Journal of Earth Sciences*, **32, 2**, 224-245.

KERRICK, D.M. 1990. The Al_2SiO_5 polymorphs. *Reviews in Mineralogy*, **22**, 406.

— & WOODSWORTH,G.J. 1989. Aluminium silicates in the Mount Raleigh pendant, British Columbia. *Journal of Metamorphic Geology*, **7**, 547-563.

KONTAK, D.J., TUACH, J., STRONG, D.F., ARCHIBALD, D.A. & FARRAR, E. 1988. Plutonic and hydrothermal events in the Ackley Granite, southeast Newfoundland, as indicated by total-fusion 40Ar/39Ar geochronology. *Canadian Journal of Earth Sciences*, **25**, 1151-1160.

LAIRD, J. 1988. Chlorites: Metamorphic petrology. *Reviews in Mineralogy*, **19**, 405-454.

— & ALBEE, A.L. 1981. High pressure metamorphism in mafic schist from northern Vermont. *American Journal of Science*, **281**, 97-126.

LAW, R.D. 1986. Relationships between strain and quartz crystallographic fabrics in the Roche Naurice Quartzites of Plougastel, western Brittany. *Journal of Structural Geology*, **8-5**, 493-515.

LEAKE, B.E. 1978. Nomenclature of amphiboles. *Mineralogical Magazine*, **42**, 533-563.

LIN, S. 1992. The stratigraphy and structural geology of the southeastern Cape Breton Highland National Park and its implications for the tectonic evolution of Cape Breton Island, Nova Scotia, with emphasis on lineations in shear zones. *PhD thesis*, Fredericton, University of New Brunswick.

—, VAN STAAL, C.R. & DUBE, B. 1994. Promontory - promontory collision in the Canadian Appalachians. *Geology*, **22**, 897-900.

LOOSEVELD, R.J.H. 1989. The synchronism of crustal thickening and low pressure facies metamorphism in the Mount Isa Inlier, Australia. Part II: fast convective thinning of mantle lithosphere during crustal thickening. *Tectonophysics*, **165**, 191-218.

— & ETHERIDGE, M.A. 1990. A model for low-pressure facies metamorphism during crustal thickening. *Journal of Metamorphic Geology*, **8**, 257-267.

LUX, D.R., DE YOREO, J.J., GUILDOTTI, C.V. & DECKER, E.R. 1986. Role of plutonism in low-pressure metamorphic belt formation. *Nature*, **323**, 794-797.

MAALØE, S. 1982. Geochemical aspects of permeability controlled partial melting and fractional crystallisation. *Geochim. Cosmochim. Acta*, **46**, 43-57.

MARILLIER, F., KEEN, C.E., STOCKMAL, G., QUINLAN, G., WILLIAMS, H., COLMAN-SADD, S.P., & O'BRIEN, S.J. 1989. Crustal structure and surface zonation of the Canadian Appalachians: Implications of deep seismic reflection data. *Canadian Journal of Earth Sciences*, **26**, 305-321.

MARUYAMA, S., SUZUKI, K. & LIOU, J.G. 1983. Greenschist-amphibole transition equilibria at low pressures. *Journal of Petrology*, **24-4**, 583-614.

Mc GONIGAL, M.H. 1973. *The Gander and Davidsville Groups: Major tectono-stratigraphic units in the Gander Lake area, Newfoundland*. Msc Thesis, Memorial University of Newfoundland St John's.

MC LENNAN, E.L. 1988. Migmatite structures in the Central Gneiss Complex, Boca de Quandra, Alaska, *Journal of Metamorphic Geology*, **6**, 517-542.

— 1989. Melt segregation in migmatite complexes. *28th International Geological Congress*, Washington D.C., USA, Abstracts, **2**: 402-403.

MEHNERT, K.R. 1968. Migmatites and the origin of granitic rocks. *Elsevier, Amsterdam*, 395.

MENGEL, F. & RIVERS, T. 1991. Decompression reactions and P-T conditions in high-grade rocks, Northern Labrador: P-T-t paths from individual samples and implications for early Proterozoic tectonic evolution. *Journal of Petrology*, **32**, 139-167.

MILLER, C. F & MC LELLAN, E.L. 1986. Textural controls on the viscosity and critical melt percentage (RCMP) of partially molten mushes: A model for melt filter-pressing in layered migmatites. *Geology Society of America, Annual Meeting*, San Antonio, Texas, Abstracts with programs, **18**, 696.

—, WATSON, E.B. & HARRISON, T.M. 1988. Perspectives on the source, segregation and transport of of granitoid magmas. *Transactions of the Royal Society of Edimburgh, Earth Science*: **79**, 135-156.

MILLER, H.G. 1988. Geophysical interpretation of the geology of the northeast Gander Terrane, Newfoundland. *Canadian Journal of Earth Sciences*, **25**, 1161-1174.

MIYASHIRO, A. 1961. Metamorphism and metamorphic belts. *Journal of Petrology*, **2**, 277-311.

—, 1973. Paired and unpaired metamorphic belts. *Tectonophysics*, **17**, 241-254.

MORAND, V.J. 1990. Low-pressure regional metamorphism in the Omeo metamorphic Complex, Victoria, Australia. 1990. *Journal of Metamorphic Geology*, **8**, 1-12.

MURRAY, A. & HOWLEY, J.P. 1881. *Reports of the Geological Survey of Newfoundland for 1866-1880*. London Edward Standford.

NEUMAN, R.B. & MAX, M.D., 1989. Penobscottain-Grampian-Finnmarkian orogenies as indicators of terrane linkages. *In.* DALLMEYER, R.D., (ED.), *Terranes in the circum-Atlantic Palaeozoic orogens*: Geological Society of America, Special Paper **230**, 31-45.

O'BRIEN, B.H., O'BRIEN, S.J., & DUNNING, G.R. 1991. Silurian cover, Late Precambrian-Early Ordovician basement and the chronology of Silurian Orogenesis In the Hermitage Flexure (Newfoundland Applachians). *American Journal of Science*, **291**, 760-799.

O'BRIEN S. J. & HOLDSWORTH, R.E. 1992. Geological Development of the Avalon Zone, the easternmost Gander Zone, and the ductile Dover Fault in the Glovertown (NTS 2D/9, east half) map area, eastern Newfoundland. *In: Current Research.* Newfoundland Department of Mines Mineral Development Division. Report, **92-1**, 171-184.

—, WARDLE, R.J. & KING, A.F. 1983. The Avalon Zone: A Pan-African terrane in the Appalachian Orogen of Canada. *Geological Journal*, **18**, 195-222.

—, O'BRIEN, B.H., O'DRISCOLL, C.F. DUNNING, G.R. HOLDSWORTH, R.E. & TUCKER, R. 1991. Silurian orogenesis and the northwest limit of the Avalonian rocks on the Hermitage Flexure, Newfoundland Appalachians. *Geological Society of America, Northeast-Southeast Combined Annual Meeting, Abstracts with Programs*, **23**, 109.

O'BRIEN, F.H.C. & SZYBINSKI, Z.A., 1989. Conodont faunas from the Catchers Pond and Cutwell groups, Central Newfoundland. *In. Current Research*: Newfoundland Department of Mines, Geological Survey of Newfoundland Report **89-1**, 121-125.

OLSEN, S.N. 1985. Mass balance in migmatites. *In*: ASHWORTH, J. R. (ED), *Migmatites*. Blackie & Son, Glasgow, U.K., 145-179.

O'NEILL, P.P. 1991. *Geology of the Weir's Pond area, Newfoundland (NTS 2E/1).* Newfoundland Department of Mines and Energy, Geological Survey Branch, Report **91-3**.

— & KNIGHT, I. 1988. Geology of the east half of the Weir's Pond (2E/1) map area and its regional significance. *In: Current Research.* Newfoundland Department of Mines Mineral Development Division. Report **88-1**, 165-176.

— & BLACKWOOD, R.F. 1989. A proposal for revised stratigraphic nomenclature of the Gander River and Davidsville Groups and the Gander River Ultrabasic Belt, of northeastern Newfoundland. *In: Current Research.* Newfoundland Department of Mines, Geological Survey of Newfoundland, Report **89-1**, 127-130.

— & LUX, D.R. 1989. Tectonothermal history and $^{40}Ar/^{39}Ar$ geochronology of the northeastern Gander Zone, Weirs Pond area (2E1). *In Current Research.* Newfoundland Department of Mines, Report **89-1**, 131-139.

— & COLMAN-SADD, S.P. 1993. *Geology of the eastern part of the Gander (NTS 2D/15) and weasern part of the Gambo (NTS 2D/16) map areas, Newfoundland.* Newfoundland Department of Mines and Energy, Geological Survey Branch, Report **93-2**.

OXBURUGH, E.R. & TURCOTTE, D.L. 1974. Thermal gradients and regional metamorphism in overthrust terrains with special reference to the Eastern Alps. *Schweiz. Mineral. Petrogr. Mitt.*, **54**, 641-622.

— & ENGLAND, P.C. 1980. Heat flow and the metamorphic evolution of the eastern Alps. *Eclogae Geol. Helv.*, **73**, 379-398.

PAJARI, G.E., PICKERILL, R.K. & CURRIE, K.L. 1979. The nature, origin and significance of the Carmanville Melange, northeast Newfoundland. *Canadian Journal of Earth Sciences*, **16**, 1439-1451.

PASSCHIER, C.W.& SIMPSON, C. 1986. Porphyroclast systems as kinematic indicators. *Journal of Structural Geology*, **8**, 831-844.

— & TROUW, R.A.J. 1996. Micro-tectonics. *Springer-Verlag, Berlin.*

—, ZWART, H.J., & VISSERS, R.L.M. 1992. Porphyroblast rotation: Eppur si muove? *Journal of Metamorphic Geology*, **10**, 283-294.

PATTISON, D.R.M. 1989. P-T conditions and the influence of graphite on pelitic phase relations in the Ballachulish aureole, Scotland. *Journal of Petrology*, **30**, 5, 1219-1244.

— & HARTE, B. 1985. A petrogenetic grid for pelites in the Ballachulish and other Scottish thermal aureoles. *Journal of the Geological Society*, London, **142**, 7-28.

PATERSON, S.R., VERNON, R.H. & TOBISCH, O.T. 1989. A review of criteria for the identification of magmatic and tectonic foliations in granitoids. *Journal of Structural Geology*, **11**, 349-363.

—, VERNON, R.H. & TOBISCH, O.T. 1989. A review of criteria for the identification of magmatic and tectonic foliations in granitoids. *Journal of Structural Geology*, **11**, 349-363.

PERCHUK, L.L. & LAVRENT'EVA, I.V. 1983. Experimental investigation of exchange equilibria in the system cordierite-biotite-garnet. *In*: SAXENA, S.K. (ED,) Kinetics and Equilibrium of Mineral Reactions, Advances in Physical Geochemistry, **3**, 199-239. Springer Verlag, New York.

PEREIRA, M. D. & BEA, F. 1994. Cordierite-producing reactions in the Pena Negra Complex, Avila batholith, central Spain: The key role of cordierite in low-pressure anatexis. *Canadian Mineralogist*, **32**, 763-780.

PIASECKI, M.A.J. 1988. A major ductile shear zone in the Bay D'Espoir area, Gander Terrane, southeastern Newfoundland. *In Current Research*. Newfoundland Department of Mines, Mineral Development Division, **Report 88-1**, 135-144.

— , WILLIAMS, H. & COLMAN-SADD, S.P. 1990. Tectonic relationships along the Meelpaeg, Burgeo and Burlington lithoprobe transects in Newfoundland. Newfoundland Department of Mines and Energy, Geological Survey Branch, **Report 90-1**, 327-339.

PLYUSNINA, L.P. 1982. Geothermometry and geobarometry of plagioclase-hornblende- bearing assemblages. *Contributions to Mineralogy and Petrology*, **80**, 140-146.

POWELL, R. & HOLLAND, T. 1990. Calculated mineralequilibra in the pelitic system, KFMASH (K_2O-FeO-MgO-Al_2O_3-SiO_2-H_2O). *American Mineralogist*, **75**, 367-380.

QUINLAN, G.M., HALL, J., WILLIAMS, H., WRIGHT, J., COLMAN-SADD, S., O'BRIEN, S.J., STOCKMAL, G. AND MARILLIER, F. 1992. Onshore seismic reflection transects across the Newfoundland Appalachians. *Canadian Journal of Earth Sciences*, **29**, 1865-1877.

RAMSEY, J.G. 1967. Folding and fracturing of rocks. McGraw-Hill, New York.

REINHARDT, J. 1992. Low-pressure, high-temperature metamorphism in a compressional tectonic setting: Mary Kathleen Fold Belt, northeastern Australia. *Geological Magazine*, **129**, 41-57.

— & RUBENACH, M.J. 1989. Temperature-time relationships across metamorphic zones: evidence from porphyroblast-matrix relationships in progressively deformed metapelites. *Tectonophysics*, **158**, 141-161.

RICHARDSON, S.W., GILBERT, M.C. & BELL, P.M. 1969. Experimental determination of kyanite-andalusite and andalusite-sillimanite equilibrium; thealuminium triple point. *American Journal of Science*, **267**, 259-272.

ROTHSTEIN, D.A. & HOISCH, T. D. 1994. Multiple intrusions and low-pressure metamorphism in the central Old Woman Mountains, southeastern California: constraints from thermal modelling. *Journal of Metamorphic Geology*, **12**, 723-734.

RUBENACH, M.J. 1992. Proterozoic low-pressure/high temperature metamorphism and an anticlockwise P-T-t path for the Hazeldene area, Mount Isa Inlier, Queensland, Australia. *Journal of Metamorphic Geology*, **10**, 333-346.

RUSHMER, 1991. Experimental deformation of paryially molten amphibolite at 8 and 12 kbars confining pressure. *Eos, Trans. Am. Geophys. Union*, **72**: 449.

— 1992. The chemical and rheological changes in amphibolite during partial melting: Experimental results between 8 and 12 kbar. *Terra Abstracts*, Abstract supplement to Terra Nova, **4**:40.

SALJE, E. 1986. Heat capacities and entropies of andalusite and sillimanite: The influence of fibrolitisation on the phase diagram of the Al_2SiO_5 polymorphs. *American Mineralogist*, **71**, 1366-1371.

SANDIFORD, M. & POWELL, R. 1986. Deep crustal metamorphism during continental extension:modern and ancient examples. *Earth and Planetary Science Letters*, **79**, 151-158.

SAWYER, E.W. 1991. Disequilibrium melting and the rate of melt-residiuum separation during migmatisation of mafic rocks from the Grenville Front Quebec. *Journal of Petrology*, **32**, 701-738.

— 1996. Melt segregation and magma flow in migmatites: Implications for the generation of granite magmas. *Transactions of the Royal Society of Edinburgh: Earth Sciences*, **87**,

SCHOFIELD, D., D'LEMOS, R., & KING, T. 1996. Evidence and implications for the syn-tectonic emplacement of the Cape Freels Granite: A Silurian pluton emplaced into the Gander Lake Subzone, northeast Newfoundland. *Current Research, Newfoundland Department of Natural Resources, Geological Survey,* Report **96-1**, 329-342.

SEDERHOLM, J.J. 1907. On granite and gneiss. *Bull. Comm. Geol. Finland*, **23**: 1-110.

SELVERSTONE, J. 1985. Petrologic constraint on imbrication, metamorphism and uplift in the SW Tauern Window, eastern Alps. *Tectonics*, **4**, 687-704.

SIMPSON, C. A. 1985. Deformation of granitic rocks across the brittle-ductile transition. *Journal of Structural Geology*, **7**, 503-511.

— 1990. Microstructural evidence for Northeastward movement on the Chocolate Mountains Fault Zone, Southeastern California. *Journal of Geophysical Research*, **95**, B1, 529-537.

SOPER, N.J.& BARBER, 1982. A model for the deep structure of the Moine Thrust Zone. *Journal of the Geology Society, London*, **139**, 127-138.

—, WEBB, B.C. & WOODCOCK, N.H. 1987. Late Caledonide (Acadian) transpression in northwest England: timing, geometry and geotectonic significance. *Proceedings of the Yorkshire Geological Society*, **46**, 175-192.

—, STRACHAN, R.A., HOLDSWORTH, R.E., GAYER, R.A. & GREILING, R.O. 1992. Sinistral transpression and the Silurian closure of Iapetus. *Journal of the Geological Society*, London, **149**, 871-880.

SPEAR, F.S. 1980. NaSi⇔CaAl exchange equilibrium between plagioclase and amphibole. An empirical model. *Contributions to Mineralogy and Petrology*, **72**, 33-41.

— 1990. Metamorphic consequences of thrust emplacement, Fall Mountain, New Hampshire. *Geological Society of America Bulletin*, **102**, 1344-1360.

— 1993. Metamorphic phase equilibria and pressure-temperature-time paths. *Mineralogical Society of America, New York.*

STEELE, D.A. & PRICE, R.C. 1985. Magmatic suites in northeastern Victoria: implications for magmatic evolution and source rocks. *In: Abstracts Victorian Lithosphere Symposium*, ed. Vandenberg, A.H.M., 22-23, Melbourne.

STEVENS, R.D., DELABIO, R.N. & LACHANCE, G.R. 1982. Age determinations and geological studies: K-Ar isotopic ages, Report 15, *Geological Survey of Canada*, **81-2**, 1-56.

STOCKMAL, G.S, BEAUMONT,C., BOUILLIER, R. 1986. Geodynamic models of convergence of conservative margin tectonics: transition from rifted margins to overthrust belt and consequences for foreland basin development. *American Association of Petroleum Geologists*, **70**, 181-190.

STOCKMAL, G.S., COLMAN-SADD, S.P., KEEN, C.E., MARILLIER, F., O'BRIEN, S.J., & QUINLAN, G.M. 1990. Deep seismic structure and plate tectonic evolution of the Canadian Appalachians. *Tectonics*, **9**, 45-62.

STRONG, D.F., DICKSON, W.L., O'DRISCOLL, C.F., KEEN, B.F. 1974. Geochemistry of eastern Newfoundland granitoid rocks. *Newfoundland Department of Mines and Energy*, Mineral Development Division, **Report 74-3**.

TCHALENKO, J.S. 1970. Similarities between shear zones of different magnitudes. *Geological Society of America Bulletin*, **81**, 1625-1640.

THOMPSON, A.B. 1976. Mineral Reactions in pelitic rocks: I Prediction of P-T-X (Fe-Mg) phase relations. *American Journal of Earth Science*, **276**, 401-424.

— 1989. Moderate overthickening of thinned sialic crust and the origin of granitic magmatism in low-p, high T-terranes. *Geology*, **17**, 520-530.

— & ALGOR, J.R. 1977. Model systems for anatexis of pelitic rocks 1. Theory of melting reactions in the system $KAlQ_2$-Al_2O_3-Si-H_2O. *Contributions to Mineralogy and Petrology*, **63**, 247-269.

— & ENGLAND, P.C. 1984. Pressure-temperatue-time paths of regional metamorphism II. Their inference and interpretation using mineral assemblages in metamorphic rocks. *Journal of Petrology*, **25**, 4, 929-955.

TRACEY, R.J. & DIETSCH, C.W. 1982. High-temperature reactions in pelitic gneiss, Central Massachusetts. *Canadian Mineralogist*, **20**, 425-437.

TRIBE, I.R. 1994. Deformation of granitoid rocks, Channel Islands, UK: implications for the structural evolution of a late Precambrian arc. *PhD thesis, Oxford Brookes University.*

— & D' LEMOS, 1996. Significance of hiatus in down-temperature fabric development within syn-tectonic quartz diorite complexes, Channel Islands, U.K. Journal of the Geological Society of London, 153, 127-138.

TUACH, J. 1987. The high-silica magmatic / metallogenic system and associated post-tectonic granites, southeast Newfoundland. *PhD thesis, Memorial University of Newfoundland, St. Johns.*

TULLIS, J. & YUND, R.A. 1987. Dynamic recrystallization of feldspar: A mechanism for ductile shear zone formation. *Geology*, **13**, 238-241.

TWENHOFEL, W.H. 1947. The Silurian of eastern Newfoundland with some data relating to physiogeography and Wisconin glaciation of newfoundland. *American Journal of Earth Science*, **245**, 65-122.

UZUAKPUNWA, A.B. 1973. Structural studies of the Gander and Davidsville groups in the Carmanville Ladle Cove areas, Newfoundland. *MSc thesis, Memorial University of Newfoundland, St. Johns.*

VAN DER PLUIJM, B.A. & VAN STAAL, C. R. 1988. Characteristics of the Central Mobile Belt, Canadian Appalachians. Journal of Geology, **96**, 535-547.

—, JOHNSON, R.J.E., & VAN DE VOO, R. 1990. Early Paleo-geography and accretionary history of Newfoundland Appalachians. *Geology*, **18**, 898-901.

VAN STAAL, C.R. 1994. The Brunswick Subduction Complex in the Canadian Appalachians: Record of the late Ordovician to late Silurian collision between Laurentia and the Gander margin of Avalon. *Tectonics*, **13**, 946-962.

— & FYFFE, L.R., 1991. Dunnage and Gander Zones, New Brunswick Canadian Appalachian region: *New Brunswick Department of Natural Resources and Energy*, Mineral Resources, Geoscience report **91-2**.

— & DE ROO, J.A. 1995. Mid-Paleozoic tectonic evolution of the Appalachian Central Mobile Belt in Northern New Brunswick, Canada: Extensional collapse and dextral transpression. *In.* HIBBARD, J.P., VAN STALL, C.R. & CAWOOD, P.A., EDS., *Current Perspectives in the Appalachian-Caledonian Orogen*: Geological Association of Canada, Special Paper **41**, 367-389.

—, SULLIVAN, R.W., & WHALEN, J.B. 1996. Provenance and tectonic history of the Gander Zone in the Caledonian/Appalachian orogen: Implications for the origin and assembly of Avalon. *Geological Society of America*, Special Paper **304**.

VAN STAAL, C.R., RAVENHURST, C. WINCHESTER, J.A., RODDICK, J.C. & LANGTON, J.P. 1990. Post Taconic blueschist suture in the northern Appalachians of New Brunswick, Canada, *Geology*, **18**, 1073-1077.

VERNON, R.H. 1978. Pseudomorphous replacement of cordierite by symplectic intergrowths of andalusite, biotite and quartz. *Lithos*, **11**, 283-298.

— 1986. Orientated growth of sillimanite in andalusite, Placitas - Juan Tabo area, New Mexico, U.S.A. *Canadian Journal of Earth Sciences*, **24**, 580-590.

— 1987. Growth of fibrous sillimanite related to heterogeneous deformation in K.feldspar-sillimanite metapelites. *Journal of metamorphic geology*, **5**, 51-68.

— & COLLINS, W.J. 1988. Igneous microstructures in migmatites, *Geology*, **16**, 1126-1129.

—, — & FOSTER. 1993. Growth and deformation of porphyroblasts in the Foothills terrane, central Sierra Nevada, California: negotiating a microstructural minefield. *Journal of Metamorphic Geology*, **11**, 203-222.

VOLL, G. 1976. Recrystallisation of quartz, biotite and feldspars from Erstfeld to the Leventina Nappe, Swiss Alps, and its geological significance. *Schweizerische Mineralogische Und Petrographische Mitteilungen*, **56**, 641-647.

WALDRON, J.F. W. & STOCKMAL, G.S. 1991. Mid-Paleozoic thrusting at the Appalachian deformation front: Port au Port Penninsula, western Newfoundland. *Canadian Journal of Earth Sciences*, **28**, 1992-2002.

WICKHAM, S.M. & OXBURGH, E.R. 1985. Continental rifts as a setting for regional metamorphism. *Nature*, **318**, 330-333.

WILLIAMS, H. 1964. The Appalachians in northeastern Newfoundland: A two-sided symetrical system. *American Journal of Science*, **262**, 1137-1158.

— 1968. Wesleyville map-area. *Geological Survey of Canada*, Map 1227A.

— 1979. Appalachian orogen in Canada. *Canadian Journal of Earth Sciences*, **16**, 792-807.

— 1984. Miogeoclines and suspect terranes of the Caledonian-Appalachian Orogen: tectonic patterns in the North Atlantic region. *Canadian Journal of Earth Sciences*, **21**, 887-901.

— 1993. Acadian Orogent in Newfoundland. *In:* ROY, D.C. & SKEHAN, J.W., EDS., *The Acadian Orogeny*: Recent studies in New England, Maritime Canada and the autochthonous foreland. Geological Society of America, Special Paper **274**, 123-133.

— & STEVENS, R.K. 1974. The ancient continental margin of eastern North America. *In*: BURK, A.C. AND DRAKE, C.L. (EDS) *The Geology of Continental Margins*. Springer Verlag, New York, 781-796.

— & HATCHER, R.D. JNR. 1983. Appalachian suspect terranes. In: HATCHER, R.D. JNR., WILLIAMS, H. & ZEITZ, I. (EDS). *Contributons to the Tectonics and Geophysics of Mountain Chains*. Memoirs of the Geological Survey of America, **158**, 33-53.

—, COLMAN-SADD, S.P., & SWINDEN, H.S. 1988. Tectonic-stratigraphic subdivisions of central Newfoundland. *Current Research, Part B, Geological Survey of Canada*, Paper **88-1B**, 91-98.

WILLIAMS, M.L. 1994. Sigmoidal inclusion trails, punctuated fabric development and interactions between metamorphism and deformation. *Journal of Metamorphic Geology*, 1994, **12**, 1-21.

WINTSCH, R.P & ANDREWS, M.S. 1988. Deformation induced growth of sillimanite: 'stress' minerals revisited. *Journal of Geology*, **96**, 143-161.

WONDERLEY, P.F. & NEUMAN, R.B. 1984. The Indian Bay Formation: fossiliferous Early Ordovician volcanogenic rocks in the northern Gander Terrane, Newfoundland and their regional significance. *Canadian Journal of Earth Sciences*, **21**, 525-532.

YODER H.S. & TILLEY, C.E. 1962. Origin of basalt magmas: an experimental study of natural and synthetic rock systems. *Journal of Petrology*, **3**, 342-352.

YOUNCE, G.B. 1970. *Structuural geology and stratigraphy of the Bonavista Bay region, Newfoundland*. PhD. Thesis, Cornell University Ithaca, New York.

Appendix A.

Full results of mineral analysis.

Figure Ap1. Representative chlorite, muscovite and plagioclase analyses for metapelitic sample Tk 94 132b.

Tk 94 132b	Chlorite						Muscovite			Plagioclase						
	9	10	11	12	13	14	1	4	7	30	39	41	49	50	51	52
SiO2	28.07	27.41	26.73	26.85	34.02	32.24	45.83	46.24	46.51	69.98	68.61	69.85	69.34	68.46	68.83	68.6
TiO2	0	0.14	0	0.15	0	0.17	0.71	0.58	0.45	0	0	0	0	0	0	0
Al2O3	21.22	21.29	21.91	20.77	20.79	20.79	31.07	30.83	29.96	20.18	20.12	19.7	19.73	20.08	20.29	20.27
FeO	26.7	27.25	26.68	26.98	22.91	26.45	4.72	4.97	5.3	0	0	0	0	0	0	0
MnO	0.4	0.54	0.45	0.49	0.34	0.22	0	0	0	0	0	0	0	0	0	0
MgO	11.61	11.62	11.45	11.97	10.18	8.2	1.31	1.43	1.58	0	0	0	0	0	0	0
ZnO	0	0	0	0	0	0	0	0	0	0	0	0	0	0	0	0
CaO	0	0	0	0	0	0	0	0	0	0.11	0	0.11	0.13	0	0	0
Na2O	0	0.78	0	0.59	2.05	1.22	0.24	0	0.28	11.52	11.4	10.82	11.11	11.05	11.04	11.45
K2O	1.12	0.51	0.96	0	0.38	0.94	11.62	11.65	11.58	0	0	0.12	0	0.12	0.1	0.12
total	89.12	89.54	88.18	87.8	90.67	90.23	95.5	95.7	95.66	101.79	100.13	100.6	100.31	99.71	100.26	100.44
	Cations per 28 oxygens						*Cations per 22 oxygens*			*Cations per 32 oxygens*						
Si	5.85	5.72	5.65	5.69	6.72	6.55	6.25	6.30	6.35	11.98	11.94	12.07	12.03	11.96	11.95	11.92
Al	5.21	5.24	5.45	5.19	4.84	4.98	5.00	4.95	4.82	4.07	4.13	4.01	4.03	4.13	4.15	4.15
Ti	0.00	0.00	0.00	0.02	0.00	0.03	0.07	0.06	0.05	0.00	0.00	0.00	0.00	0.00	0.00	0.00
Fe	4.65	4.76	4.71	4.78	3.79	4.49	0.54	0.57	0.61	0.00	0.00	0.00	0.00	0.00	0.00	0.00
Mn	0.07	0.10	0.08	0.09	0.06	0.04	0.00	0.00	0.00	0.00	0.00	0.00	0.00	0.00	0.00	0.00
Mg	3.61	3.62	3.60	3.78	3.00	2.48	0.27	0.29	0.32	0.00	0.00	0.00	0.00	0.00	0.00	0.00
Zn	0.00	0.00	0.00	0.00	0.00	0.00	0.00	0.00	0.00	0.00	0.00	0.00	0.00	0.00	0.00	0.00
Ca	0.00	0.00	0.00	0.00	0.00	0.00	0.00	0.00	0.00	0.02	0.00	0.02	0.02	0.00	0.00	0.00
Na	0.00	0.32	0.00	0.24	0.79	0.48	0.06	0.00	0.07	3.82	3.85	3.62	3.74	3.74	3.72	3.86
K	0.30	0.14	0.26	0.00	0.10	0.24	2.02	2.02	2.02	0.00	0.00	0.03	0.00	0.03	0.02	0.03
A	0.21	0.22	0.22	0.23	0.25	0.23										
F	0.56	0.57	0.57	0.56	0.56	0.64										
XAn										0.01	0.00	0.01	0.01	0.00	0.00	0.00
XAb										0.99	1.00	0.99	0.99	0.99	0.99	0.99
XAl	0.39	0.38	0.40	0.38	0.42	0.42										
XMg	0.44	0.43	0.43	0.44	0.44	0.36										

Figure Ap 2. Analyses of Chlorite, muscovite and plagioclase for metapelitic sample Tk 94 135b.

Tk 94 135b	Chlorite								Muscovite				Plagioclase				
	13	24	25	26	27	28	29	30	2	9	10	12	18	19	21	22	23
SiO2	23.72	23.38	23.39	24.09	23.61	23.22	23.59	23.64	45.87	46.66	45.9	47.26	68.12	68.39	68.58	68.48	68.55
TiO2	0.23	0	0	0.17	0.21	0.13	0	0	0.75	0.64	0.56	0.74	0.00	0.00	0.00	0.00	0.00
Al2O3	21.48	21.64	21.72	21.44	21.11	22.03	21.4	21.38	31.24	30.66	32.09	31.73	19.74	20.07	19.97	20.23	20.09
FeO	29.79	28.84	28.67	28.41	28.44	28.8	28.7	28.4	5.12	4.73	4.05	4.69	0.19	0.00	0.23	0.17	0.00
MnO	0.19	0.56	0.66	0.48	0.51	0.5	0.58	0.46	0	0	0	0	0.00	0.00	0.00	0.00	0.00
MgO	11.91	12.06	12.18	12.67	12.44	12.34	11.72	12.55	1.68	1.61	1.64	1.45	0.00	0.00	0.00	0.00	0.00
ZnO	0	0	0	0	0	0	0	0	0	0	0	0	0.00	0.00	0.00	0.00	0.00
CaO	0	0	0	0	0	0	0	0	0	0	0	0	0.00	0.00	0.00	0.00	0.00
Na2O	0	0	0	0	0	0	0	0	0.3	0.35	0	0	11.12	11.30	10.94	11.13	11.37
K2O	0.13	0	0	0	0	0	0	0	11.54	11.52	11.89	11.36	0.00	0.09	0.00	0.10	0.00
total	87.45	86.48	86.62	87.26	86.32	87.02	85.99	86.43	96.5	96.17	96.13	97.23	99.17	99.85	99.72	100.11	100.01
	Cations per 28 oxygens								*Cations per 22 oxygens*				*Cations per 32 oxygens*				
Si	5.16	5.13	5.12	5.21	5.18	5.06	5.20	5.17	6.21	6.32	6.20	6.30	11.97	11.94	11.97	11.93	11.94
Al	5.51	5.60	5.61	5.47	5.46	5.66	5.56	5.52	4.98	4.89	5.11	4.98	4.09	4.13	4.11	4.15	4.13
Ti	0.04	0.00	0.00	0.03	0.03	0.02	0.00	0.00	0.08	0.07	0.06	0.07	0.00	0.00	0.00	0.00	0.00
Fe	5.42	5.29	5.25	5.14	5.22	5.25	5.29	5.20	0.58	0.54	0.46	0.52	0.03	0.00	0.03	0.02	0.00
Mn	0.04	0.10	0.12	0.09	0.09	0.09	0.11	0.09	0.00	0.00	0.00	0.00	0.00	0.00	0.00	0.00	0.00
Mg	3.86	3.94	3.97	4.09	4.07	4.01	3.85	4.09	0.34	0.32	0.33	0.29	0.00	0.00	0.00	0.00	0.00
Zn	0.00	0.00	0.00	0.00	0.00	0.00	0.00	0.00	0.00	0.00	0.00	0.00	0.00	0.00	0.00	0.00	0.00
Ca	0.00	0.00	0.00	0.00	0.00	0.00	0.00	0.00	0.00	0.00	0.00	0.00	0.00	0.00	0.00	0.00	0.00
Na	0.00	0.00	0.00	0.00	0.00	0.00	0.00	0.00	0.08	0.09	0.00	0.00	3.79	3.83	3.70	3.76	3.84
K	0.04	0.00	0.00	0.00	0.00	0.00	0.00	0.00	1.99	1.99	2.05	1.93	0.00	0.02	0.00	0.02	0.00
XAn													0.00	0.00	0.00	0.00	0.00
XAb													1.00	0.99	1.00	0.99	1.00
A	0.23	0.23	0.23	0.23	0.23	0.23	0.23	0.23									
F	0.58	0.57	0.57	0.56	0.56	0.57	0.58	0.56									
XAl	0.37	0.38	0.38	0.37	0.37	0.38	0.38	0.37									
XMg	0.42	0.43	0.43	0.44	0.44	0.43	0.42	0.44									

Figure Ap 3. Analyses of biotite, muscovite, plagioclase, staurolite and andalusite for metapelitic sample TK 94 157b.

TK 157

	Biotite						Muscovite			Plagioclase					
anal. #	1	3	4	33	34	37	42	43	45	47	49	50	51	48	52
SiO2	34.77	34.32	34.77	34.43	34.29	34.36	44.16	44.31	43.93	60.17	59.99	60.08	59.83	59.6	59.55
TiO2	2.34	2.21	2.26	2.15	2.06	2.2	0.87	0.88	0.83	0	0	0	0	0	0
Al2O3	18.34	18.62	18.83	19.04	18.93	18.29	35.07	35.13	34.82	24.85	24.6	24.69	24.99	24.72	25.78
FeO	20.69	21.11	20.45	20.38	20.56	21.18	2.61	2.75	2.84	0.34	0.44	0.35	0.53	0.35	0.76
MnO	0.26	0.24	0	0.15	0.3	0.17	0	0	0	0	0	0	0	0	0
MgO	9.47	9.44	9.59	9.6	9.33	9.59	0.5	0.59	0.65	0	0	0	0	0	0
ZnO	0	0	0	0	0	0	0	0	0	0	0	0	0	0	0
CaO	0	0	0	0	0	0	0	0	0	5.76	5.92	5.89	6.53	6.02	5.4
Na2O	0.37	0.35	0.49	0.55	0.44	0.34	0.94	0.91	0.86	8	7.65	7.81	7.26	7.85	7.75
K2O	10.22	10.11	9.83	10.09	10.14	10.07	10.67	10.67	10.74	0	0.12	0.1	0.13	0.13	0.12
total	96.46	96.4	96.22	96.39	96.05	96.2	94.82	95.24	94.67	99.12	98.72	98.92	99.27	98.67	99.36
	Cations per 22 oxygen						*Cations per 22 oxygens*			*Cations per 32 oxygens*					
Si	5.31	5.26	5.30	5.25	5.26	5.28	5.99	5.98	5.98	10.79	10.80	10.80	10.73	10.75	10.66
Al	3.30	3.36	3.38	3.42	3.42	3.31	5.60	5.59	5.58	5.25	5.22	5.23	5.28	5.26	5.44
Ti	0.27	0.25	0.26	0.25	0.24	0.25	0.09	0.09	0.08	0.00	0.00	0.00	0.00	0.00	0.00
Fe	2.64	2.70	2.61	2.60	2.64	2.72	0.30	0.31	0.32	0.05	0.07	0.05	0.08	0.05	0.11
Mn	0.03	0.03	0.00	0.02	0.04	0.02	0.00	0.00	0.00	0.00	0.00	0.00	0.00	0.00	0.00
Mg	2.16	2.16	2.18	2.18	2.13	2.19	0.10	0.12	0.13	0.00	0.00	0.00	0.00	0.00	0.00
Zn	0.00	0.00	0.00	0.00	0.00	0.00	0.00	0.00	0.00	0.00	0.00	0.00	0.00	0.00	0.00
Ca	0.00	0.00	0.00	0.00	0.00	0.00	0.00	0.00	0.00	1.11	1.14	1.13	1.25	1.16	1.04
Na	0.11	0.10	0.14	0.16	0.13	0.10	0.25	0.24	0.23	2.78	2.67	2.72	2.52	2.75	2.69
K	1.99	1.98	1.91	1.96	1.98	1.97	1.85	1.84	1.86	0.00	0.03	0.02	0.03	0.03	0.03
XMg	0.45	0.44	0.46	0.45	0.44	0.44									
XK	0.95	0.95	0.93	0.92	0.94	0.95									
XAn										0.28	0.30	0.29	0.33	0.30	0.28
XAb										0.72	0.70	0.70	0.66	0.70	0.72

Figure Ap 3 continued.

TK 157	Staurolite					Andalusite		
	7	11	17	20	27	55	57	58
SiO2	28.63	26.46	27.14	26.91	30.12	34.55	34.22	34.28
TiO2	0.47	0.31	0.7	0.8	0.56		0.16	
Al2O3	53.91	56.19	54.73	55.24	52.32	63.25	63.49	63.46
FeO	10.64	11.94	12.18	12.33	12.05	1.27	1.21	1.5
MnO	0.69	0.58	0.57	0.59	0.77	0	0	0
MgO	0.76	1.29	1.38	1.43	1.37	0.22	0.2	0.24
ZnO	0	0	0	0	0	0	0	0
CaO	0	0	0	0	0	0	0	0
Na2O	0.33	0.33	0.29	0.25	0.533	0	0	0
K2O	1.68	0	0.09	0	0	0	0	0
total	97.11	97.1	97.08	97.55	97.723	99.29	99.28	99.48
	Cations per 24 oxygens					*Cations per 20 oxygens*		
Si	4.85	4.48	4.60	4.54	5.05	5.31	5.26	5.26
Al	10.76	11.21	10.94	10.99	10.35	11.45	11.50	11.48
Ti	0.06	0.04	0.09	0.10	0.07	0.00	0.02	0.00
Fe	1.51	1.69	1.73	1.74	1.69	0.16	0.16	0.19
Mn	0.10	0.08	0.08	0.08	0.11	0.00	0.00	0.00
Mg	0.19	0.33	0.35	0.36	0.34	0.05	0.05	0.05
Zn	0.00	0.00	0.00	0.00	0.00	0.00	0.00	0.00
Ca	0.00	0.00	0.00	0.00	0.00	0.00	0.00	0.00
Na	0.11	0.11	0.10	0.08	0.17	0.00	0.00	0.00
K	0.36	0.00	0.02	0.00	0.00	0.00	0.00	0.00

Figure Ap 4. Analyses of garnet, epidote, chlorite and plagioclase from retrogressed pelitic sample TK 158.

TK 158	Garnet						Epidote			Chlorite			Plagioclase		
anal. #	1	3	4	5	6	7	15	18	20	8	9	10	26	27	28
SiO2	35.87	35.95	36.31	36.01	36.22	35.84	37.04	36.78	36.78	31.20	30.35	30.58	59.80	58.30	57.69
TiO2	0.00	0.22	0.24	0.23	0.00	0.15	0.00	0.00	0.41	1.17	0.92	1.22	0.00	0.00	0.00
Al2O3	20.39	20.42	20.52	20.46	20.65	20.71	21.20	21.26	21.75	19.11	18.50	18.56	26.00	26.56	26.48
FeO	18.84	16.89	16.94	16.87	16.73	18.51	15.84	15.08	14.88	18.31	18.17	17.54	0.00	0.00	0.19
MnO	20.81	21.47	21.39	21.14	21.61	20.30	0.18	0.30	0.00	0.49	0.46	0.48	0.00	0.00	0.00
MgO	2.41	2.93	3.05	3.07	2.79	2.46	0.00	0.25	0.00	19.03	18.98	18.31	0.00	0.00	0.00
ZnO	0.00	0.00	0.00	0.00	0.00	0.00	0.00	0.00	0.00	0.00	0.00	0.00	0.00	0.00	0.00
CaO	2.28	3.21	3.20	3.20	2.63	2.74	24.28	23.91	24.24	0.20	0.15	0.14	6.75	7.98	7.90
Na2O	0.00	0.00	0.00	0.00	0.00	0.00	0.00	0.00	0.00	0.36	0.40	0.32	7.63	7.15	6.80
K2O	0.00	0.00	0.00	0.00	0.00	0.00	0.00	0.00	0.00	0.99	0.98	1.45	0.10	0.00	0.00
total	100.60	101.09	101.65	100.98	100.63	100.71	98.54	97.58	98.06	90.86	88.91	88.60	100.28	99.99	99.06
Cations per O			*24*					*12.5*			*28*			*32*	
Si	5.85	5.82	5.83	5.82	5.86	5.82	3.07	3.06	3.04	6.10	6.14	6.14	10.62	10.42	10.40
Al	3.92	3.90	3.88	3.90	3.94	3.96	2.07	2.09	2.12	4.40	4.41	4.39	5.44	5.60	5.63
Ti	0.00	0.00	0.03	0.03	0.00	0.02	0.00	0.00	0.03	0.17	0.00	0.18	0.00	0.00	0.00
Fe	2.57	2.29	2.27	2.28	2.27	2.51	1.10	1.05	1.03	2.99	3.07	2.94	0.00	0.00	0.03
Mn	2.87	2.95	2.91	2.89	2.96	2.79	0.01	0.02	0.00	0.08	0.08	0.08	0.00	0.00	0.00
Mg	0.59	0.71	0.73	0.74	0.67	0.60	0.00	0.03	0.00	5.54	5.72	5.47	0.00	0.00	0.00
Zn	0.00	0.00	0.00	0.00	0.00	0.00	0.00	0.00	0.00	0.00	0.00	0.00	0.00	0.00	0.00
Ca	0.40	0.56	0.55	0.55	0.46	0.48	2.15	2.13	2.15	0.04	0.03	0.03	1.28	1.53	1.53
Na	0.00	0.00	0.00	0.00	0.00	0.00	0.00	0.00	0.00	0.14	0.16	0.12	2.63	2.48	2.38
K	0.00	0.00	0.00	0.00	0.00	0.00	0.00	0.00	0.00	0.25	0.25	0.37	0.02	0.00	0.00
Xan										0.33	0.38	0.39			
Xab										0.67	0.62	0.61			
Xal															
Xmg	0.19	0.24	0.24	0.24	0.23	0.19				0.34	0.33	0.34			
Xfe	0.81	0.76	0.76	0.76	0.77	0.81									
Xgrs	0.01	0.09	0.09	0.09	0.07	0.07									
Xsps	0.45	0.45	0.45	0.45	0.47	0.44									
Xprp	0.09	0.11	0.11	0.11	0.11	0.09									
Xalm	0.40	0.35	0.35	0.35	0.36	0.39									
Ps							0.51	0.50	0.49						

Figure Ap 5. Analyses of garnet, biotite, chlorite and plagioclase from retrogressed metapelitic sample TK ON 725.

ON87725	Garnet					Biotite		Chlorite		Plagioclase	
anal. #	1(r)	3(r)	5(c)	7(c)	8(r)	1	2	19	25	23	25
SiO2	36.48	36.23	36.14	35.72	36.10	35.09	35.09	32.13	43.53	63.33	63.66
TiO2	0.23	0.21	0.27	0.15	0.19	1.93	1.93	1.72	0.53	0.11	0.00
Al2O3	20.70	20.79	20.28	20.22	20.40	17.93	17.93	17.67	32.07	22.67	22.43
FeO	31.36	31.31	31.07	30.86	31.32	21.00	21.00	21.67	2.72	0.36	0.46
MnO	8.84	9.34	9.32	9.12	9.33	0.25	0.25	0.18	0.00	0.00	0.00
MgO	2.33	2.39	2.27	2.43	2.17	9.03	9.03	9.39	1.31	0.00	0.00
ZnO	0.00	0.00	0.00	0.00	0.00	0.00	0.00	0.00	0.00	0.00	0.00
CaO	1.51	1.48	1.79	1.40	1.48	0.00	0.00	0.00	0.00	3.36	3.43
Na2O	0.00	0.00	0.00	0.00	0.00	0.40	0.40	0.44	0.90	10.59	10.67
K2O	0.00	0.00	0.00	0.00	0.00	9.88	9.88	8.46	10.48	0.07	0.07
total	101.45	101.75	101.14	99.90	100.99	95.51	95.51	91.66	91.54	100.49	100.72
Cations per O			*24*			*22*		*28*		*32*	
Si	5.90	5.84	5.87	5.87	5.87	5.41	5.41	6.61	7.84	11.19	11.23
Al	3.95	3.95	3.88	3.92	3.91	3.26	3.26	4.28	6.80	4.72	4.66
Ti	0.00	0.03	0.03	0.02	0.02	0.22	0.22	0.27	0.00	0.01	0.00
Fe	4.24	4.22	4.22	4.24	4.26	2.71	2.71	3.73	0.41	0.05	0.07
Mn	1.21	1.28	1.28	1.27	1.29	0.03	0.03	0.03	0.00	0.00	0.00
Mg	0.56	0.57	0.55	0.59	0.53	2.07	2.07	2.88	0.35	0.00	0.00
Zn	0.00	0.00	0.00	0.00	0.00	0.00	0.00	0.00	0.00	0.00	0.00
Ca	0.26	0.26	0.31	0.25	0.26	0.00	0.00	0.00	0.00	0.64	0.65
Na	0.00	0.00	0.00	0.00	0.00	0.12	0.12	0.18	0.31	3.63	3.65
K	0.00	0.00	0.00	0.00	0.00	1.94	1.94	2.22	2.41	0.02	0.02
Xan										0.15	0.15
Xab										0.85	0.85
Xal								0.39	0.90		
Xmg	0.12	0.12	0.12	0.12	0.11	0.43	0.43	0.44	0.46		
Xfe	0.88	0.88	0.88	0.88	0.89						
XK						0.94	0.94				
Xgrs	0.00	0.04	0.04	0.05	0.04						
Xsps	0.20	0.19	0.20	0.20	0.20						
Xprp	0.09	0.09	0.09	0.09	0.09						
Xalm	0.67	0.68	0.67	0.66	0.67						

Figure Ap 6. Analyses of garnet from metapelitic sample TK 95 122.

Tk 95 122 anal. #	Garnet										
	60	61	72	73	74	75	76	77	96	97	99
SiO2	35.81	36.05	35.76	36.23	35.84	36.28	36.17	36.19	35.50	35.98	35.66
TiO2	0.00	0.00	0.00	0.15	0.00	0.00	0.00	0.00	0.00	0.14	0.00
Al2O3	20.84	20.66	21.01	20.84	20.45	20.75	20.79	21.08	20.64	20.84	20.69
FeO	38.77	39.08	39.13	38.83	38.28	39.30	39.00	38.61	38.39	38.30	38.29
MnO	2.55	2.50	2.43	2.42	2.34	2.45	2.37	2.45	2.26	2.17	2.08
MgO	1.89	1.81	1.72	1.81	1.80	1.68	1.97	1.94	1.86	1.96	1.96
ZnO	0.00	0.00	0.00	0.00	0.00	0.00	0.00	0.00	0.00	0.00	0.00
CaO	2.61	2.54	2.65	2.59	2.59	2.40	2.62	2.55	2.78	2.64	2.73
Na2O	0.00	0.00	0.00	0.00	0.00	0.00	0.00	0.00	0.00	0.00	0.00
K2O	0.00	0.00	0.00	0.00	0.00	0.00	0.00	0.00	0.00	0.00	0.00
total	102.47	102.64	102.70	102.87	101.30	102.86	102.92	102.82	101.43	102.03	101.41
	Cations per 24 oxygen										
Si	5.78	5.81	5.77	5.81	5.84	5.83	5.81	5.80	5.79	5.81	5.80
Al	3.97	3.93	3.99	3.94	3.93	3.93	3.94	3.99	3.97	3.97	3.97
Ti	0.00	0.00	0.00	0.02	0.00	0.00	0.00	0.00	0.00	0.02	0.00
Fe	5.23	5.27	5.28	5.21	5.22	5.28	5.24	5.18	5.23	5.17	5.21
Mn	0.35	0.34	0.33	0.33	0.32	0.33	0.32	0.33	0.31	0.30	0.29
Mg	0.45	0.43	0.41	0.43	0.44	0.40	0.47	0.46	0.45	0.47	0.48
Zn	0.00	0.00	0.00	0.00	0.00	0.00	0.00	0.00	0.00	0.00	0.00
Ca	0.45	0.44	0.46	0.45	0.45	0.41	0.45	0.44	0.49	0.46	0.48
Na	0.00	0.00	0.00	0.00	0.00	0.00	0.00	0.00	0.00	0.00	0.00
K	0.00	0.00	0.00	0.00	0.00	0.00	0.00	0.00	0.00	0.00	0.00
Xmg	0.08	0.08	0.07	0.08	0.08	0.07	0.08	0.08	0.08	0.08	0.08
Xfe	0.92	0.92	0.93	0.92	0.92	0.93	0.92	0.92	0.92	0.92	0.92
Xgrs	0.01	0.01	0.01	0.01	0.01	0.01	0.01	0.01	0.01	0.01	0.01
Xsps	0.05	0.05	0.05	0.05	0.05	0.05	0.05	0.05	0.05	0.05	0.04
Xprp	0.07	0.07	0.06	0.07	0.07	0.06	0.07	0.07	0.07	0.07	0.07
Xalm	0.81	0.81	0.81	0.81	0.81	0.82	0.81	0.81	0.81	0.81	0.81

Figure Ap 7. Analyses of biotite from metapelitic sample TK 95 122.

Tk 95 122

	Biotite											
anal. #	57	58	64	65	66	67	68	87	89	91	92	93
SiO2	33.37	32.68	33.02	33.79	33.31	33.37	33.42	33.52	33.08	33.85	33.94	32.71
TiO2	1.78	1.77	1.67	1.87	1.81	1.80	2.01	1.92	1.55	1.84	2.01	1.72
Al2O3	18.95	18.83	18.93	18.90	18.88	18.95	18.83	19.42	19.13	19.24	19.34	19.27
FeO	26.40	26.91	26.53	25.31	26.32	25.62	26.14	25.83	26.00	25.52	25.41	26.71
MnO	0.00	0.00	0.00	0.21	0.00	0.19	0.00	0.00	0.00	0.00	0.00	0.00
MgO	6.55	6.55	6.80	6.60	6.70	6.36	6.23	6.08	6.50	6.10	6.02	6.35
ZnO	0.00	0.00	0.00	0.00	0.00	0.00	0.00	0.00	0.00	0.00	0.00	0.00
CaO	0.00	0.00	0.00	0.00	0.00	0.00	0.00	0.00	0.00	0.00	0.00	0.00
Na2O	0.33	0.00	0.28	0.00	0.00	0.00	0.00	0.00	0.00	0.00	0.45	0.00
K2O	9.28	8.90	9.21	9.72	9.41	9.78	9.52	9.70	8.81	9.78	10.00	8.68
total	96.66	95.64	96.44	96.40	96.43	96.07	96.15	96.47	95.07	96.33	97.17	95.44
	Cations per 22 oxygens											
Si	5.21	5.16	5.17	5.26	5.21	5.23	5.24	5.23	5.22	5.28	5.25	5.16
Al	3.49	3.51	3.49	3.47	3.48	3.50	3.48	3.57	3.56	3.53	3.53	3.58
Ti	0.21	0.21	0.20	0.22	0.21	0.21	0.24	0.23	0.18	0.22	0.23	0.20
Fe	3.44	3.56	3.47	3.30	3.44	3.36	3.43	3.37	3.43	3.33	3.29	3.52
Mn	0.00	0.00	0.00	0.03	0.00	0.03	0.00	0.00	0.00	0.00	0.00	0.00
Mg	1.52	1.54	1.59	1.53	1.56	1.49	1.46	1.41	1.53	1.42	1.39	1.49
Zn	0.00	0.00	0.00	0.00	0.00	0.00	0.00	0.00	0.00	0.00	0.00	0.00
Ca	0.00	0.00	0.00	0.00	0.00	0.00	0.00	0.00	0.00	0.00	0.00	0.00
Na	0.10	0.00	0.09	0.00	0.00	0.00	0.00	0.00	0.00	0.00	0.14	0.00
K	1.85	1.79	1.84	1.93	1.88	1.96	1.90	1.93	1.77	1.94	1.97	1.75
XMg	0.31	0.30	0.31	0.32	0.31	0.31	0.30	0.30	0.31	0.30	0.30	0.30
XK	0.95	1.00	0.96	1.00	1.00	1.00	1.00	1.00	1.00	1.00	0.94	1.00

Figure Ap 8. Analyses of biotite, cordierite, plagioclase and alkali feldspar from migmatitic sample TK 94 92.

TK 94 92

	Biotite					Cordierite							
anal. #	8	10	19	20	22	1	2	3	4	5	6	7	12
SiO2	34.38	34.29	34.14	34.25	34.10	46.80	47.21	46.99	46.78	47.28	47.1	46.71	46.38
TiO2	2.70	2.93	2.66	2.86	2.87	0.00	0	0	0	0	0.133	0	0
Al2O3	18.88	18.79	19.11	18.71	18.75	33.43	33.44	33.28	33.33	33.46	33.51	33.16	32.75
FeO	22.60	22.16	22.56	22.72	23.04	9.81	9.46	9.28	9.15	9.69	9.58	9.23	9.64
MnO	0.38	0.34	0.38	0.37	0.52	0.97	1	0.85	0.95	0.91	0.75	0.87	0.89
MgO	7.75	7.66	7.25	7.15	7.41	7.11	6.96	7.09	6.98	7.04	7.1	7.06	7.11
ZnO	0.00	0.00	0.00	0.00	0.00	0.00	0	0	0	0	0	0	0
CaO	0.00	0.00	0.00	0.00	0.00	0.00	0	0	0	0	0	0	0
Na2O	0.39	0.00	0.00	0.00	0.00	0.66	0.55	0.55	0.57	0.55	0.5	0.54	0.58
K2O	10.54	10.31	10.29	10.26	10.03	0.00	0	0	0	0	0	0	0
total	97.62	96.48	96.39	96.32	96.72	98.78	98.62	98.04	97.76	98.93	98.673	97.57	97.35
	Cations normalised for 22 Oxygens					*Cations normalised for 18 oxygens*							
Si	5.25	5.27	5.27	5.29	5.25	4.87	4.91	4.91	4.90	4.90	4.89	4.90	4.89
Al	3.40	3.41	3.47	3.41	3.40	4.10	4.10	4.10	4.11	4.09	4.10	4.10	4.07
Ti	0.31	0.34	0.31	0.33	0.33	0.00	0.00	0.00	0.00	0.00	0.01	0.00	0.00
Fe	2.89	2.85	2.91	2.94	2.97	0.85	0.82	0.81	0.80	0.84	0.83	0.81	0.85
Mn	0.05	0.04	0.05	0.05	0.07	0.09	0.09	0.08	0.08	0.08	0.07	0.08	0.08
Mg	1.76	1.76	1.67	1.65	1.70	1.10	1.08	1.10	1.09	1.09	1.10	1.10	1.12
Zn	0.00	0.00	0.00	0.00	0.00	0.00	0.00	0.00	0.00	0.00	0.00	0.00	0.00
Ca	0.00	0.00	0.00	0.00	0.00	0.00	0.00	0.00	0.00	0.00	0.00	0.00	0.00
Na	0.12	0.00	0.00	0.00	0.00	0.13	0.11	0.11	0.12	0.11	0.10	0.11	0.12
K	2.05	2.02	2.02	2.02	1.97	0.00	0.00	0.00	0.00	0.00	0.00	0.00	0.00
XMg	0.38	0.38	0.36	0.36	0.36	0.56	0.57	0.58	0.58	0.56	0.57	0.58	0.57
XK	0.95	1.00	1.00	1.00	1.00								
XAn													
XAb													
XOr													

Figure Ap 8 continued

TK 94 92

	Plagioclase							K-Feldspar					
anal. #	8	9	10	11	12	13	14	2	3	4	5	6	7
SiO2	62.48	62.06	62.62	62.46	62.22	61.88	60.49	64.31	64.66	64.38	64.67	64.49	64.47
TiO2	0	0	0	0	0.11	0	0	0.22	0.21	0.21	0.16	0.14	0.22
Al2O3	23.15	22.36	23.08	22.93	22.84	22.42	24.49	18.88	19.03	19.08	18.74	18.85	18.87
FeO	0	0	0	0	0	0	0	0	0	0	0	0	0
MnO	0	0	0	0	0	0	0	0	0	0	0	0	0
MgO	0	0	0	0	0	0	0	0	0	0	0	0	0
ZnO	0	0	0	0	0	0	0	0	0	0	0	0	0
CaO	0	0	0	0	0	0	0	0	0	0	0	0	0
Na2O	10.08	10.39	10.54	10.4	10.23	10.26	9.91	1.42	1.53	1.88	2.19	2.57	1.16
K2O	0.24	0.3	0.22	0.2	0.21	0.18	0.17	15.96	15.73	14.37	14.41	14.8	16.18
total	100.03	98.74	100.52	100	99.6	98.43	100.43	100.79	101.16	99.92	100.17	100.85	100.9
						Cations normalised for 32 oxygens							
Si	11.10	11.17	11.09	11.11	11.10	11.16	10.77	11.83	11.84	11.85	11.89	11.83	11.85
Al	4.85	4.74	4.82	4.81	4.80	4.77	5.14	4.10	4.11	4.14	4.06	4.08	4.09
Ti	0.00	0.00	0.00	0.00	0.01	0.00	0.00	0.03	0.03	0.03	0.02	0.02	0.03
Fe	0.00	0.00	0.00	0.00	0.00	0.00	0.00	0.00	0.00	0.00	0.00	0.00	0.00
Mn	0.00	0.00	0.00	0.00	0.00	0.00	0.00	0.00	0.00	0.00	0.00	0.00	0.00
Mg	0.00	0.00	0.00	0.00	0.00	0.00	0.00	0.00	0.00	0.00	0.00	0.00	0.00
Zn	0.00	0.00	0.00	0.00	0.00	0.00	0.00	0.00	0.00	0.00	0.00	0.00	0.00
Ca	0.78	0.70	0.77	0.76	0.76	0.71	1.02	0.00	0.00	0.00	0.00	0.00	0.00
Na	3.47	3.63	3.62	3.59	3.54	3.59	3.42	0.51	0.54	0.67	0.78	0.91	0.41
K	0.05	0.07	0.05	0.05	0.05	0.04	0.04	3.75	3.67	3.38	3.38	3.46	3.79
XMg													
XK													
XAn	0.16	0.17	0.17	0.18	0.16	0.23	0.00						
XAb	0.83	0.82	0.82	0.81	0.83	0.76	0.12						
XOr								0.88	0.87	0.83	0.81	0.79	0.90

Figure Ap 9. Analyses of cordierite and plagioclase for migmatite sample TK 94 115.

TK 94 115	Cordierite							Plagioclase				
anal. #	1	2	3	4	5	6	7	3	4	5	6	7
SiO2	48.2	48.34	48.12	47.91	47.63	47.56	47.769	60.97	60.04	60.52	60.64	60.28
TiO2	0	0	0	0	0	0	0	0	0	0.11	0.12	0.15
Al2O3	34.07	33.8	33.78	33.58	33.87	33.8	33.597	23.93	23.51	24.03	23.89	23.73
FeO	5.515	5.33	5.6	5.41	5.61	5.59	5.51	0	0	0		0
MnO	0.797	0.7	0.69	0.78	0.74	0.72	0.67	0	0	0		0
MgO	9.716	9.9	9.87	9.72	9.93	9.7	9.76	0	0	0		0
ZnO	0	0	0	0	0	0	0	0	0	0		0
CaO	0	0	0	0	0	0	0	5.22	5.33	5.2	5.09	5.19
Na2O	0	0	0	0	0	0	0.351	9.62	9.15	9.62	9.42	9.53
K2O	0	0	0	0	0	0	0	0.15	0.24	0.19	0.23	0.31
total	98.30	98.07	98.06	97.40	97.78	97.37	97.66	99.89	98.27	99.67	99.39	99.19
			cations per 18 oxygens						*cations per 32 oxygens*			
Si	4.92	4.94	4.92	4.93	4.89	4.90	4.91	10.88	10.89	10.84	10.87	10.85
Al	4.10	4.07	4.07	4.07	4.10	4.11	4.07	5.04	5.03	5.07	5.05	5.04
Ti	0.00	0.00	0.00	0.00	0.00	0.00	0.00	0.00	0.00	0.01	0.02	0.02
Fe	0.47	0.46	0.48	0.47	0.48	0.48	0.47	0.00	0.00	0.00	0.00	0.00
Mn	0.07	0.06	0.06	0.07	0.06	0.06	0.06	0.00	0.00	0.00	0.00	0.00
Mg	1.48	1.51	1.50	1.49	1.52	1.49	1.50	0.00	0.00	0.00	0.00	0.00
Zn	0.00	0.00	0.00	0.00	0.00	0.00	0.00	0.00	0.00	0.00	0.00	0.00
Ca	0.00	0.00	0.00	0.00	0.00	0.00	0.00	1.00	1.04	1.00	0.98	1.00
Na	0.00	0.00	0.00	0.00	0.00	0.00	0.07	3.33	3.22	3.34	3.28	3.33
K	0.00	0.00	0.00	0.00	0.00	0.00	0.00	0.03	0.06	0.04	0.05	0.07
XMg	0.76	0.77	0.76	0.76	0.76	0.76	0.76					
XK												
XAn								0.18	0.18	0.18	0.18	0.18
XAb								0.81	0.81	0.81	0.81	0.81
XOr												

Figure A 10. Analyses of amphibole for metabasite sample TK 94 151.

TK 94 151								
	Amphibole							
anal. #	8	9	14	23	24	25	26	30
SiO2	44.63	45.09	45.04	44.90	44.37	43.07	44.92	45.11
TiO2	1.27	1.09	1.12	1.64	1.55	1.51	1.42	1.34
Al2O3	10.17	10.69	11.11	9.00	10.24	12.32	10.75	9.95
Cr2O3	0.00	0.00	0.00	0.00	0.00	0.00	0.00	0.00
FeO	16.09	15.90	16.10	15.82	15.89	15.37	15.86	15.67
MnO	0.41	0.34	0.33	0.27	0.27	0.22	0.32	0.31
MgO	11.68	11.59	11.11	11.96	11.30	10.26	11.42	11.76
ZnO	0.00	0.00	0.00	0.00	0.00	0.00	0.00	0.00
CaO	11.67	11.72	11.91	11.86	11.91	12.84	11.95	11.81
Na2O	1.17	1.28	1.39	1.26	1.17	1.34	1.47	1.11
K2O	0.58	0.47	0.45	0.86	0.73	0.61	0.54	0.53
total	97.67	98.16	98.56	97.57	97.41	97.54	98.65	97.60
				Cation per 23 oxygens				
Si	6.49	6.51	6.48	6.53	6.47	6.27	6.45	6.56
Al - IV	1.51	1.49	1.52	1.47	1.53	1.73	1.55	1.44
Al - VI	0.23	0.33	0.37	0.07	0.24	0.38	0.27	0.27
Fe3+	1.13	1.05	1.06	1.25	1.10	1.20	1.16	0.97
Ti	0.14	0.19	0.12	0.18	0.17	0.17	0.15	0.15
Cr	0.00	0.00	0.00	0.00	0.00	0.00	0.00	0.00
Mg	2.53	2.50	2.39	2.59	2.46	2.23	2.45	2.55
Ni	0.00	0.00	0.00	0.00	0.00	0.00	0.00	0.00
Fe2+	0.83	0.87	0.78	0.68	0.84	0.67	0.75	0.93
Mn	0.05	0.04	0.04	0.03	0.03	0.03	0.04	0.04
Ca	0.09	0.10	0.25	0.21	0.16	0.33	0.19	0.09
Fe2+								
Mn								
Ca	1.72	1.72	1.59	1.64	1.70	1.67	1.65	1.75
Na	0.28	0.29	0.39	0.36	0.30	0.33	0.35	0.25
Ca								
Na	0.05	0.07			0.03	0.05	0.06	0.06
K	0.11	0.09	0.08	0.16	0.14	0.10	0.10	0.10
SUM	15.16	15.25	15.07	15.17	15.17	15.16	15.17	15.16
Mg #	0.75	0.74	0.75	0.79	0.75	0.77	0.77	0.73

Figure Ap 11. Analyses of plagioclase for metabasite sample TK 94 151.

TK 94 151

	Plagioclase								
anal. #	2	3	17	18	20	22	21	33	36
SiO2	53.60	53.14	52.83	53.90	54.70	55.73	54.58	54.58	54.97
TiO2	0.00	0.00	0.00	0.00	0.00	0.00	0.00	0.19	0.00
Al2O3	29.34	30.00	30.46	29.62	29.21	28.96	28.63	29.31	28.79
FeO	0.21	0.29	0.20	0.00	0.18	0.18	0.18	0.25	0.00
MnO	0.00	0.00	0.00	0.00	0.00	0.00	0.00	0.00	0.00
MgO	0.00	0.00	0.00	0.00	0.00	0.00	0.00	0.00	0.00
ZnO	0.00	0.00	0.00	0.00	0.00	0.00	0.00	0.00	0.00
CaO	11.34	11.67	12.33	11.07	10.84	10.34	10.58	10.58	10.39
Na2O	5.25	5.08	4.64	5.26	5.45	5.99	5.68	5.34	5.72
K2O	0.00	0.00	0.00	0.00	0.00	0.00	0.00	0.18	0.00
total	99.74	100.18	100.46	99.85	100.38	101.20	99.65	100.43	99.87
			Cations per 32 oxygens						
Si	9.72	9.61	9.53	9.74	9.83	9.92	9.88	9.81	9.91
Al	6.27	6.39	6.48	6.31	6.19	6.08	6.11	6.21	6.12
Ti	0.00	0.00	0.00	0.00	0.00	0.00	0.00	0.03	0.00
Fe	0.03	0.04	0.03	0.00	0.03	0.03	0.03	0.04	0.00
Mn	0.00	0.00	0.00	0.00	0.00	0.00	0.00	0.00	0.00
Mg	0.00	0.00	0.00	0.00	0.00	0.00	0.00	0.00	0.00
Zn	0.00	0.00	0.00	0.00	0.00	0.00	0.00	0.00	0.00
Ca	2.20	2.26	2.38	2.14	2.09	1.97	2.05	2.04	2.01
Na	1.85	1.78	1.62	1.84	1.90	2.07	1.99	1.86	2.00
K	0.00	0.00	0.00	0.00	0.00	0.00	0.00	0.04	0.00
XAn	0.54	0.56	0.59	0.54	0.52	0.49	0.51	0.52	0.50
XAb	0.46	0.44	0.41	0.46	0.48	0.51	0.49	0.48	0.50

Figure Ap 12. Analyses of amphibole for metabasite samples TK 95 226, TK 95 232 and TK 95 231.

	TK 95 226					TK 95 232						
anal. #	62	63	66	67	69	1	11	18	19	20	21	23
SiO2	44.74	44.25	44.58	44.40	44.36	44.96	43.74	45.21	45.43	46.28	44.96	45.91
TiO2	1.48	1.57	1.37	1.68	1.69	0.55	0.52	0.82	1.09	0.53	1.12	0.89
Al2O3	9.3	9.75	8.88	9.83	9.81	9.79	9.94	9.03	8.04	8.09	8.69	7.99
Cr2O3	0.00	0.00	0.00	0.00	0.00	0.00	0.00	0.00	0.00	0.00	0.00	0.00
FeO	18.38	17.59	18.43	17.37	18.13	20.17	19.62	18.83	18.92	18.81	19.49	18.42
MnO	0.3	0.26	0.36	0.25	0.27	0.29	0.39	0.43	0.31	0.33	0.33	0.42
MgO	10.5	10.66	10.35	10.76	10.90	9.28	9.18	9.82	10.34	10.62	9.79	10.74
ZnO	0.00	0.00	0.00	0.00	0.00	0.00	0.00	0.00	0.00	0.00	0.00	0.00
CaO	12.61	12.54	12.63	12.99	12.71	12.90	12.55	12.40	13.04	12.89	12.74	12.94
Na2O	1.05	1.08	1.03	1.05	1.07	1.46	1.28	1.33	1.20	1.33	1.51	1.39
K2O	0.97	1.01	0.96	1.03	1.01	0.46	0.58	0.51	0.41	0.35	0.43	0.44
Total	99.33	98.71	98.59	99.36	99.95	99.86	97.80	98.38	98.78	99.23	99.06	99.14
	cations per 23 oxygens								*cations per 23 oxygen*			
Si	6.55	6.50	6.58	6.48	6.44	6.57	6.53	6.69	6.70	6.78	6.62	6.72
Al - IV	1.45	1.50	1.42	1.52	1.56	1.43	1.47	1.31	1.30	1.22	1.38	1.28
Al - VI	0.16	0.19	0.13	0.17	0.12	0.26	0.28	0.27	0.10	0.18	0.13	0.10
Fe3+	0.74	0.76	0.75	0.77	0.86	0.85	0.86	0.63	0.66	0.67	0.81	0.75
Ti	0.16	0.17	0.15	0.18	0.18	0.06	0.06	0.09	0.12	0.06	0.12	0.10
Cr	0.00	0.00	0.00	0.00	0.00	0.00	0.00	0.00	0.00	0.00	0.00	0.00
Mg	2.29	2.33	2.28	2.34	2.36	2.02	2.04	2.17	2.28	2.32	2.15	2.34
Ni	0.00	0.00	0.00	0.00	0.00	0.00	0.00	0.00	0.00	0.00	0.00	0.00
Fe2+	1.51	1.40	1.53	1.35	1.34	1.62	1.59	1.71	1.67	1.63	1.58	1.51
Mn	0.04	0.03	0.05	0.03	0.03	0.04	0.05	0.05	0.04	0.04	0.04	0.05
Ca	0.10	0.12	0.11	0.16	0.11	0.15	0.12	0.08	0.13	0.10	0.17	0.15
Fe2+ / Mn												
Ca	1.88	1.85	1.89	1.87	1.87	1.87	1.89	1.89	1.93	1.92	1.84	1.88
Na / Ca	0.12	0.15	0.11	0.13	0.13	0.13	0.11	0.11	0.07	0.08	0.16	0.12
Na	0.18	0.16	0.19	0.17	0.17	0.28	0.26	0.27	0.27	0.3	0.27	0.28
K	0.18	0.19	0.18	0.19	0.19	0.09	0.11	0.1	0.08	0.07	0.08	0.08
XMg	0.60	0.62	0.60	0.63	0.64	0.55	0.56	0.56	0.58	0.59	0.58	0.61

Cont...	TK 95 232					TK 95 231					
	24	71	72	73	4	7	8	23	26	28	29
	44.87	44.21	46.56	43.85	43.68	44.00	43.73	43.37	43.20	43.37	42.56
	1.20	0.83	0.75	1.00	1.00	1.07	1.19	1.42	0.94	0.96	0.80
	8.66	9.71	8.33	9.94	10.40	10.94	10.66	10.98	11.44	11.13	11.71
	0.00	0.00	0.00	0.00	0.00	0.00	0.00	0.00	0.00	0.00	0.00
	19.42	19.37	18.93	19.58	16.95	16.97	16.91	18.05	17.72	17.25	17.83
	0.38	0.37	0.33	0.42	0.34	0.24	0.26	0.24	0.28	0.35	0.34
	9.76	9.89	10.67	9.66	10.92	10.88	10.93	10.51	10.51	10.54	10.21
	0.00	0.00	0.00	0.00	0.00	0.00	0.00	0.00	0.00	0.00	0.00
	12.83	12.46	13.03	12.64	12.49	12.35	12.55	12.38	12.57	12.36	12.44
	1.38	1.54	1.34	1.51	1.69	1.81	1.64	1.82	1.86	1.65	1.90
	0.44	0.52	0.42	0.54	0.38	0.41	0.41	0.42	0.35	0.43	0.45
	98.94	98.90	100.36	99.14	97.85	98.67	98.28	99.19	98.87	98.04	98.24
						cations per 23 oxygen					
	6.62	6.49	6.74	6.44	6.41	6.40	6.40	6.30	6.28	6.36	6.23
	1.38	1.51	1.26	1.56	1.59	1.60	1.60	1.70	1.72	1.64	1.77
	0.13	0.17	0.16	0.16	0.21	0.28	0.24	0.18	0.24	0.29	0.25
	0.76	0.97	0.68	1.01	1.00	0.97	0.94	1.09	1.16	0.97	1.27
	0.13	0.09	0.08	0.11	0.11	0.12	0.13	0.16	0.10	0.11	0.09
	0.00	0.00	0.00	0.00	0.00	0.00	0.00	0.00	0.00	0.00	0.00
	2.15	2.17	2.30	2.11	2.39	2.36	2.38	2.28	2.28	2.31	2.23
	0.00	0.00	0.00	0.00	0.00	0.00	0.00	0.00	0.00	0.00	0.00
	1.64	1.41	1.62	1.40	1.09	1.10	1.13	1.11	1.00	1.14	0.92
	0.05	0.05	0.04	0.05	0.04	0.03	0.03	0.03	0.03	0.04	0.04
	0.14	0.14	0.12	0.16	0.16	0.14	0.15	0.15	0.19	0.14	0.20
	1.89	1.82	1.9	1.83	1.81	1.78	1.82	1.78	1.77	1.80	1.75
	0.11	0.18	0.1	0.17	0.19	0.22	0.18	0.22	0.23	0.20	0.25
	0.29	0.26	0.28	0.26	0.29	0.29	0.29	0.29	0.29	0.27	0.29
	0.08	0.1	0.08	0.1	0.07	0.08	0.08	0.08	0.07	0.08	0.08
	0.57	0.61	0.59	0.60	0.69	0.68	0.68	0.67	0.70	0.67	0.71

Figure Ap 13. Analyses of plagioclase for metabasite samples TK 95 226, TK 95 232 and TK 95 231.

	TK 95 226				TK 95 232					
anal. #	71	75	76	77	2	3	10	27	28	29
SiO2	54.11	53.87	52.55	52.31	61.19	60.56	61.30	61.39	61.99	62.55
TiO2	0.00	0.00	0.00	0.00	0.00	0.00	0.00	0.00	0.00	0.00
Al2O3	30.37	30.59	31.50	31.47	24.69	25.37	24.64	24.49	24.52	24.20
FeO	0.21	0.30	0.36	0.49	0.30	0.41	0.29	0.50	0.51	0.37
MnO	0.00	0.00	0.00	0.00	0.00	0.00	0.00	0.00	0.00	0.00
MgO	0.00	0.00	0.00	0.00	0.00	0.00	0.00	0.00	0.00	0.00
ZnO	0.00	0.00	0.00	0.00	0.00	0.00	0.00	0.00	0.00	0.00
CaO	11.90	11.81	13.17	13.44	5.86	6.36	5.74	5.51	5.27	4.80
Na2O	5.15	5.10	4.12	4.18	8.12	7.98	8.21	8.41	8.52	8.83
K2O	0.14	0.14	0.11	0.00	0.00	0.00	0.00	0.00	0.00	0.00
Total	101.88	101.81	101.81	101.89	100.16	100.68	100.18	100.30	100.81	100.75
							cations per 32 oxygens			
Si	9.62	9.59	9.38	9.34	10.85	10.71	10.87	10.88	10.92	11.00
Al	6.37	6.42	6.63	6.63	5.16	5.29	5.15	5.12	5.09	5.02
Ti	0.00	0.00	0.00	0.00	0.00	0.00	0.00	0.00	0.00	0.00
Fe	0.03	0.04	0.05	0.07	0.04	0.06	0.04	0.07	0.08	0.05
Mn	0.00	0.00	0.00	0.00	0.00	0.00	0.00	0.00	0.00	0.00
Mg	0.00	0.00	0.00	0.00	0.00	0.00	0.00	0.00	0.00	0.00
Zn	0.00	0.00	0.00	0.00	0.00	0.00	0.00	0.00	0.00	0.00
Ca	2.27	2.25	2.52	2.57	1.11	1.21	1.09	1.05	0.99	0.90
Na	1.78	1.76	1.43	1.45	2.79	2.74	2.82	2.89	2.91	3.01
K	0.03	0.03	0.03	0.00	0.00	0.00	0.00	0.00	0.00	0.00
XAn	0.56	0.56	0.63	0.64	0.29	0.31	0.28	0.27	0.25	0.23
XAb	0.44	0.44	0.37	0.36	0.71	0.69	0.72	0.73	0.75	0.77

	TK 95 232				TK 95 231						
Cont...	31	32	78	79	16	19	20	32	35	37	38
	61.09	61.61	61.39	61.37	61.05	60.61	61.81	59.11	62.16	61.32	61.63
	0.00	0.00	0.00	0.00	0.00	0.00	0.00	0.00	0.00	0.00	0.00
	24.53	24.42	23.79	23.97	24.12	24.14	24.85	24.30	24.30	24.97	24.42
	0.47	0.36	0.37	0.38	0.52	0.46	0.33	0.29	0.18	0.25	0.00
	0.00	0.00	0.00	0.00	0.00	0.00	0.00	0.00	0.00	0.00	0.00
	0.00	0.00	0.00	0.00	0.00	0.00	0.00	0.00	0.00	0.00	0.00
	0.00	0.00	0.00	0.00	0.00	0.00	0.00	0.00	0.00	0.00	0.00
	5.46	5.30	4.89	4.95	5.50	5.62	5.47	5.78	5.00	5.70	4.96
	8.06	8.34	8.49	8.67	8.38	8.05	8.61	7.83	8.51	8.39	8.90
	0.00	0.00	0.00	0.00	0.00	0.00	0.00	0.00	0.00	0.00	0.00
	99.61	100.03	98.93	99.34	99.57	98.88	101.07	97.31	100.15	100.63	99.91
	10.88	10.92	11.00	10.96	10.90	10.89	10.86	10.80	10.99	10.83	10.93
	5.15	5.10	5.02	5.05	5.08	5.11	5.15	5.23	5.06	5.20	5.11
	0.00	0.00	0.00	0.00	0.00	0.00	0.00	0.00	0.00	0.00	0.00
	0.07	0.05	0.06	0.06	0.08	0.07	0.05	0.04	0.03	0.04	0.00
	0.00	0.00	0.00	0.00	0.00	0.00	0.00	0.00	0.00	0.00	0.00
	0.00	0.00	0.00	0.00	0.00	0.00	0.00	0.00	0.00	0.00	0.00
	0.00	0.00	0.00	0.00	0.00	0.00	0.00	0.00	0.00	0.00	0.00
	1.04	1.01	0.94	0.95	1.05	1.08	1.03	1.13	0.95	1.08	0.94
	2.78	2.87	2.95	3.00	2.90	2.80	2.93	2.77	2.92	2.87	3.06
	0.00	0.00	0.00	0.00	0.00	0.00	0.00	0.00	0.00	0.00	0.00
	0.27	0.26	0.24	0.24	0.27	0.28	0.26	0.29	0.25	0.27	0.24
	0.73	0.74	0.76	0.76	0.73	0.72	0.74	0.71	0.75	0.73	0.76

Figure Ap 14. Analyses of clinopyroxene for metabasic sample TK 95 226 and TK 95 232.

	TK 95 226						TK 95 232		
anal #.	25	26	28	29	46	47	36	38	39
SiO2	52.92	52.78	52.56	52.56	52.82	53.11	53.61	53.65	53.27
TiO2	0.00	0.20	0.21	0.23	0.24	0.00	0.29	0.19	0.19
Al2O3	1.04	1.09	1.73	1.18	1.17	1.05	0.67	0.75	0.82
FeO	10.13	10.08	10.63	10.46	9.82	9.82	10.43	9.94	10.43
MnO	0.51	0.63	0.48	0.57	0.50	0.52	0.42	0.37	0.48
MgO	12.08	11.98	12.32	12.25	12.42	12.31	12.10	12.32	11.77
CaO	23.86	24.03	23.25	23.26	23.87	23.63	23.79	24.26	24.01
Na2O	0.41	0.40	0.38	0.51	0.44	0.53	0.54	0.57	0.46
Cr2O3	0.00	0.00	0.11	0.00	0.00	0.00	0.00	0.00	0.00
Total	100.95	101.18	101.68	101.02	101.28	100.96	101.84	102.06	101.44
				cations per 6 oxygens					
Si	1.97	1.96	1.94	1.95	1.96	1.97	1.98	1.97	1.98
Al - IV	0.03	0.04	0.06	0.05	0.04	0.03	0.02	0.03	0.02
Fe3+									
Al - VI	0.02	0.01	0.05	0.01	0.01	0.02	0.01	0.01	0.01
Ti			0.01	0.01	0.01		0.01		
Fe3+	0.04	0.05	0.05	0.06	0.05	0.05	0.03	0.06	0.05
Cr3+	0.00	0.00					0.00		
Mg2+	0.67	0.66	0.68	0.68	0.69	0.68	0.67	0.68	0.65
Fe2+	0.27	0.27	0.24	0.25	0.25	0.25	0.29	0.25	0.28
Mn2+		0.01						0.01	0.01
Mg2+									
Fe2+			0.04	0.02	0.01	0.01	0.01		
Mn2+	0.02	0.01	0.02	0.02	0.02	0.02	0.03		0.01
Ca2+	0.95	0.96	0.92	0.93	0.95	0.94	0.94	0.96	0.95
Na+	0.03	0.03	0.03	0.04	0.03	0.04	0.04	0.04	0.03
XMg	0.71	0.71	0.74	0.73	0.73	0.73	0.70	0.73	0.70

Figure Ap 15. Analyses of amphibole for retrogressed metabasite sample TK 94 125.

TK 94 125	Amphibole										
anal. #	1	11	13	15	22	34	37	38	41	58	59
SiO2	44.92	48.02	43.83	44.56	43.96	48.21	51.28	50.25	49.33	45.33	45.96
TiO2	0.88	0.29	1.25	1.15	0.92	0.33	0.17	0.19	0.26	1.26	0.81
Al2O3	9.31	7.50	8.97	8.98	10.18	6.99	4.64	5.45	6.24	8.20	8.83
Cr2O3	0.00	0.00	0.00	0.00	0.00	0.00	0.00	0.00	0.00	0.14	0.00
FeO	18.43	15.90	18.24	17.74	18.02	15.61	14.07	14.81	14.57	17.70	17.16
MnO	0.33	0.35	0.38	0.39	0.46	0.44	0.46	0.40	0.37	0.35	0.36
MgO	10.50	12.15	10.37	10.51	9.99	12.24	14.24	13.33	13.13	11.29	11.29
ZnO	0.00	0.00	0.00	0.00	0.00	0.00	0.00	0.00	0.00	0.00	0.00
CaO	13.11	13.07	12.70	12.84	12.72	13.05	13.23	13.12	13.13	12.95	12.89
Na2O	1.20	0.80	0.90	1.15	1.04	0.84	0.71	0.88	0.81	1.01	0.90
K2O	0.96	0.43	1.07	1.00	1.12	0.27	0.24	0.29	0.36	0.89	0.83
Total	99.64	98.51	97.70	98.29	98.42	97.98	99.03	98.73	98.20	99.11	99.04
						Cations per 23 oxygens					
Si	6.46	6.94	6.53	6.49	6.40	7.01	7.33	7.22	7.12	6.63	6.63
Al - IV	1.54	1.06	1.47	1.51	1.60	0.99	0.67	0.78	0.88	1.37	1.37
Al - VI	0.04	0.22	0.10	0.03	0.15	0.21	0.11	0.14	0.18	0.05	0.13
Fe3+	1.51	0.77	0.84	1.42	1.43	0.69	0.45	0.59	0.62	0.77	1.15
Ti	0.09	0.03	0.14	0.13	0.10	0.04	0.02	0.02	0.03	0.14	0.09
Cr	0.00	0.00	0.00	0.00	0.00	0.00	0.00	0.00	0.00	0.02	0.00
Mg	2.25	2.62	2.30	2.28	2.17	2.65	3.03	2.85	2.82	2.46	2.43
Ni	0.00	0.00	0.00	0.00	0.00	0.00	0.00	0.00	0.00	0.00	0.00
Fe2+	0.70	1.16	1.43	0.74	0.77	1.21	1.23	1.19	1.14	1.40	0.92
Mn	0.04	0.04	0.05	0.05	0.06	0.05	0.06	0.05	0.05	0.04	0.04
Ca	0.37	0.16	0.14	0.35	0.33	0.15	0.11	0.16	0.17	0.13	0.24
Fe2+											
Mn											
Ca	1.65	1.86	1.89	1.65	1.66	1.88	1.92	1.86	1.86	1.90	1.75
Na	0.33	0.14	0.11	0.32	0.29	0.12	0.08	0.14	0.14	0.10	0.25
Ca											
Na		0.08	0.15			0.12	0.11	0.10	0.09	0.19	0.01
K		0.08	0.20			0.05	0.04	0.05	0.07	0.17	0.15
SUM	14.98	15.16	15.35	14.96	14.96	15.17	15.16	15.15	15.17	15.37	15.16
Mg #	0.76	0.69	0.62	0.75	0.74	0.69	0.71	0.71	0.71	0.64	0.73

Figure Ap 16. Analyses of plagioclase, chlorite and epidote for retrogressed metabasite sample TK 94 125.

TK 94 125	Plagioclase											Chlorite			Epidote		
anal. #	6	12a	17	19	23	29	32	33	47	63	64	10	11	16	68	69	70
SiO2	61.66	58.03	58.48	58.50	62.61	58.12	57.92	58.00	61.52	57.78	60.32	30.59	29.90	28.76	37.70	37.85	37.35
TiO2	0.00	0.00	0.00	0.00	0.00	0.00	0.00	0.00	0.00	0.00	0.00	0.90	0.67	0.23	0.20	0.19	0.00
Al2O3	23.79	26.29	25.07	24.90	24.51	27.05	27.03	27.07	24.33	26.10	24.54	15.33	14.92	16.47	25.32	25.69	25.15
FeO	0.28	0.19	0.00	0.00	0.32	0.00	0.26	0.18	0.21	0.29	0.22	23.18	23.68	21.15	10.96	10.63	10.58
MnO	0.00	0.00	0.00	0.00	0.00	0.00	0.00	0.00	0.00	0.00	0.00	0.19	0.22	0.49	0.17	0.32	0.36
MgO	0.00	0.00	0.00	0.00	0.00	0.00	0.00	0.00	0.00	0.00	0.00	14.48	15.09	16.08	0.00	0.00	0.00
ZnO	0.00	0.00	0.00	0.00	0.00	0.00	0.00	0.00	0.00	0.00	0.00	0.00	0.00	0.00	0.00	0.00	0.00
CaO	4.90	7.71	7.28	7.31	4.80	8.33	8.45	8.49	5.54	7.49	5.61	0.00	0.11	2.27	25.15	25.00	24.98
Na2O	8.79	7.20	7.19	7.46	8.92	6.91	6.94	7.05	8.29	7.14	8.06	0.00	0.00	0.00	0.00	0.00	0.00
K2O	0.00	0.00	0.00	0.11	0.00	0.00	0.09	0.00	0.10	0.00	0.00	2.99	1.81	0.00	0.00	0.00	0.00
total	99.42	99.42	98.02	98.28	101.16	100.41	100.69	100.79	99.99	98.80	98.75	87.66	86.40	85.45	99.50	99.68	98.42
				Cations per 32 oxygen									*Cations per 28 O*			*Cations per 12.5 O*	
Si	11.00	10.44	10.63	10.63	10.97	10.35	10.31	10.31	10.92	10.45	10.84	6.46	6.39	6.12	3.01	3.01	3.01
Al	5.00	5.57	5.37	5.33	5.06	5.68	5.67	5.67	5.09	5.56	5.20	3.81	3.76	4.13	2.38	2.41	2.39
Ti	0.00	0.00	0.00	0.00	0.00	0.00	0.00	0.00	0.00	0.00	0.00	0.14	0.11	0.04	0.01	0.01	0.00
Fe	0.04	0.03	0.00	0.00	0.05	0.00	0.04	0.03	0.03	0 04	0.03	4.09	4.23	3.77	0.73	0.71	0.71
Mn	0.00	0.00	0.00	0.00	0.00	0.00	0.00	0.00	0.00	0 00	0.00	0.03	0.04	0.09	0.01	0.02	0.02
Mg	0.00	0.00	0.00	0.00	0.00	0.00	0.00	0.00	0.00	0 00	0.00	4.55	4.81	5.10	0.00	0.00	0.00
Zn	0.00	0.00	0.00	0.00	0.00	0.00	0.00	0.00	0.00	0 00	0.00	0.00	0.00	0.00	0.00	0.00	0.00
Ca	0.94	1.49	1.42	1.42	0.90	1.59	1.61	1.62	1.05	1 45	1.08	0.00	0.03	0.52	2.15	2.13	2.16
Na	3.04	2.51	2.53	2.63	3.03	2.39	2.39	2.43	2.85	2 50	2.81	0.00	0.00	0.00	0.00	0.00	0.00
K	0.00	0.00	0.00	0.03	0.00	0.00	0.02	0.00	0.02	0 00	0.00	0.81	0.49	0.00	0.00	0.00	
XAn	0.24	0.37	0.36	0.35	0.23	0.40	0.40	0.40	0.27	0 37	0.28						
XAb	0.76	0.63	0.64	0.65	0.77	0.60	0.60	0.60	0.73	0.63	0.72						
Ps															0.38	0.37	0.37
XAl												0.31	0.29	0.32			
XMg												0.53	0.53	0.58			

Appendix B.

Analytical procedures.

B.1. Instrument, setup and operating conditions for microanalysis.

Backscatter and secondary electron images (BEI / SEI) were acquired using the Oxford Brookes University JEOL JSM-840 Scanning Electron Microscope. The following operating conditions were used; acelerating voltage = 20 KV, beam current = 2nA; working distance = 32mm. The SEM uses an energy dispersive x-ray detector (EDX) operated by LINK-XL software for and enables quantatative microanalysis using the ZAF4 calculation program.

B.2. Normalisation procedures and chemical parameters.

Selected representative microprobe analyses for metapelites, migmatites and metabasites from the Gander Lake Subzone are presented in Appendix A. Analyses are given both as weight percent oxide and as cations per formula unit.

Alkali feldspar and Plagioclase

Mole fractions of albite, anorthite and orthoclase were calculated using the following equations;

$$X_{An} = Ca / (Ca+Na+K)$$
$$X_{Ab} = Na / (Ca+Na+K)$$
$$X_{Or} = K / (Ca+Na+K)$$

where Ca, Na and K have been calculated on the basis of 32 oxygens.

Garnet

Mole fractions of almandine, pyrope, spessartine and grossular were calculated using the following equations on the basis of 24 oxygens;

$$X_{Alm} = Fe / (Fe + Ca + Mg + Mn)$$
$$X_{Prp} = Mg / (Fe + Ca + Mg + Mn)$$
$$X_{Sps} = Mn / (Fe + Ca + Mg + Mn)$$
$$X_{Grs} = Ca / (Fe + Ca + Mg + Mn)$$

Biotite

Biotite formula units were normalised to 22 cations and X_{Mg} and X_K values calculated using the following equations;

$$X_{Mg} = Mg / (Mg+Fe^{total})$$
$$X_K = K / K + Na$$

Muscovite

Muscovite was calculated on the basis of 22 oxygens and X_{Mg} values calculated as above.

Cordierite

Cordierite was analysed on the basis of 18 oxygens; X_{Mg} values were calculated using equation

$$X_{Mg} = Mg / (Mg+Fe^{total}).$$

Amphibole

Amphiboles were analysed on the basis of 23 oxygens and recalculated to account for the ferric iron using the Schumacher spreadsheet (comprising 8 cations in the tetrahedral sight and 5 in octahedral sites). The nomenclature and terminology used follows Leake (1978). The following calculation was made $X_{Mg} = Mg^{2+} / (Mg^{2+} + Fe^{2+})$.

Chlorite

Chlorite was analysed on the basis of 28 oxygens and the following calculations made;

$$X_{Al} = Al / (Al + Fe + Mg)$$

$$X_{Mg} = Mg / (Mg + Fe).$$

Epidote

Epidote formula units were normalised to 12.5 oxygens. Ps content was calculated using equation:

$$Ps = FeO / (FeO + Al_2O_3).$$

Clinopyroxene

Clinopyroxene was analysed on the basis of 6 oxygens per formula unit and recalculated by hand using the method described by Mormoto, 1988. The following calculations were made;

$$X_{Mg} = Mg^{2+} / (Mg^{2+} + Fe^{2+}).$$

Classification of the clinopyroxene is based on the scheme of Morimoto (1988).

B.3. Calibrations of geothermometry

The calibrations of the garnet-biotite Fe-Mg exchange thermometer applied to assemblage TK 95 122 in domain 3 are shown below:

Calibrations of Garnet-biotite Fe-Mg exchange thermometry

Ferry & Spear (1978)	$T = 2089 + 0.00956P / 0.7820 - \ln K_2$
Hodges & Spear (1982)	$T = 2089 + 0.00956P + 1661X_{Ca}^{Grt} / \ln K_3 + 0.782 + 0.755X_{Ca}^{Grt}$
Ganguly & Saxena (1984)	$T = 1175 + 0.00945P + 1 / 1.987$ (Wfe - Mg (XFe - Xmg) + 3000 (XCa = XMn))$^{Grt} / \ln K_3 + 0.782$ where WFe - Mg = 2500 (XFe / (XFe + XMg)) + 200 (XMg / (XMg + XFe))
Indares & Martignole (1985b)	$T = 12454 - 0.057P + 3(mX_{Al}^{Bt} + nX_{Ti}^{Bt}) - (\Delta WCaX_{Ca}^{Grt} + \Delta WMnX_{Mn}^{Grt}) / 4.662 - 5.9616\ln K1$ where $m = (W_{FeTi}^{Bt} - W_{MgTi}^{Bt}) = -464$ or 1590 $n = (W_{FeTi}^{Bt} - W_{MgTi}^{Bt}) = -676$ or -1451
Perchuk & Lavrent'eva (1983)	$T = 7843.7 + \Delta V (P - 6000) / 1.987 \ln K1 + 5.699$ where $\Delta V = -0.0577$ cal.bar

$\ln K_1 = Fe^{Grt} . Mg^{Bt} / Mg^{Grt} . Fe^{Bt}$
$\ln K_2 = (Mg / Fe)^{Grt} / (Mg / Fe)^{Bt}$
$\ln K_3 = (Fe/Mg)^{Grt} / (Fe / Mg)^{Bt}$
$T = °K$, $P = kbar$, $R = 0.008314$ kJ k^{-1}

where,
$X_{Fe} = 1-X_{Mg}$
$X_{Ca} = X_{Ca} / X_{Ca} + X_{Mn} + X_{Fe} + X_{Mg}$
$X_{Mn} = X_{Mn} / X_{Mn} + X_{Ca} + X_{Fe} + X_{Mg}$
$X_{Ti} = X_{Ti} / X_{Ti} + X_{Al}^{6} + X_{Fe} + X_{Mg} + X_{Mn}$
$X_{Al}^{6} = X_{Al} / X_{Al}^{6} + X_{Ti} + X_{Fe} + X_{Mg} + X_{Mn}$